Uncertainty in the First Principle Model Based Condition Monitoring of HVAC Systems

By

Richard Andrew Buswell

Submitted in partial fulfilment of the requirements for the degree of Doctor of Philosophy

at

Loughborough University

Loughborough, Leicestershire

June 2001

Table of Contents

List of Tables

List of Figures

Abstract

Model based techniques for automated condition monitoring of HVAC systems have been under development for some years. Results from the application of these methods to systems installed in real buildings have highlighted robustness and sensitivity issues. The generation of false alarms has been identified as a principal factor affecting the potential usefulness of condition monitoring in HVAC applications. The robustness issue is a direct result of the uncertain measurements and the lack of experimental control that are characteristic of HVAC systems. This thesis investigates the uncertainties associated with implementing a condition monitoring scheme based on simple first principles models in HVAC subsystems installed in real buildings.

The uncertainties present in typical HVAC control system measurements are evaluated. A sensor validation methodology is developed and applied to a cooling coil subsystem installed in a real building. The uncertainty in steady-state analysis based on transient data is investigated. The uncertainties in the simplifications and assumptions associated with the derivation of simple first principles based models of heat-exchangers are established. A subsystem model is developed and calibrated to the test system. The relationship between the uncertainties in the calibration data and the parameter estimates are investigated. The uncertainties from all sources are evaluated and used to generate a robust indication of the subsystem condition. The sensitivity and robustness of the scheme is analysed based on faults implemented in the test system during summer, winter and spring conditions.

Key Words: Uncertainty Analysis, Model Uncertainty, Model Structure, Measurement Uncertainty, Fault Detection, Condition Monitoring, Air-Conditioning, Heat Exchanger, Physical Modelling, Sensors, HVAC, Information Poor Systems.

Acknowledgements

I'm here in the final hours of the thesis and I want to write something witty and poignant. Something that will bring laughter and tears in equal measure. I'm thinking I should've thought about this before. The only observation I can make is *what possessed me to start the thing in the first place?* What should have been a few joyful years of intellectual stimulation (er, and climbing) felt like an eternity at times; the most fitting description of which was given by David Lodge in his book *The Picturegoers*, 'Think of a ball of steel as large as the world, and a fly alighting on it once every million years. When the ball of steel is rubbed away by the friction, eternity will not even have begun.' And to be honest, at times, I don't know whether I've been the fly or the steel ball. On at least one occasion I have felt like rolling off the edge of something.

It is now complete and I would like to acknowledge the financial support of ASHRAE through RP1020 and the Grant in Aid scheme. I would like to thank my supervisors Dr. Jon Wright and Dr. Phil Haves for their contributions during my time at Loughborough. I would especially like to recognise the patience of Dr. Tim Salsbury who, with quite saint like calm, answered my every question when I was learning 'C'. Considering he was at the same stage in his thesis as I am now, when presented with a question like, 'so . . . why *do* you need a semicolon after *every* line?', he would have been forgiven for answering physically. In addition to these characters are the occupants of the Control Lab, class of 2000, going on 2002. Lunches have never been quite so enjoyable. Or lasted quite so long. And for that matter, afternoons have never had such a caffine induced buzz (courtesy of the nice double espresso served at the library).

It's over now and that is what I must keep telling myself. Although it, or my first degree, would not have been completed if it wasn't for the unending support of my family. I would also like to thank Richard House, who as listened to my ups an downs along the way and made days out climbing so enjoyable. There is, however, one person without whom I would have never started either of my degrees. Moreover, I would only be a fraction of the person I am today had we never met. I would like to thank Sara for her part in everything.

Nomenclature

α	Risk of rejecting hypothesis (-)
β	Valve curvature coefficient (-)
γ	Valve authority (-)
δ	Differencing interval (-)
ε	Effectiveness (-)
η	Fin efficiency (-)
θ	Sensitivity coefficient (-)
λ	Forgetting factor (-)
ν_a	Air-side conductance resistance velocity power (-)
ν_w	Water-side conductance resistance velocity power (-)
ρ_a	Density of air (kgm^{-3})
ρ_w	Density of water (kgm^{-3})
ρ_M	Uncertainty correlation coefficient (-)
ρ_b	Uncertainty correlation coefficient in the bias errors (-)
σ	Variance (-)
$\sigma^{\cdot}$	Effective variance (-)
σ_{min}	Minimum variance (-)
σ_{max}	Maximum variance (-)
τ	Time constant (s)
ω	Hysteresis (-)
υ	Degrees of freedom (-)
ϕ	Diameter (m)
ς	Partial substitution factor (-)
ξ	Error or convergence criterion (-)
μ	Population mean (-)
ϖ	Distance (radians)

κ	Heat transfer coefficient ($WK^{-1}m^{-2}$)
κ_a	Air-side heat transfer coefficient ($WK^{-1}m^{-2}$)
κ_w	Water-side heat transfer coefficient ($WK^{-1}m^{-2}$)
ϱ	Time (s)
Θ	Vector of sensitivity coefficients (-)
Φ	Matrix of correlated derivatives (-)
Ψ	Vector of sensitivity coefficients (-)
a_l	Low activation point (-)
a_h	High activation point (-)
A_s	Secondary air-side surface area (m^2)
A_o	Air-side surface area (m^2)
A_f	Coil face area (m^2)
A_t	Total area available for water flow in coil (m^2)
b	Estimate of covariance (-)
b_f	Bypass factor (-)
B	Bias uncertainty (-)
B'	Correlated portion of bias uncertainty (-)
B_y	Bias uncertainty component in the uncertainty in a result (-)
B_T	Bias uncertainty in temperature (K)
$B_{T_{rad}}$	Bias uncertainty due to radiation (K)
$B_{T_{uni}}$	Bias uncertainty in spatially uniform temperature measurement(K)
$B_{T_{dist}}$	Bias uncertainty due to spatial distributed temperature (K)
B_{v_a}	Bias uncertainty due to spatial distributed velocity (% of ms^{-1})
$\dot{C}_a$	Air-side capacity rate (WK^{-1})
$\dot{C}_w$	Water-side capacity rate (WK^{-1})
C_{min}	Minimum capacity rate (WK^{-1})
C_r	Capacity rate ratio (-)
C_{P_a}	Specific heat capacity of air ($Jkg^{-1}K^{-1}$)
C_{P_a}	Specific heat capacity of water ($Jkg^{-1}K^{-1}$)
d	Distance (m)
g_{ai}	Moisture content of air onto the coil ($kgkg^{-1}_{air}$)
h_{ai}	Air inlet enthalpy ($kJkg^{-1}$)
h_{ao}	Air outlet enthalpy ($kJkg^{-1}$)
h_s	Effective mean enthalpy of the air at the coil surface conditions ($kJkg^{-1}$)

H_{aa}	Relative humidity of the ambient air (%)
H_{ra}	Relative humidity of the return air (%)
H_{sa}	Relative humidity of the supply air (%)
I_n	Sample interval (s)
I_{max}	Maximum likely value of uncertainty (-)
j	Outside air fraction (-)
J	Number of variables (-)
k'	Amplification factor (-)
k	Thermal conductivity ($WK^{-1}m^{-1}$)
K	Coverage factor (-)
l_f	Coil face length (m)
l_h	Coil face height (m)
l_l	Coil fin thickness (m)
l_{fin}	Fin length (m)
L	Number of elemental uncertainties (-)
$\dot{m}_a$	Mass flow rate of air (kgs^{-1})
$\dot{m}_w$	Mass flow rate of water (kgs^{-1})
$\dot{m}_{w_{max}}$	Maximum water mass flow rate (kgs^{-1})
$\dot{m}'_w$	Primary circuit water mass flow rate (kgs^{-1})
$\hat{m}_w$	Estimated water mass flow rate (kgs^{-1})
$\boldsymbol{m}$	Elemental uncertainty matrix (-)
$\widetilde{M}$	Sum squared uncertainty matrix (-)
M	Sum squared uncertainty vector (-)
M_r	Random or bias uncertainty estimate (-)
n'	Effective number (-)
n	Number (-)
n_r	Number of rows in heat-exchanger (-)
n_c	Number of circuits in heat-exchanger (-)
N_{tu}	Number of heat transfer units (-)
$\boldsymbol{N}$	matrix of correlated uncertainties (-)
P	Random uncertainty (-)
P_y	Random uncertainty component in the uncertainty in a result (-)
P_v	Velocity pressure (Pa)
q	Heat flux (W)
q_{max}	Maximum heat flux (W)

Q_s	Sensible heat transfer (kW)
Q_t	Total heat transfer (kW)
Q'_t	Predicted total heat transfer (kW)
r_a	Air-side conductive resistance coefficient ($_{(\text{rows})}\text{Km}^2\text{s}^{\nu}\text{W}^{-1}\text{m}^{-\nu}$)
r_w	Water-side conductive resistance coefficient ($_{(\text{rows})}\text{Km}^2\text{s}^{\nu}\text{W}^{-1}\text{m}^{-\nu}$)
R_m	Conductive resistance of tube wall in heat-exchanger ($_{(\text{rows})}\text{m}^2\text{KW}^{-1}$)
s	Valve stem position (-)
s^{sq}	Squashed valve stem position (-)
$\hat{s}$	Estimated valve stem position (-)
S	Standard deviation (-)
$\dot{S}$	Standard deviation integrated over time (-)
S_P	Pooled standard deviation (-)
SHR	Specific heat ratio (-)
S_{UA}	UA scaling factor (-)
t	Students-t statistic (-)
T_{max}	Maximum temperature (℃)
T_{min}	Minimum temperature (℃)
T_a	Air temperature (℃)
T_w	Water temperature (℃)
T_{ai}	Air inlet temperature (℃)
T_{ao}	Air outlet temperature (℃)
T_{wi}	Water inlet temperature (℃)
T_{wo}	Water inlet temperature (℃)
T_s	Surface temperature (℃)
T_{sat}	Saturation temperature (℃)
$T_{h_{ai_{sat}}}$	Saturation temperature at h_{ai} (℃)
u_c	Combined standard uncertainty (-)
u_{cc}	Cooling coil valve control signal (-)
u_{mb}	Mixing box damper control signal (-)
u_{sq}	Normalised active range (-)
U_x	Uncertainty in a variable (-)
$U_{\bar{x}}$	Uncertainty in an averaged variable (-)
U_ϵ	Uncertainty in effectiveness (-)

U_{ADD}	Summed uncertainty combination (-)
U_{RSS}	Root sum-squares uncertainty combination (-)
U_{smp}	Uncertainty in the sampling regime (-)
U_{trn}	Uncertainty due to transient data (-)
U_{EMS}	Uncertainty in the model structure (-)
U_t	Total uncertainty (-)
U_{CC}	Uncertainty in the convergence criterion (-)
U_y	Uncertainty in the result or output (-)
U	Overall conductance for heat transfer ($WK^{-1}m^{-2}$)
U_a	Overall conductance for heat transfer with respect to the air-side ($WK^{-1}m^{-2}$)
v_a	Air velocity (ms^{-1})
v_w	Water velocity (ms^{-1})
V_{aa}	Volumetric flow rate of ambient air (m^3s^{-1})
V_{ra}	Volumetric flow rate of return air (m^3s^{-1})
V_{sa}	Volumetric flow rate of supply air (m^3s^{-1})
w	Window length (-)
x	Variable (-)
$\bar{x}$	Mean (-)
$\bar{x}'$	Effective Mean (-)
X	'Lingering' control parameter (-)
y	Output or result variable (-)
Y	'Waiting' control parameter (-)
Z	Non-operator element of a model (-)

Chapter 1

Introduction

In safety critical or high performance engineering, there is a pressing need to account for the inevitable uncertainties present in the measurement and control of processes. The principles used to engineer heating ventilating and air conditioning (HVAC) systems are often derived from such applications. HVAC systems are designed to provide a thermally comfortable environment. Recently, there has been a global effort to improve the efficiency and performance of buildings in order to reduce the emissions that are attributed to global warming and to extend the life of fuel reserves. To accomplish this, research has been directed towards the development of Fault Detection and Diagnosis or Condition Monitoring techniques for building control systems. Taken largely from 'safety critical' industries such as nuclear energy production and augmented by the reduction in the cost of computing power, techniques over the last eight years have been under development to detect faulty operation in building plant. Once detected, faults can be corrected thus saving energy that would otherwise be wasted.

Much of the initial developmental work of condition monitoring for HVAC systems was carried out using simulations or laboratory test equipment. In the last five years there has been a move to test and validate the many condition monitoring approaches on systems installed in *real* buildings. This lead to the realisation that the application of the methods developed in simulation to systems in real buildings was not a trivial task. While there has been some degree of success, frustrations have been compounded by the ambiguous results generated by such tools in these applications (Norford et al., 2000).

The reasons for the apparent poor performance of condition monitoring techniques are in-part due to the inadequacies of systems installed in real buildings in terms of 'expected' performance. A major factor is the lack of 'experimental control'. The condition monitoring methods are expected to be applicable to a wide range of systems. HVAC plant and installations, however, are generally bespoke. For example, in HVAC a 'generic tool' is considered to be one that applies to all typical sizes and configurations of, say, air-to-water heat-exchangers; the engineer applying a 'tool' to a batch of the same nominally identical jet engines may consider that tool to be 'generic'. In addition, the operational characteristics of the plant are heavily influenced by unpredictable and often unquantifiable disturbances. There is a growing realisation that the sensing and measurement capabilities of typical HVAC plant is poor and that this is a major contributing factor to ambiguity in analysing system performance and/or characteristics. There will always be some uncertainty surrounding results from analysis of real systems; the real question is . . . *how much?*

1.1 HVAC Systems

Many of the environments in offices and other commercial buildings are maintained by HVAC Variable Air Volume (VAV) systems. Although the installation of such systems has been declining in recent years, these systems offer a rigorous test for analytical procedures, such as condition monitoring.

The plant is typically centralised, supplying the building from one location through a network of pipes and ducts. An Air Handling Unit (AHU) is used for controlling the air condition and usually comprises of a section to mix outside and recirculated air from the conditioned space, heating and cooling coils, a humidifier and supply and extract fans. A number of sensors are installed to control the output of these components. The typical scheme is shown in Figure 1.1. An AHU can be broken down into a number of subsystems, although these are not easy to define. A component may be connected to another system, such as a cooling coil which is connected to a chiller that serves other coils. Typically the coil control valve and the sensor that controls the valve set point would be defined as the elements that make up the cooling coil subsystem. Modelling, however, may be done at

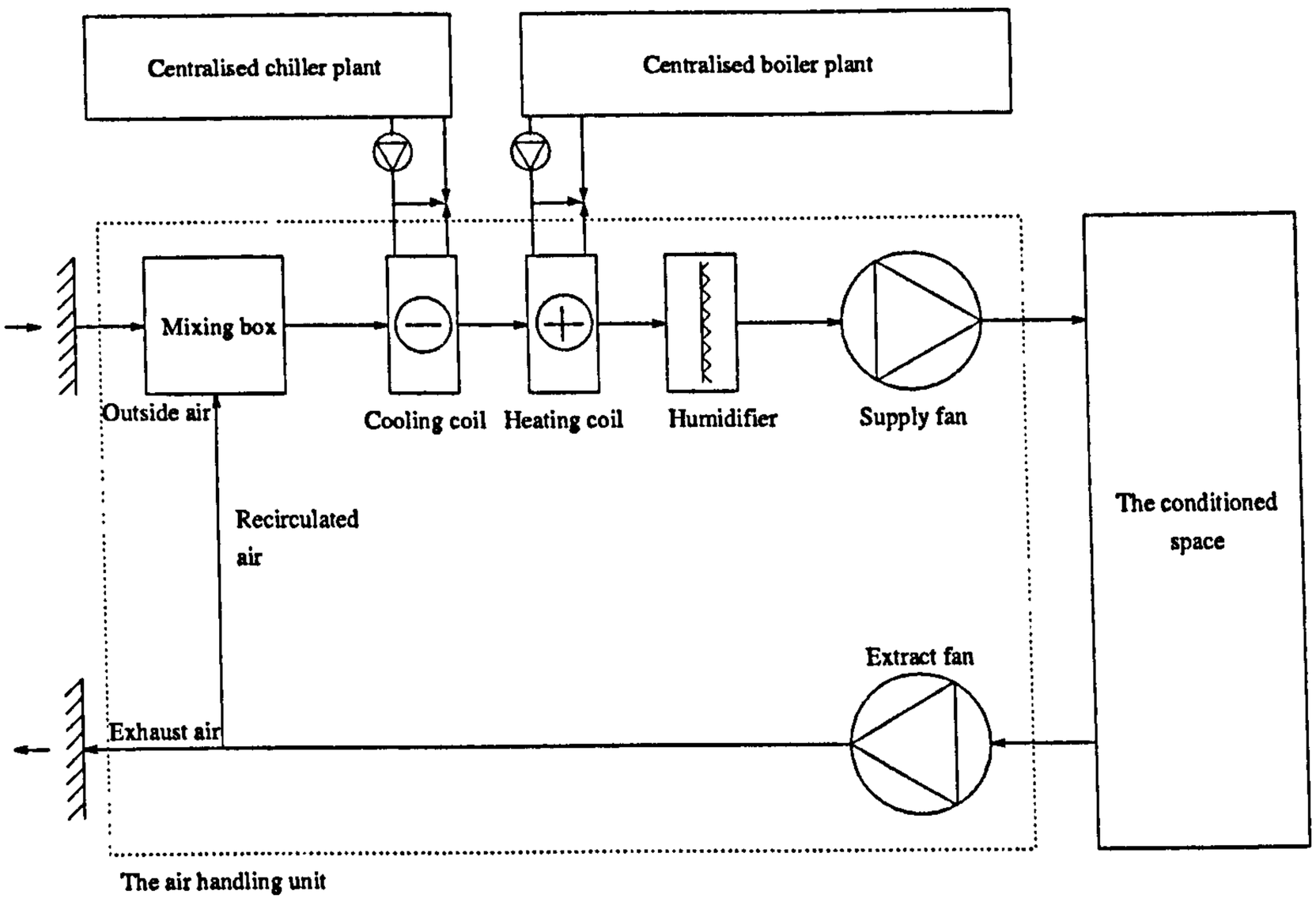

Figure 1.1: The Layout of Typical HVAC Plant Installation.

any level, which can be component, subsystem or whole system.

Typical characteristics of measurement schemes in HVAC plant are:

- minimal instrumentation;
- significant uncertainty in the measurements;
- and high levels of non-linearity.

In general, HVAC plant is constructed to perform the design task for the least cost. To this end, control is implemented by the minimum number of sensors and the placement of these can be questionable. Unmeasured disturbances such as wind speed and direction; noise and bias in the measurements; and interactions with other systems can affect the subsystem processes and the control measurements. The non-linear process characteristics also complicate the modelling aspects.

1.2 Information Processing Technologies

As systems that control processes become more complicated, computer based technologies are required to assist operators in the operation, control and maintenance of the system. Condition Monitoring is an example of this. Information is processed to generate indications of a system's operational status. The application of this technology to information-poor systems offers a challenge.

HVAC systems are a category of information-poor systems that are typically associated with high measurement uncertainty. This type of system generates significant robustness issues for information handling technologies. For condition monitoring applications, the trade-off between sensitivity and robustness is an issue over which there has been much discussion. In general, the reliability measures implemented involve statistics. These are often applied in a somewhat ad-hoc manner and little if no consideration is given to the causes of the uncertainties. Uncertainty Analysis offers a generic approach to evaluating the uncertainty in system measurements and data processing and has the potential to generate robust reliability measures about model predictions. The application of Uncertainty Analysis to the condition monitoring of HVAC subsystems serves as a rigorous test of the available techniques.

1.2.1 Model Based Condition Monitoring

If a system is not operating to the standard required, then there is an error present in the system. This error is commonly termed a 'fault'. 'Fault detection' describes what is done to identify that the system is not operating 'correctly', or at least, 'as expected'. 'Fault diagnosis' is the process by which the probable cause of the faulty operation is established. However, a fault implies that something *unacceptable* is wrong with the system. If a decision is to be made as to whether a fault is to be rectified, the effects of the fault need to be evaluated against some criteria, such as cost and benefit (Rossi and Braun, 1994). A significant change in the operation of the system could occur but may be acceptable and therefore may *not* be considered a fault. 'Condition Monitoring' is the term used to refer to the process of monitoring the operational condition of a system for a

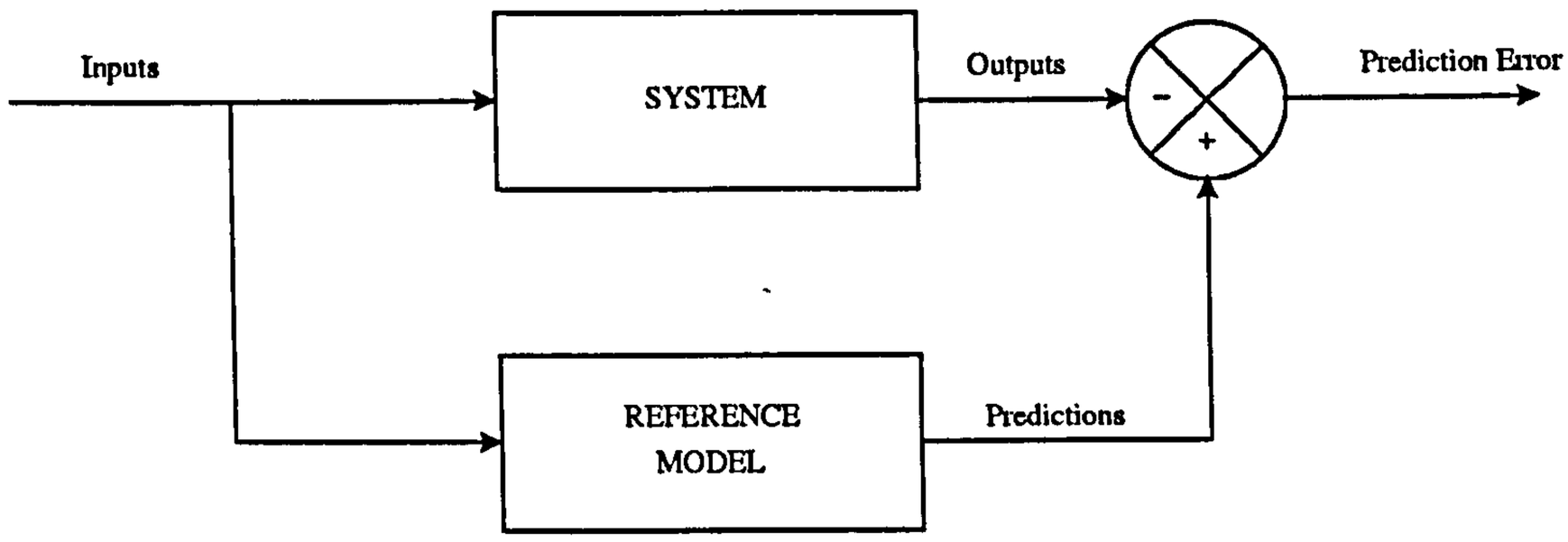

Figure 1.2: Model Based Fault Detection Showing the Generation of Prediction Error.

significant change in performance. It is at this point where the uncertainty in the system has significant impact on the determination of the system state.

The model based approach to condition monitoring generally considers a reference model of the system operating correctly. The system inputs are shared by the system and the model and the outputs are compared as depicted in Figure 1.2. Any difference in the outputs is termed the 'prediction error'. The system input and output measurements will have a degree of uncertainty associated with the measured values. It can be envisioned that uncertainty present in the input measurements affect the model output and will therefore contribute to the degree of uncertainty surrounding the prediction error. In real systems it is unlikely that the prediction error will ever be zero. In essence, if the prediction error magnitude lies outside that which is expected under normal operation, then a change in the system can be identified. The uncertainty estimate for the prediction error calculation can form a statistical threshold against which the prediction error magnitude may be compared.

Model Types

Any condition monitoring procedure must incorporate knowledge about the behaviour of the relevant process. Some process knowledge is generic (applying to all members of a particular class of system). Generic knowledge can be obtained from a first principles based analysis or from experiments. The operational characteristics of each instance of a particular class of system will vary from system to system. The model of a particular

instance, therefore, will usually require the generic process knowledge to be supplemented by information that is obtained from the specific system.

Reference operation can be represented by a computer based mathematical model and there are two primary categories:

- qualitative,
- and quantitative.

The qualitative model is typically an expert rule base that describes the process and can be implemented in some logical programming language (Bratko et al., ; Glass et al., 1995; Kaptipamula et al., 1999). These methods use system measurements to fire rules that result in a qualitative description of the system condition. One disadvantage of this approach is that the creation of expert systems is difficult since often all outcomes need to be considered. Uncertainty in the system will affect the output, but the variations in the interpretation of the output that result, may be a source of ambiguity. The functional transparency of the condition monitoring system can be an important issue (Visier et al., 1999) and there can be a lack of transparency in the derivation of an output due to the complexity of the rule system. Threshold setting can also become problematical as the number of rules increases and there are often many rules required (Norford et al., 2000; Buswell and Wright, 1998; House and Whitcomb, 1999).

Quantitative modelling approaches give a numerical output and deals with absolute values and can potentially contain more information about a specific system than qualitative models. The category can be further subdivided into two basic types (Benouarets et al., 1994):

- black box models, empirical models that embody no prior knowledge of the system;
- and physical models; models based on first principles analysis of the system.

Black box models do not require, nor can they make use of, any prior knowledge of the process. They must be configured using training data generated either by the target

system itself or by a simulation of it. The main advantage of black box models is that they offer great flexibility in the selection of the input/output relationships and can model highly complex and/or poorly understood, non-linear processes. One advantage of physical models is that the prior knowledge that they embody improves their ability to extrapolate to regions of the operating space for which no training data are available. They also require fewer parameters for a given degree of model accuracy.

Uncertainty analysis in physical systems necessitates the proper consideration of the process being examined and requires an understanding of the components in a process that can affect the uncertainty in the measurements, from ISO (1993);

> '*The evaluation of uncertainty is neither a routine task nor a purely mathematical one; it depends on detailed knowledge of the nature of the measurand*[1] *and of the measurement. The quality and utility of the uncertainty quoted for the result and measurement therefore ultimately depend on the understanding, critical analysis, and integrity of those who contribute to the assignment of its value'.*

Analytical models provide the most insight into the underlying process present in physical systems. It can be expected that observation irregularities may be better understood for this reason. In addition, the proper formulation of the relationships between errors through the use of any data reduction equations can be made on a first principles basis.

1.3 Uncertainty in Model Comparison to Data

When collecting any data for the purpose of analysis, uncertainty will *always* be present. The uncertainty in the desired output (the result) can be affected by typical experimental errors that can be characterised as:

- limitations on the precision and accuracy of the measurements;

[1]The *measurand* is the term used by the ISO Standard to refer to the quantity being measured (ISO, 1993)

- extraneous influences, exacerbated by the level of experimental control;
- unrepresentative data inadvertently used to calculate the result (the inclusion of data containing transients in a steady-state analysis, for example);
- disturbances induced by the presence of the observation equipment itself;
- human error.

There are a number of other important issues when considering the analysis of data (Holman, 1984; ASHRAE, 1996; Reddy et al., 1999):

- the type of error under consideration;
- the difference in the significance of the effect of the maximum error compared to the most probable error on the uncertainty in the result;
- the data sampling regime;
- the propagation of errors through the system in relation to the models employed;
- and the approximation to Gaussian or Normal distribution.

The data sampling regime is critical when considering statistical analysis. The sample type affects the way in which the data can be treated and can be categorised as either *single sample*: where a single reading or a succession of readings are taken at the same or different times, but under identical conditions, or, *multi sample*: where repeated measurement of a fixed quantity is affected using different test conditions, such as different observers or different instrumentation. In practice, using control measurements typically found in HVAC plant, there will be one set of sensors available. At certain operating conditions, two sensors may sample the same fluid stream properties, and may therefore approximate to a form of multi sample data. However, most of the data collected will be time dependent, single sample. The disadvantage of using single sample data is that certain errors associated with the sensor measurement will only ever be sampled once, regardless of repetition. This will undoubtedly increase the level of uncertainty that cannot be statistically treated.

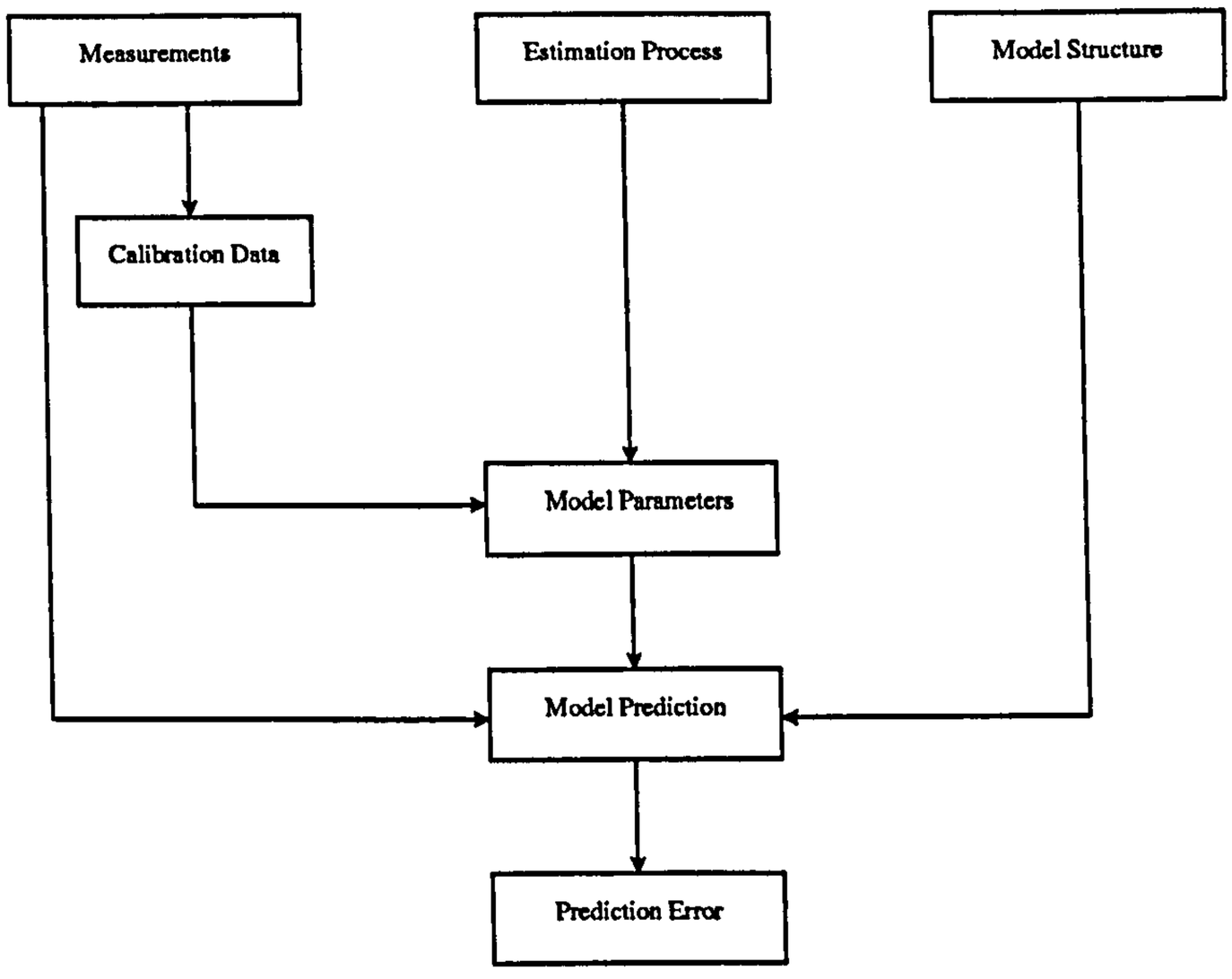

Figure 1.3: Condition Monitoring Scheme Uncertainty Flow Diagram.

Table 1.1: Sources of Uncertainty Associated with General Uncertainty Categories

Measurements	Model Structure	Model Parameters
sensor	detail limitation	calibration data
data handling	computational limitation	model structure
noise	information quality	region of operation

1.3.1 Categorising Sources of Uncertainty

Figure 1.3 maps the uncertainty flow path of a model based condition monitoring scheme where the prediction error is the desired result. The sources of uncertainty that contribute to the effectiveness and reliability of a model based condition monitoring scheme can be placed in one of three main categories. Table 1.1 lists the sources of uncertainty in these three categories of uncertainty factors. It should be noted that the region of operation is not a source of uncertainty, but a factor that the errors associated with the model parameters are dependent upon. Further to Table 1.1, the effects associated with the correct, accurate and precise fluid state measurement in HVAC systems can be attributed to (Oughton, 1985):

sensor: type and design; published characteristic/conversion tables; associated dynamics; age.

data handling: installation, such as lengths of cable etc. (Sontay, 1998); data handling, such as truncation and rounding; analogue to digital conversion.

noise: flow rate and flow regime in terms of the heat transfer coefficient at the sensing element; radiation, from other surfaces such as coils, or the sun; approximation to the mean fluid temperature that is implied by the measurement; noise induced in the analogue signal by external factors.

These uncertainties impact on the sensitivity and/or robustness of any condition monitoring scheme and so a method of evaluation is necessary. Uncertainty due to the design and type of sensor and data handling can usually be gained from manufacturers data sheets. These figures are typically quoted as a percentage of the full scale range of the device at a confidence level of 95% (ASHRAE, 1996). The integrity of the stated manufacturers uncertainties is an important consideration in the use of these values. The noise component of the measurement signal is used here to describe the elements of the real system operation that are not explained by the system model (Dobson, 1983). The effects of the influences of noise are evident in the variation in the data signal. These variations will be system specific and the sources listed above will vary in significance. Work detailed by Carling (1998a) demonstrates that major influences on air temperature measurements in HVAC systems are the nature of the air flow, i.e. approximation to the real fluid average temperature which is complicated by stratification and radiation on the sensor. It should be noted that accuracy is a separate issue that affects the uncertainty of a measurement. Inaccuracy may be corrected, or at least improved, by calibration. Statistical techniques can be applied to the noise and combined with the other uncertainties to give confidence bounds for a given measurement.

The assessment of model structural uncertainty is an issue that has not been addressed in the literature. This uncertainty can be present where iterations are required to solve model's equations. The convergence criteria introduces some uncertainty into the model prediction. The simplifications and assumptions that allow the construction of simple models must by definition contain some uncertainty. These simplifications are based on

information about the system. The quality and understanding of this information will, therefore, influence the uncertainty evaluation process.

When a model is calibrated, or 'fitted', to data collected from the target system, the uncertainty present in the data becomes embodied in the model parameter estimates. This links the model structural uncertainty with the parametric uncertainty. The information in the data is critical to the precision of the model in prediction especially when the model is expected to extrapolate.

1.4 Aims and Objectives

The overall objective of this work is to investigate the uncertainties evident in monitoring the performance of typical HVAC heat-exchanger systems. The work is targeted at developing a holistic approach to identifying and evaluating uncertainties so that robust predictions of real system performance using simple first principles models cans be realised. The aims of the work are:

- to critically review uncertainty analysis techniques and uncertainty applications used in HVAC engineering (Chapter 2);
- to investigate uncertainties in data acquisition and to review and develop methods of evaluating spatially induced bias uncertainties in typical HVAC sensor measurements (Chapter 3);
- to investigate the uncertainty in the data sampling regime and to develop a procedure for evaluating the uncertainty generated in steady-state model predictions, when the input data contains transients (Chapter 4);
- to examine the uncertainties inherent in the structure of a simple heat-exchanger model structure and to develop an uncertainty assessment approach to describe these ambiguities, demonstrating the methodology through parametric study on heat and heat-and-mass transfer examples (Chapter 5);
- to describe a test sub-system installed in a full scale test facility and to investigate

uncertainties and bias in the measurements, developing and validating an *in situ* sensor validation methodology (Chapter 6);

- to describe a model parameter identification procedure that allows the assessment of uncertainty introduced from the calibration data and to evaluate the performance of model based condition monitoring on the test system described in Chapter 6, based on all the uncertainties present in the system (Chapter 7);

- to draw conclusions and suggest areas where there is potential to conduct further research (Chapter 8).

Chapter 2

Literature Review

In engineering systems, a key issue is the quality of measurement used for control and monitoring purposes. Uncertainty is inevitable in all measurements and is introduced at every stage in the measurement process. It is usually caused by a variety of reasons and some will be more significant than others. Uncertainty analysis is concerned with identifying the significant influences on measurement quality so that these can be controlled in order to render useful information. This chapter gives a brief history of the development of uncertainty analysis and then reviews work in related areas, highlighting the significant issues for this work. Condition monitoring and uncertainty analysis used in HVAC is reviewed, identifying the need for the application of uncertainty analysis to generate robust condition monitoring.

2.1 Uncertainty Analysis

It is only since the early part of the 20th century that the developing industrialised society realised the importance of properly calibrated instruments in engineering. This realisation occurred as mass produced parts required increasing levels of interchangeability and therefore replicable degrees of quality control and precision (Dietrich, 1973). Increasing the precision to which components are manufactured requires assessment of critical dimensions or properties. Measurement instruments are required, and these need to be calibrated to provide some assurance that the instrument reading is correct. The term

'calibration' originates from the early eighteenth century. 'Calibre' or 'calliper' both referred to an instrument used for measuring bores. The calibre-scale is used for measuring gun bores and it is in this way that the term 'to calibrate' is associated with measurement and scales. During the mid-nineteenth century the term was associated with the measurement of physical quantities, such as temperature and pressure. Calibration was used as the term for correcting instrument scales for irregularities in the bores of the tubes in the instrument. The term has now become associated with the correction of measurement instruments that are already graduated. More generally, improved calibration, results in a more precise measurement. As the confidence in the value of a measurement increases, the uncertainty decreases. The analysis of how uncertainty behaves is a powerful, if not essential, tool in any information gathering process. In applications where information is processed for the purpose of decision making, the expression of uncertainty is critical if the information is to be trusted and hence used to its maximum potential.

2.1.1 Uncertainty Propagation

At the time of the publication of the paper by Kline and McClintock (1953), there was virtually no published work describing the treatment of uncertainties in single-sample experiments. Single-sample experiments occur more frequently than multi-sample experiments in engineering. The difference between the approaches is in the number of observers used to monitor the process; multiple observers yielding richer information. Observations made by single observers were generally found to give inconsistent results ((Pearson, 1902) referenced in (Kline and McClintock, 1953)). This is because if a single instrument is used to make repeated observations, some error would always exist. It is the reduction of this error by the application of different observers that separates single-sample from multi-sample data.

Kline and McClintock suggested that the uncertainties in an experiment should be established through expert judgement to give an interval within which the true value would lie given certain odds and that these uncertainties could be used to calculate an uncertainty in the result. The equation proposed is essentially founded on the premise that if a process

is described correctly by an equation $y = f(x_1, x_2, ..., x_J)$, then the uncertainty surrounding the true value of the J^{th} variable (x_J) U_J, would contribute to the uncertainty of the result, U_y, as a function of the derivative of U_J with respect to y, and so,

$$U_y = \left[\left(\frac{\partial y}{\partial x_1} U_1\right)^2 + \left(\frac{\partial y}{\partial x_2} U_2\right)^2 + \ . \ . \ . \ . \ + \left(\frac{\partial y}{\partial x_J} U_J\right)^2\right]^{\frac{1}{2}}. \qquad (2.1)$$

The addition in quadrature means that the signs associated with the variable uncertainties or the gradients are negated, resulting in $\pm U_y$, and consequently an even distribution about the best estimate of y. This method of calculating the uncertainty in the result has been universally adopted and is the foundation of contemporary uncertainty analysis.

The ASME[1], prompted by the ISO[2] 5168 Standard (1976), set up a committee to prepare a US standard on uncertainties in flow measurement. Later, the ANSI[3]/ASME MFC - 2M Standard on uncertainties in flow measurement was published (1983). The methodology described in the standard is presented in Abernethy et al. (1985). The approach develops that of Kline and McClintock (1953). The uncertainties in each variable in Equation 2.1 are treated as single values. Abernethy et al. (1985) identifies a difference between 'bias' (often referred to as 'systematic') and 'random' uncertainties and defines the terms 'precision' and 'accuracy'. Figure 2.1 demonstrates these terms. Their approach calculates *total uncertainty* as the sum of the total bias and total random errors in a variable. These are treated separately until the final combination to generate the uncertainty in the result. The random errors are treated statistically. The bias error is estimated by the experimenter. In the absence of rigorously proved methods for combining the two uncertainty types, two combination options were offered which gave a maximum error, U_{ADD}, and a most likely error, U_{RSS},

$$U_{ADD} = B + tS_{\bar{x}} \qquad (2.2)$$

$$U_{RSS} = [B^2 + (tS_{\bar{x}})^2]^{\frac{1}{2}} \qquad (2.3)$$

where B, t and $S_{\bar{x}}$ are the total bias uncertainty, student-t value and total random error respectively. U_{ADD} and U_{RSS}[4] provided a coverage interval, within which the true value

[1] American Society of Mechanical Engineers.
[2] International Organization for Standardization.
[3] American National Standards Institute.
[4] There is an error in the publication by Abernethy et al. (1985). The square root of the right hand side of Equation 2.3 is not taken. It is shown correctly here.

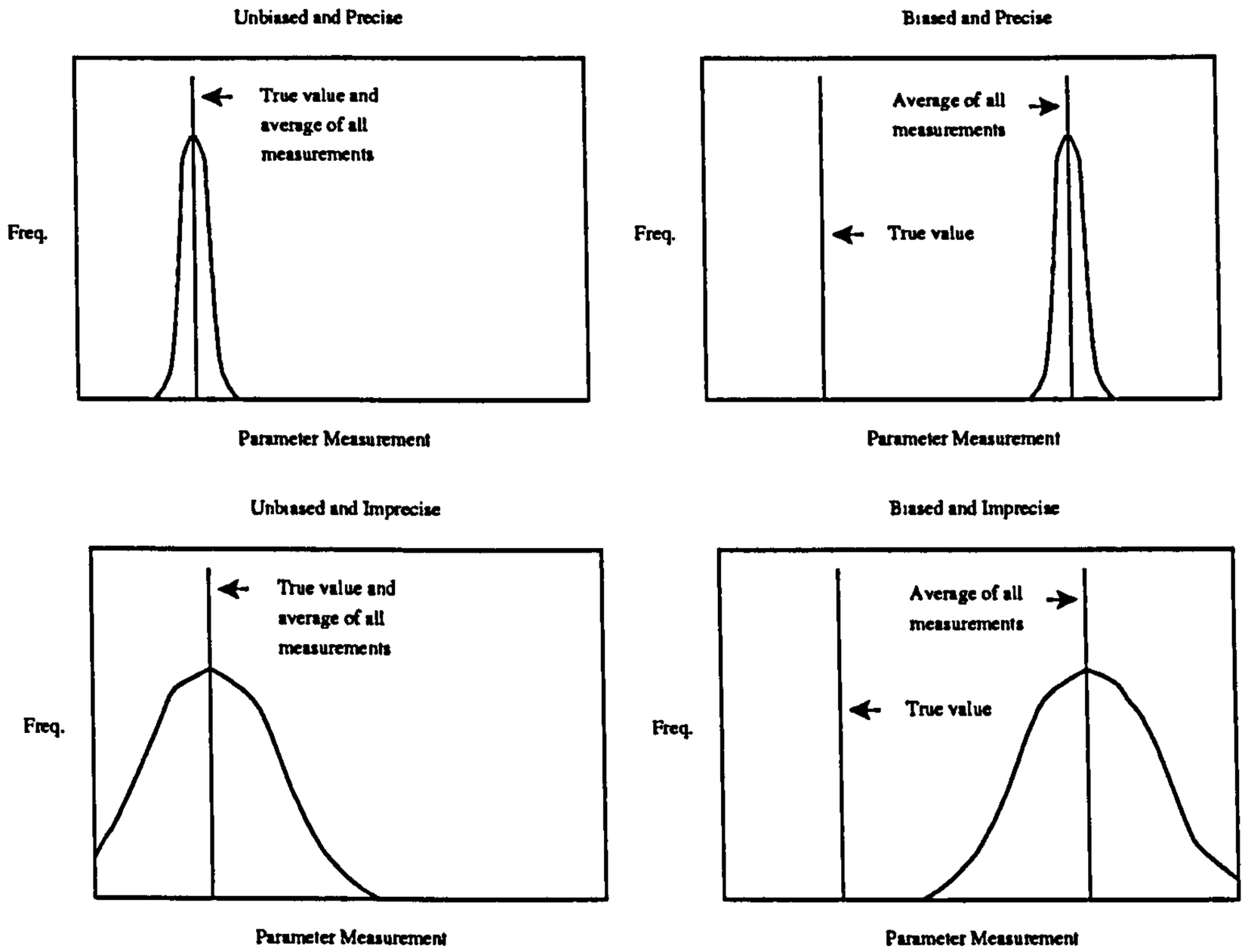

Figure 2.1: Graphical Representation of the Relationship Between the Terms Precision and Bias in the Context of Uncertainty

will lie at an approximation to the 99% confidence level and at an approximation to the 95% confidence level respectively.

Up until the 1990s the evaluation of random uncertainty was considered to be a matter of applying statistics. Steele et al. (1993) argued that a simple statistical evaluation of the precision uncertainty would only be possible if a result was considered over a finite time window. In more typical engineering applications, however, variables are held in steady-state for a set time period and not over the entire time frame of interest. The results obtained from these 'local' conditions are then often expected to apply globally. This can be described as the extrapolation of uncertainty. If there are factors that affect the precision in terms of this extrapolation, the estimated precision limit[5] may be under-predicted. This can occur when there are certain effects that cause a measured variable

[5]From Steele et al. (1993): 'Precision limit: The $\pm P_y$ interval about a result y (single or averaged) is the experimenter's 95% confidence estimate of the band within which the mean of many such results would fall if the experiment were repeated many times under the same conditions using the same equipment. The precision limit is thus an estimate of the scatter or lack of repeatability caused by random errors and unsteadyness.'

value to fluctuate on a longer time scale than the data sample is collected over. Clearly, if the precision limit is to be correct for experimental replication, it is important that effects such as these are correctly evaluated.

The investigation by Steele et al. (1993), considered the determination of precision limit by comparing two methods of calculation, assuming no bias uncertainty. They compared the ANSI/ASME Standard approach where the test variables x_i are measured n_i times, where n_i could be different for each variable i. The result, $y = f(\bar{x}_1, \bar{x}_2, ..., \bar{x}_J)$. P_y is then given by $P_y = tS_y$, where t is the student-t value at the appropriate probability level and S_y is determined from the uncertainty propagation equation (Equation 2.1) that uses the standard deviation about $\bar{x}_i$,

$$S_y = \left[\sum_{i=1}^{J}(\theta_i S_{\bar{x}_i})^2\right]^{\frac{1}{2}}, \tag{2.4}$$

where $\theta_i = \frac{\partial y}{\partial \bar{x}_i}$ and $S_{\bar{x}_i}$ is the standard deviation. The alternative approach given by Coleman and Steele (1999) was calculating P_y by,

$$P_y = \left[\sum_{i=1}^{J}(\theta_i P_{\bar{x}_i})^2\right]^{\frac{1}{2}}, \tag{2.5}$$

where $P_{\bar{x}_i}$ is the precision limit of the mean for the variable x_i and $P_{\bar{x}_i} = t_i S_{\bar{x}_i}$.

Using a Monte Carlo simulation[6] the two methods were assessed against a set of hypothesised true variable values and uncertainty distributions for an engineering data reduction equation, in the absence of bias error. A range of sample sizes were run and a check made to see how often the estimated interval centered about the current variable value contained the hypothetical true value. The conclusion was that using either method to predict the interval within which the result from a separate experiment would lie with small sample sizes (i.e. $n_i = 4$) could lead to significant over or under prediction of the range that contains the true value.

Rather than increasing the sample size to generate more reliable precision limits, the second consideration was to use sets of previously gathered large data samples, (10, 20 and 31 samples), to calculate the standard deviations of the uncertainty distributions. The precision interval for the small sample case was then calculated with respect to the

[6]Computer based simulation based on the Monte Carlo Method; used in statistics to estimate a solution to a numerical problem using the random sampling of numbers (Binder and Heermann, 1992).

large sample data and to the current sample size. The coverage of the true value with the estimated interval using the larger sample size information was much improved. The key outcome from the work was that during the set up phase of experiments, the standard deviations from different data samples should be compared and then used to estimate more reliable precision limits around data taken in the future from smaller sample sizes.

The ISO published the 'Guide to the Expression of Uncertainty in Measurement' (1993), virtually setting an international standard for the expression of uncertainty in measurement. In 1978 the worlds highest authority in metrology, the Comit International des Poids et Mesures, requested that the Bureau International des Poids et Mesures address the lack of international consensus on the expression of uncertainty in measurement. A set of recommendations were developed and the ISO were assigned the task of developing a detailed guide. Working contributions from organisations in the areas of chemistry, physics, metrology and electro-technical were made. The guide describes the nomenclature to be used, details calculation procedures, outlines a reporting methodology, gives an overview of statistics and gives example uncertainty calculations.

Coleman and Steele (1995) found the ISO approach to uncertainty analysis to be consistent with previously published approaches. ISO (1993) gives the uncertainty propagation equation[7] in terms of the *combined standard uncertainty*, u_c, is given by,

$$u_c^2 = \sum_{i=1}^{J} \theta_i^2 b_i^2 + 2 \sum_{i=1}^{J-1} \sum_{k=i+1}^{J} \theta_i \theta_k b_{ik} + \sum_{i-1}^{J} \theta_i^2 S_i^2 + 2 \sum_{i=1}^{J-1} \sum_{k=i+1}^{J} \theta_i \theta_k S_{ik}, \qquad (2.6)$$

where $\theta_i = \frac{\partial y}{\partial x_i}$ and y is the result[8] related to the J measured variables by the data reduction equation represented by $y = f(x_1, x_2, ..., x_J)$. The term b_i^2 is the estimate of the variance of the bias error distribution of the variable x_i and b_{ik} an estimate of the covariance of the bias errors. The other terms for precision error are analogous to the bias error term descriptions. The uncertainty propagation equation is derived via a first-order Taylor series approximation to the data reduction equation, see Coleman and Steele (1995), ANSI/ASME-MFC-2M (1983) or ISO (1993). The function is assumed to be continuous and have continuous partial derivatives in the neighbourhood of the evaluation of the result. If the non-linearity of the data reduction equation is significant, then it may

[7]Sometimes referred to as the *law of propagation of uncertainty* (Taylor and Kuyatt, 1994; ISO, 1993).
[8]The 'result' is then term used to describe the calculated variable of interest in the analysis.

be necessary to consider the higher order terms of the Taylor series expansion.

To obtain a coverage interval for the standard uncertainty at a specified confidence level, u_c is multiplied by a coverage factor, K, to give the *expanded uncertainty*, U_y,

$$U_y = K u_c, \tag{2.7}$$

where K is the appropriate student-t value and a discussion of the estimation of the degrees of freedom required are given by Coleman and Steele (1995). Coleman and Steele do not provide clear comment on how the probability levels involved in establishing the uncertainty intervals for the separate uncertainties interact with the calculation of U_y. Intuitively, the chosen probability level should remain constant throughout the uncertainty estimation process.

The approach of the ASHRAE (1996)[9] Guideline is that if the uncertainties associated with all the variables are at a specified level of confidence, then after application of Equation 2.1 the uncertainty in the result is at the same stated confidence level. The ASHRAE Guideline is not, therefore, in harmony with the ISO Standard (1993).

Coleman and Steele (1995) compared the published approaches for calculating the expanded uncertainty. Various methods were investigated including Abernethy et al. (1985), given in Equations 2.2 and 2.3 and ISO (1993) given in Equations 2.6 and 2.7. Their own approach was also introduced. This was similar to the ISO approach, but differed in that it accounted for correlations in the bias errors. The U_{ADD}/U_{RSS} approach of Abernethy et al. could not be rigorously justified against the derivation of the uncertainty propagation equation given by Coleman and Steele (1995). Apart from these comments, the methods were found to be similar.

Correlations in the Bias Errors

A bias error correlation occurs when the source of uncertainty cause two or more variables to be biased in the same direction; this often occurs when instruments are calibrated to the same standard. Coleman et al. (1995) showed that improper handling of correlated

[9]American Society of Heating, Refrigerating and Air-Conditioning Engineers

bias error can lead to significant effects on the bias limit. An additional conclusion was that the existence of correlated bias errors can reduce the uncertainty in the result and so it cannot, therefore, be considered conservative to ignore such effects.

Brown et al. (1996) demonstrated that the approaches to the treatment of correlated bias error varied tremendously. Two treatment methodologies were used: neglecting them all together and applying the 'root-sum-squares' approach. In this approach the bias correlations were treated by estimating the covariance, b_{ik}, at the 95% confidence limit using $b_{ik} = \rho_{b_{ik}} B_i B_k$, where $\rho_{b_{ik}}$ is the correlation coefficient appropriate for the bias errors in the variables, x_i and x_k. Assuming that there exists perfect correlation between the variables that are considered to be correlated, $\rho_{b_{ik}} = 1$ and therefore, $b_{ik} = B_i' B_k'$ where B_i' is given by,

$$B_i' = \sqrt{\sum_{j=1}^{L} (B_i)_j^2}, \tag{2.8}$$

where B_i' and B_k' are the portions of B_i and B_k that are correlated and there are L elemental systematic errors common for the measurements of the variables x_i (with similar terms for k). The desired coverage of the estimated interval for both these methods was found to be much less consistent than the approach proposed by Brown et al. (1996) where the treatment is by estimating the covariance, B_{ik}, directly using,

$$B_{ik} = \sum_{j=1}^{L} (B_i)_j (B_k)_j, \tag{2.9}$$

and is called the 'sum-of-products' approach. The approach described in Equation 2.9 is, therefore, preferred.

Conclusions: Uncertainty Propagation

A brief history and review of the work that has contributed to the theory behind the propagation of uncertainty has been presented. There are a number of approaches available and each is based on Equation 2.1, proposed by Kline and McClintock (1953). The approach described in Coleman and Steele (1995) (and subsequently in Coleman and Steele (1999)) calculates the 95% estimate of the uncertainty in the result where the random and bias uncertainties are quoted at the 95% level;

$$U_y^2 = B_y^2 + P_y^2, \tag{2.10}$$

where, U_y is the uncertainty in the result, y and B and P represent the 95% estimates of the bias and random uncertainties denoted by M in the general equation,

$$M_y^2 = \sum_{i=1}^{J} \theta_i^2 M_i^2 + 2 \sum_{i=1}^{J-1} \sum_{k=i+1}^{J} \theta_i \theta_k \rho_{M_{ik}} M_i M_k. \tag{2.11}$$

where J is the number of variable and $\theta_i = \frac{\partial_y}{\partial x_i}$. Given the standard deviation S_i and assuming the large sample assumption is applicable, $P_i = 2S_i$. $\rho_{M_{ik}}$ is the correlation coefficient that relates the correlations between uncertainty sources which can be estimated using Equation 2.9. This method is preferred because:

- it has a rigorous derivation;
- no coverage factor needs to be estimated;
- it handles correlations in the uncertainties.

The derivation of the uncertainty code used in Chapter 7 is given in Appendix C and is based on Equations 2.10 and 2.11.

Two powerful Uncertainty Analysis tools given in Coleman and Steele (1999) are the Uncertainty Percentage Contribution (UPC) and the Uncertainty Magnification Factor (UMF), described in Equations 2.12 and 2.13 respectively,

$$UPC = \left(\frac{\partial y}{\partial x_i}\right)^2 \left(\frac{U_{x_i}}{U_r}\right)^2, \tag{2.12}$$

$$UMF = \frac{\partial y}{\partial x_i} \frac{x_i}{y}, \tag{2.13}$$

where y is the result and x_i is a measured variable participating in the calculation of the result. U denotes the uncertainty associated with the variables and $\frac{\partial y}{\partial x_i}$ is the respective sensitivity coefficient. Both techniques are employed in Chapters 4, 5 and 7.

2.1.2 Application of Uncertainty Analysis

Moffat (1982) acknowledges that there exists a multiplicity of factors that influence the variance of data measurements, some of which can be controlled directly, some indirectly, some cannot be controlled and some are not even observable. An analysis methodology

is presented that considers the levels of experimental replication that allows the structured consideration of all the contributions to uncertainty made through elemental errors present. An experiment in which the fixed or systematic errors, or rather the effects, can be considered insignificant compared to the random (and therefore measurable) perturbations in the measured variables are called 'Zero-Centered' in the work. Moffat bases his analysis technique on the fact that this goal is practically achievable. Discussion by two independent reviewers of the work, however, claim that Zero-Centered data is unlikely to be achievable in practice and is therefore a weakness in the methodology. In a later publication, Moffat (1985) gives an example of using uncertainty analysis in pre-test, or *priori*, testing using his uncertainty order methodology. The uncertainty order methodology described related to three levels, Zeroth, First and Nth order. The Zeroth-order considers the errors associated with the instrument only. The First-order considers the variation in a reading during a steady-state experiment. The errors would include natural fluctuations in the experiment and the instrument; essentially the random component in a series of measurements. The Nth-order considered all uncertainties associated with the experiment and would be the level at which other independent experiments would be expected to agree with. The application of the analysis method allows for the detailed consideration of all elemental errors affecting a result.

Moffat (1988) describes the application of uncertainty analysis to measurements and pays particular attention to the errors present in measurement systems. Moffat presents the proposition that the 'true' value of the measurand is not 'absolute', but in fact subject to a definition cast by the experimenter, that is affected by the choice of measurement and analysis. This can be illustrated by considering a thermocouple probe in a hot gas stream in a duct with cold walls; the 'true' definition of the temperature, (Moffat, 1988) could be considered as:

- the temperature of the thermocouple junction (the achieved value);
- the temperature of the gas at the junction location (the available value);
- the temperature the gas at the junction location would have had if the instrumentation system had not disturbed the distribution (the undisturbed value);

- the mass-flow-weighted average temperature the gas in the duct would have had, at the axial location of the thermocouple probe, had the instrument system not disturbed either the temperature or the flow distribution (the conceptual value).

In systems that have permanently installed sensors, such as in process control, the disturbance caused by the sensor can be considered as part of the system characteristics or configuration. The important issue is that careful consideration and definition of the result is necessary to ensure that the *conceptual* errors implicit in the data reduction process are kept to a minimum. Moffat suggests simple methods of correcting the listed system/sensor errors, but, in general, the successful application of corrections is primarily a function of the accuracy of the assumptions and approximations applied to the situation. The uncertainties associated with the assumptions and corrections therefore need to be accounted for in the analysis. However, Moffat recognised that these errors are often significant and that some measurement bias can be introduced through effects dependent on other variables. For example, an offset appearing in a temperature sensor due to radiation from the duct walls: if the wall temperature differs, so too will the offset. These types of error were termed 'variable but deterministic'.

Moffat also considered that if measurement sampling was carried out at a faster rate than the process varied at, then the data would contain some information about the measurement system. Moffat called this multiple-sample data. This is contrary to the classical view but it does highlight a subtle difference in the type of data that may be acquired. Considering the 'ideal' sampling case (infinite size) for each example, descriptions of the possible data types in descending order of quality are:

Multi-Sample 1: *An infinite number of observers used to measure data sets created from infinite sample sizes taken over the entire domain of interest at sufficient sample rate to characterise the measurement system variations.* In this case, since all the bias errors will vary randomly, and the sample sizes are infinite, the mean of the overall uncertainty distribution will be the true value of the measurand (assuming a Guassian distribution).

Single-Sample 1: *A single observer used to measure data sets created from infinite sample sizes taken over the entire domain of interest at sufficient sample rate to characterise the measurement system variations.* Here, the random variations are accounted for perfectly; the measurement system random errors are accounted for but since the measurement system stays the same, some bias will always exist.

Single-Sample 2: *A single observer used to measure data sets created from infinite sample sizes taken over the entire domain of interest.* Here, the random variations in the **system only** are accounted for, since the measurement system stays the same, some bias will always exist and there will be an additional random component that is unexplained.

Single-Sample 3: *A single observer used to measure data sets created from infinite sample sizes taken over some of the domain of interest.* Here, **some** of the random variations in the system are accounted for, since the measurement system stays the same, some bias will always exist and there will be an additional random component that is unexplained.

Single-Sample 4: *A single observer used to measure a data set created from an infinite sample size taken at a single point in the domain of interest.* Here, **none** of the random variations in the system are accounted for, since the measurement system stays the same, some bias will always exist and there will be an additional random component that is unexplained.

Practical considerations and the lack of experimental control in measurements taken from 'permanently' installed instruments will usually result in single-sample data somewhere between type 2 and 4. In addition, classic statistics state that as sample size decrease the quality of estimates from the sample will also degrade. A further observation is that careful consideration of the information required is needed to select a suitable sampling rate.

2.1.3 Causes of Uncertainty

Causes of uncertainty in terms of the calibration of scientific measurements and quality control in manufacturing processes were given by Dietrich (1973) as:

- uncertainties in standards or in calibration equipment;
- uncertainties due to operator error;
- resolution or discrimination uncertainties;
- environmental uncertainties (eg. variation of temperature);
- instability uncertainties (eg. lack of repeatability);
- functional uncertainties (eg. from malfunctioning equipment);
- uncertainties caused by a lack of cleanliness;
- uncertainties due to poor quality surface texture and incorrect geometry;
- uncertainties associated with the lapse of time (eg. where there could be change in the equipment).

Causes of uncertainty in measurement is given in ISO (1993), which notes that these may not be independent effects:

- incomplete definition of the measurand[10];
- imperfect realisation of the definition of the measurand;
- nonrepresentative sampling (the sample measured may not represent the defined measurand);
- inadequate knowledge of the effects of environmental conditions on the measurement or imperfect measurement of environmental conditions;
- personal bias in reading analogue instruments;

[10]The 'measureand' is the term used to describe the measurement of interest.

- finite values of measurement standards and materials;
- inexact values of constants and other parameters obtained from external sources and used in the data-reduction algorithm;
- approximations and assumptions incorporated in the measurement method and procedure;
- variation in repeated observations of the measurand under apparently identical conditions.

The above lists assist in the identification of uncertainty sources and should be considered in any analysis and influences the investigation in Chapters 3, 4, 6, and 7.

2.1.4 Uncertainty and Models

There is little work that discusses the uncertainty in modelling in the literature. Coleman and Steele (1999) and Brown et al. (1998) derive an expression for the uncertainty propagation in classical linear regression. Sensitivity analysis is often performed in conjunction with uncertainty analysis (Hofer, 1999). This can be a powerful tool in the identification of the main contributors to uncertainty in the result and is sometimes termed 'Uncertainty Importance Analysis'. The effort and analysis time can be reduced by targeting the major influences on uncertainty. The analysis can demonstrate whether the investigative resources should be directed into either:

- further model development,
- improved understanding of the process being modelled.

A sensitivity analysis can also assist model developers and users in identifying errors in the model and identifying when the model is not valid for a given application. In computationally intensive applications, model quality assurance is important (Hofer, 1999) and uncertainty/sensitivity analysis can contribute in a number of ways:

- error flags can be incorporated into the analysis runs, catching computational problems that may otherwise be undetected;
- the analysis output can highlight associations that should not exist, or do not show those that should, indicating the possibility of an implementation error in the code, the data handling system or the model;
- the identifications of possible areas for execution efficiency improvements;
- the identification of computed or measured outputs that are outside the complementary boundaries of uncertainty, indicating the existence of possible errors in the uncertainty assumptions/estimates used.

The model performance (principally in terms of the output prediction uncertainty) can be improved by an iterative process of model validation and verification (Hasselman et al., 1998). Validation is a qualitative process that investigates how faithfully the underlying process physics are represented in the model. Validation evaluates the model structure and may involve the selective testing of different models, with varying levels of the degree to which physical complexities are represented. The verification process is quantitative and includes:

- calibration or tuning of model parameters with data from physical measurements;
- analysis of parameter estimates for statistical significance and consistency.

Certain statistical properties can be obtained after calibration and three useful information measures applied to the new model parameter estimates:

- verification that changes in the parameter estimates are statistically consistent with the initial estimates;
- comparison of the revised parameter uncertainties to the initial uncertainties to estimate the degree of new information extracted from the data;
- and the correlation structure of the estimates which is an indication of how much information has been gained about individual parameters as opposed to correlated

sets of parameters (the less parameters are correlated, the more is known about individual parameters).

These processes need to be considered with respect to model parameters identification; applied in Section 7.2. There is, however, no research reported in the literature that addresses uncertainty in the modelling assumptions and simplifications associated with the creation of simple non-linear first principles based models. Chapter 5 addresses this deficiency with respect to heat-exchanger models.

2.1.5 Uncertainty Analysis in HVAC Applications

Uncertainty analysis is a developing technology. Major applications and developments have been in Metrology and experimental Physics and Chemistry (ISO, 1993; Eurachem, 1995). Much of the development has been through the desire to standardise the expression of uncertainty throughout the international community. Early work was driven by the requirements associated with laboratory experiments but the application has broadened to engineering disciplines, such as thermal hydraulics, waste disposal performance assessments, and structural mechanics and into safety critical applications, such as, structural risk analysis and accident consequence assessment (ISO, 1976; ANSI/ASME-MFC-2M, 1983; ANSI/ASME-PTC-19.1, 1986; Hofer, 1999; Bilal, 1998).

Increasingly, the engineering community at large is appreciating the tools and methodologies offered by uncertainty analysis. One such field is HVAC, although the use of the available techniques is relatively uncommon. There have been several publications in recent years, although much of this work has been directed towards estimation of uncertainties associated with economic factors (Kammerud et al., 1999), or at in-situ plant testing (Phelan et al., 1997a; Phelan et al., 1997b).

Phelan et al. (1997a, 1997b) consider the measurement of fans pumps and chillers for the purpose of establishing the plant energy consumption. The work describes guidelines aimed at the testing of installed plant in-situ such that energy analysis can be performed on the data with respect to assessing energy savings from various economy improving strategies. The methods described used measured data, subjective information regarding

the building loads, and manufacturers data. An uncertainty analysis procedure is developed to estimate the uncertainty in the energy savings predictions. One challenge facing the work was that standard methods of testing mechanical equipment were directed for laboratory use, and did not extend to in-situ applications. Problems associated with the application of experimental type approaches necessitated the adjustment of these methods to account for effects of system installation, operation and control. In particular the work highlighted the major sources of uncertainty as (Phelan, Brandemuehl, and Karti 1997b):

- calibration errors in the instrumentation associated with the installation of the sensors;
- random errors associated with the noise in the instrumentation system and with the various processes being measured;
- regression prediction uncertainty;
- uncertainty of the subjective information (load profiles).

The use of uncertainty analysis was implemented to generate bounds of uncertainty on the prediction of a linear regression model. Phelan et al. (1997a) applied uncertainty analysis to a temperature dependent chiller[11] model. The uncertainty in the estimation of the chiller efficiency ($1/COP$[12]) is calculated by propagating the uncertainty in the measurements through the chiller model equation.

Uncertainty analysis on the testing of air-to-air heat-exchangers installed in buildings has also been investigated by Johnson et al. (1998). The aim of the work was to examine the installed performance of typical heat recovery devices. The work recognised that uncertainties in air flow measurements exist due to non-uniform fluid flow. Flow non-uniformity is inevitable in real systems due to fittings; tees/elbows, dampers, etc. Recommended 'best practice' plant installation (such as that given in BSRIA (1993a) and (1993b)) are often restricted by a lack of space and therefore good locations for measurement rarely exist. In addition, non-uniform temperature distributions were found to increase uncertainty in the analysis and were attributed to:

[11] A chiller is a refrigeration unit used for cooling fluids, usually some water solution in HVAC applications, so that the cooling capacity can be transported to the point of application.
[12] COP: Coefficient of Performance

- ducting leaks;
- stratification;
- non-uniform heating or cooling of coils;
- and losses or gains from the ducting walls.

One outcome of the work was to demonstrate that the ASHRAE Standard 84 (ASHRAE, 1991) applicable to laboratory testing, was not entirely suitable for field testing (Ciepliski et al., 1998). Similar findings were reported in the work by Phelan et al. (1997a, 1997b).

The bias uncertainty quoted in Johnson et al. (1998), was estimated from calibration tests and the precision uncertainty was estimated from field data. Corrections were made to the bias uncertainty estimates to account for the non-uniformity in temperature. The total bias uncertainty, B_T (K) was given as,

$$B_T = \sqrt{(B_{T_{dist}})^2 + (B_{T_{uni}})^2}, \tag{2.14}$$

where $B_{T_{uni}}$ is estimated from calibration of the sensors. $B_{T_{dist}}$ is given by,

$$B_{T_{dist}} = \frac{T_{max} - T_{min}}{n}, \tag{2.15}$$

where n is the number of independent temperature sensors and T_{max} and T_{min} (℃) are the maximum and minimum temperatures measured. It was found that these effects were significant in some of the measurements taken.

The benefits of using uncertainty analysis has also been found when considering the evaluation of energy and cost savings associated with alternative methods of cooling (Reddy et al., 1999). The methodology presented took measurements from the target system over a short periods of time both before and after energy conservation methods were implemented. The energy savings were then calculated together with an estimate of the uncertainty in this value. In addition to uncertainty arising from measurement errors and the prediction uncertainty in the regression model determined from the data, the work also considered cases where models supplied variables to other models. The prediction uncertainty from regression models was attributed to the following factors:

model mis-specification uncertainty: where the regression model does not adequately approximate the true functional form of the process modelled, such as where relevant regressor variables are not included or where linear approximations are made;

model prediction uncertainty: arises due to the imperfect nature or structural deficiencies of the model;

model extrapolation uncertainty: where the mode is used for predictions outside the training data region of operating space.

A suggestion was that to minimise the model mis-specification uncertainty, the physical behaviour of the system is considered to gain an insight into the 'true' nature of the process. The work also includes the variability of the input variables in the category of model prediction uncertainty and treats the bias and random errors together.

Conclusions: Uncertainty Analysis in HVAC Applications

Uncertainty analysis is little used in HVAC applications, although guideline documents (of which ASHRAE (1991) and ASHRAE (1996) are examples) exist. The fuller, more correct uncertainty analysis techniques demonstrated in Section 2.1.1 have not been used in published research to date. Appendix C and the subsequent application in Chapter 7 sees the introduction of the contemporary approach to uncertainty propagation to HVAC applications. Published research has incorporated the evaluation of uncertainties and there has been some decision on sources on uncertainty that are common in the HVAC environment. Estimates of bias uncertainty have also been presented. Chapter 3 and 6 build on these techniques and findings.

2.2 Condition Monitoring in HVAC Systems

Once building control systems[13] gained the potential to record control measurements, the feasibility of condition monitoring in HVAC systems was realised. Over recent years there

[13] Computer based systems that traditionally control the operation of the mechanical and electrical plant used to condition the occupied spaces. Today, these systems increasingly provide complete centralised control for all building systems, including lighting, security, etc.

have been considerable research efforts into developing condition monitoring technologies for HVAC equipment. At the forefront has been the work of Annex 25 of the International Energy Agency[14]. Different approaches were developed and the principles tested were generally in simulation (Hyvärinen, 1997b; Hyvärinen, 1997a; Hyvärinen, 1997c). The current IEA Annex 34 is close to completion and has investigated the practical application and demonstration of some of the technologies developed in Annex 25.

2.2.1 Approaches to Condition Monitoring

The practical implementation of condition monitoring in HVAC systems have the following requirements:

- inexpensive computationally;
- low rate of false alarms;
- quick detection of developing faults;
- robust to atypical disturbances;
- model the processes under consideration to the desired accuracy;
- differentiate between faults that are important and those that are insignificant;
- able to model different types of plant.

The lack of computational effort of condition monitoring schemes is becoming less of an issue with the ever decreasing cost of computational power and is not considered a prohibitive constraint in this work. Low false alarm rates (robustness) are satisfied by the application of the correct reliability measures; a critical issue in the successful application of these technologies.

There are two main approaches to the application of model based condition monitoring in buildings:

[14]The International Energy Agency was established in 1974 with the aim of fostering co-operation among twenty-one participating countries to increase energy security through energy conservation, development of alternative energy sources and energy research development and demonstration , (Hyvärinen, 1997b). Here-on-in referred to as the IEA.

- whole building energy simulation ('energy monitoring and targeting');
- component level condition monitoring.

The models used in energy monitoring and targeting are often very simple; using models based on degree-days, for example. Detailed analytical models such as those in DOE-2 and black box models have been investigated for this application (Bronson et al., 1992; Kreider and Haberl, 1994). In most cases, these models are configured to represent correct operation, and so condition monitoring can be implemented.

Component level model based condition monitoring, involves the use of models of individual items of equipment. These models may either be analytical, first principles, or empirical models (Fargus and Dexter, 1994; Benouarets et al., 1994). In general, the models are simple, usually for reasons of computational efficiency and ease of configuration.

In principle, reference models used in condition monitoring should treat dynamic behaviour as well as steady-state behaviour. However, the variations in operating point encountered in HVAC systems are often slow enough that most items of equipment can be regarded as being in a quasi steady-state, such that the error produced by using a static reference model is acceptably small. Static reference models are simpler to develop and configure; the dynamic behaviour of HVAC equipment is often non-linear and poorly understood. Static models can be used for condition monitoring if it is possible to determine when their predictions are valid, and when measurements can be used safely to estimate their parameters. Several steady-state detectors have been produced by Annex 25 participants (Hyvärinen, 1997a; Hyvärinen, 1997b; Hyvärinen, 1997c). Work by Norford et al. (2000) has found that the effective determination of steady-state, with respect to precise model predictions is difficult. The tuning of steady-state detector parameters tends to become a heuristic process and does not guarantee transient free data is used with the model. This can lead to poor prediction precision and Chapter 4 presents an alternate approach to address this problem.

If condition monitoring is expected to indicate abnormal operation, the models used in the condition monitoring methods *must* represent the correctly operating system. Performance validation is the process of inspecting the system to ensure at least *acceptable* operation

is achieved and configuring the models of correct operation to the acceptably operating system. The models used in the condition monitoring scheme may require data from the target system for configuration purposes (Salsbury, 1996; Haves et al., 1995). These tasks can be combined and automated (Buswell et al., 1997; Ngo and Dexter, 1999a). Section 7.2 presents the approach adopted in this work.

2.2.2 Technology Review

There have been many approaches to condition monitoring in HVAC. Some of the techniques include the application of fuzzy logic, artificial neural networks, parameter estimation, rule bases and hybrid approaches, such as combining physical modelling techniques with radial basis function networks (Hyvärinen, 1997c; Salsbury, 1996; Geshwiler, 1996). All approaches use the same source of data; the only differences being the manner in which the data are processed.

Kaptipamula et al. (1999) presented a condition monitoring method applied to the mixing box (or economiser) in an AHU[15]. The method used an expert rule base to detect and diagnose problems. Development of the user interface was addressed, and the tool is currently installed in two real buildings, although results to date are from testing in simulation. A recent presentation by Kärki and Karjalainen (1999) proposed a plant life cycle approach to condition monitoring. Their approach was to link certain performance factors to the condition monitoring phase. Fault detection was affected by a characteristic curves approach, a method that models the correct operation by the comparison of polynomial curve fits to interesting quantities (Hyvärinen, 1997c). Diagnosis is implemented with a fault tree, but there were no test results from real buildings.

Expert rule bases are a popular condition monitoring medium. Obtaining knowledge to generate data bases required to affect an expert rule base from real system data was investigated by Han et al. (1999). House and Whitcomb (1999) demonstrated a rule based condition monitoring approach based on data from a real AHU plant. Statistical estimates of the measured variables were used to generate some robustness and it was

[15] Air Handling Unit, containing several HVAC components; typically consisting of coils, fans, filters and a mixing section.

envisioned that these thresholds would mature as the application to more systems refined the values to generic levels. This echoes the sentiments of Buswell and Wright (1999). A disadvantage of House and Whitcomb's technique was that twenty-six rules were used to model the system performance, all requiring a threshold to identify abnormal operation. False alarms were evident.

Arguably the most advanced condition monitoring demonstration scheme in HVAC is currently being implemented in France. An artificial neural network has been used to identify six fault cases using three measurements. The application has been designed to reduce the engineering effort involved in monitoring the status of many buildings' hydronic heating systems simultaneously (Li et al., 1996; Li et al., 1997). Simplicity has been the key approach. The work is demonstrating that method simplicity and transparency are important issues with the end users, particularly with regard to diagnosis. Users also found the raw data was important for building confidence in both the diagnosis and the technology (Visier et al., 1999). A distinct set of faults were defined at the conception of the method, which simplifies the diagnosis process, and the system has been warmly received by the users. One outstanding issue still to be resolved, however, is a high false alarm rate.

Seem et al. (1999) presented a prototype condition monitoring residing in local digital controllers implemented on VAV boxes. The new controllers have been implemented in a real building and are currently under trial. Simple indices are calculated and can be displayed in graphical format. The approach operates on a pseudo-redundancy scheme, where detection is by visual recognition that the performance of say, one or two, VAV units exhibits largely different performance to the majority. A similar approach that uses on-line recursive parameter estimation to tune a dynamic process model to the current system operation was presented by Yoshida and Kumar (1999). VAV boxes were monitored and a visual inspection of plots of the frequency response of the model identify abnormally operating systems.

Significant progress has been made in the development of practical condition monitoring techniques for vapour compression equipment. Rossi and Braun (1994) showed that the operating costs of such equipment could be minimised through optimal maintenance

scheduling. Later work developed a statistically based condition monitoring technique for vapour compression equipment (Rossi and Braun, 1997). The approach was evaluated by Breuker and Braun (1997), (1998) and (1999). The method uses data collected from the target system to estimate the parameters of polynomial models that characterise the system operation. Detection is by statistical significance of the residual magnitude, generated by the measurements and the correct operation model. Diagnosis identifies the cause as one of five possible faults. A disadvantage is that the amount of training data required to establish the models is significant although this is offset by the application to mass produced units. One unit can be tested and the data *should* apply identical units. A subset of the technology developed is currently under trial in computer assisted maintenance packages.

There have been two recently completed research projects, the aim of which was to apply condition monitoring to real HVAC plant installed in real buildings. One considered the cooling coil subsystem of a constant air volume AHU operating over an entire cooling season. Three condition monitoring methods were applied using:

- first principles model and rule based diagnosis;
- first principles model combined with parameter estimation;
- and fuzzy model incorporating a fuzzy matching scheme for diagnosis.

The first two methods used identical physical models (Salsbury, 1996; Buswell et al., 1997; Buswell and Wright, 1998; Buswell and Wright, 1999). The rule based approach affected detection by checking the innovations magnitude against the calibration error. Larger innovations were taken as evidence of abnormal operation. The innovations were then issued to one of three 'bins' where the diagnosis information accumulated. The bins represented low, medium and high operation, and the expert rules were applied to the information in the bins. The recursive parameter estimation re-estimated certain model parameters designed to represent faults. As faults occur, the parameters change and identify the current operating condition of the system. In both cases the first principles models are tuned to the target system using data gathered across the operating range of the plant.

The fuzzy logic based approach uses a generic cooling coil model generated in simulation, characterised using data from a similar class of heat-exchanger. Beliefs are issued with statements about the current operating condition. The beliefs are generated by comparing different models of faulty and normal operation to the current operating data. The beliefs represent a measure of the degree of representation offered by the respective models to the current system state (Dexter and Benouarets, 1995; Dexter and Benouarets, 1996; Ngo and Dexter, 1999b; Ngo and Dexter, 1998). In addition to these three fault detection and diagnosis methods, an automated commissioning tool which reduces effort involved in the calibration data collection procedure (Ngo and Dexter, 1999a) and a data archiving protocol were developed (Buswell, 1998).

All three methods gave similar results over the test period. The principal differences in performance were that the first principles model approaches seemed more sensitive, but prone to inconsistent alarm output, whereas the fuzzy model approach gave more ambiguous output, but was more robust. The main issues highlighted by the work were:

- the lack of information available for diagnosis when the plant is left to its normal operational cycle;
- the degree of uncertainty, and lack of consistency in typical HVAC measurements;
- and the engineering time involved in setting up the methods.

Updated versions of the first principles model based approaches were subject to further research. The developments in the rule based version primarily involved applying statistical methods to determine confidence limits around the innovation (Section 1.2.1). The approach used a statistical test to generate $(1-\alpha)100\%$ confidence limits about the difference between two means $(\mu_1 - \mu_2)$: one was recursively estimated given the current sample and the other was a reference variable established by calibration testing;

$$(\bar{x}_1 - \bar{x}_2) - t_{\alpha/2} S_P \sqrt{\frac{1}{n_1} + \frac{1}{n_2}} < \mu_1 - \mu_2 < (\bar{x}_1 - \bar{x}_2) + t_{\alpha/2} S_P \sqrt{\frac{1}{n_1} + \frac{1}{n_2}} \qquad (2.16)$$

where $\bar{x}$ is the sample mean, n is the number of data in the samples, S_P is the pooled estimate of the population standard deviation and $t_{\alpha/2}$ is the student-t value with $v = n_1 + n_2 - 2$ degrees of freedom. Both sample population variances were assumed to be

equal, but unknown (Walpole and Myres, 1989). The mean and standard deviation for the innovations in calibration data in each bin was compared to the current innovation. The innovations were also corrected for differences in the trained model prediction and the calibration data. The fault models for the parameter estimation technique were developed to increase the independent nature of the parameters. The detection of faults in the mixing box, cooling coil and supply air systems were investigated (Norford et al., 2000).

A third fault detection and diagnosis method was implemented called non-intrusive load monitoring, or, NILM. This technique used correlations between electrical energy consumption and flow rates or control signals to represent normal operation. Statistical intervals are used to generate robustness. One advantage of this approach is that the electrical energy consumption is monitored, and so the impact of faults can be assessed in terms of energy directly (Norford et al., 2000; Norford and Leeb, 1996). Additional sensors to those normally used for control were installed for the NILM method, whereas the first principles approach only uses the sensors already installed for control purposes.

A range of abrupt[16] and degradation[17] faults were introduced into the three monitored systems. These were two full size AHU test systems connected to test spaces, and one AHU serving live office space. The test periods covered summer, winter and a swing (spring) season. The main issues that came from the work were:

- some faults drive the system to saturation, therefore increasing the difficulty of diagnosis;
- in general, abrupt faults could be detected;
- in general, degradation faults had to be quite large before detection was unambiguous;
- and the reliability measures were not sufficiently robust, resulting in difficulty in selecting suitable fault thresholds.

[16] Abrupt, sometimes termed catastrophic, faults are those that affect an instant and (usually) dramatic effect on the performance of the system, such as a broken fan belt

[17] Degradation faults are those that reduce the performance of the system over time, such as as fouling on the water-side of a cooling coil.

The conclusions from the current research is that the data available from HVAC systems is highly uncertain. In general, the condition monitoring methods that are being actively investigated at present are not mature with respect to these inherent uncertainties, which is the principal contributing factor to the ambiguity and lack of robustness in the condition monitoring output.

2.3 Conclusions

A review of uncertainty analysis theory and engineering application was presented together with a review of HVAC system condition monitoring. It was identified that the use of uncertainty analyis techniques in HVAC engineering research was minimal. This work introduces the contemporary methods given in Appendix C. Specific comments are:

- The proper handling of uncertainty in measurement is critical in establishing the usefulness of the results of analysis. Non-uniform temperatures was identified as an important issue with respect to the quality of measurement. There has been little published work addressing the evaluation of uncertainty in HVAC sensors. Chapter 3 addresses these issues;

- The appropriate sampling characteristics were identified as an important issue in obtaining the required system information. The problems with existing steady-state detectors were identified. Both issues are considered in Chapter 4;

- It was identified that there currently exists no method of evaluating the uncertainty in the assumptions and simplifications that allow the creation of first principles based models. Chapter 5 investigates this issue with respect to heat-exchangers;

- Causes of uncertainty in generic terms and specific problems identified in HVAC systems were highlighted. There is no standard approach for evaluating sensor bias using *in situ* measurements. Chapter 6 introduces a methodology for this purpose;

- First principles based models were shown to be able to yield precise predictions of HVAC component performance. The robustness issues surrounding the practical implementation of condition monitoring techniques were identified. Uncertainty

analysis is applied to a first principles model based condition monitoring scheme to generate robust predictions in Chapter 7.

Chapter 3

Sensors and Uncertainty in Measurements

HVAC control systems have the capability of recording measurements used to control the processes, an essential feature that has allowed the application of condition monitoring techniques. Uncertainties in measurements are introduced during the data acquisition process in three distinct phases:

- in the process of converting (fluid) properties and quantities to electronically usable information;
- in the calibration of the sensing element;
- and in the characteristics of the location of the sensing element.

This chapter considers the uncertainty sources that contribute to these three categories, focusing on typical HVAC sensor arrangements and measurements.

Sensing and data acquisition technology is described in the context of the uncertainties they introduce to the measurements. Spatially induced sensor bias is highlighted as a particularly significant source of uncertainty, especially in air measurements. Methods of evaluation of spatially induced uncertainty reported in the literature are considered. Where no such methods exist new approaches are formulated.

3.1 HVAC Data Acquisition

The quality of the data acquisition available at any one HVAC installation will be generally restricted by the control system hardware specification. Although this specification is strongly influenced by cost, the resolution and data handling capabilities of the hardware in contemporary installations are likely to be quite adequate in terms of the other uncertainties present in the system (See Table 6.2 and Chapter 6).

The principal components of the data acquisition system can be classified into three separate hardware tiers:

- sensing elements;
- information processing;
- and data recording.

Sensing elements have either an electro-physical or electro-mechanical property that converts a physical quantity or property into an electrical signal. The information processing tier converts the analogue signal from the sensor to a digital one. Any post processing of the data, such as Condition Monitoring, is likely to be carried out at the data recording level.

Building control systems are often split into *supervisors* and *outstations*. At the supervisory level the operations of the buildings systems are monitored and it is at this level that the data recording would take place. The *outstations* execute the minute-by-minute control and will generally contain the information processing tier. The hardware system consists of the following main components:

- signal conditioner;
- amplifier;
- filter;
- multiplexer;

- analogue to digital converter.

The above list can be classified in two groups; the actions executed by the first three are termed 'conditioning'; the last two are termed 'conversion' (Taylor, 1986).

3.1.1 Signal Conditioning

The signal conditioner can be described as the interface between the sensor and the converter. The following functions must be provided by the components of the conditioner listed above:

1. provide sensor excitation;
2. compensate for signal offsets;
3. provide system and sensor calibration;
4. provide amplification of the input signal to match converter input requirements;
5. accommodate differences in zero potential references;
6. limit signal bandwidth.

A constant current or constant voltage needs to be applied across most sensors since sensing elements are often passive. In building control system measurements, 0-12v or 4-20mA are common. The stability of the voltage is an important factor and a lack of stability and/or excessive noise will contribute to the uncertainty in the measurement as a function of the signal amplification and conversion. The amplification component scales the converter's input signal to accommodate differences in zero potential. If dynamic measurements are required, consideration of the response of the amplifier is necessary. The amplifier settling time and slew rate specifications are measures of the components ability to track changes in the measurement.

The uncertainty associated with such components are often not quoted for HVAC equipment. This is because, in correctly operating systems, their influence should be negligible

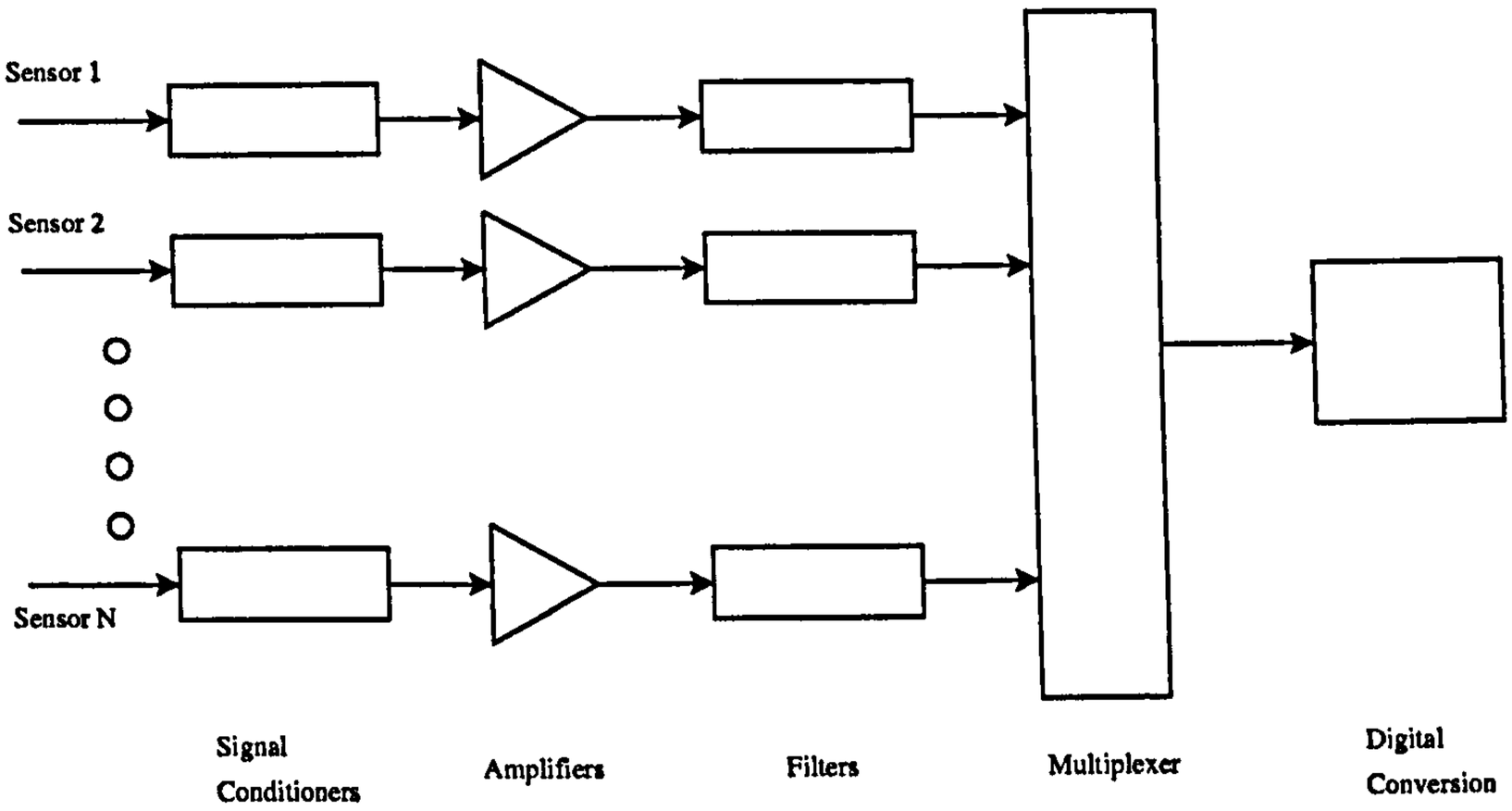

Figure 3.1: A High Level *Multiplexing* Data System.

compared to other sources, such as signal conversion (discussed in the next section). The assessment of voltage stability is time consuming. In the context of the practical implementation of a condition monitoring scheme, this is likely to be prohibitive and so the uncertainty from these elemental sources are unlikely to be evaluated. Such influences on the measurements will therefore appear as random fluctuations. The uncertainties can be accounted for indirectly by the assessment of random uncertainty described in Chapter 4.

3.1.2 Conversion

In order to reduce the cost of data acquisition or control systems, *hardware multiplexing* is often employed. This allows a reduction in the duplication of components. An example of a high level *multiplexing* data system is shown in Figure 3.1. *Multiplexing* allows the use of one set of conversion equipment to process signals from many sensors. Measurement uncertainty can be affected by cross-talk between various channels when the signals are closely coupled. The accuracy of the measurement can also be affected by switching between channels through the switch resistance, frequency, thermally induced voltages, source impedance and settling time. Once again these uncertainties are practically impossible to evaluate directly, but can be accounted for by the application of a random uncertainty assessment.

The converter is an error source and the magnitude of uncertainty is quantifiable. The continuous analogue signal is converted into discrete steps so that it can be represented by digital code. This process is called *quantization*. The resolution of the converted signal is a function of the bit-size of the converter. An 8-bit converter has $2^8 - 1 = 255$ 'steps'. A $0 \rightarrow$ 10 volt signal is therefore represented by bands of $\frac{10}{255} = 0.039$ volts/bit. For a temperature scale that relates $0 \rightarrow 10$ volts to $-50°C \rightarrow 50°C$, this equates to $\frac{(50-(-50))}{255} = 0.392°C$. Each instantaneous point is represented by one level. The *quantization error* is therefore given by $\pm\frac{1}{2}$LSB (Least Significant Bit). In the example this would be $\frac{0.039}{2} = 0.020$ volts, which yields an uncertainty of $\pm 0.195°C$. Contemporary HVAC control systems typically use 12-bit converters. Examples of the uncertainties that can be expected for various measurements can be found in Section 6.4.

In condition monitoring, the control signals can also be used as measured input (see Section 7.1). In a similar manner to the analogue to digital conversion, the reverse conversion is used in the generation of the analogue control signal and so will also contain some uncertainty. The error in the control signal in a 12-bit converter is $\frac{1}{4095} \times 100 = 0.02\%$. In some manufacturers equipment, the digital to analogue conversion is operated on a lower resolution (10-bit). In general, in calculations where there are many analogue to digital conversions and relatively few digital to analogue conversions, the uncertainties due to the latter source can be neglected. This is often the case with model based condition monitoring.

3.1.3 Data Recording

Uncertainty in the data recording phase accounts for the handing of the converted measurement and recording. If no further filtering or data manipulation is carried out, the error (and hence uncertainty) associated with the recorded data will lie in the number of significant figures left after any truncation or rounding operations.

3.2 Sensing Elements

There are many different types of sensors available (Holman 1984; Taylor 1982). A comprehensive review of those commonly found in building systems control can be found in Underwood (1999). According to Underwood (1999), there are twelve factors that specify a sensor in terms of performance and economy. Half of these have implications for uncertainty:

Range; the range of the measured variable for which the following characteristics are maintained at stated values.

Accuracy; the degree to which the measured output compares with some known benchmark.

Repeatability; the ability of the sensor to reproduce consistently the same output from the same measured value.

Sensitivity; the smallest detectable change in measured value that results in an output change by the sensor.

Drift; the degree to which the sensor fails to give consistent performance throughout stated life.

Response time; the rate of response with respect to time of the output following an input change.

The range has implications for uncertainty at the information processing level. Analogue to digital conversion discretises the analogue signal. The smaller the range and the higher the resolution of the converter, the less uncertainty present in the measurement. This is pertinent where no choice in the converter resolution is available. The uncertainty can then only be reduced by limiting the range. Accuracy is obviously fundamental to the overall accuracy of the measurement value. The manufacturer's calibration accuracy is often specified at a given value, or as a percentage of the full scale deflection. This value is usually specified at the 95% confidence level.

Aspects of the installation of the sensor will affect the uncertainty. Taylor (1986) gives the factors affecting the repeatability of a measurement as the following:

- hysteresis;
- electrical noise;
- time variations of the measurement;
- thermal drift;
- cross talk;
- common mode voltage.

Taylor regards these effects as contributions to the random error uncertainty component and the practical evaluation of these has been discussed in Section 3.1.2 and 3.1.1.

Response time is largely insignificant if the time scale of the process dynamics and/or the data sampling interval is slow compared with the time constant associated with the sensing element. Sensitivity is not usually an issue in HVAC systems, because sensors tend to be 'standardised' and are sufficiently sensitive compared to the uncertainties from other sources.

The following sections describe the principles and uncertainties associated with the most common sensors used in HVAC control applications. Special attention is given to the estimation of the uncertainty associated with measurements used to represent fluid bulk averages.

3.2.1 Temperature Measurement

A temperature measurement device usually consists of an element that changes resistance with temperature. The change in resistance is then measured by the subsequent variation in voltage or current connected across the element. Some signal conditioning will be applied to the voltage or current such that the range of the measured quantity can be

scaled to suit some useful range. The length of the sensor installation cabling can influence the measurement, although various wiring arrangements are commonly employed to compensate for this (Holman, 1984).

The sensing element is constructed from a material for which useful temperature/resistance characteristics are derivable. The two types that are commonly found in HVAC control systems are Thermistors and Resistance Temperature Detectors (RTDs). Figure 3.2 demonstrates the characteristic differences in the element sensitivity between these sensors. A thermistor is a semiconductor that has a negative coefficient of resistance and an exponential characteristic. One main advantage of this device is sensitivity. There is a large change in resistance to a small change in temperature. Holman (1984) quotes a possible uncertainty in the region of $\pm$0.01K. The RTD is a metal based element. Although it has a polynomial characteristic, the temperature/resistance relationship is very linear over the majority of the application range. These devices have a positive coefficient of resistance and are characterised by a much smaller change in resistance for a given change in temperature than the Thermistor. RTDs are low cost devices whose characteristics can be easily tailored to suit a particular application. A typical level of uncertainty is approximately $\pm$0.15K. The magnitude of the inaccuracies contribute to the uncertainty in the measurement. Clearly, the Thermistor is an order of magnitude better than the RTD in this respect.

There are two types of air temperature measurement; point and averaging. Considering air flow in a duct, a point measurement at any location will only measure the properties of the fluid at that location. The application of that measurement to the entire flow area (estimation of the bulk average) becomes less robust as the flow area increases. One major influence is stratification, which is exacerbated by duct leakage; duct heat loss or gain; long uninterrupted flow paths or two air streams mixing at dissimilar temperatures. An average reading over the flow area is desirable and can be practically achieved in two ways:

- A long sensing element[1] is installed so that it is exposed to different proportions of the duct area.

[1] Termed an 'averaging' sensor and is often an RTD.

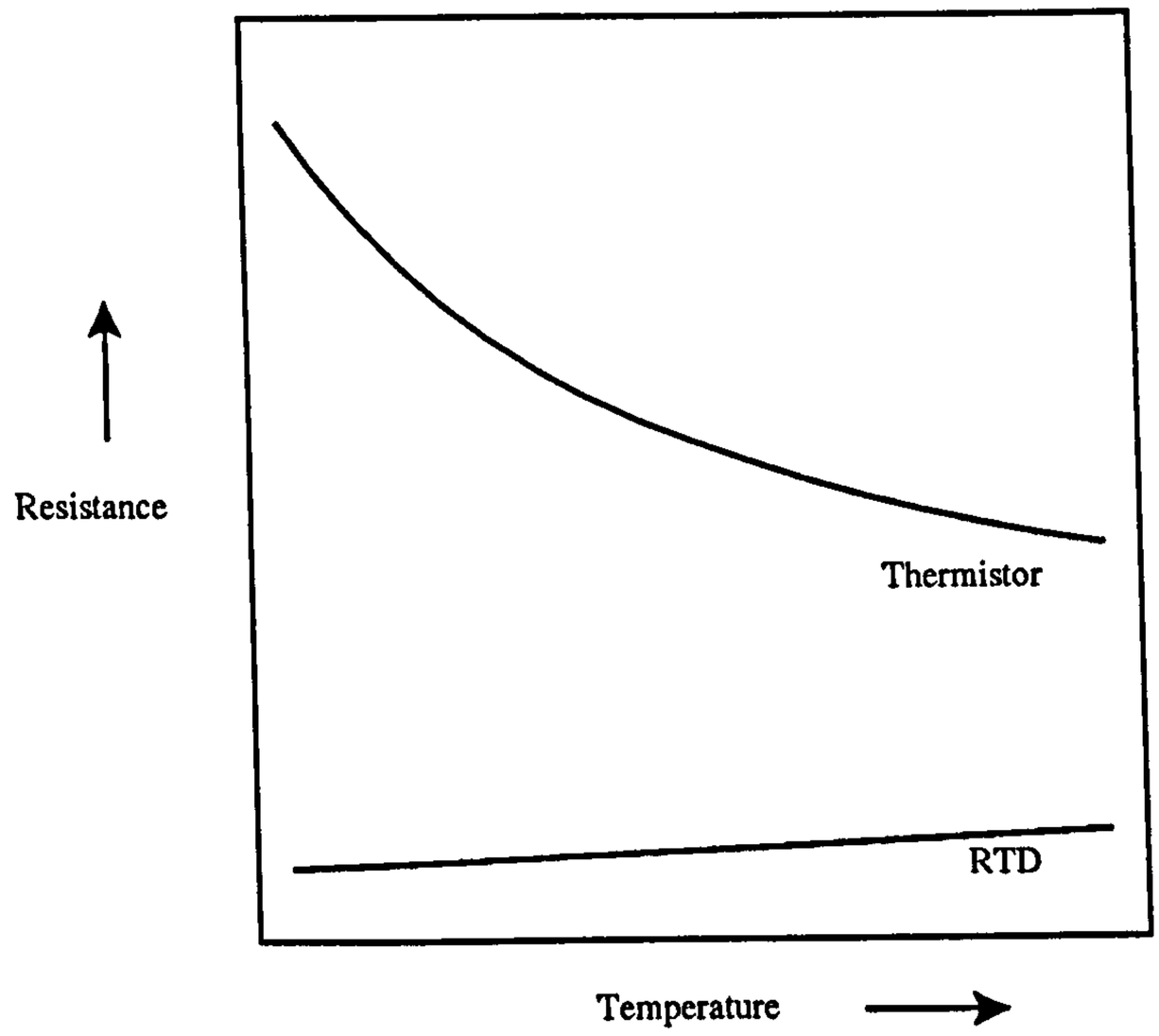

Figure 3.2: Thermistor and RTD Resistance Temperature Characteristics.

- Multiple sensors are installed and readings from these are then averaged. One disadvantage with this approach is that the data communication and processing is more expensive.

Averaging sensors can give good approximations to the bulk mean average temperature. Unfortunately, the readings from these sensors are often heavily influenced by installation and air flow characteristics. Measurements that are influenced to the greatest extent are generally those that follow a flow merge whose inlet air conditions are at different temperatures. In HVAC systems this is usually found in the 'mixing box' section (see Section 1.1), just prior to the heating and cooling coils.

This investigation, enforced by findings reported by Carling (1999), Robinson (1999), Kelso et al. (2000) and Lee (2000), leads to the conclusion that if averaging sensors are installed perpendicular to the dominating stratification direction, reasonable estimates of the bulk average can be expected. Figure 3.3 demonstrates this in comparison to some undesirable installation configurations.

Johnson et al. (1998) handled the uncertainty using multiple measurements using the

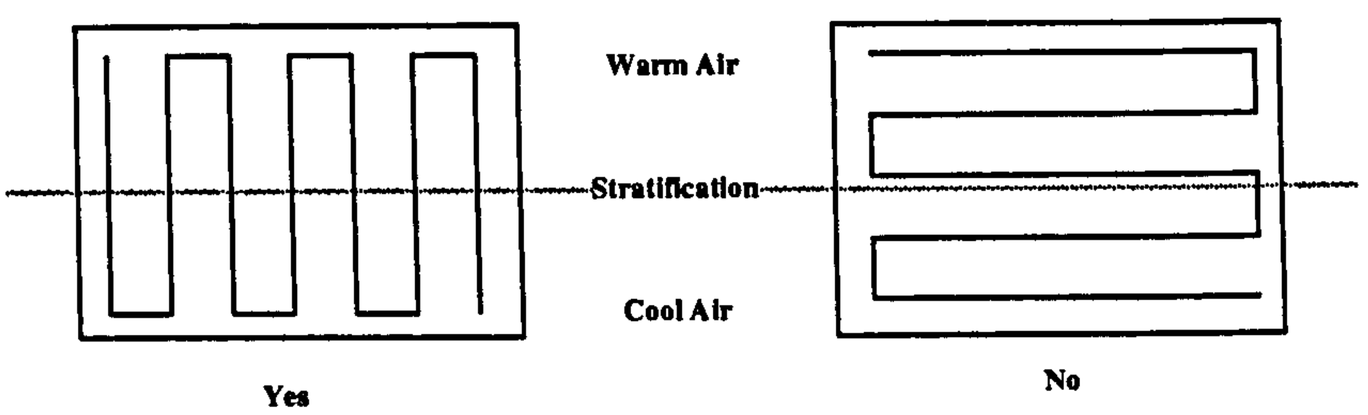

Figure 3.3: Suggested Configuration of an Air Temperature Averaging Sensor Compared to Some Common Installation Arrangements.

following calculation,

$$B_{T_{dist}} = \frac{T_{max} - T_{min}}{n}, \tag{3.1}$$

where $B_{T_{dist}}$ (K) is the measurement bias due to the non-uniform distribution, T_{max} and T_{min} (℃) are the maximum and minimum temperatures observed and n for $n \geq 2$ is the number of independent temperature sensors used to calculate the average measurement value.

To date there are no methods for the estimation of the uncertainty in averaging or single point measurements reported in the literature. The problem is dependent on the configuration of the sensor in relation to the stratification characteristics. A new approach to this problem is to estimate the likely bias in the bulk average temperature by analysis of a simple model. In the simplest case, the stratification effects can be assumed to form two perfect layers and an estimate of the likely temperature difference between the two layers can be made given a knowledge of the system. A simple resistance model, based on the manufacturer's sensor temperature/resistance characteristics can be configured to represent the sensor geometry in relation to the duct cross-sectional area and the stratification effects. The resistance of the element is calculated given a knowledge of the length on the element exposed to either temperature. The temperature that the control system

will 'see' can be estimated by applying the compound resistance to the known temperature/resistance characteristics. Since the temperatures entering the flow merge are known, the true bulk average is known. Based on a comparison of these two values, judgement can be used to establish a reasonable magnitude of uncertainty at the 95% confidence level. This approach is applied in Section 6.3.2.

Moffat (1988) suggests a correction should be made for the bias induced by radiation incident in the sensing element from other bodies. Radiative heat exchange can be a complex process, but it is likely that where sensors are sited in close proximity to heat-exchangers, this source will dominate. There are no simple methods for assessing uncertainty due to radiation in the literature. In experiments reported by Carling (1999), errors of approximately 0.2K were observed when sensors measuring air temperature were mounted closely to a coil. Although this value is situation dependent, it can be used to estimate the uncertainty in other similar configurations. If it is assumed that the radiation effects reduce in proportion to the square of the distance, a nominal estimate of uncertainty (taken to be the 95% confidence level) for radiative effects is proposed as,

$$B_{T_{rad}} = \frac{0.2}{(\frac{d}{0.1})^2}, \tag{3.2}$$

where d (m) is the distance between the heat-exchanger and the plane of the sensor 0.1m is an estimate of the distance of the sensor plane to the face of the heat-exchanger in the experiment[2].

3.2.2 Air Flow Measurement

Flow measurement usually relies on a pressure or temperature measurement. The accuracy of an instrument often depends on the accuracy to which the pressure or temperature can be measured. There are two common air flow measurement methods; a pitot effect device and hot-wire anemometer. The former relates pressure to flow and the latter, temperature to flow. The pitot tube measures total pressure and static pressure at a particular locality. This is achieved by the application of a double walled tube. The face area of the central

[2]Carling (1998b) depicts the experimental arrangement and comments 'The evaluated sensors mounted on the frame which is placed next to the heating coil'. 0.1m has been assumed to be a reasonable estimate of the distance used .

bore is perpendicular to the fluid flow and therefore measures the pressure due to the velocity of the fluid and the static component. The outer tube is exposed to the fluid stream such that the area of the opening is parallel to the flow, hence measuring the static pressure only. Deduction yields the velocity pressure, P_v (Pa), from which the fluid velocity, v_a (ms^{-1}), can then be calculated from $P_v = \frac{1}{2}\rho_a v_a^2$, where ρ_a (kgm^{-3}) is the density of the air. If there is a large flow plane area, single local measurements are unlikely to be representative of the velocity profile and traverses taking multiple readings need to be employed. Rules of thumb exist for the planning of in duct measurements (BSRIA, 1993b). Where the information from repeated air flow measurement traverses is required, arrays of pressure measuring devices can be employed and permanently installed. An example is the *veloprobe*. With this device, exemplified in Underwood (1999), the total pressure is measured through holes along the side of a circular unit and gives an effective mean pressure reading. One disadvantage of this type of configuration is its sensitivity to the yaw angle between the direction of flow and the openings which can generate uncertainty in the measurements through the introduction of bias.

The conversion of pressure measurement to an electrical signal is achieved by *displacement transducers* that measure the displacement of a diaphragm (Underwood, 1999). The diaphragm movement induced by air flow measurements from building ventilation systems could be measured using the electro-magnetic induction principle. Here the diaphragm moves a ferrite core linking two coils to varying degrees. A potential difference is connected to one core and the measurement is made by monitoring the voltage or current in the other. The hot-wire anemometer exploits the variation in heat transfer coefficient between a fine heated wire and air as a function of air velocity. The current is varied to maintain the wire at a given temperature. An additional temperature sensor maintains a constant wire/air temperature difference and so the supplied current is proportional to the air velocity. This method is sensitive, but less robust than the *veloprobe* technique. Fluctuations in the potential difference used to excite either sensor can be a source of random uncertainty, as discussed at the beginning of the section.

The accuracy of a *veloprobe* is largely dependent on the number of measurement points used by the probe. Hot wire anemometers have very short time constants and have been used extensively for turbulence measurements (Holman, 1984) and are therefore

characteristically sensitive to fluctuations in the air flow patterns. Both methods, however have a limited number of measurements in relation to the estimation of the velocity profile. There will, therefore, be some uncertainty in the estimation of the bulk average air flow rate. Some estimation could be made by studying the velocity profiles using traverse measurements. This is time consuming and there are no other simple methods for the estimation of this uncertainty in the literature. A new method, based on sensor geometry, is proposed here.

Consider then, fully developed laminar air flow in a duct, depicted in Figure 3.4. For the purposes of this research the flow front is assumed to have an approximately sinusoidal velocity profile, in cross-section. An assessment of the approximation to the measurement to the bulk average is derived by comparing the area under the assumed velocity profile, to the area of the rectangular profile. The greater the number of measurement points, the finer the resolution of the measurement approximation and hence, the smaller the uncertainty. Figure 3.4 depicts three measurements points. The 'real' flow profile will also develop with time, particularly where air flow rate is a control variable. Identifying the correct flow profile in terms the bias uncertainty applicable to *on-line* measurements is practically indeterminable. The proposed approach attempts to give a pragmatic solution to the evaluation of this uncertainty.

Working in Radians, the sinusoidal velocity profile can be considered as half a period of a sine wave, where $\sin\frac{\pi}{2} = 1$. The maximum velocity at the centre of the section. A general expression for the estimation of uncertainty can be calculated by,

$$B_{v_a} = \left(a^2 + b^2 + c\right)^{\frac{1}{2}}, \tag{3.3}$$

where B_{v_a} (% of ms^{-1}) represents the difference between the areas of the sinusoidal velocity profile and the rectangular profile defined by the location of the sensors and the duct wall. a and b describe the difference between the areas of the section adjacent to the duct walls (labelled 'A' and 'B' in Figure 3.4), given by,

$$\begin{aligned} a &= \sin\left(\frac{\pi}{2n}\right)\left(\frac{\pi}{2n}\right) - \int_0^{\frac{\pi}{2n}} \sin(\varpi), \\ b &= \sin\left(\frac{n\pi}{n+1}\right)\left(\frac{n\pi}{n+1}\right) - \int_{\frac{n\pi}{n+1}}^{\pi} \sin(\varpi), \end{aligned}$$

where n is the number of measurements across the duct and ϖ is the the distance from the initial duct wall in radians. In Figure 3.4, the wall in section 'A' is denoted as $\varpi = 0$ and in section 'B', $\varpi = \pi$. c describes the area difference in the middle sections (labelled 'C' in Figure 3.4) and is calculated by,

$$c = \sum_{i=2}^{n-1} \left\{ \left(\sin\left(\frac{(i-1)\,\pi}{n+1}\right) d - \int_{e}^{f} \sin(\varpi) \right)^2 + \left(\sin\left(\frac{i\pi}{n+1}\right) d - \int_{f}^{g} \sin(\varpi) \right)^2 \right\},$$

where i is an incremental counter from $0 \rightarrow n$ and d, e, f and g are given by,

$$\begin{aligned} d &= \left(\frac{\frac{i\pi}{n+1} - \frac{(i-1)\pi}{n+1}}{2} \right), \\ e &= \frac{(i-1)\,\pi}{n+1}, \\ f &= \left(d + \frac{(i-1)\,\pi}{n+1} \right), \\ g &= \frac{i\pi}{n+1}. \end{aligned}$$

Using Equation 3.3 a 0.4m high duct with two measurements of velocity, equally spaced would generate a bias error of 6% of the measured velocity.

For flow in ducts this could be carried out in both planes, neglecting complex edge effects, and the uncertainties could be calculated through the double integrals to compare volumes. A simpler approach would be to carry out the two-dimensional methods in both planes, combining the uncertainties using a sum-of-the-squares approach. Where a hot-wire anemometer is used, the uncertainty in the plane parallel to the flow would be accounted for by the effects of the varying heat transfer coefficient on the wire. The approach would therefore only needed to be carried out in one direction.

3.2.3 Air Humidity Measurement

Humidity measurement can be achieved by employing sensing elements that respond to air moisture content by varying the resistive or capacitive qualities of the element. Commercially available sensors can achieve a sensitivity down to 2% of relative humidity (Underwood, 1999) although these sensors can be sensitive to long term exposure to high humidities.

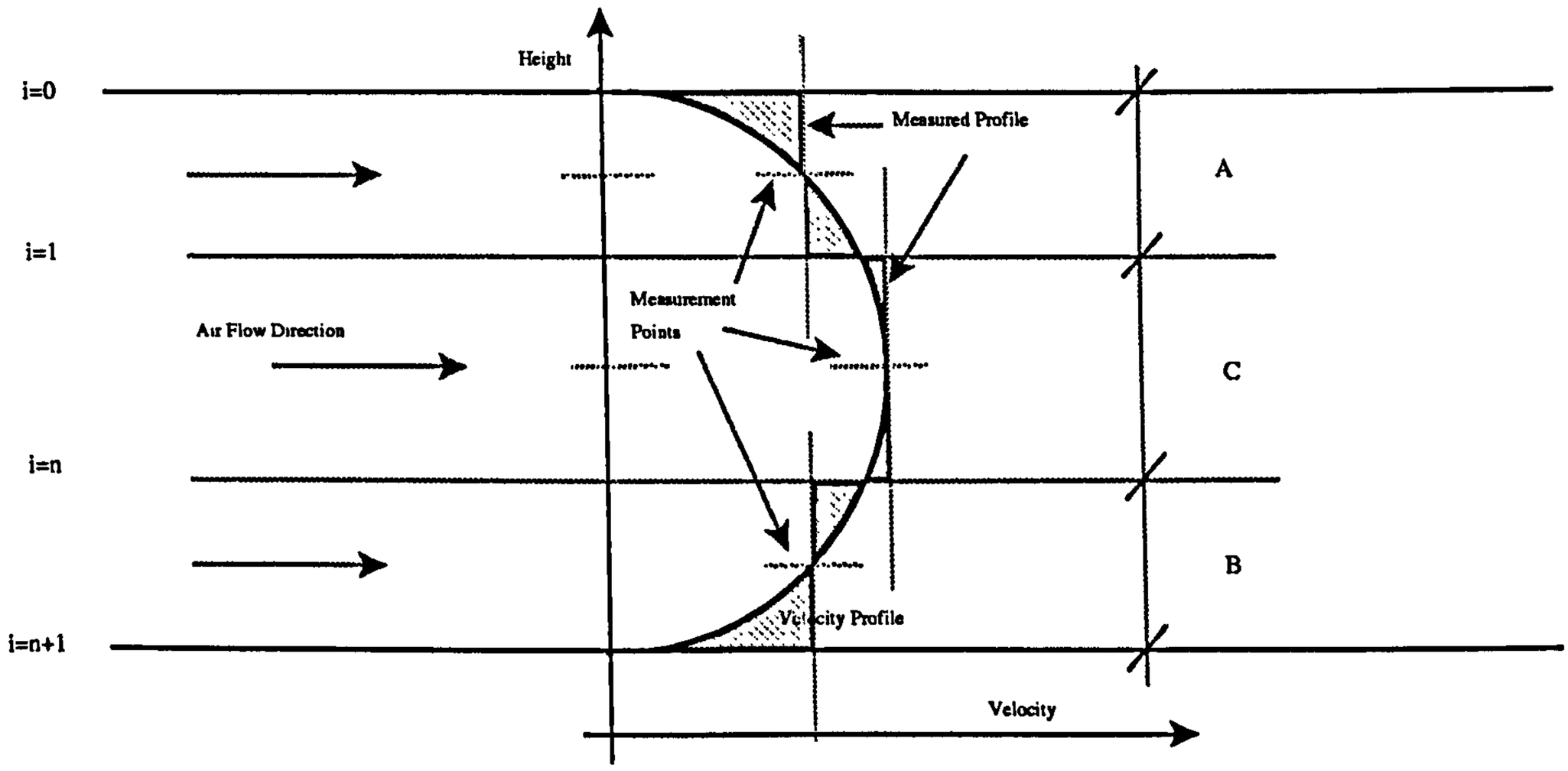

Figure 3.4: Laminar Air Flow Velocity Profile in a Duct.

Humidity measurements are usually point sensors and the uncertainty will suffer in much the same way as the point temperature measurement where the fluid is poorly mixed with respect to the moisture content. This would be less of an influence where the air is well mixed. It is often, however, the humidity ratio ($kgkg_{air}^{-1}$) that is of interest in calculations. This needs to be calculated using the relative humidity and an air temperature measurement as well as a psychrometric function. The uncertainties due to the introduction of the psychrometric function can be neglected because they are based on thermodynamic principles. Some functions make use of constants and internal iterations and these can be selected such that they introduce insignificant uncertainty. In principle, the uncertainty in the measurements (inputs to the function) will be far greater than those implicit in the function derivation. In fact, the air temperature measurement is most likely to be the significant source of uncertainty as discussed in Section 3.2.1.

3.2.4 Water Temperature

Where the sensor is submerged in the fluid flow in a small duct, spatial differences can be neglected. Devices that clamp onto the pipe wall are subject to radiation and heat effects if not insulated correctly. Correct contact with the pipe wall is also an issue. It

is also possible that the heat transfer coefficient associated with the velocity of fluid in variable flow systems could affect readings. This is related to the calibration process that should endeavour to emulate the test conditions such that no additional uncertainty need be added (Abernathy, 1973). The largest bias uncertainty is usually associated with the location of the sensing element. If at some distance from the point of use relative to the data reduction equation, then heat losses/gains should be expected. With a knowledge of the distance, insulation and ambient conditions, the measurement could be corrected for this bias error.

3.2.5 Water Flow Measurement

A common method used for water flow rate measurements in a digital based monitoring scheme is by turbine flow meter. This instrument is a calibrated turbine which is placed in the fluid line. The flow drives the impeller which is attached to a permanent magnet. A reluctance pickup generates a pulse, due to the magnet, on every revolution. The pulse count is then proportional to the flow as a function of the turbine design and fluid properties. There is little or no uncertainty due to spatial averaging when in line turbine meters are used to measure water flow rate. Often however, in HVAC systems, the mass flow rate through the coil is not measured and needs to be inferred (Buswell et al., 1997). This can be achieved using a model, but there will be uncertainty associated with its predictions. Appendix B details such a model and the uncertainties generated by the derivation of the model's characteristic parameters and the associated uncertainty is discussed further in Section 7.2.

3.3 Conclusions

This chapter has described a typical HVAC data acquisition process. Uncertainties in respect of the key stages of this process have been discussed. The operational principles behind some of the most common sensors used in HVAC control were reviewed. The uncertainties associated with typical measurements were discussed, focusing on the uncertainty (due to inconsistent spatial distribution) introduced through estimation of bulk average

fluid properties. Existing methods that address the spatial uncertainty estimation were identified. Where no such methods exist in the literature, new methods were introduced. Specific comments are:

- the resolution of contemporary HVAC equipment data acquisition systems is sufficient for condition monitoring purposes in terms of measurement accuracy;
- the uncertainties associated in the signal conditioning and elements of the conversion process will contribute to the random uncertainty component in a measurement, the practical assessment of which is described in Chapter 4;
- analogue to digital conversion can be a significant source of uncertainty, however, the reverse conversion can be neglected in model based condition monitoring applications;
- a thermistor measurement is preferable to a RTD because of the higher precision, however, RTDs are commonly configured as averaging sensors that can yield good approximations to the fluid bulk average temperature in the right configuration;
- stratification was identified as one of the most influential effects on air temperature measurement in ducts;
- a new model based approach to assessing the impact of sensor configuration and stratification characteristics on the uncertainty in the approximation of measurement to the bulk average temperature was introduced;
- a new method of assessing the uncertainty in the approximation of air flow measurement to the bulk average was introduced.

All the above issues are carried to Chapter 6, where the measurement uncertainties in a real system are evaluated.

Chapter 4

Uncertainty in Transient Measurements

Chapter 3 principally discussed sources of bias uncertainty in typical HVAC measurements. Certain elemental uncertainty sources were identified as being practically unquantifiable. These uncertainties contribute to the 'random' uncertainty observed in measurements. This chapter considers a variance based approach to the evaluation of such uncertainties, suitable for both *on-line* and batch implementation. It is demonstrated that the evaluation method itself introduces uncertainty into the measurement. The evaluation of these uncertainties are investigated using two widely used first order filter techniques. Recommendations for the preferred filter technique is made on the basis of the method that introduces the least uncertainty into the measurement. The filtering process is developed to account for the uncertainties in using transient data in calculations that are only applicable to steady-state conditions; introducing a new approach to this problem.

4.1 Preliminaries

When time continuous measurements are discretised, some information is lost and uncertainty in the discrete measurement is introduced. In many applications, the processing of system information requires further sampling of this discrete data. This is often performed by a fixed length window or exponential filter, which is used to generate a mean value for a given variable over some period of time. The deviation in the data about the mean

can be used to calculate the sample variance. There are generally two approaches to the treatment of the variance that can be generated from the filter:

1. The variation in the measurements about the mean can be considered to be 'white noise'. The stochastic nature of the variation results in the cancellation of the positive and negative variations over the sample window and hence the variance is zero.

2. The variation in the measurements about the mean cannot be considered to be truly stochastic or that such a consideration would lead to practical robustness issues. Hence, the variance must contain some information about the uncertainty in the measured variable.

Where the zero variance assumption cannot be proved; or where the sampling interval of the discrete data is coarse with respect to the time window; the sample size is small; and/or there exists influences on the process that are largely unquantifiable; application of the latter option is more robust than the former. HVAC measurements are subject to many unquantifiable disturbances and as such the zero-variance assumption is not applicable.

4.2 Sampling Data

The sampling rate is critical in characterising the variations present in the data (Moffat 1988). The sample interval should be selected on the basis of the information that is of interest. This evaluation is simplified when the observed system is in steady-state. In addition, allowing the variables to be measured when the whole system is in steady-state is desirable, because generally, the analysis of steady-state systems is simpler than for the dynamic alternative. Practically, however, it is not possible and transients will always be present to some extent. The dominant dynamic effects associated with each measured variable used in a calculation need to be considered to establish a sample interval that is suitable for the application.

4.2.1 Sample Interval

The selection of the sampling interval is influenced by a number of considerations:

- information required from the test system or process;
- system or process characteristics;
- limitations of the data collection system;
- cost constraints.

The aim of the sample of discrete data with respect to measurements of single quantities, is to evaluate the components that contribute to the random uncertainty associated with the measured value. To this end, the system characteristics can be further described:

- the time constants associated with the dominating process dynamics;
- the time constants associated with the control process dynamics (if applicable);
- the time constants associated with the measurement system dynamics (although these are usually insignificant compared to effects at the process level);
- the time scale associated with any variations in the location of the measurement value in the domain of measurement.

Table 4.1 describes the differences in information that might be expected through different sampling intervals applied to the data from a heat-exchanger in a HVAC system under close loop control. When sample intervals of fractions of a second are considered, the sample information will describe details of the measurement system. The lower frequency sample intervals (1 Hour) are generally useful for energy consumption and cost performance predictions. The area that is of specific interest to information related to model based condition monitoring are those sample intervals that can describe the process and process control dynamics. If this information can be observed from the data, it is possible to establish when systems are in (or close to) steady-state, and hence when uncertainty should be at a minimum. This range is between the 1 second and 1 minute scale.

Table 4.1: The Sample Interval Spectrum Applicable to a Heat Exchanger System Used to Control the Air Temperature of a Space.

Time Scale	Information
< 1 Second	Detailed measurement system information, i.e. sensor dynamics
1 Second	Measurement system information and detailed process dynamics
1 Minute	General process and control system dynamics information
15 Minutes	Changes in steady-state conditions, but no dynamic information
60 Minutes	Detailed daily changes in general operating conditions
6 Hourly	Detailed seasonal variations, i.e. daily peaks etc.
24 Hourly	General seasonal variations

In many cases it is often desirable to acquire the most detailed data possible. The data can then be used to evaluate effects that would otherwise be indeterminable. A practical upper limit for a sample interval for building control systems is often 1 Minute. This is typically due to limitations in the bandwidth of the control system network available for additional data traffic.

4.2.2 The Effect of Sample Size

A number of consecutive, discrete samples need to be taken from the data and used to calculate the sample mean and variance. The sample variance can then be used as a basis for the estimate of the random uncertainty associated with the sample mean. The reliability of this value will be dependent on the size of the sample and it should be maximised.

Student's t distribution approximates to a normal distribution when the the sample size, $n \geq 30$, but also provides small sample coverage. This makes this distribution attractive for practical applications. To evaluate the effect of sample size on the reliability of the variance calculation; an analogy can be drawn between the uncertainty associated with the mean and the confidence attributed to an interval about that mean, containing the population mean. If there is no bias error present, uncertainty can be considered as the inverse of confidence. Then the uncertainty describes an interval in which the true value lies, where the true value is the population mean. Figure 4.1 demonstrates the increase in confidence associated with a sample by the reduced t-value. The t-value is affected

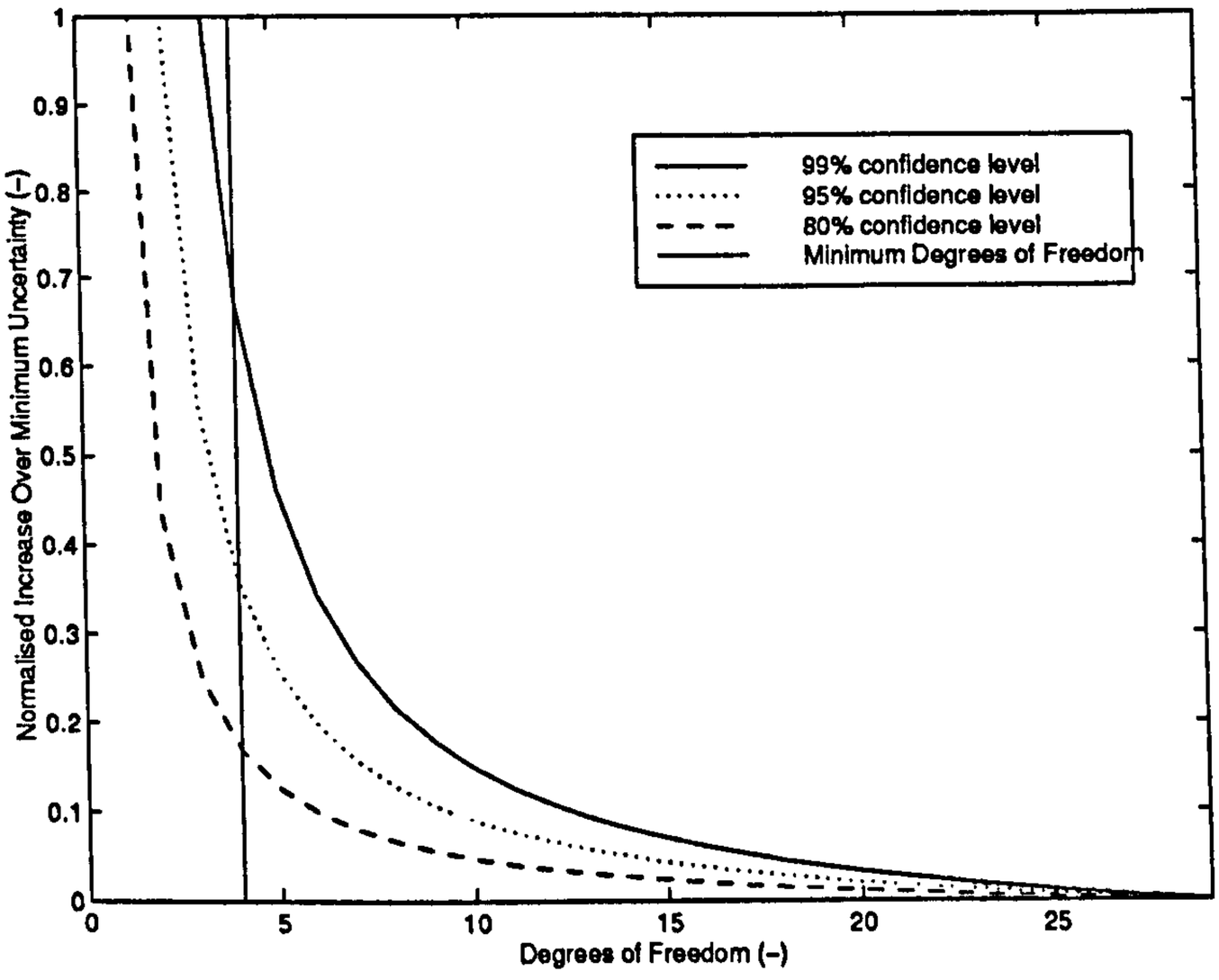

Figure 4.1: The Effect of Sample Size on the t-value Associated With Student's t Distribution for varying levels of confidence.

directly by the number of degrees of freedom associated with a sample. The uncertainty in Figure 4.1 is depicted by plotting degrees of freedom ($v = n - 1$) against a normalised t-value, t_α^{norm}, where α represents the $(1-\alpha)100\%$ confidence limit. t_α^{norm} is calculated by;

$$t_\alpha^{norm} = \frac{t_\alpha^{v=i} - t_\alpha^{v=29}}{t_\alpha^{v=29}}, \tag{4.1}$$

where i is an integer in the range $1 \leq i \leq 29$. If there are no degrees of freedom, i.e. $v = 0$, there is no information in the data and we have no confidence in the estimate of the population mean. In these circumstances, uncertainty is at its maximum. Conversely, when $v = \infty$, there is complete confidence and no uncertainty is associated with the estimate. For practical purposes, $v > 29$ contains enough information to ensure a good estimate of the population mean. The t-value at $v = 29$ provides an indicator of the practical minimum level of uncertainty achievable using sampled data. Figure 4.1 also demonstrates the change in the level of uncertainty associated with different levels of confidence. A value of 1.0 on the y axis indicates a 100% increase in uncertainty over the practical minimum at $v = 29$. There is a steep decline in the uncertainty as $v \to 29$, however, all the curves at each α are under $t_\alpha^{norm} = 1$ at $v = 4$, equivalent to a sample size

of $n = 5$. $n = 5$ is duly taken as a minimum sample size from which to obtain a reasonable estimate the population mean and variance.

4.2.3 Data-Time Association

Recorded data will be associated with a specific instance in time. Comparisons between different measurements at an instance in time yield correct results if both measurements were observed at the same instance in time. Ideally, each data would be recorded at identical moments. Realistically there will always be some difference. For HVAC systems, such differences are likely to be small. Any small differences that do exist are unlikely to have a significant effect on the data accuracy compared to the uncertainty generated by the presence of transients. In addition, as the system approaches steady-state, the effect on uncertainty will diminish.

4.3 Analysis of Sampling Uncertainty

The following section investigates the error generated when averaging functions are employed to evaluate sample mean and variance in the presence of dynamic effects. The responses generated by a first order system to various forcing functions are used to represent the true values of the measurements. The mean calculated by the filters that sample the true value differ. In the absence of bias error, this difference can be regarded as the total error. The total error and the calculated variance are used to evaluate the performance of the filters. The more desirable filter has a smaller variance and one that coincides with the total error.

4.3.1 Time Averaging Functions

The fixed time window approach averages consecutive data samples over the length of the window. The number of samples is represented by the window length and the current mean is calculated including the new data point, disregarding the oldest. This is represented by

Equation 4.2 and 4.3.

$$\bar{x}_n = \frac{1}{w}\sum_{k=0}^{w} x_{(n-k)}, \tag{4.2}$$

$$\sigma_n = \frac{1}{w-1}\sum_{k=0}^{w}(\bar{x}_n - x_{(n-k)})^2, \tag{4.3}$$

where $\bar{x}_n$ is the mean of the measurements $x_{(n-k)}$ at sample number n, w is the window length and σ_n is the sample variance. Using this approach, the data at each point in the window contributes to the calculations in equal proportions.

The exponentially weighted approach degrades the influence that each data has in the calculations with time. The rate at which this 'forgetting' occurs is controlled by a forgetting factor, λ. Equation 4.4 and 4.5 give the calculation of the effective sample mean, $\bar{x}_n^{\cdot}$ and effective sample variance, $\sigma_n^{\cdot}$.

$$\bar{x}_n^{\cdot} = \lambda\bar{x}_{n-1}^{\cdot} + (1-\lambda)x_n, \tag{4.4}$$

$$\sigma_n^{\cdot} = \lambda\sigma_{n-1}^{\cdot} + (1-\lambda)(\bar{x}_n^{\cdot} - x_n)^2, \tag{4.5}$$

The number of samples is represented by the effective number of samples, $n^{\cdot}$ and is given by,

$$n^{\cdot} = nearest\ integer\{\lambda(n-1)+1\}. \tag{4.6}$$

Figure 4.2 demonstrates the relationship between λ and $n^{\cdot}$ in the left hand plot. The right hand plot indicates the number of samples that are included in the weighted calculations. The data used were generated by applying Equation 4.6, rounding up the effective number of samples to the nearest whole sample. The number of samples considered was taken as the nearest higher integer when the difference between consecutive samples of the number of considered samples was < 0.005. The plot demonstrates that the exponential weighting considers considerable amounts of past history data. For example; a sample size of 30 from a system where the data acquisition system sampling interval is 1.0 minute, would consider all the data from approximately the last 2 Hours and 40 Minutes (Figure 4.2). The Figure shows that practical values for the forgetting factor are in the range $0.8 \leq \lambda \leq 0.967$, corresponding to effective sample sizes of $5 \leq n^{\cdot} \leq 30$.

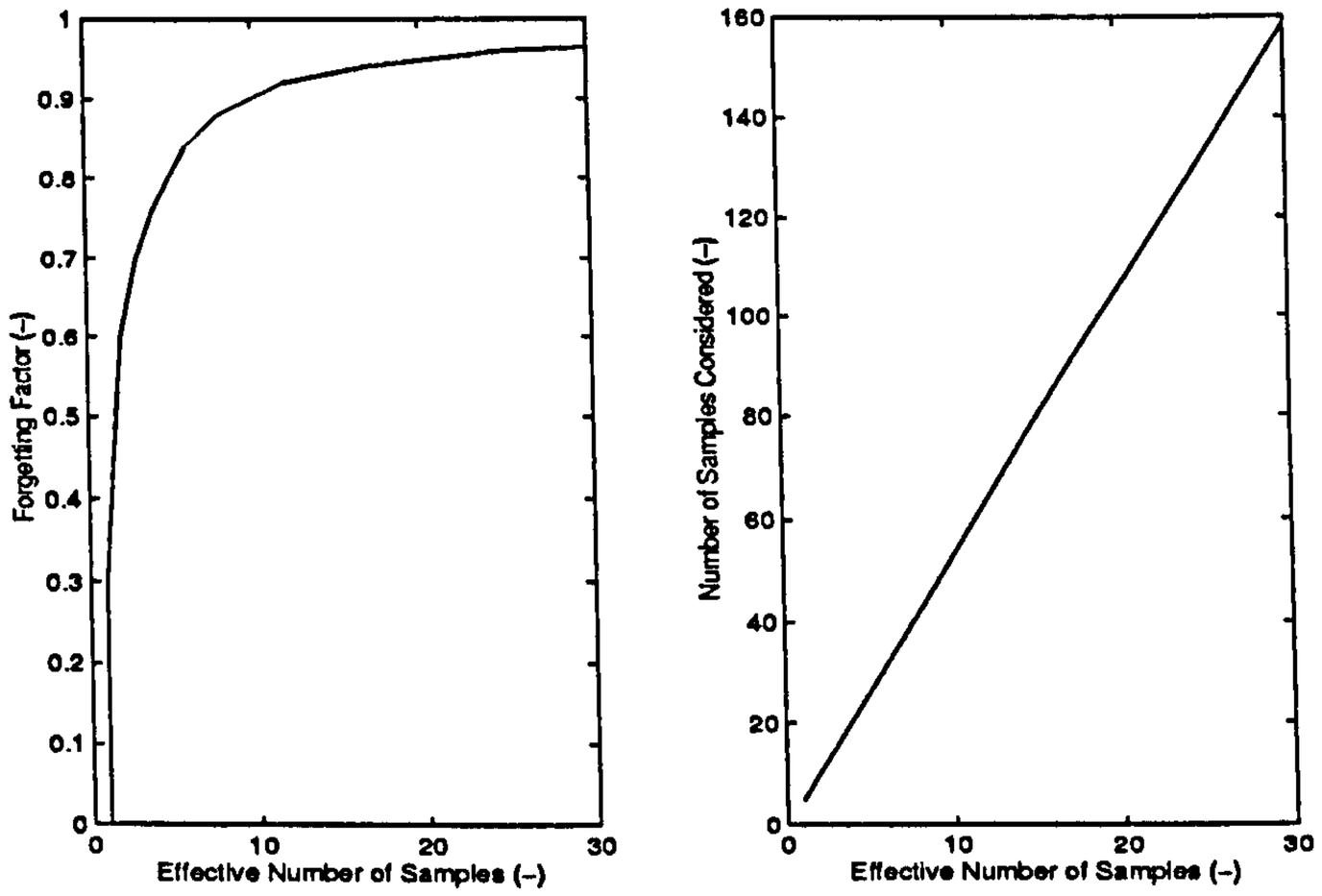

Figure 4.2: The Relationship Between Effective Sample Size and the Forgetting Factor.

4.3.2 Test Functions

The additional uncertainty induced by the sampling regime, as the measurements reflect a shift in the operation condition of the process, has been tested by employing test functions. These were selected to exercise the averaging methods over three likely system inputs,

- step,
- ramp,
- and impulse.

The first order system responses to these inputs are represented by Equations 4.7, 4.8 and 4.9 (Schwarzenbach and Gill, 1992).

$$c(\varrho)_{step} = 1 - e^{-\varrho/\tau}, \tag{4.7}$$

$$c(\varrho)_{ramp} = k'(\varrho - \tau + \tau e^{-\varrho/\tau}), \tag{4.8}$$

$$c(\varrho)_{impulse} = \frac{1}{\tau} e^{-\varrho/\tau}. \tag{4.9}$$

where ϱ is time (s), τ is the system time constant (s) and k' controls the magnitude of the rate of increase in the ramp input. The number of samples in a given period is given by

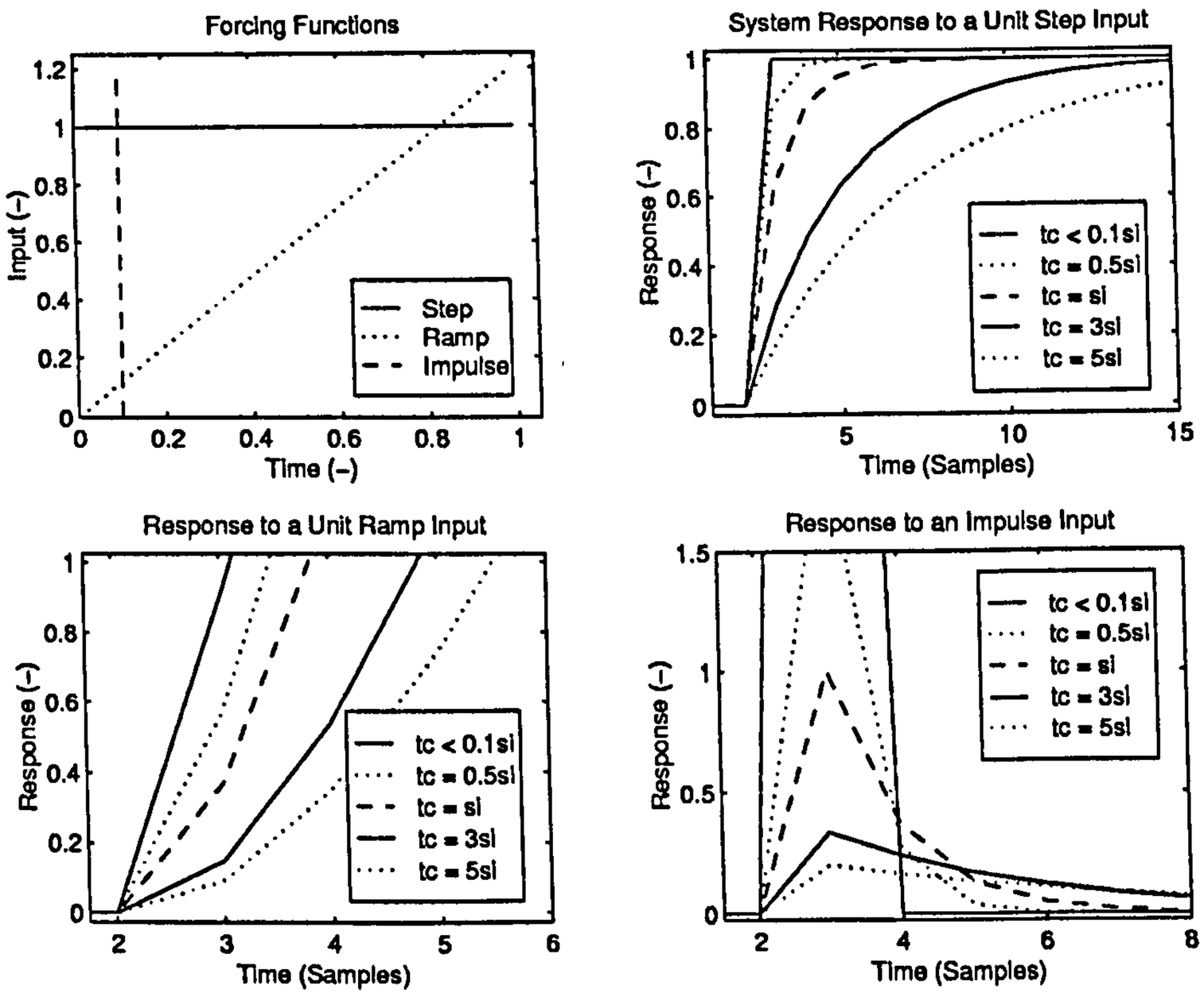

Figure 4.3: The First Order System Response to a Step, Ramp and Impulse Input for Various System Time Constants.

$n = \frac{\rho}{I_n}$ where I_n is the time sample interval (s) . Figure 4.3 shows these responses relative to time measured in data samples, for systems with various time constants. On the plot, 'tc' and 'si' refer to 'time constant' and 'sample interval' respectively.

In the absence of any bias or random uncertainty effects, the responses to the forcing functions can be considered to be the true value of a result. We can sample this true value and evaluate the sample variance. A non-zero value for the variance indicates uncertainty associated with the sampling process alone. Since the true value is known, the total error can be calculated. For this test case the total error is taken as the uncertainty to be described by the variance associated with the sample regime. Ideally, we require the sample variance and total error to be at a minimum and for the variance to reflect the distribution of the total error, i.e. both having coincident maxima.

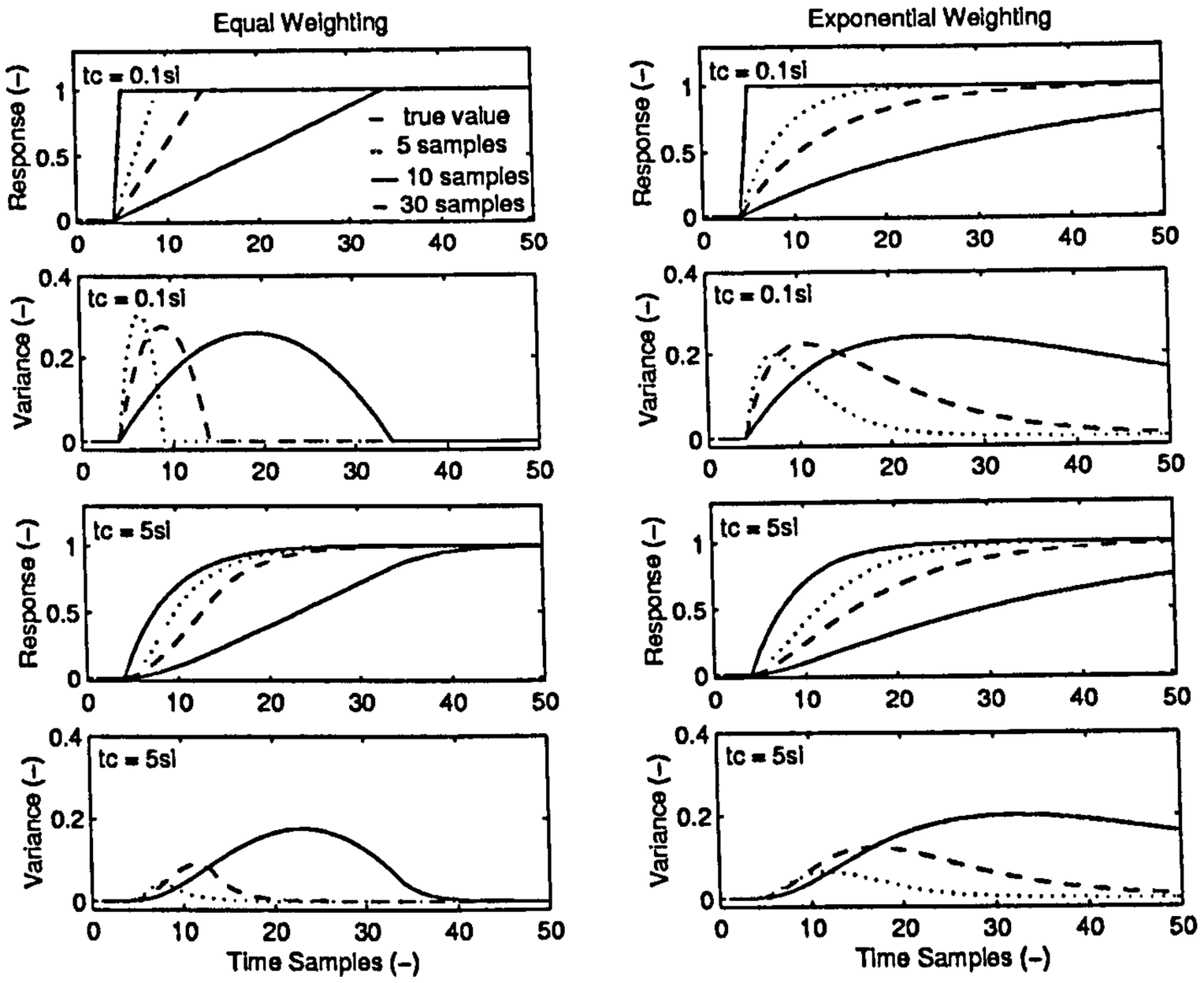

Figure 4.4: The Effects on Sample Uncertainty Due a First Order Response to a Unit Step Input for Different Sample Sizes and System Time Constants For Equally and Exponentially Weighted Sampling Methods.

4.3.3 Comparison of Mean Calculations

Response to a Step Input

Figure 4.4 shows the true value, sample response and sample variance for the different system time constants and sample sizes for both the equal and exponentially weighted sampling methods. The figure shows that for both approaches, the effect of the sampling regime is to give rise to a second order response by introducing a source of inertia in the mean value calculation. This is more predominant in the equal weighting case and the effect increases as the sample size increases. The total sample variance increases accordingly. One difference between the two filters is that the exponentially weighted method gives a smaller peak variance at the shorter time constants, whereas when τ is larger, the equal weighting has a smaller peak variance. In the equal weighting example; for short system time constants, the smaller sample size has a higher peak variance over the larger, whereas in the $\tau = 5I_n$ case the reverse is true. The exponentially weighted

Table 4.2: The Total Uncertainty Associated With the Test Sampling Methods Over a Period of 60 Samples For a Unit Step Input.

System Time Constant (Sample Intervals)	Sample Size (Number)	Equal Weight Method	Exponential weight Method
0.1	5	1.0	1.778
0.1	10	1.833	4.222
0.1	30	5.167	9.599
5	5	0.214	0.850
5	10	0.654	2.751
5	30	3.315	7.343

case shows the same trend, but to a lesser extent. As the rate of response of the system decreases ($\tau \uparrow$), the lag times associated with the sampled response of smaller sample sizes decreases and the greater they are affected. In addition, as the sample period becomes short compared to the system time constant, the total error, and hence the uncertainty associated with the same sizes, will be reduced.

The total variance over a predetermined period can be used as a measure of the total uncertainty generated by the sampling method. The total uncertainty in relation to time samples is given by the integral of the sample variance. It can be shown that, from Equations 4.2, 4.4 and 4.7 for the equal weighting case,

$$S_n^2 = \frac{1}{w-1}\sum_{k=1}^{w}\left(\left[\frac{1}{w}\sum_{i=1}^{w}\left(1-\tau e^{\frac{-\varrho_{n-i}}{\tau}}\right)\right] - \left(1-\tau e^{\frac{-\varrho_{n-k}}{\tau}}\right)\right)^2, \tag{4.10}$$

and so,

$$\dot{S}_n^2 = \int_{n=0}^{n=x} S_n^2 d\varrho, \tag{4.11}$$

which for discrete samples can be approximated to,

$$\dot{S}_n^2 \approx \sum_{n=0}^{n=x} I_n \left\{\frac{1}{w-1}\sum_{k=1}^{w}\left(\left[\frac{1}{w}\sum_{i=1}^{w}\left(1-\tau e^{\frac{-(n-i)}{\tau}}\right)\right] - \left(1-\tau e^{\frac{-(n-k)}{\tau}}\right)\right)^2\right\}, \tag{4.12}$$

where x is the time associated with the end of the evaluation period. Table 4.2 shows the integral for unit sample interval for the responses shown in Figure 4.4 over 60 samples. There is nearly twice the uncertainty associated with the exponential than with the equal weighting approach. Figure 4.5 demonstrates the coincidence of the total error and variance maxima. There are three observations;

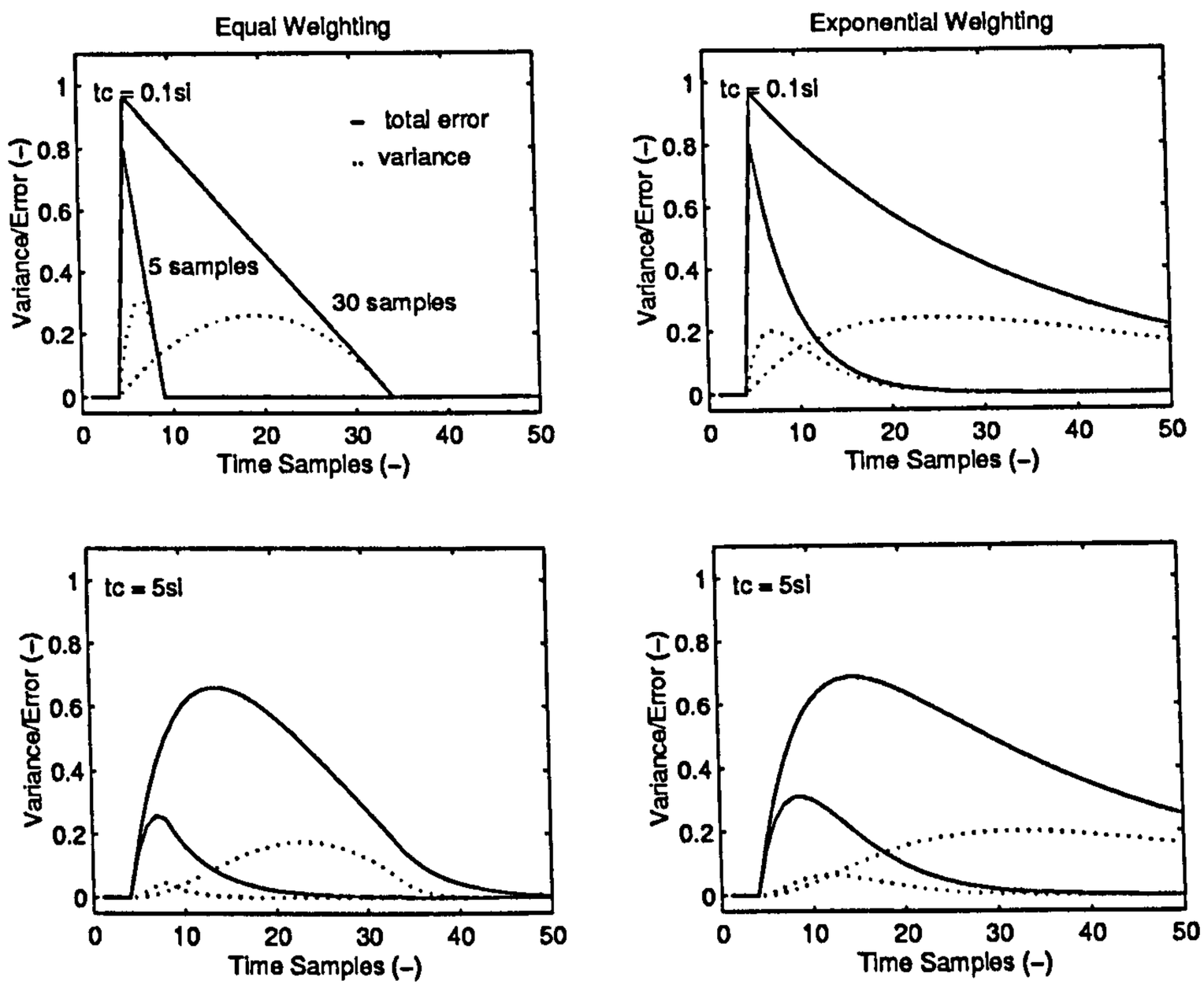

Figure 4.5: Representation of the Total Error by the Uncertainty Estimate Using the Sample Variance for an Unit Step Input.

- the total error associated with the equal weight approach is less than for the exponential method (demonstrated by the areas under the plots);
- the smaller the sample size, the greater the coincidence of the peak values;
- the larger the system time constant is in relation to the sample size, the closer the coincidence.

Response to a Ramp Input

Figure 4.6 shows similar plots to Figure 4.4 but for a unit ramp input. The ramp functions have been stopped at an arbitrary point to demonstrate the rate at which uncertainty reduces after the disturbance. The steady-state error for a first order response to a ramp input is given by $k'\tau$ where $k' = 1$ for a unit input. After the initial transients, the equal weight method therefore gives constant variance related to the sample size and ramp gradient. The uncertainty is independent of system time constants after the initial

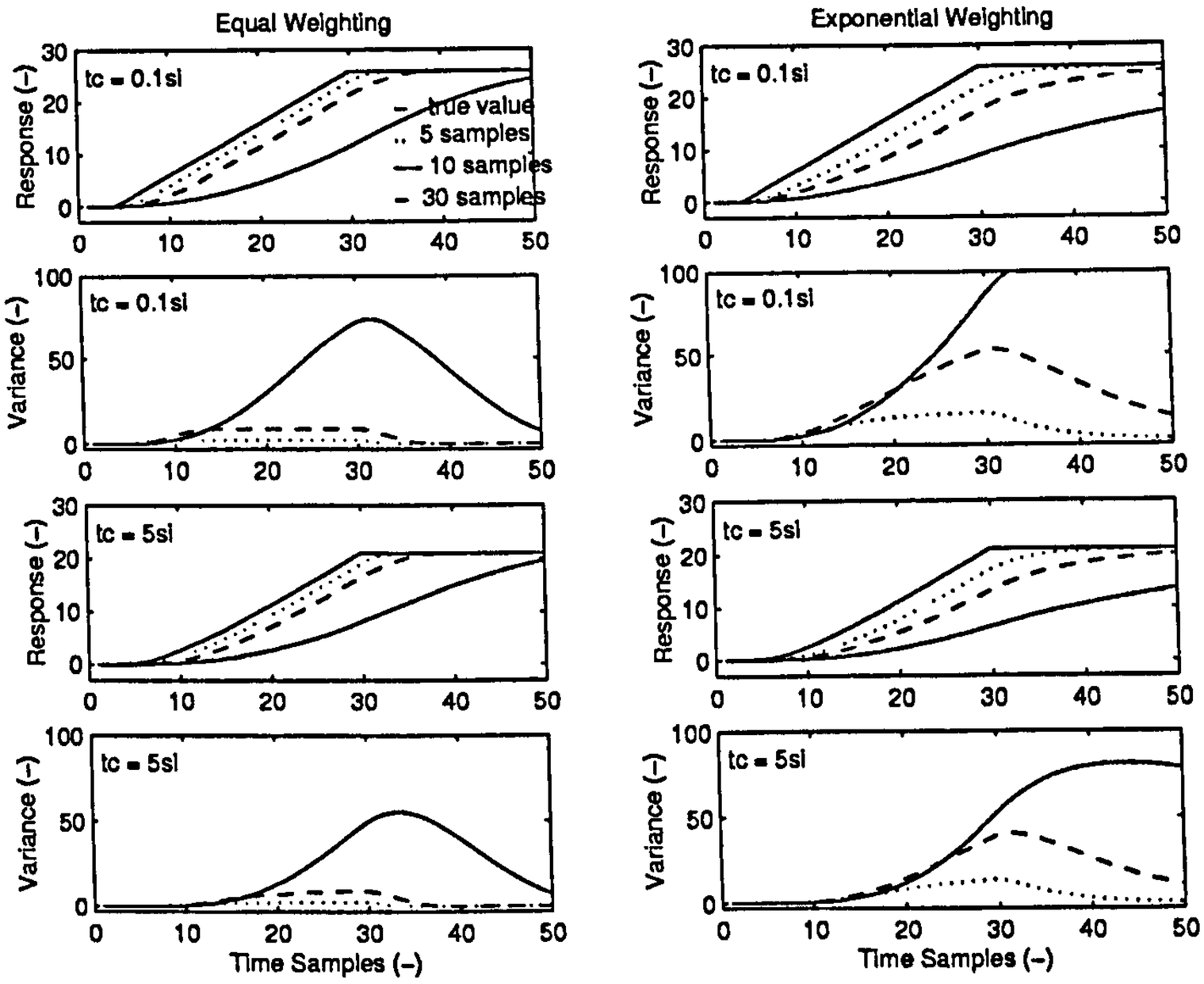

Figure 4.6: The Effects on Sample Uncertainty Due a First Order Response to a Unit Ramp Input for Different Sample Sizes and System Time Constants For Equally and Exponentially Weighted Sampling Methods.

transients. Figure 4.7 details the effects due to different input ramp gradients. The most striking feature is the slow response on the exponentially weighted method to return to zero, after the ramp has been stopped. Both Figures 4.6 and 4.7 show the exponential weighting method to generate greater uncertainty than the alternate approach.

Response to an Impulse Input

Figure 4.8 detail similar plots for a first order response to a unit impulse. For this case it is clear that the exponentially weighted method demonstrates the following over the equal weighting approach:

- lower peak uncertainty;
- lower total uncertainty;
- and a quicker initial reduction in uncertainty.

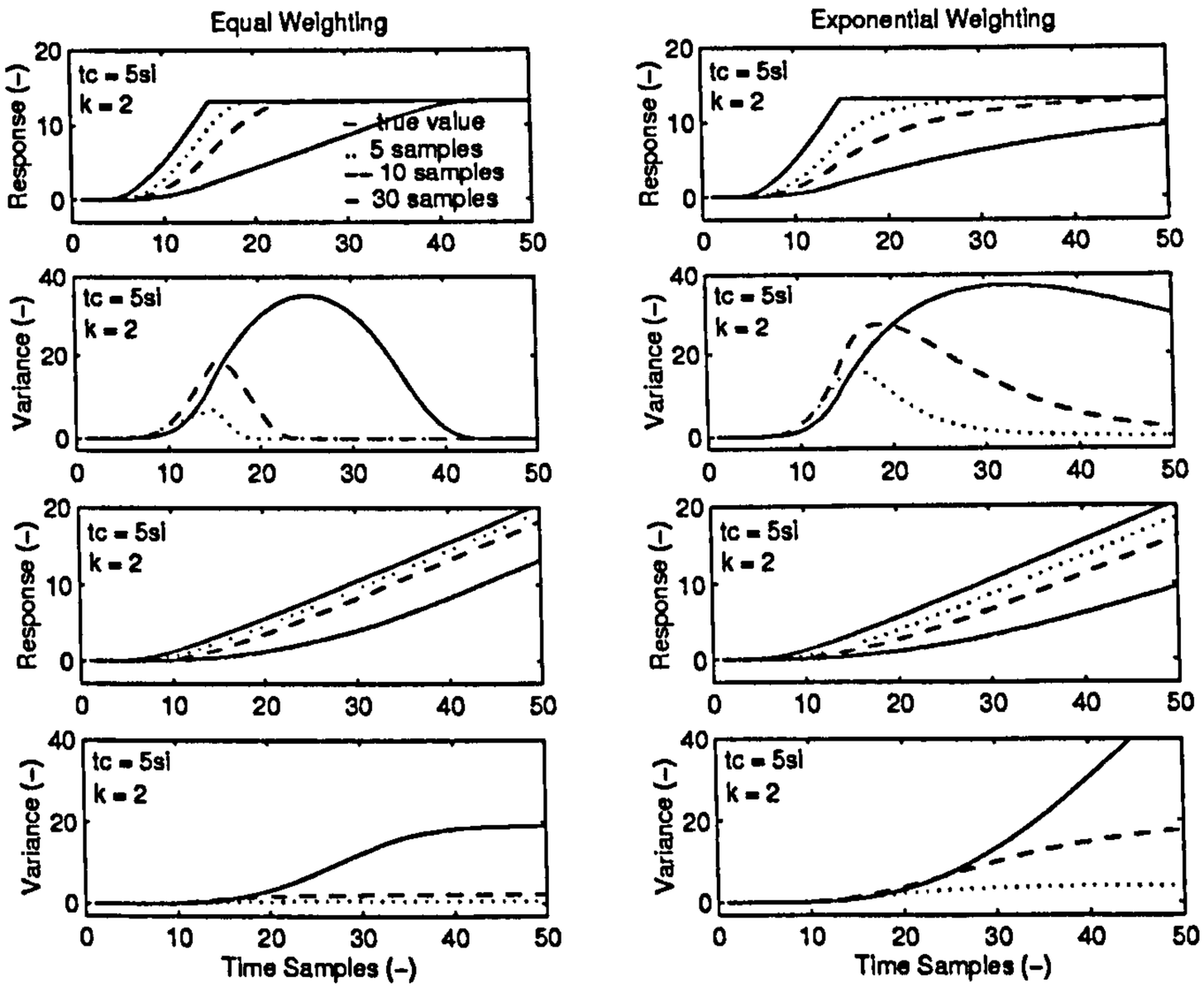

Figure 4.7: The Effects on Sample Uncertainty Due a First Order Response to Two Rates of Ramp Input for a System Time Constant of $5I_n$ for Equally and Exponentially Weighted Sampling Methods.

Table 4.3 shows the integrals associated with the total variance similar to that shown in Table 4.2. These results are calculated by substituting Equation 4.4 and 4.5 for Equation 4.2 and 4.3 in the derivation of Equation 4.12. Although the reduction in uncertainty is initially quicker than for the equal weighting, the exponential method is slower to return to zero. Figure 4.9 shows the relationship between the total error and the sample variance for both methods. As the system time constant increases, the uncertainty becomes less significant. One interesting feature is that due to the rapidity of the system input response and the slower decay of the sampling functions, a sign change in the total error is evident. At $\tau = 5I_n$ both approaches are similar, however as τ decreases, the exponential method gives a much better uncertainty response.

4.3.4 Conclusions: Analysis of Sampling Uncertainty

The exponential method considers more samples than the fixed length window method. The 'memory' of the variance, therefore, lingers causing sluggish response to the total

Table 4.3: The Total Uncertainty Associated With the Test Sampling Methods Over a Period of 60 Samples For a Unit Impulse Input.

System Time Constant (Sample Intervals)	Sample Size (Number)	Equal Weight Method	Exponential weight Method
0.1	5	99.998	71.110
0.1	10	99.999	84.845
0.1	30	100.000	77.665
5	5	0.038	0.045
5	10	0.058	0.071
5	30	0.091	0.079

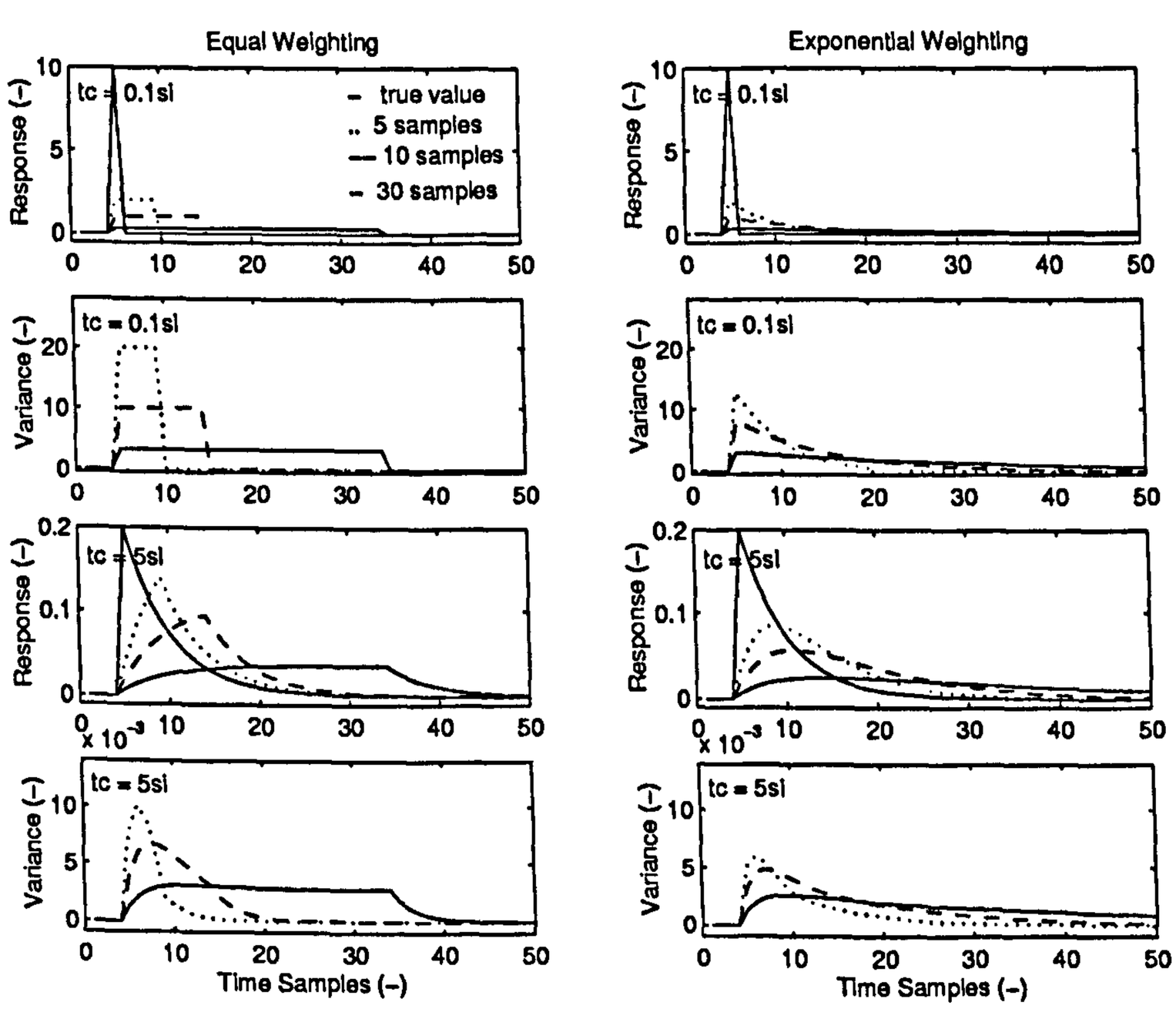

Figure 4.8: The Effects on Sample Uncertainty Due a First Order Response to a Unit Impulse Input for Different Sample Sizes and System Time Constants For Equally and Exponentially Weighted Sampling Methods.

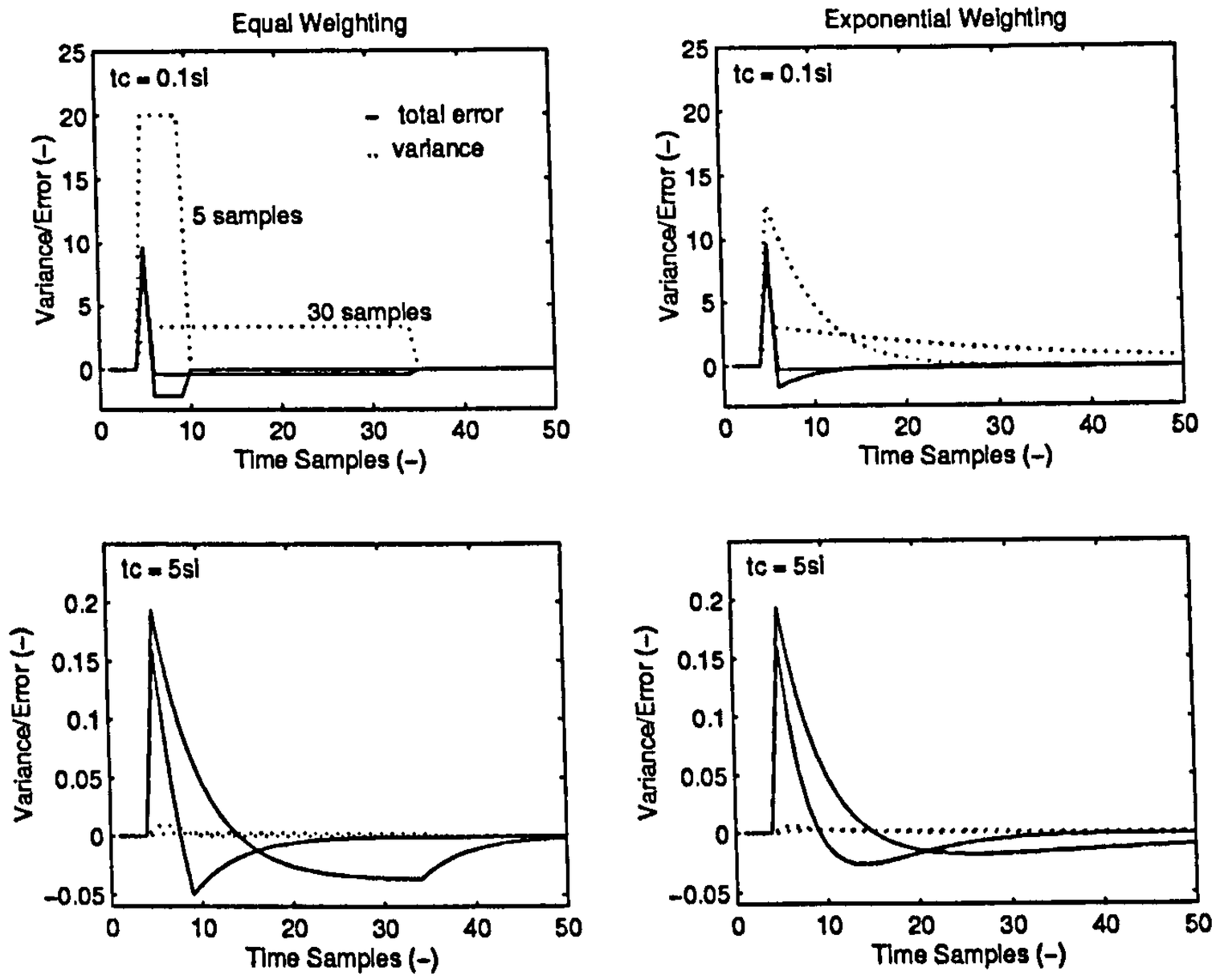

Figure 4.9: Representation of the Total Error by the Uncertainty Estimate Using the Sample Variance for an Unit Impulse Input.

error for ramp and step inputs. Conversely, the equal weighting method generates higher uncertainties when an impulse input is considered, which is particularly apparent when τ is small. However there is little to distinguish between the filters in terms of the coincidence of the total error with maximum variance; a desirable feature since the variance is the 'description' of uncertainty. In conclusion, if measurements are taken from a system having predominantly impulse inputs, the exponential method will generate less uncertainty. If the system is subject to predominantly ramp and step inputs, as is the case with most typical HVAC systems, the equal weighting method will generate less uncertainty.

4.4 Steady-State Predictions Using Transient Data

Steady-state models of HVAC processes have been used to a considerable extent for condition monitoring (Salsbury, 1996; Hyvärinen, 1997c; Hyvärinen, 1997a). HVAC systems spend a large amount of time at or close to steady-state and steady-state models have been proven to yield a reasonable representation of real HVAC system performance (Buswell

et al., 1997; Buswell and Wright, 1998; Norford et al., 2000).

Excessive transients present in the data can generate unacceptable degrees of accuracy in the model predictions. To ensure that the predictions from a steady-state model are valid, the approaches reported in the literature commonly use filtering techniques. These are termed *steady-state detectors* and filter out the unwanted transient data. The model is then only applied to the data that is considered to be in steady-state. One such approach is described by Salsbury (1996). One of the main problems with this approach is that the decision whether to discard the data is based on a threshold. The satisfactory selection of this threshold can be subjective and difficult to achieve in practice (Buswell and Wright, 1999). Subsequently, transient data can be incorrectly classified as steady-state, which has implications for the accuracy of the model predictions.

To avoid the accuracy issues that arise due to incorrectly classified data, a new approach has been developed. The proposed alternative is to consider all available data with the steady-state models and to evaluate the additional uncertainty attributed to the transients present. This section develops this approach basing mean and variance calculations on a 10 sample, fixed averaging window. The selection of filter type and window size is suitable for the system characteristics for HVAC thermal systems as discussed in Sections 4.2 and 4.3.

4.4.1 Estimating Uncertainty due to Transients

The previous sections discussed the uncertainty involved in sampling discrete measurements. In real systems, however, we do not know the true value of the measurement, we can only observe the system. Here, the observation tools are the mean and variance generated by the filter. Figure 4.10 demonstrates the relationship between the sampling uncertainty and the uncertainty due to dynamics forced by a step input in a first order system. After the excitation, the system response and measurement thereof, approach the resultant value. The moment the input occurs, steady state analysis is no longer concerned with the original operating condition, but considers only the anticipated resultant steady state condition. It can be stated, therefore, that the uncertainty in the value of the observation is at a maximum the moment after the input and is at a minimum when

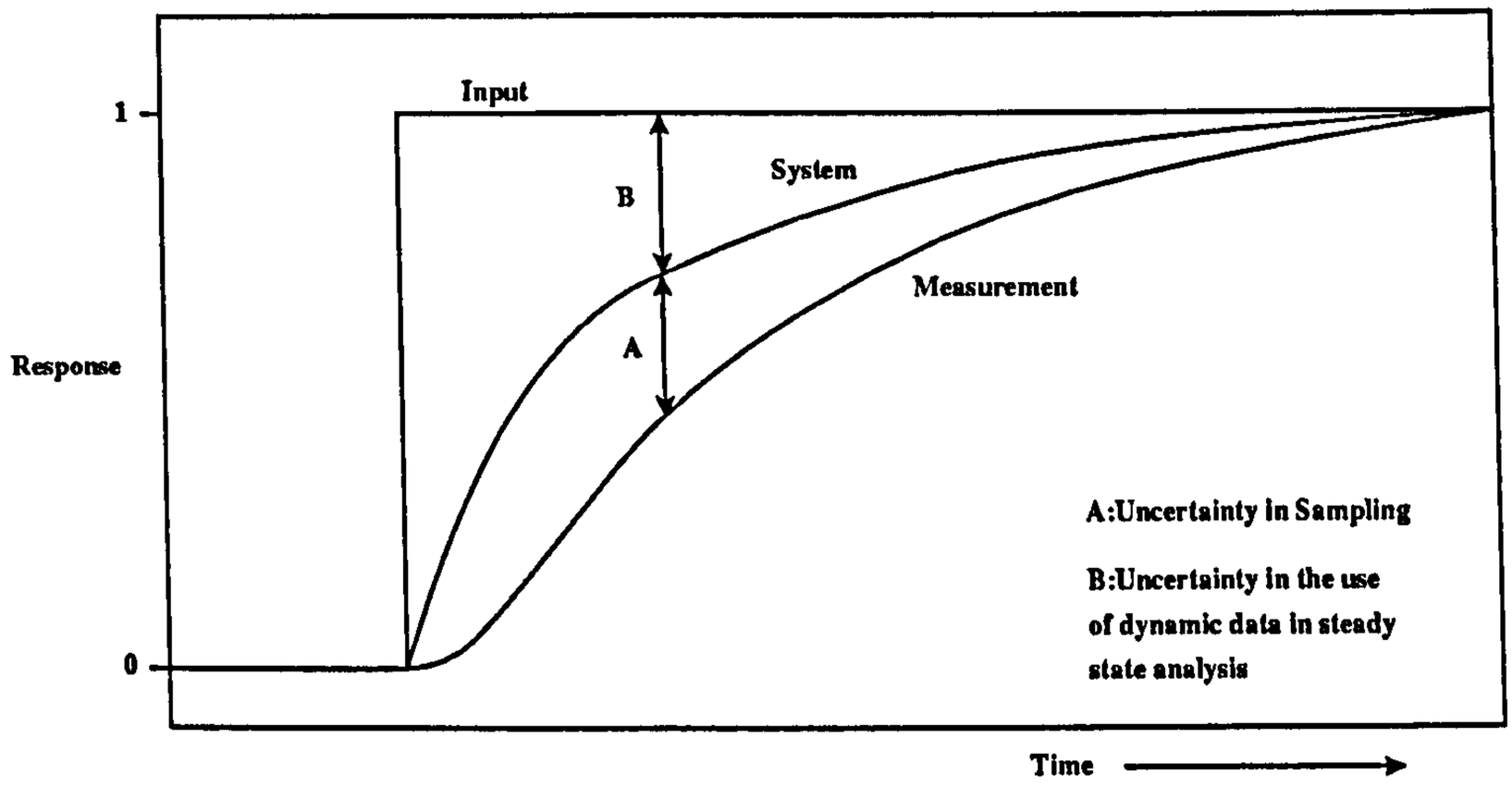

Figure 4.10: The Relationship Between the Uncertainty Due to Sampling the Data and that Due to the Use of Dynamic Data in Steady State Analysis.

the new steady-state condition is considered to exist.

The inputs to HVAC systems are generally unknown in terms of time and magnitude. Since the variance is the only observation that describes the system activity, a relationship between the variance and uncertainty is required.

The uncertainty in the measurement noise, sampling regime and transients can be classified as the random uncertainty component of a measurement, P. From consideration of Figure 4.10,

$$P = U_{smp} + U_{trn}, \tag{4.13}$$

where U_{smp} and U_{trn} are the uncertainties due to the sampling regime and due to the presence of transients respectively. Note that the combination of the uncertainties is not considered to be in quadrature. This is because the uncertainty in the sampling regime depends on the uncertainty due to the transient system response. The uncertainty in the measurement noise will be implicit in the sampling uncertainty, which is given by,

$$U_{smp} = \frac{t\sqrt{\sigma_n}}{\sqrt{n-1}}. \tag{4.14}$$

U_{trn} can be described by,

$$U_{trn} = I_{max} \cdot f(\varrho, \tau, \sigma_n), \tag{4.15}$$

where I_{max} is the maximum likely value of uncertainty, which is taken to be the estimate of the 95% confidence level. Practically, this is equivalent to the maximum likely step change in the system. $f(\varrho, \tau, \sigma_n)$ is a function whose normalised output factors I_{max} to yield the uncertainty due to transients. The function relates the variance to the estimated uncertainty and is derived as follows.

Derivation of Transient Uncertainty Measure

If the system is approximated to first order, the characteristics of the true value of the measurement generated after a step input, can be described by,

$$\bar{x}(\varrho) = 1 - e^{-\frac{\varrho}{\tau}}. \tag{4.16}$$

$\bar{x}(\varrho) = e^{-\frac{\varrho}{\tau}}$, therefore, represents the level of uncertainty between the true value and the *desired-future* true value due to the ensuing dynamic activity. Since steady-state can be considered to exist when the output is at 95% of its final value (Gruber, 1996), this expression can be normalised to give,

$$\bar{x}(\varrho)' = \frac{e^{-\frac{\varrho}{\tau}} - a}{1 - a}, \tag{4.17}$$

where $a = e^{-\frac{\varrho^{95\%}}{\tau}}$ and $\varrho^{95\%}$ is the time after the excitation which the response falls within 5% of the final value.

Equation 4.17 represents the relationship between uncertainty and proximity to steady-state. The variance is a measure of the activity in the data and we can estimate the likely maximum and minimum magnitudes from data collected from the system. σ_n' is calculated by normalising the current variance between these limits by,

$$\sigma_n' = \frac{\sigma_n - \sigma_{n_{max}}}{\sigma_{n_{min}} - \sigma_{n_{max}}}. \tag{4.18}$$

The function $f(\varrho, \tau, \sigma_n)$ is given by,

$$f(\varrho, \tau, \sigma_n) = \frac{e^{-\frac{\sigma_n' \varrho^{95\%}}{\tau}} - \eta}{1 - \eta}. \tag{4.19}$$

Different measurements observe different system time constants. To avoid the requirement of selecting suitable parameters associated with the time constants for each measurement, a

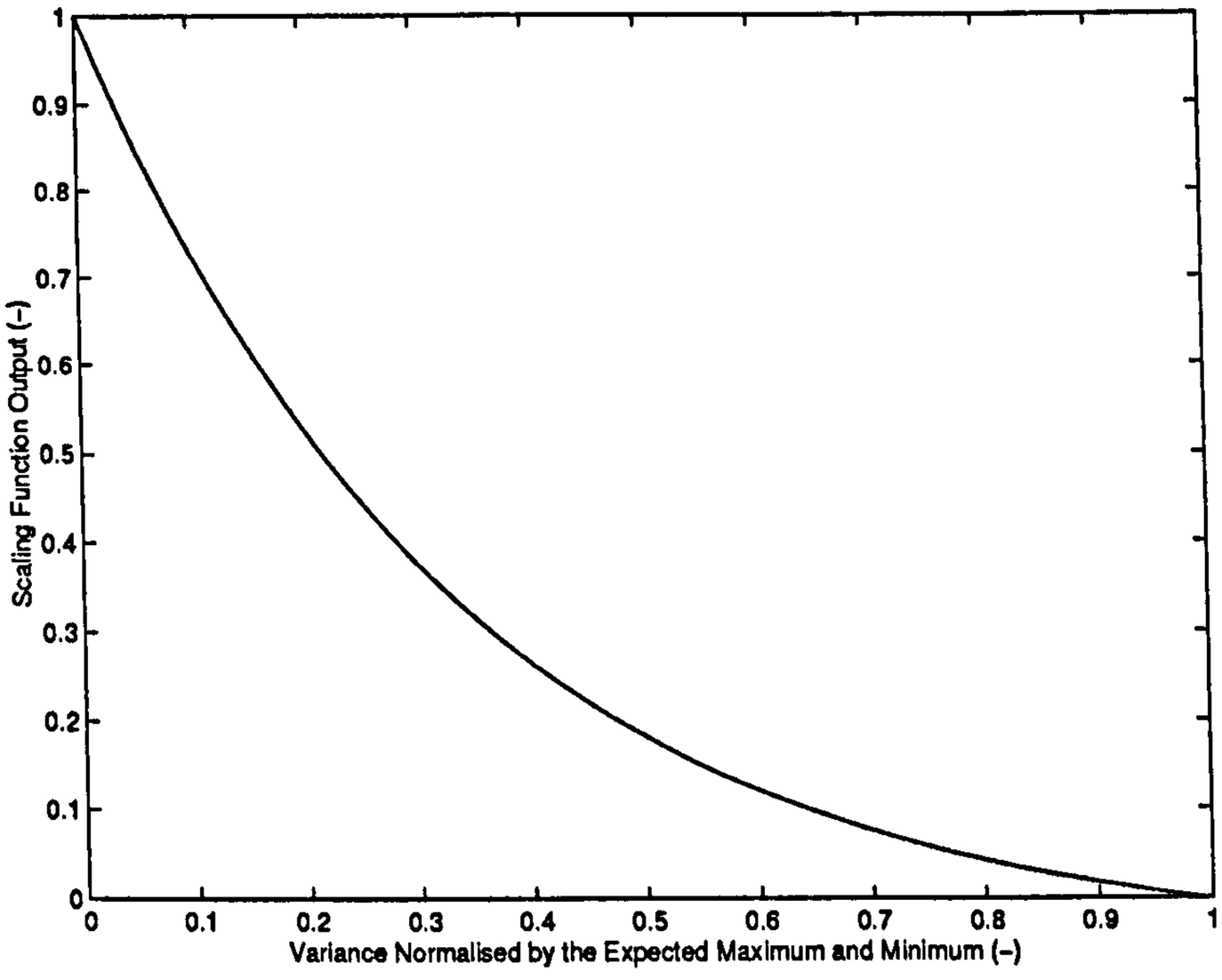

Figure 4.11: The Relationship Between σ'_n and the Function $f(\varrho, \tau, \sigma_n)$, Used to Scale the Maximum Likely Uncertainty Given by I_{max}.

simplification is to assume the relationship between σ'_n and $f(\varrho, \tau, \sigma_n)$ is similar for different measurements. The relationship can be based on one measurement; the measurement that observes the maximum system time constant. Observations made on the the HVAC system described in Section 6.1 showed that the maximum observable values associated with the cooling coil are approximately $\varrho^{95\%} = 600\,\text{Seconds}$ and $\tau = 180\,\text{Seconds}$. Equation 4.19 can then be approximated by,

$$f(t, \tau, \sigma_n) = 1.053e^{-2.996\sigma'_n} - 0.053, \tag{4.20}$$

and be applied to all measurements. Figure 4.11 demonstrates the relationship described by Equation 4.20.

4.5 Application of Uncertainty Evaluation Method

Under closed loop control, under-damped systems will generate more uncertainty on the approach to steady-state due to the excitation of the system. The additional variation across the filter window will be implicitly evaluated as extra transients and noise. Further

Table 4.4: Parameter Values for Equation 4.15 for Typical HVAC Measurements.

Measurement	$\sigma_{n_{min}}$	$\sigma_{n_{max}}$	I_{max}	Units
Temperature	0.070	59.8	15	K
Air Volumetric Flow Rate	0.000	0.862	1.0	kgs^{-1}
Air Relative Humidity	0.018	176.0	20	%

measures to account for uncertainty due to excessive control dynamics are not, therefore, required.

The assessment of uncertainty described in Section 4.4.1 is applied to each measurement used in a particular calculation. The uncertainty P is then combined with the bias uncertainties for each measurement and used to calculate the uncertainty in the result. See Sections 6.4 and 7.1 and Appendix C.

The parameters required for Equation 4.15, estimated for the system measurements described in Section 6.1, are presented in Table 4.4. Using these parameters, the approach is demonstrated on a typical air temperature measurement, at sample intervals of 60 Seconds.

The system is a cooling coil installed in an HVAC system serving a real building and is described fully in Section 6.1. The system output observations are made on the outlet air temperature. The system output excitation comes from the variation of three principal inputs; control signal that governs the mass flow rate of chilled water through the coil; the air temperature onto the coil; and the air mass flow rate. The top plot of Figure 4.12 shows the 95% confidence limits about the system output, due to P. The normalised system input excitation is detailed in the bottom plot. The centre plot shows the uncertainty percentage contributions to P from the uncertainty due to the sampling regime and the uncertainty due to the presence of transients. This shows that the uncertainty in the sampling is typically dominant unless there is significant excitation of the system. The plot also demonstrates that the total uncertainty is of the same order of magnitude as the step input and as such is a good estimation of the uncertainty in the dynamics.

Section 7.3 demonstrates that when the system experiences excessive dynamic activity, the evaluation of the P is critical to generate robust calculations. This often occurs in

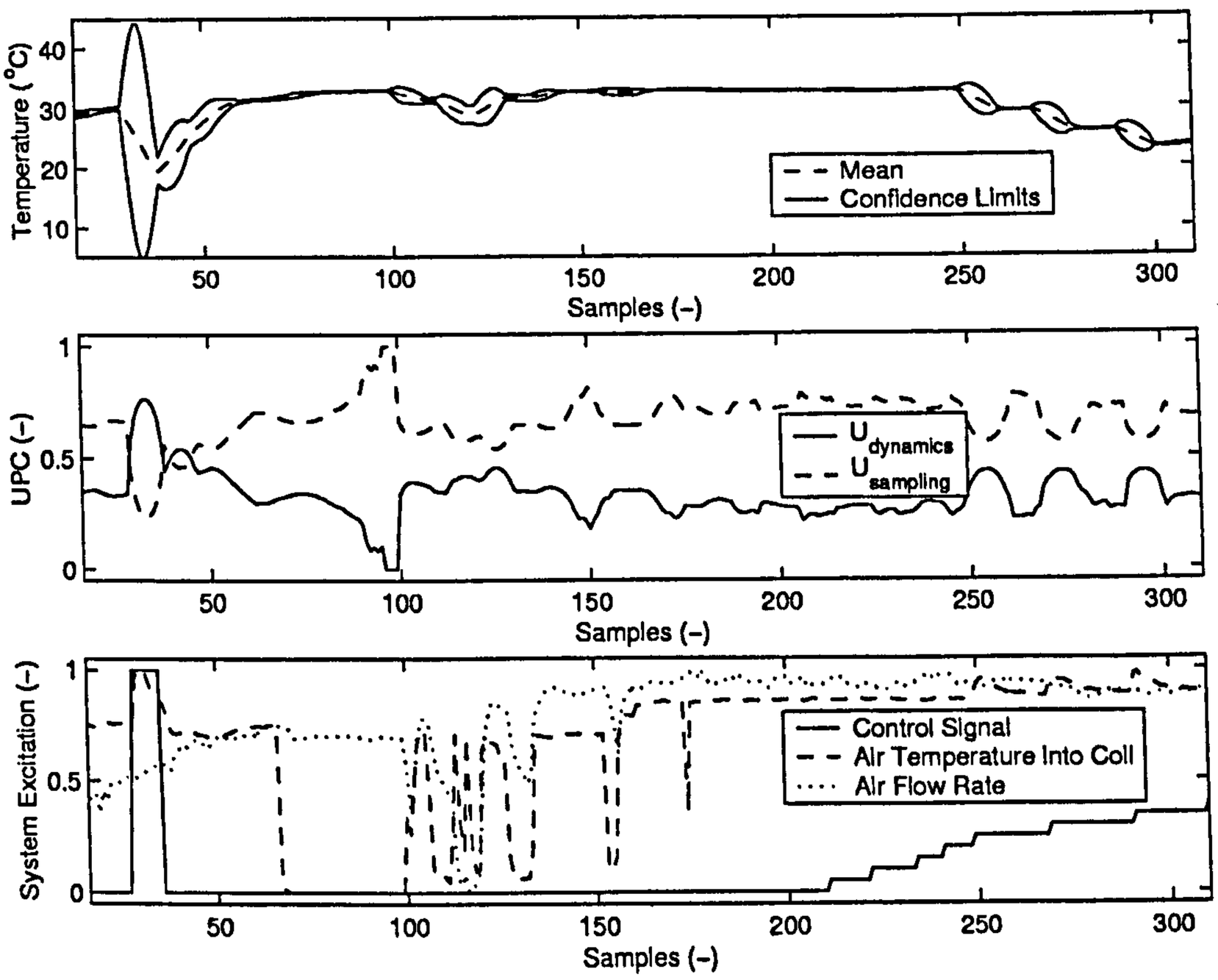

Figure 4.12: The Total Uncertainty Evaluation Regime Applied to Test Data.

HVAC systems when the systems start up from a dormant period, typically night-time shut down. The uncertainty due to the transients under nominal operating conditions, however, becomes insignificant when compared to the uncertainty due to the bias in the measurements.

4.6 Conclusions

In this chapter, the calculation of the random uncertainty component associated with HVAC measurements was considered. It was shown that the uncertainty in the data sampling is influenced by disturbances in the data. It was established that in HVAC systems, the disturbances are usually not quantifiable and therefore advocates the rejection of the zero mean variance assumption. The performance of two first order filters in the presence of persistent dynamic activity were evaluated in terms of the uncertainty they generate in a measurement. The properties of the variance generated by the filter was exploited to develop a new approach that allows the legitimate use of transient data with

steady-state calculations. Specific Comments are:

- a suitable sample interval for HVAC component performance is 1 minute and a suitable filter window length is 10 samples;
- the temporal alignment of simultaneous variable data records can be considered to be negligible;
- the fixed length window filter demonstrated better performance then the exponential filter in terms of the magnitude of uncertainty generated in characteristic HVAC system inputs;
- a new approach to the filtering of transient data for use in steady-state calculations was introduced;
- the variance from HVAC measurements can be related to a theoretical maximum uncertainty, equivalent to the maximum likely step input to that measurement;

Chapters 6 and 7 use the demonstrated transient uncertainty assessment technique developed here and apply the approach to the condition monitoring problem.

Chapter 5

Uncertainty in Heat-Exchanger Models

There will always be some degree of approximation or generalisation in a mathematical representation of a real process. Assumptions and simplifications are practically necessary to generate a simple first principles based model of a system. These assumptions and simplifications introduce uncertainty into the model structure. In order to generate robust predictions from such models, the *model structural uncertainty* cannot be neglected. To date, there are no methods available to carry out this assessment reported in the literature. This chapter addresses this issue by introducing a new uncertainty assessment methodology. The approach is applied to heat transfer and heat and mass transfer heat-exchangers of the class commonly found in HVAC systems.

Uncertainty evaluation techniques are classified and the simplified first principles based models are presented. The uncertainty in the heat-exchanger configuration and the primary and secondary fluid flow regimes are investigated. The sensitivity of the model characteristic parameters are studied in relation to the model output. Issues surrounding uncertainty in the model parameters are further developed in Section 7.2. The influence of the uncertainty in the physical constants used in the calculations are studied. In relation to the heat and mass transfer model, the additional uncertainty associated with internal iterations are considered.

5.1 Uncertainty Assessment Methodology

In engineering calculations uncertainty is often described statistically. This is an approach which allows the engineer to calculate the uncertainty associated with one parameter or variable in isolation. This approach expedites the assessment of uncertainty in the structure of the model. The principal stages required to account for uncertainty in modelling assumptions are:

1. understanding the implications for the model output;
2. describing the uncertainty in terms of the model structure;
3. and generating the variance estimate.

The basis for the description of uncertainty relies heavily on the implementation of the model and its application to the process. The structured methodology, presented in Figure 5.1, demonstrates the proposed approach to uncertainty identification. The uncertainties in the data used for parameter identification need to be evaluated. Uncertainty in data is covered in Chapters 3 and 4 and uncertainty in the parameters and parameter identification from data is covered in Section 7.2. For the investigation in this chapter, the uncertainty in the data is assumed to be zero and hence this work is only concerned with the evaluation of the model structural uncertainty.

Initially the assumptions affecting the model output need to be established. Treated in turn, these need evaluation by employing one of the following methods:

Empirical Quantification is desirable but not commonly applicable. This method requires the uncertainty in the model structure to be quantifiable from data. Clearly, the uncertainty in the data acquisition process needs to be sufficiently small to render the model useful.

Differential Complexity involves employing a more detailed process model and comparing the outputs (or some calculated variable of interest) to a simpler model (used to generate the analysis results). The method is founded on the premise that the

process is represented by the detailed model to an extent where the difference between the simple and detailed model (in terms of the *truth* in the representation of the process) is *much* greater than between the detailed model and the real process. The detailed model complexity can be prohibitive and, of course, the detailed model is not free of uncertainty.

Absolute Range is particularly applicable to estimating uncertainty in tabulated physical properties where the data uncertainty is fossilised[1]. Applied to a variable or parameter, the maximum feasible range with respect to the process is estimated. This range can be assumed to contain the true value with 99.9% certainty, and then scaled to the appropriate level (typically 95%).

Differential Composition can be used where the structural uncertainty is a function of the process operating region. In this approach, the model is composed of different structural elements that give an upper and lower limit to an internally calculated variable, from which the mean is calculated (and used in any subsequent calculations). The uncertainty is calculated by applying the absolute range technique to these limits. The sensitivity coefficient of the internally calculated variable with respect to the model output needs to be derivable. The sensitivity coefficient (see Section 2.1.1 for definition) needs to be implemented in addition to the gradient calculation method used to calculate the uncertainties of the other parameters and variables associated with the output/result (see Section 7.2 and Appendix C). For this method to be implemented, however, the construction of the structural composition must be realisable in the calculations that form the model.

The key issues that allow the representation of uncertainty in the model are that: the uncertainty effects must be realisable in terms of some parameter, variable, constant or an internally calculated value; and that the uncertainty can be described by an estimation of some variance.

[1]'Fossilised' uncertainty describes the uncertainty associated with empirically derived data, generally taken to be the truth. Examples are tables of fluid thermodynamic and transport properties.

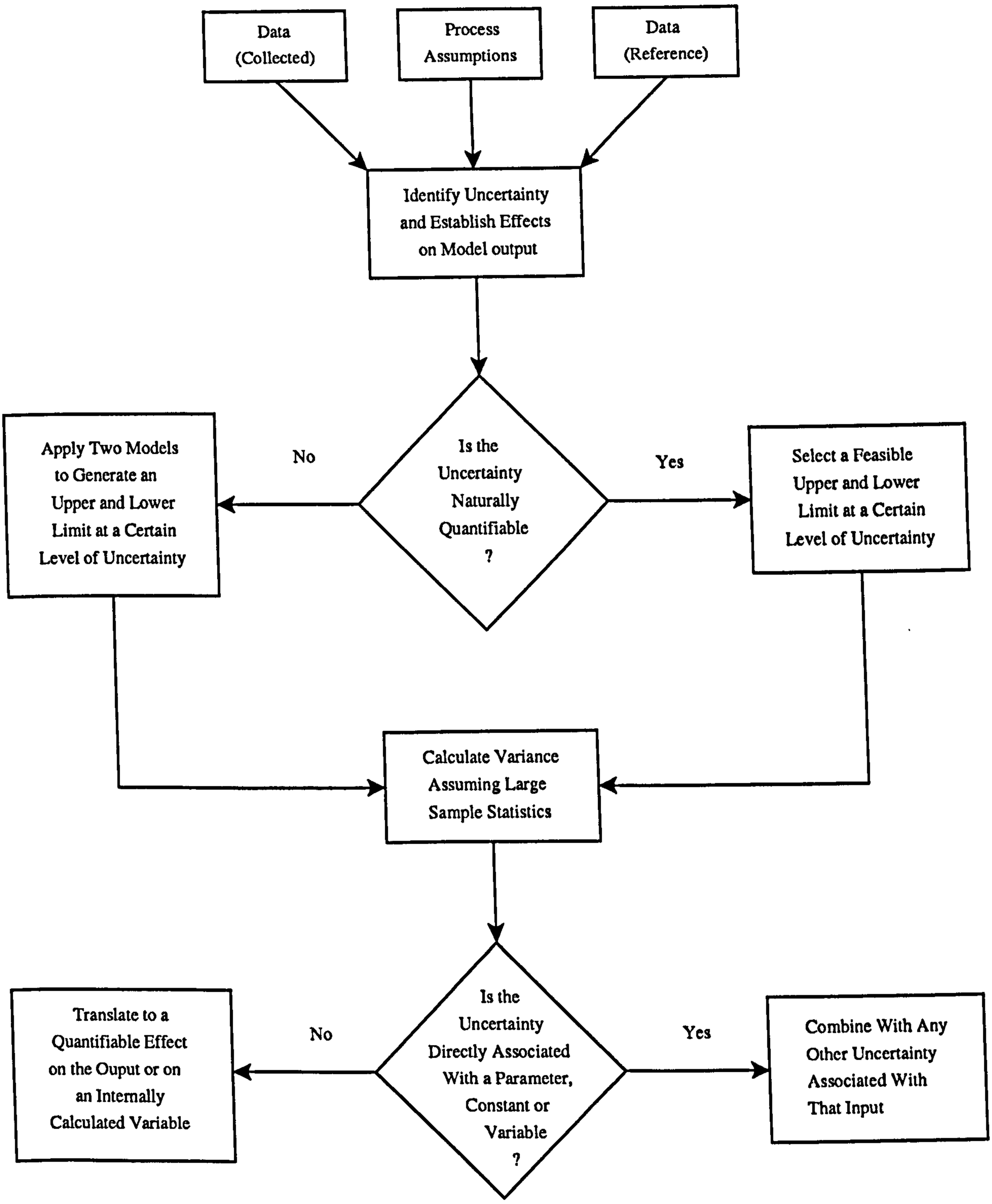

Figure 5.1: Methodology for Assessing the Uncertainty in the Model Structure.

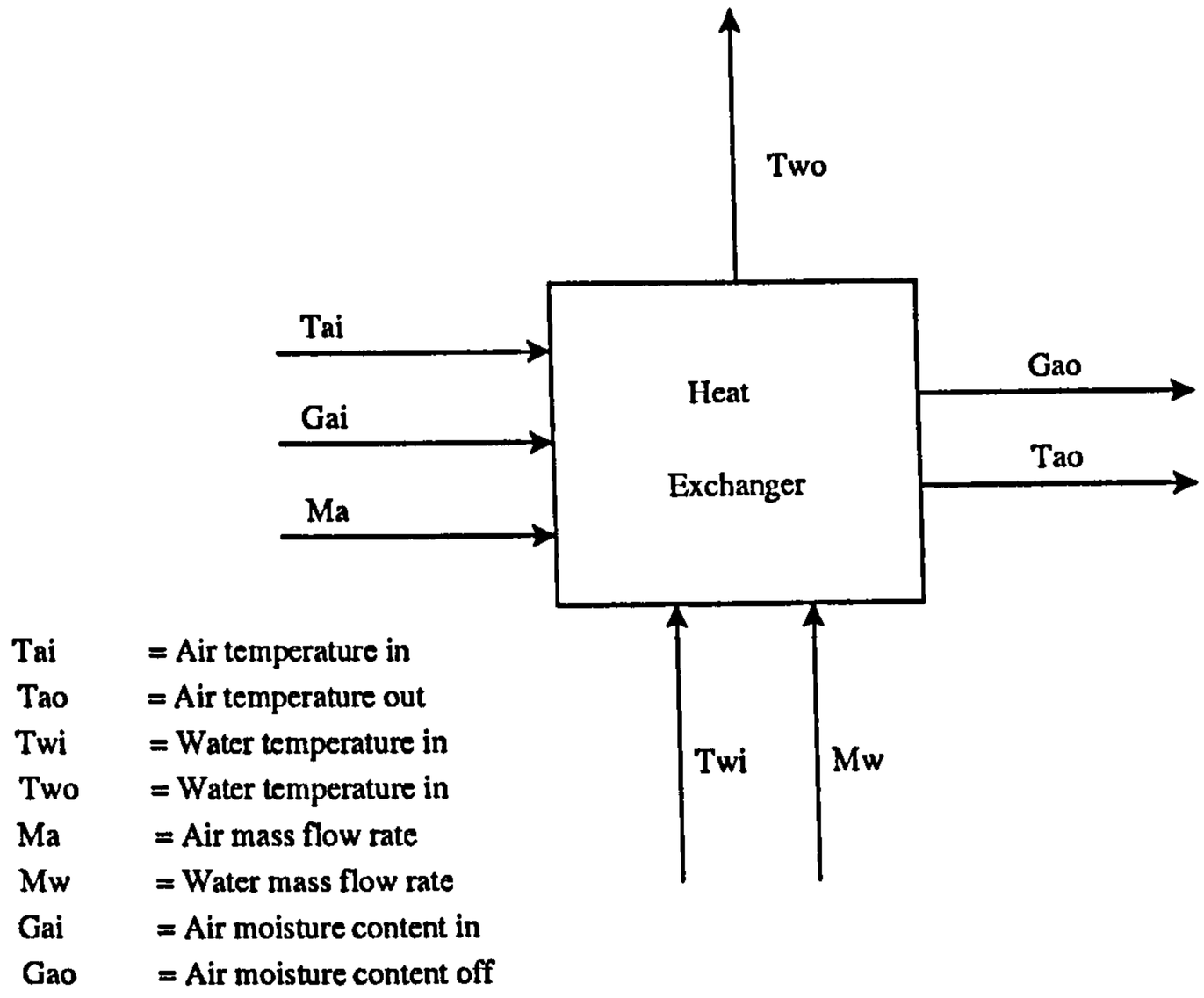

Figure 5.2: The Critical Fluid Quantities and Properties Associated with a Heat Exchanger

5.2 Heat Exchangers

Heat exchangers are used in a wide range of process applications. A typical configuration in HVAC applications uses (primarily) water to heat or cool a variable air flow rate, controlled by varying the water mass flow rate. Figure 5.2 demonstrates the fluid quantities and properties of interest.

5.2.1 The ε-N_{tu} Model

Kays and London (1984) describe the heat-exchanger by two analytically derivable characteristics: effectiveness, ε and dimensionless quantity called the Number of Heat Transfer Units, N_{tu}. The heat-exchanger performance is based on U ($\mathrm{WK^{-1}m^{-2}}$), an overall conductance for heat transfer that combines the convective and conductive heat transfer mechanisms. Equation 5.1 demonstrates U as unit conductance at a section where there is a temperature difference $T_a - T_w$ between the air temperature, T_a (℃), and the water temperature, T_a,

$$\frac{dq}{dA} = U(T_a - T_w), \tag{5.1}$$

where $\frac{dq}{dA}$ ($\mathrm{Wm^{-2}}$) is the heat flux per unit area. Continuing the analogy to Ohm's law then, the overall resistance with respect to the air-side, $\frac{1}{U_a}$, can be represented by,

$$\frac{1}{U_a} = \frac{1}{\eta_{o,a}\kappa_a} + \frac{b}{(A_k/A_a)k} + \frac{1}{(A_w/A_a)\eta_{o,w}\kappa_w}, \tag{5.2}$$

where k ($\mathrm{WK^{-1}m^{-1}}$) is the conductance of the wall material and b (m) is the wall thickness. κ ($\mathrm{WK^{-1}m^{-2}}$) denotes the air/water-side convective heat transfer coefficients that are complex functions of the coil surface geometry, fluid properties and flow conditions. A_x ($\mathrm{m^2}$) are areas in relation to the air-side heat transfer area A_a. η_a and η_w are the temperature effectiveness, or fin efficiencies of the respective areas. It should be noted that it is not typical to find extended surfaces on the water side of heat-exchangers used in HVAC processes.

The N_{tu} value can be derived from the UA ($\mathrm{WK^{-1}}$) where A is the air-side heat transfer area,

$$N_{tu} = \frac{UA}{C_{min}}, \tag{5.3}$$

$$C_{min} = minimum\{\dot{C}_a, \dot{C}_w\}, \tag{5.4}$$

where $\dot{C}_a$ and $\dot{C}_w$ ($\mathrm{WK^{-1}}$) are the fluid capacity rates given by $\dot{m}_a Cp_a$ and $\dot{m}_w Cp_w$ respectively. $\dot{m}$ ($\mathrm{kgs^{-1}}$) and Cp ($\mathrm{Jkg^{-1}K^{-1}}$) are the air and water mass flow rates and specific heat capacities. The effectiveness can be defined as,

$$\varepsilon = \frac{q}{q_{\max}} = \frac{\dot{C}_a(T_{ai} - T_{ao})}{\dot{C}_{\min}(T_{ai} - T_{wi})} = \frac{\dot{C}_w(T_{wi} - T_{wo})}{\dot{C}_{min}(T_{wo} - T_{ai})}, \tag{5.5}$$

where the subscripts 'i' and 'o' indicate fluids entering and leaving the coil respectively. The capacity ratio C_r is defined as $\frac{\dot{C}_{min}}{\dot{C}_{max}}$ and allows the effectiveness to be expressed as,

$$\varepsilon = f(N_{tu}, C_r), \tag{5.6}$$

as some function of the flow arrangement. Two such common arrangements for water to air heat-exchangers are:

Crossflow; characterised by perpendicular fluid flow directions and where one of the fluids is typically considered to be mixed. An example would be a single row configuration, where the air passes over the water coil once.

Counterflow; characterised by opposing fluid flow directions, a condition that is approached in water-to-air heat exchangers when there are many rows of water coils in the air path.

Kays and London gives,

$$\varepsilon_{cross} = 1 - e^{-\frac{1}{C_r}(1-e^{-N_{tu}C_r})}, \tag{5.7}$$

for when $\dot{C}_{min} = mixed$ and $\dot{C}_{max} = unmixed$ and

$$\varepsilon_{cross} = \frac{1}{C_r}\left(1 - e^{-C_r(1-e^{-N_{tu}})}\right), \tag{5.8}$$

for the opposite case. The counterflow effectiveness is given by,

$$\varepsilon_{counter} = \frac{1 - e^{-N_{tu}(1-C_r)}}{1 - C_r e^{-N_{tu}(1-C_r)}}. \tag{5.9}$$

Apart from the inherent structural uncertainty, the quality of the calculations hinges on the estimates of the heat transfer coefficients and associated efficiencies. In addition, it may be desirable to have an equation that will give a good representation of the heat-exchanger performance over the whole range of operation, not just at one operating point. Holmes (1982) proposed to simplify the formulation of the parameters and calculate the overall heat transfer, UA, shown in Equation 5.2 with,

$$UA = \frac{n_r A_f}{r_a v_a^{\nu_a} + R_m + r_w v_w^{\nu_w}}, \tag{5.10}$$

where n_r is the number of rows in the coil and A_f (m^2) is the coil face area. R_m ($_{(rows)}m^2KW^{-1}$), r_a and r_w ($_{(rows)}Km^2s^{\nu}W^{-1}m^{-\nu}$) represent notional overall factors that control the resistance of the air, coil material and water to heat transfer that can be estimated from manufacturer's data. v_a and v_w (ms^{-1}) are the air face velocity and the water velocity respectively. ν_a and ν_w are powers that approximate the control of the heat transfer relationship to be governed by the fluid flow rates. This approach has been demonstrated to be a reasonable simplification in Salsbury (1996), Buswell et al. (1997), Buswell et al. (1997), Norford et al. (2000). Figure 5.3 demonstrates the surface of T_{ao} for such a coil. The analysis is based on a six row coil with eighteen parallel circuits constructed of tubes with a nominal 0.013 mm bore and a face area of $0.557m^2$. The thermal resistance factors are r_a =$0.596_{(rows)}Km^2s^{\nu}W^{-1}m^{-\nu}$, r_w =$0.217_{(rows)}Km^2s^{\nu}W^{-1}m^{-\nu}$, R_m =$0.286_{(rows)}m^2KW^{-1}$, $\nu_a = -0.8$ and $\nu_w = -0.8$ (taken from Holmes (1982)). The

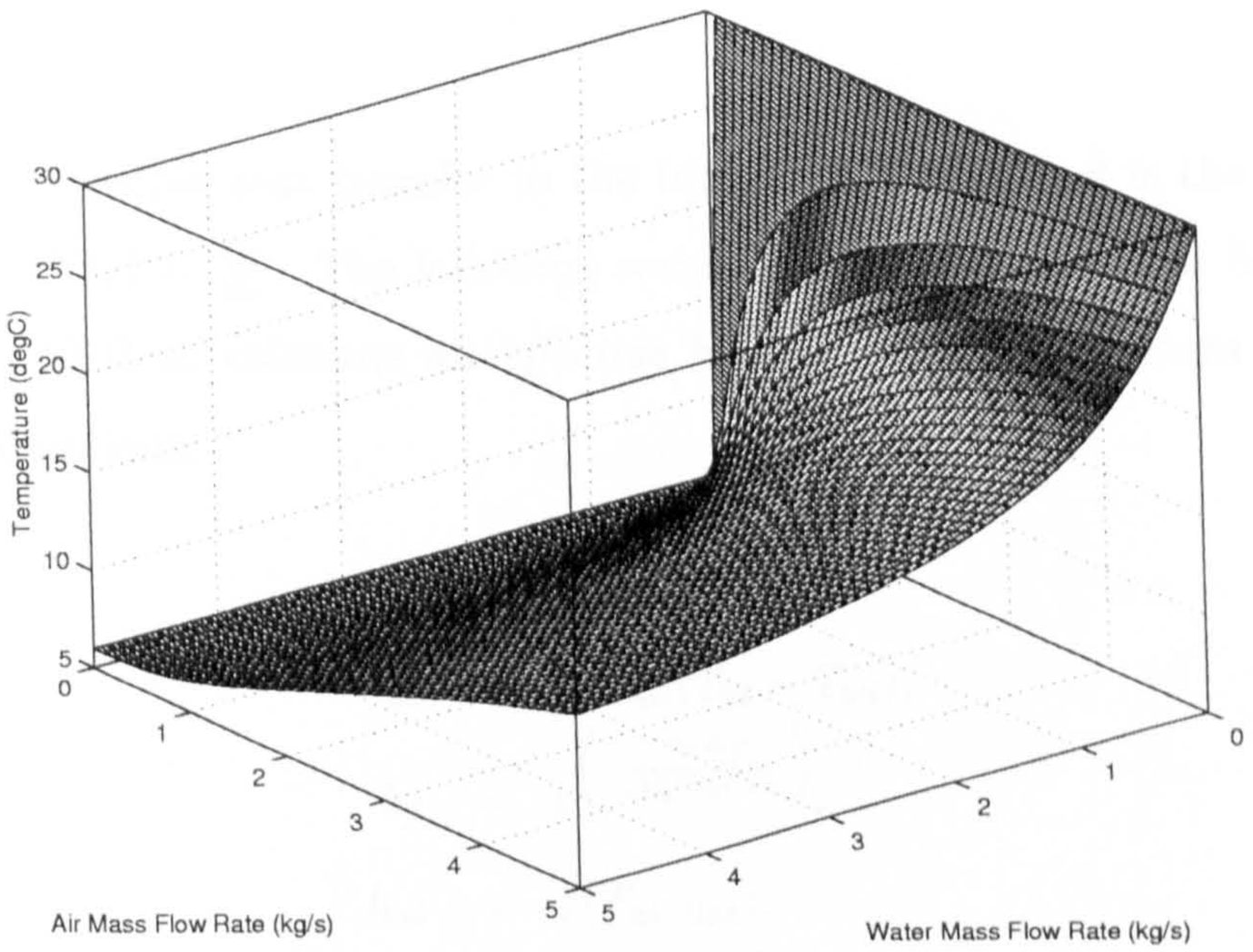

Figure 5.3: The Heat-exchanger Model Result Surface For T_{ao}

configuration cools air at 30℃ with water at 6℃. The air is assumed to be dry for the heat transfer analysis and to be moist to a specified degree for the heat and mass transfer investigation. Both fluid steams are varied from 0kgs^{-1}to 5kgs^{-1}.

5.2.2 The SHR-ε-N$_{tu}$ Model

As hot air is passed over a cold surface, the temperature of the air is reduced. When the temperature of the surface drops below the dew point temperature of moist air, water condenses on the surface and the heat transfer is part latent and part sensible. The ε-N$_{tu}$ model can be extended to model both heat and mass transfer. Two common methods are the Sensible Heat Ratio, SHR, method and the 3-line method. Both methods are well used and are detailed in Carrier et al. (1940). Arguments for the method of preference have been made by Stephan and Gruschka (1994) and based on this work, by Salsbury (1996). Both methods are similar in performance, with the exception that the 3-line method can be applied to the consideration of wet and dry areas of the coil. The SHR model has been successfully used in a number of applications for modelling real heat-exchanger systems (Salsbury, 1996), (Buswell et al., 1997), (Buswell and Wright, 1998), (Norford et al., 2000).

The SHR method has been adopted to demonstrate the uncertainty analysis used in this investigation.

The ratio of the sensible heat transfer to the total heat transferred is the SHR at those conditions, i.e. $SHR = \frac{Q_s}{Q_t}$. The following series of equations can then be employed to incorporate the SHR to calculate an *effective* heat transfer effectiveness to be used in subsequent calculations:

$$\begin{aligned}
\varepsilon &= f(N_{tu}, C_r), && (5.11)\\
Q_t &= \varepsilon \dot{C}_{min}(T_{ai} - T_{wi}), && (5.12)\\
b_f &= e^{\left(\frac{-n_r A_f}{r_a v_a^{\nu} \dot{m}_a C_{pa}}\right)}, && (5.13)\\
h_{ai} &= f(T_{ai}, g_{ai}), && (5.14)\\
T_s &= \frac{T_{ao} - b_f T_{ai}}{1 - b_f}, && (5.15)\\
T_{adp} &= f(g_{ai}), && (5.16)
\end{aligned}$$

where Q_t (kW) is initialised to the value of total heat transfer if $SHR = 1$, g_{ai} (kgkg_{air}^{-1}) is the moisture content of the air entering the coil and $h_{ai} = f(T_{ai}, g_{ai})$ and $T_{adp} = f(g_{ai})$ are psychrometric functions. A test for wet coil surface can be carried out and so if the (*effective mean*) surface temperature, T_s is less than the apparatus dew point, T_{adp}, latent heat transfer is considered to occur. Subsequent substitution can be employed to iterate on the total heat transfer[2] via the following equations;

$$\begin{aligned}
h_{ao} &= h_{ai} - \frac{Q_t}{\dot{m}_a}, && (5.17)\\
h_s &= \frac{h_{ao} - b_f h_{ai}}{1 - b_f}, && (5.18)\\
T_s &= f(h_s), && (5.19)\\
T_{ao} &= b_f(T_{ai} - T_s) + T_s, && (5.20)\\
SHR &= \frac{Cp_a(T_{ai} - T_{ao})}{h_{ai} - h_{ao}}, && (5.21)\\
\dot{C}_a &= \dot{m}_a \frac{Cp_a}{SHR}, && (5.22)\\
\dot{C}_w &= \dot{m}_w Cp_w, && (5.23)\\
\dot{C}_{min} &= min\left\{\dot{C}_a, \dot{C}_w\right\}, && (5.24)
\end{aligned}$$

[2]See Appendix A for discussion on convergence using subsequent substitution.

$$\dot{C}_r = \frac{\dot{C}_{min}}{max\left\{\dot{C}_a, \dot{C}_w\right\}}, \tag{5.25}$$

$$UA = \frac{n_r A_f}{SHR\, r_a v_a^{\nu_a} + R_m + r_w v_w^{\nu_w}}, \tag{5.26}$$

$$N_{tu} = \frac{UA}{\dot{C}_{min}}, \tag{5.27}$$

$$\varepsilon = f(N_{tu}, \dot{C}_r), \tag{5.28}$$

$$Q_t = \varepsilon \dot{C}_{min}(T_{ai} - T_{wi}), \tag{5.29}$$

where h_{ao} and h_{ai} (kJkg^{-1}) are the enthalpies of the air entering and leaving the heat-exchanger. h_s is the effective mean enthalpy of the air at the assumed conditions at the surface of the heat-exchanger. b_f is the bypass factor as defined in Carrier et al. (1940) and $f(h_s)$ is a psychrometric function.

5.3 Uncertainty in Heat Transfer

Figure 5.2 shows the relationships between the inputs and outputs of the heat-exchanger model and Table 5.1 lists the parameters, variables and constants associated with the calculation of effectiveness. The relationships of these, in terms of the propagation of uncertainty, is demonstrated by the flow diagram in Figure 5.4 where; 'D', 'A', 'M', 'V', 'R', 'C' and 'v', refer to density, area, mass flow rate, velocity, resistance, capacity rate and velocity coefficient respectively. The subscripts 'a', 'w' and 'm' refer to air, water and coil tube material. 'Lf', 'Wf' and 'Af' are the coil face length, width and area; and 'At', 'dt' and 'Nc' are the water-side tube area, diameter and number of circuits. 'Ntu and 'UA' are self explanatory and 'e' denotes effectiveness. 'Config.' refers to the uncertainty in the configuration of the effectiveness calculation. The uncertainty can be described by considering four aspects of the model: the calculation of UA, the effectiveness, the physical constants and the fluid flow regime. Each is discussed individually in this section.

5.3.1 Effectiveness Calculation

The use of the effectiveness calculations relies on the specification of the fluid flow configuration. Most applications utilise cross or counter flow arrangements. Often, however,

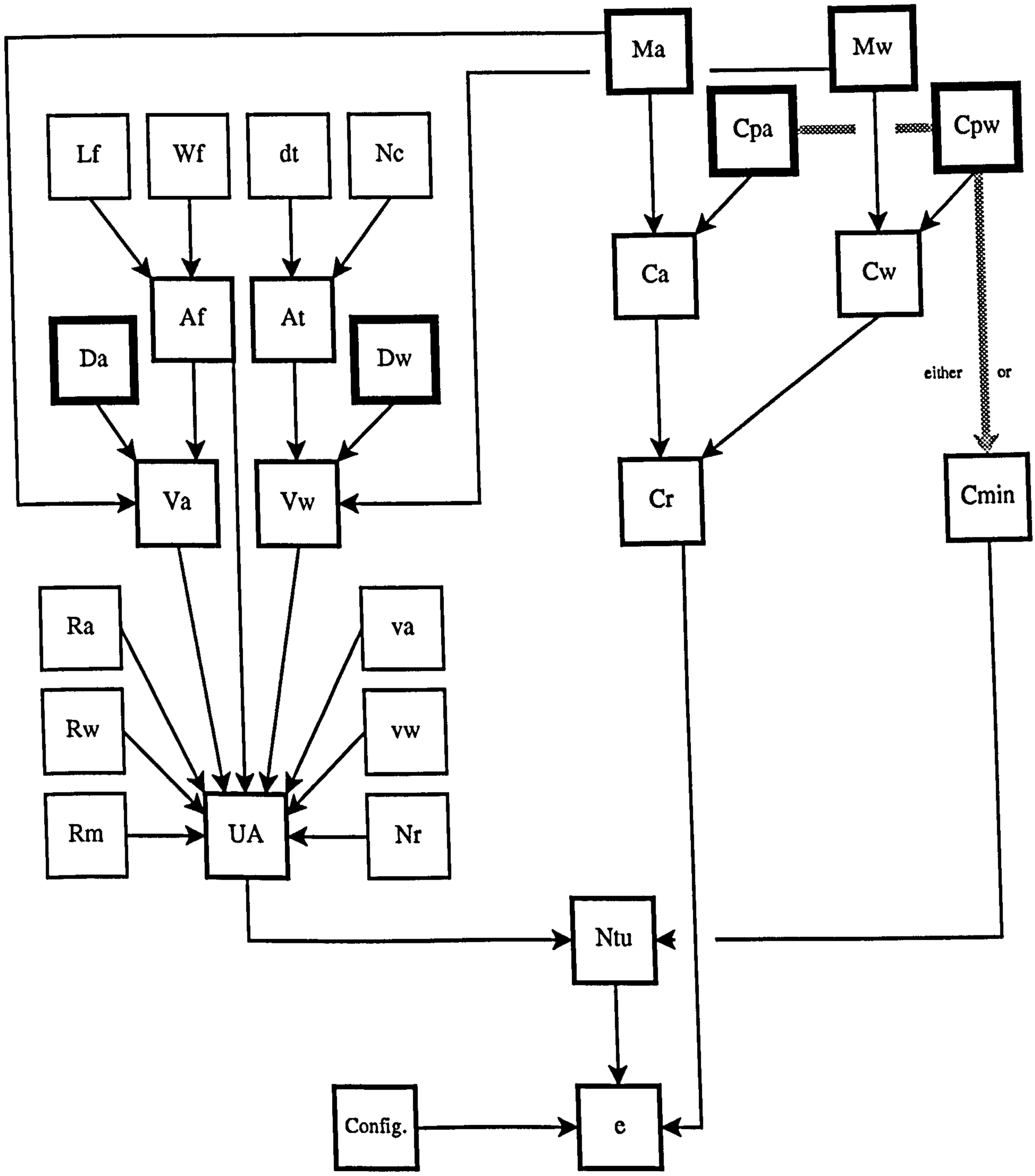

Figure 5.4: The Relationships Between the Uncertainty Components and the Calculation of the Result

Table 5.1: The Uncertainty Inputs Associated with the Calculation of effectiveness.

Parameters	Variables	Constants	Intermediaries
r_a	$\dot{m}_a$	C_{p_w}	A_f
r_w	$\dot{m}_w$	C_{p_a}	A_t
R_m	T_{ai}	ρ_w	v_a
ν_a	T_{wi}	ρ_a	v_w
ν_w	-	-	$\dot{C}_a$
l_f	-	-	$\dot{C}_w$
l_h	-	-	C_r
ϕ_t	-	-	UA
n_r	-	-	N_{tu}
$n_{circuits}$	-	-	-

HVAC heat-exchanger systems do not fall into either category precisely and so some degree of approximation is implied by the calculation constraints. The implications of these assumptions are:

Fluid Mixing: If the application of a cross flow arrangement is considered, the fluid flow mixing characteristics need to be estimated according to Kays and London (1984). An *unmixed* fluid is one where the fluid passage through the heat-exchanger is divided into small tubes, such that no cross mixing of the fluid is possible. The effectiveness is then based on the mixed mean temperature of the outlet fluid. A *mixed* fluid considers perfect cross mixing of the fluid in the heat-exchanger. Although this is not explicitly stated by Kays and London, this would imply that the outlet temperature was uniform. Observation of real systems demonstrates that reality lies near to these ideals, and hence, some uncertainty is inherent in the application of these assumptions to calculations relating to real systems.

Assignment of Fluid Mixing Conditions: In calculations of ε for crossflow arrangements, the application of the effectiveness calculation for one fluid mixed and the other unmixed is common. Kays and London depict a cross flow arrangement that allows the mixed fluid to pass over each of the unmixed fluid passages in series. A typical arrangement for a single row, finned, water-to-air heat-exchanger, is to have the mixed flow (air) perpendicular to the unmixed (water) where the mixed flow passes over the unmixed flow passages simultaneously. Evidently, there is a

difference. As the number of rows increases, the coil deepens and air flow passages become longer. It is arguable that the air flow is now unmixed also, although the plan view of the coil and fluid flow passages reflect that shown in Kays and London more closely.

Uncertainty can thus be evident in the application of the effectiveness calculation to a given system. Often the above coil configuration can be considered to be a counterflow arrangement. Holmes (1982) suggests a good approximation when the number of rows is equal to two or more. Stephan and Gruschka (1994) suggest four rows and above. The performance of the crossflow arrangement in relation to counterflow is poor. It is logical to assume, therefore, that the *true effectiveness* lies between these limits and since the effectiveness is operating condition dependent. Differential Composition can be applied to estimate this uncertainty. If we assume that the true effectiveness lies between the calculated effectiveness for crossflow and counterflow with 95% confidence, the mean of the two can be used as the best estimate of the true effectiveness.

Calculating the mean in this way requires either the water to be considered to be mixed and the air unmixed, or vice-versa. The largest difference generated between the calculated effectiveness' is the difference between counterflow and crossflow when the mixed stream is the stream with the maximum capacity rate as depicted in the upper left hand plot of Figure 5.5. The air-side capacity rate controls the heat transfer in these heat-exchanger systems. The largest difference will therefore be generated when the air-side is considered to be mixed.

The parameter values required (Holmes, 1982) for Equation 5.10 are given in Table 5.2. These values are typical of HVAC cooling coils and are used on the calculations to generate Figure 5.5. The upper right plot of Figure 5.5 shows the effectiveness uncertainty. The main feature is the large spike close to the origin which extends further, but is restricted by the plot mesh size. This is due to the increasing gradient of the relationship as it approaches zero N_{tu}. At the lower water flow rates, the heat transfer is controlled by the water mass flow rate, and hence the mixing of the streams relative to the maximum capacity rate changes and a different crossflow equation is used.

Table 5.2: Cooling Coil Parameter Values.

Parameter	Value	Units
r_a	0.596	$_{(\text{rows})}\text{Km}^2\text{s}^{\nu}\text{W}^{-1}\text{m}^{-\nu}$
r_w	0.217	$_{(\text{rows})}\text{Km}^2\text{s}^{\nu}\text{W}^{-1}\text{m}^{-\nu}$
R_m	0.286	$_{(\text{rows})}\text{m}^2\text{KW}^{-1}$
ν_a	-0.8	(-)
ν_w	-0.8	(-)
A_f	0.555	m^2
A_t	0.0023	m^2

The two lower plots on Figure 5.5 show the effectiveness and N_{tu} relationship with fluid mass flow rate when the water stream is considered unmixed and the air is considered mixed. The lower left plot demonstrates the mean effectiveness as a function of the fluid flow rates. The 'valley' is the obvious feature. Maximum theoretical performance occurs when $C_r \to 0$; conversely the poorest performance occurs when $C_r \to 1$. When two variable capacity rate fluids are considered, some combination of flow rates $\dot{C}_{min}$ and C_{max} will be applicable to the opposite fluid. This will occur when $C_r = 1$. The valley is a function of the capacity ratio line and gives the *minimum* effectiveness that will occur in that coil configuration. The last plot shows N_{tu} as a function of the flow rates. The plot points have been stopped just short of the zero-axes for clarity as $N_{tu} \to \infty$, the mass flow rates approach zero. This is a function of the dependence on the thermal resistances to the fluid velocities raised to a fractional negative power. Demonstrated also is the control of the heat transfer by the air-side flow rate.

5.3.2 UA Calculation

Two assumptions apply to the calculation of UA:

- the heat transfer process is driven by some notional overall temperature/enthalpy difference;
- the heat transfer is controlled by some notional overall heat transfer coefficient.

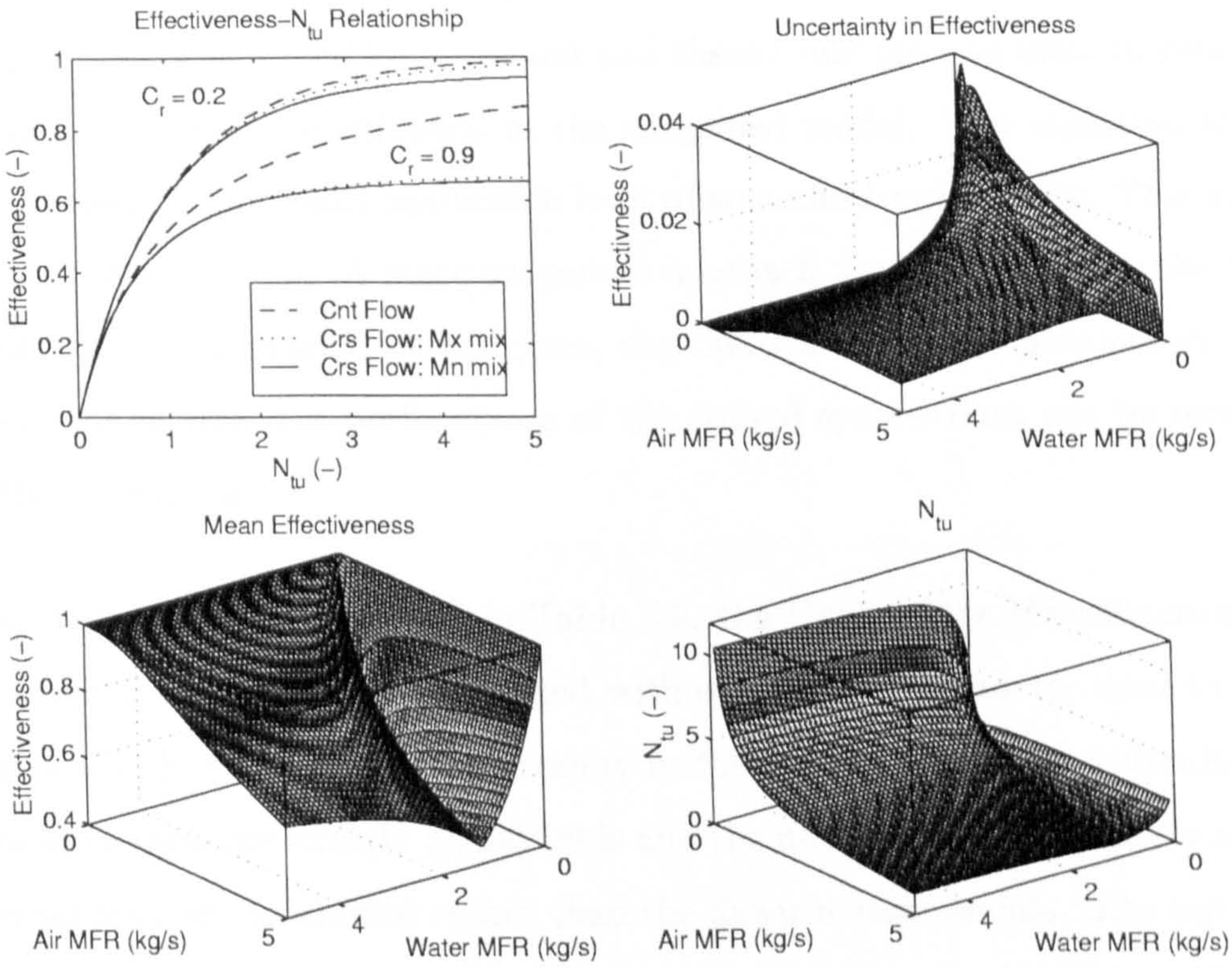

Figure 5.5: The ε-N_{tu} Relationship Characteristics.

In reality the temperature difference and heat transfer coefficient are complex, interrelated issues, which are highly dependent on fluid properties, flow and heat-exchanger geometry. In addition, fluid properties are not temperature independent. The heat transfer from the water to the air through the heat-exchanger matrix will be far from uniform.

The temperature difference and the heat transfer coefficient at a given condition can be viewed as means, about which there is some degree of uncertainty. However, a focal point for the uncertainty assessment is required and this involves the selection of model parameters. The parameters that are selected should be capable of representing the structural uncertainty over the operating conditions required. In the UA calculation, the structural uncertainty can be embodied in the resistance coefficients, since an estimation of the overall heat transfer coefficient for given temperature conditions is based on the total heat transferred, which is a function of both heat transfer coefficient and temperature difference. The uncertainty can be evaluated using the Differential Complexity approach. The heat transfer and the resistance to heat transfer for both fluid films and the wall material could be generated as an output from the detailed model at every evaluation

point for each position in the operating space. From that data, the average coefficients for each operating point could be evaluated and these could then be used to generate the flow dependent resistance coefficients in the simplified model. The variation about the mean would then be a globally applicable level of structural uncertainty. This approach, however, is time-consuming. A more pragmatic approach would be to apply the Absolute Range method. Using manufacturers' data, the thermal resistance parameters for heat-exchangers that 'bound' the performance of the desired system data can be used for the bases of the estimation.

Using the characteristic parameters in Table 5.2, the Uncertainty Magnification Factors (see Section 2.1.1 for definition) associated with each model parameter used to calculate UA are shown in Figure 5.6. The uncertainty in the number of rows and circuits is taken to be zero since these are exactly quantifiable and the uncertainty in the coil face area and tube internal area are considered rather than the linear measurements. The top left hand surface shows the mean effectiveness and is plotted on reverse axes for clarity. The air-side parameters and R_m generally increase in sensitivity with increasing mass flow rate. This is due to the powers controlling the denominator in the partial derivative calculations given in Equations 5.30 and 5.31,

$$U_r^2\left(\frac{\partial UA}{\partial r}\right) = U_r^2\left(\frac{-n_r A_f}{r^2 v^\nu}\right), \tag{5.30}$$

$$U_{R_m}^2\left(\frac{\partial UA}{\partial R_m}\right) = U_{R_m}^2\left(\frac{-n_r A_f}{R_m^2}\right), \tag{5.31}$$

$$U_\nu^2\left(\frac{\partial UA}{\partial \nu}\right) = U_\nu^2\left(\frac{-n_r A_f \ln v_a}{r^2 v^\nu}\right), \tag{5.32}$$

where U is the uncertainty. One additional feature on the plot for ν_a is the *zero crease* at $\dot{m}_a \approx 0.5\text{kgs}^{-1}$which is caused by the absolute nature of the uncertainty. Equation 5.32 yields a gradient that is positive and negative with respect to the operating space. This effect is reciprocated for ν_w also. The parameters associated with the waterside are most sensitive to parameter uncertainty when $\dot{C}_{min} = \dot{C}_w$. This is due to the crossflow equation that is used to describe the effectiveness when the minimum capacity rate is unmixed (the waterside). If either capacity rate is zero, $\dot{C}_{min} \to 0$ and $\text{N}_{tu} = \frac{UA}{\dot{C}_{min}} \to \text{N}_{tu_{max}}$ where $\text{N}_{tu_{max}} = f(R_m, A_f, n_r)$. These functions therefore have a finite response. In addition, when $\dot{C}_{min} = 0$, $\dot{C}_r = 0$ which results in $\varepsilon = 0$. In the crossflow equations this is because $\dot{C}_r$ controls the equation. The counterflow arrangement is controlled by N_{tu}. Under the same

Table 5.3: Physical Constants and Their Associated Uncertainty Variances.

Constant	Mean/Median	Units	95% Confidence
ρ_a	1.231	kgm^{-3}	0.040 (3.3%)
ρ_w	999.7	kgm^{-3}	0.599 (>0.1%)
C_{P_a}	1.018	$Jkg^{-1}K^{-1}$	0.011 (1.1%)
C_{P_w}	4.215	$Jkg^{-1}K^{-1}$	0.003 (>0.1%)

conditions, $\dot{C}_{min} = 0$ generates large values for N_{tu}, which raises e to a negative power in the numerator of Equation 5.9, thus giving $\epsilon = 0$. Each contribution to the uncertainty in the calculation of UA will be reduced in size by between 10% and 30%. The air-side parameters have a more global effect on the performance of the model, although at low flow rates ($< 2.0 kgs^{-1}$) the effect of the water-side parameters is at least equivalent to the air-side parameters.

5.3.3 Physical Constants

Tabulated physical constants are not published without a degree of uncertainty because they are the result of observations and some best estimate is used to derive the listed values. The Absolute Range method can be readily applied to these values to establish some level of uncertainty. Table 5.3 details the mean/median constant values and the associated confidence limits at the 95% level, based on data from Rogers and Mayhew (1988). Using these values, the uncertainty in the effectiveness calculation is demonstrated in Figure 5.7. The Figure shows the Uncertainty Percentage Contribution. The surface of the top right hand corner shows the 95% uncertainty interval over the operating space considered. The most striking feature is that the uncertainties in the constants associated with water flow are negligible. The uncertainty in the configuration assumptions is clearly dominant although the uncertainty in the density of air prevails as the air flow rate approaches zero. The density here has been used in the conversion of mass flow rate to velocity, demonstrating that even simple conversions can have a significant impact on the uncertainty in a result. Evident in all six plots is the *capacity ratio line* where the minimum capacity rate switches from the water stream to the air stream, using different crossflow effectiveness calculations as a result. One important conclusion is that for any model there will be some

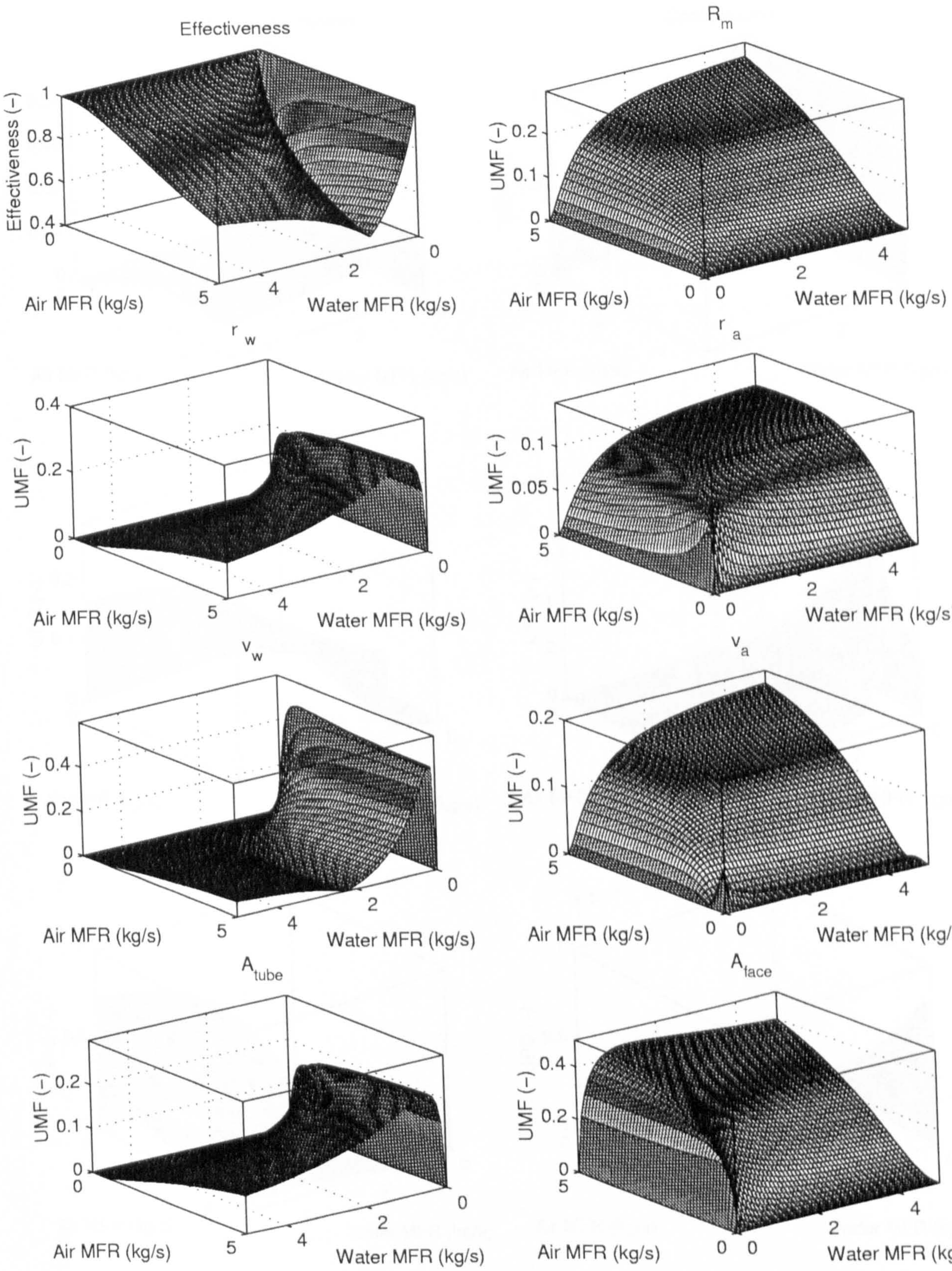

Figure 5.6: The Uncertainty Magnification Factors Associated with the Model Parameters.

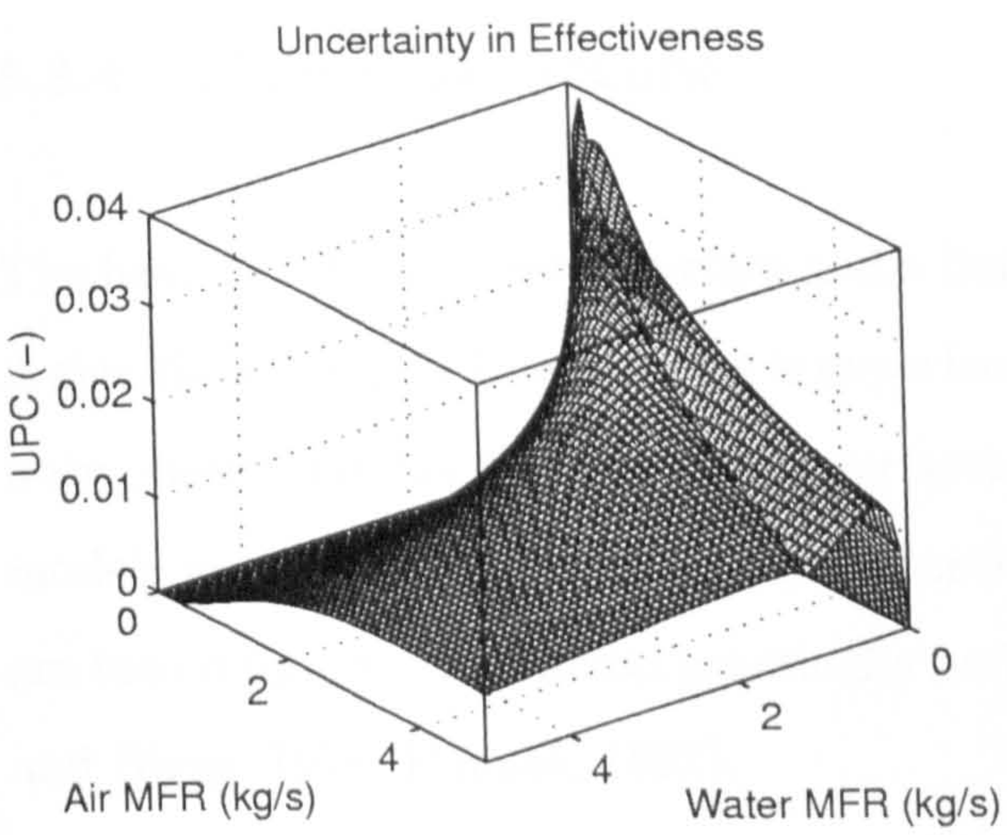

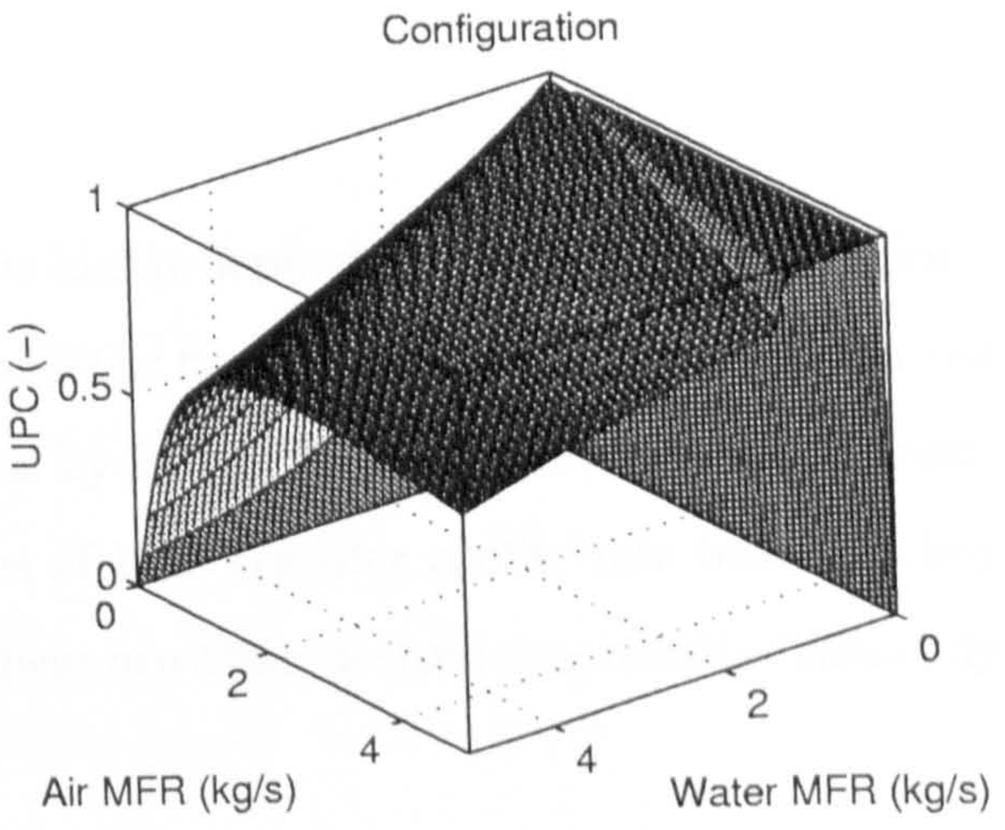

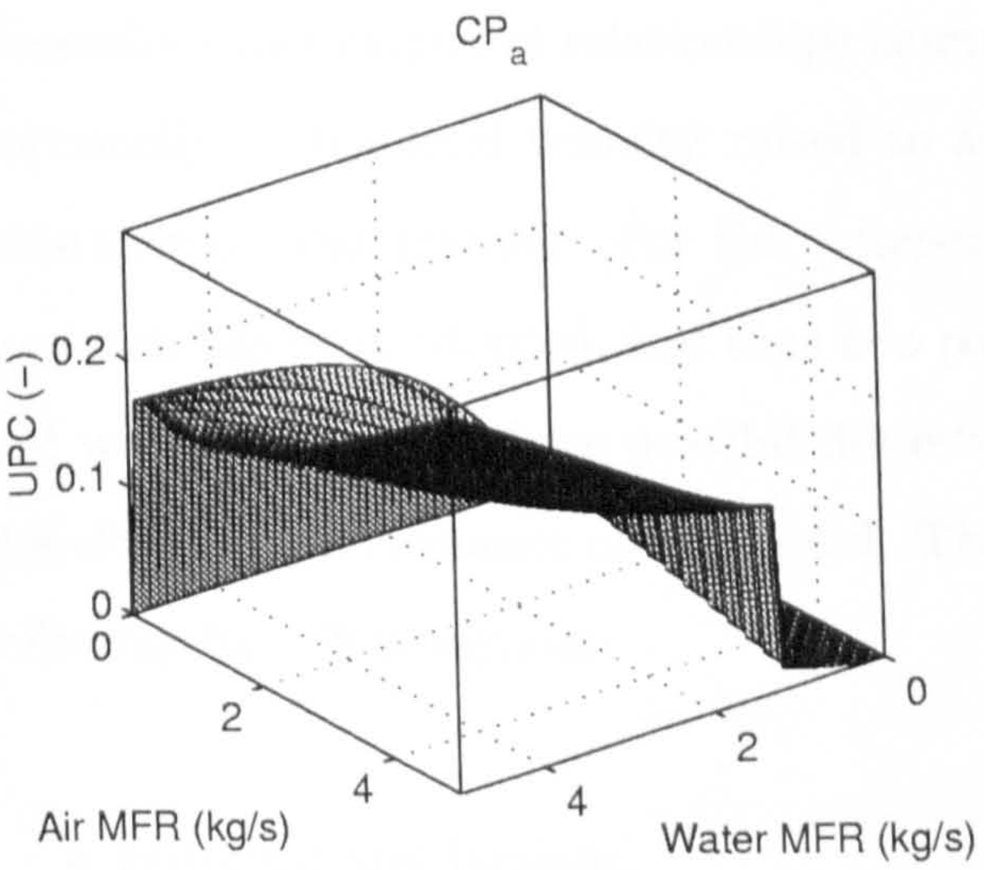

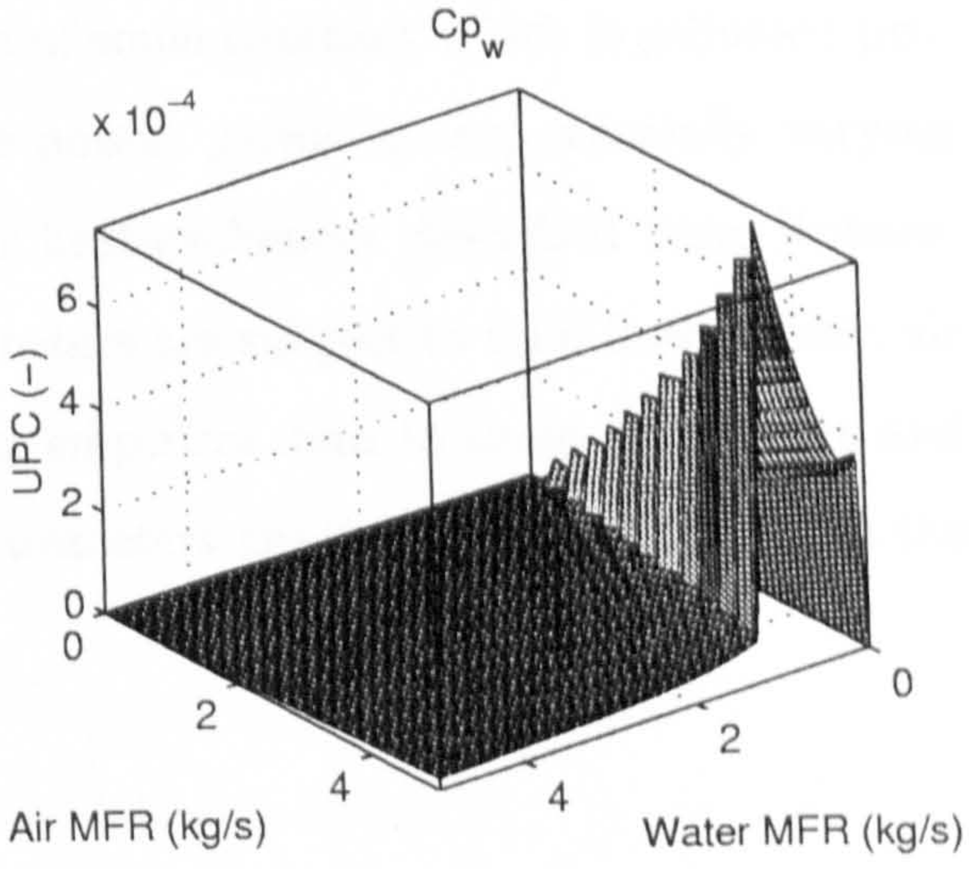

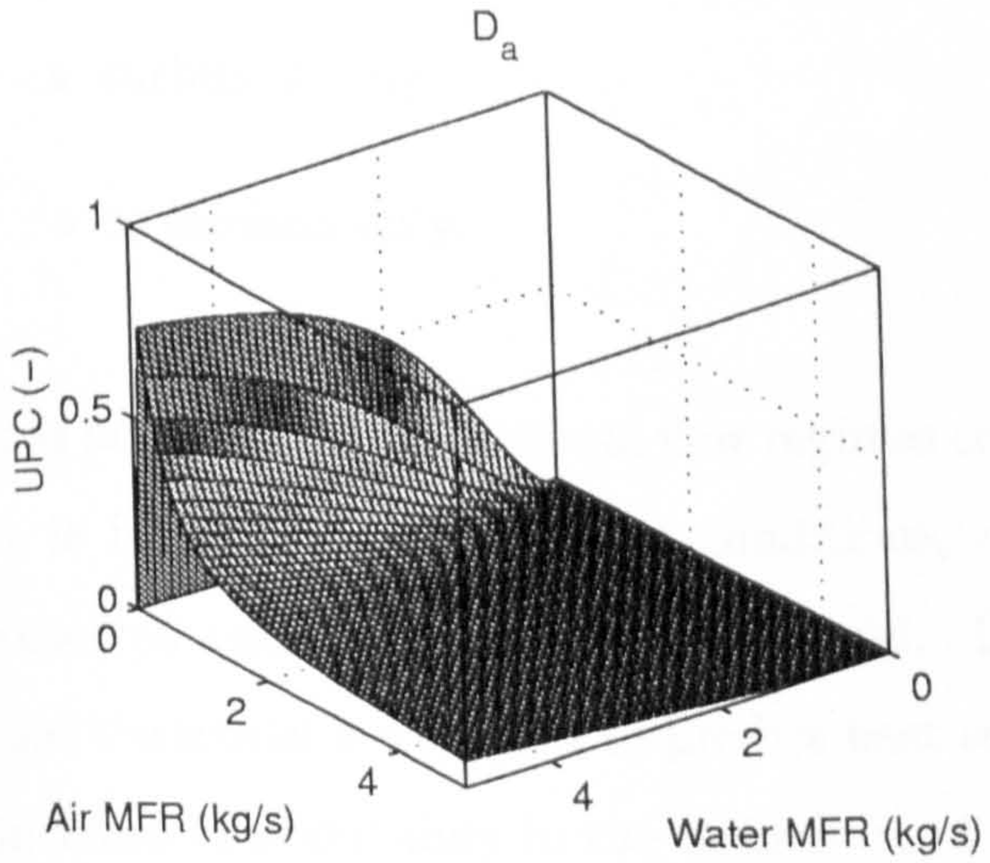

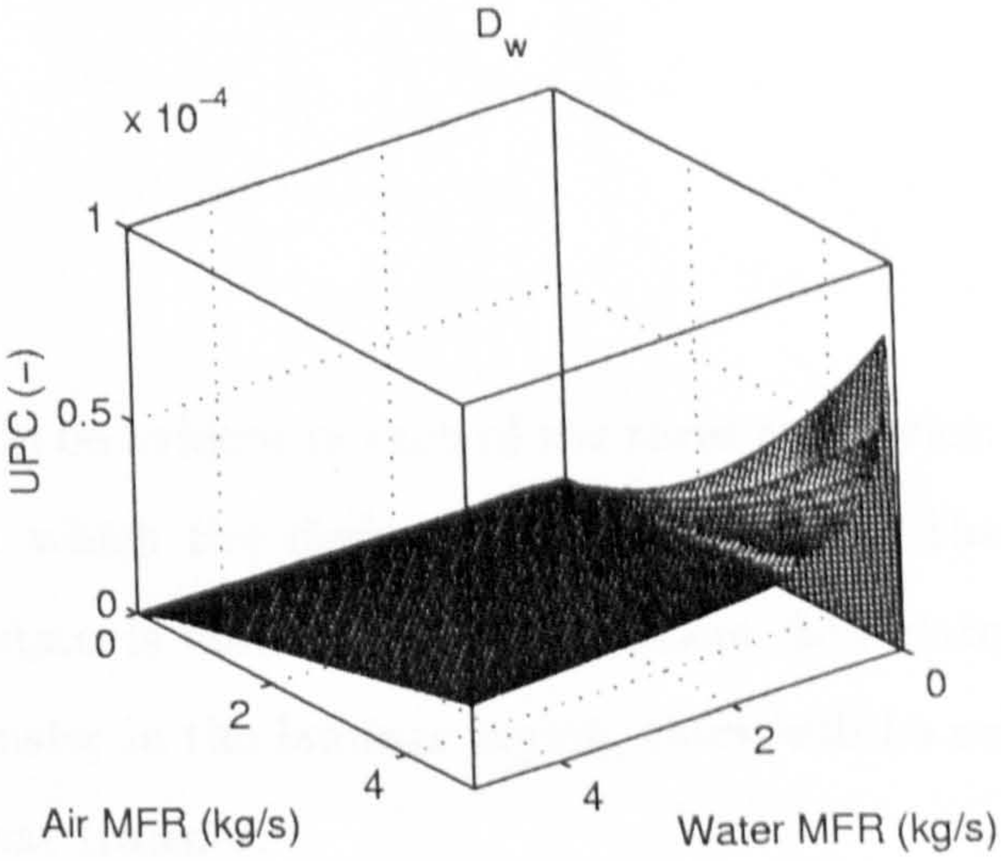

Figure 5.7: The Uncertainty Percentage Contributions to Uncertainty in the Effectiveness Calculation.

level of uncertainty introduced by the use of physical constants.

5.3.4 Fluid Flow Regime

The heat transfer between a surface and a fluid is highly dependent on the fluid flow regime. A significant drop in heat transfer is experienced if the flow is laminar. Evidence of this has been observed in HVAC heat-exchanger systems by Buswell et al. (1997). Heat exchanger models generally use simplified representations of heat transfer coefficients because they are too complicated to model practically and these are often derived empirically (Elmahdy and Biggs, 1979; Holmes, 1982).

Generally these empirical relationships comprise of some constant which is adjusted proportionally to the fluid velocity raised to some power, giving an exponentially varying resistance to heat transfer. For the water-to-air heat-exchanger described here, Holmes' approach has been adopted, and thus two parameters are subject to fluid flow regime; air and water. There are three possibilities relating empirical data to these parameters and therefore the performance of the model. The parameters are defined using data from the following fluid flow regimes:

- turbulent and laminar,
- turbulent only,
- or laminar only.

It is possible that transitional flow regimes could be evident in each of the three categories. It is important that the flow conditions, on which the derivation is based, cover the expected operating region of the model. If data is collected from turbulent flow data and the model is expected to predict heat transfer in the laminar region, there will be an increase in uncertainty in the estimation of heat transfer.

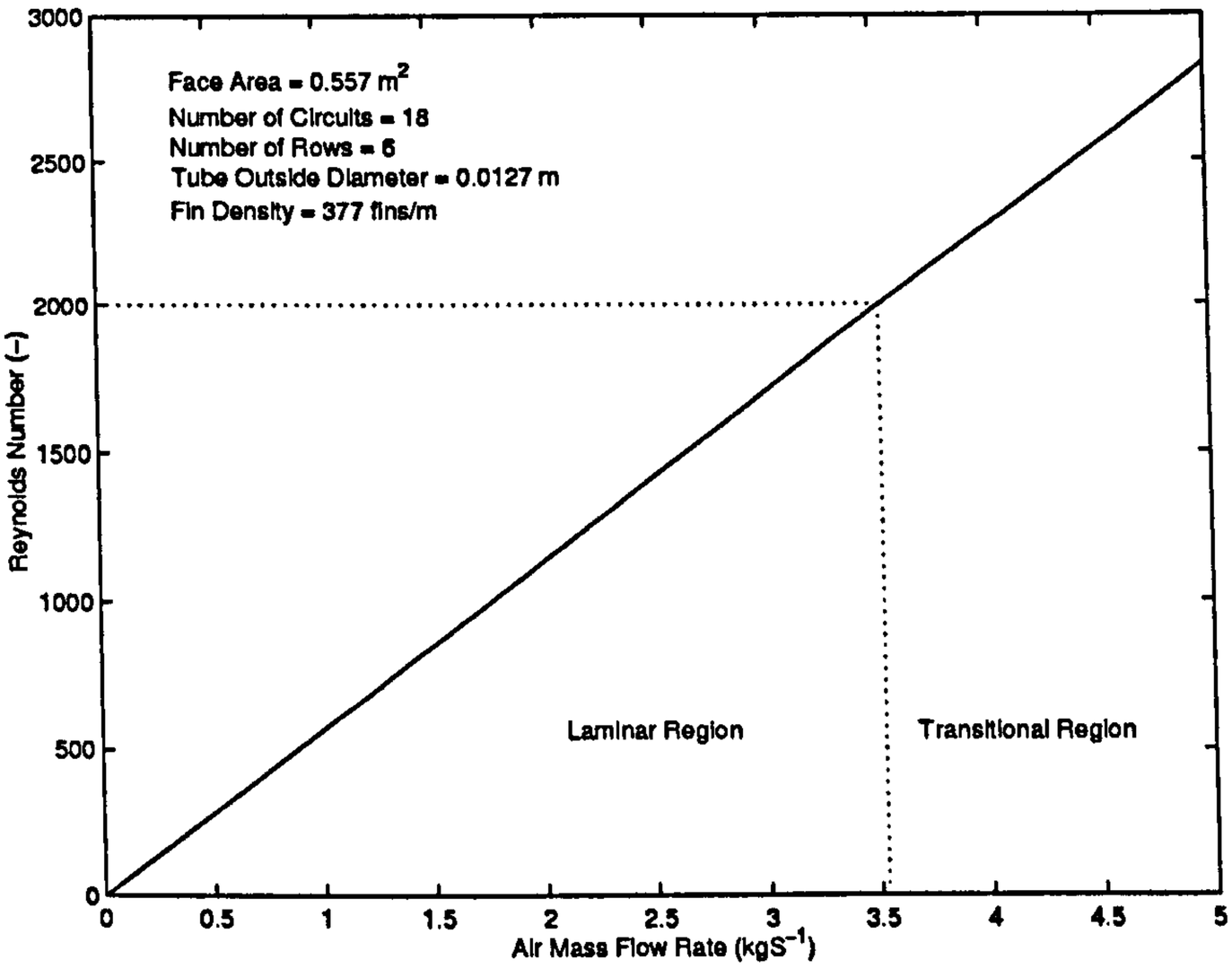

Figure 5.8: The Relationship Between Air Mass Flow Rate and Reynolds Number for a Typical HVAC Water-to-Air Heat Exchanger.

Air Side Heat Transfer

In typical applications of the water-to-air arrangement, the air-side controls the heat transfer rate. Assuming constant properties, Figure 5.8 demonstrates the air mass flow rate relationship with Reynolds Number[3] for a typical HVAC coil configuration. Clearly, for most HVAC applications, the air flow will be either in the laminar or transitional flow region, confirmed by Underwood (2000). It is reasonable to suppose that empirical relations for heat transfer derived for the application of such plant will cover this region, and so no additional uncertainty will be present in the model due to air flow regime.

Water Side Heat Transfer

Water side heat transfer in HVAC coils is often controlled through variable mass flow rate. This can mean that the coil will operate under laminar, transitional and turbulent flow regimes. For a typical coil the relationship between water mass flow rate and Reynolds

[3]The Reynolds Number is calculated on the basis of the free flow area and hydraulic diameter detailed in Threlkeld (1970) and used in the ASHRAE Secondary Toolkit Brandemuehl et al. (1993).

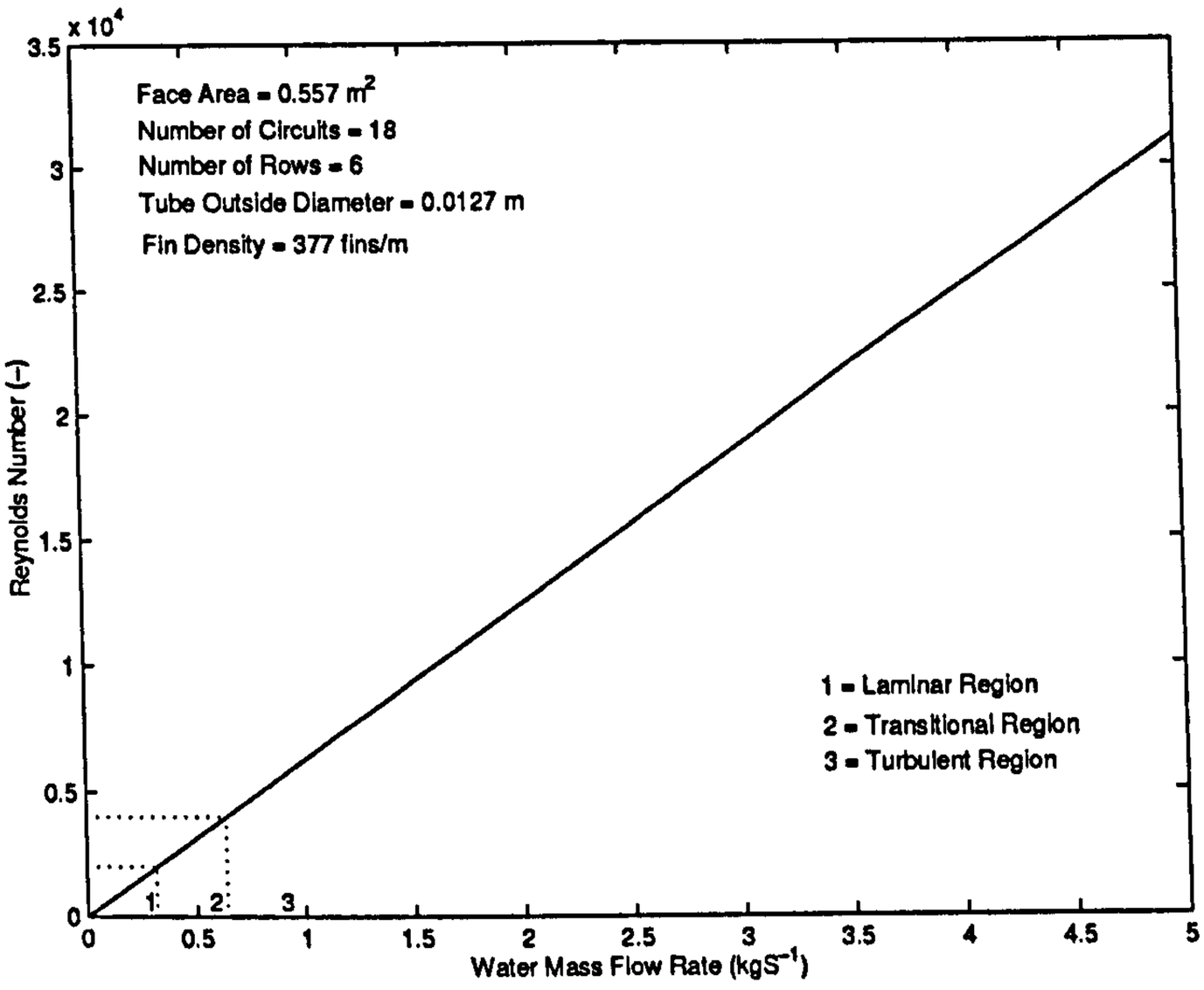

Figure 5.9: The Relationship Between Water Mass Flow Rate and Reynolds Number for a Typical HVAC Water-to-Air Heat Exchanger.

Number, assuming constant properties, is shown in Figure 5.9. If data from the laminar and transitional regions are included when the resistance parameters are defined, then no additional uncertainty due to the flow regime need be taken into account. If the data is from the turbulent region only, then there will be some additional uncertainty associated with the model predictions in the laminar region.

These can be accounted for by considering the total heat transferred. The model will over predict the heat transfer, and hence in the laminar region we can be 99.9% sure that the *true overall* heat transfer coefficient lies between the current prediction and zero. In the absence of more detailed information, it is reasonable to assume that the uncertainty is zero at zero heat transfer and at the boundary between turbulent and transitional region and is greatest at the laminar/transitional regions. The uncertainty is estimated over the region by calculating the velocity relating to the approximate laminar/transitional flow regime boundary. The total heat transfer at this velocity is calculated. This value becomes the 99.9% limit. Scaling assuming large sample statistics yields the 95% limit. Linear interpolation from: this value to zero at zero velocity; and this value to zero at the velocity that marks the transitional/turbulant boundary; yields the additional uncertainty over

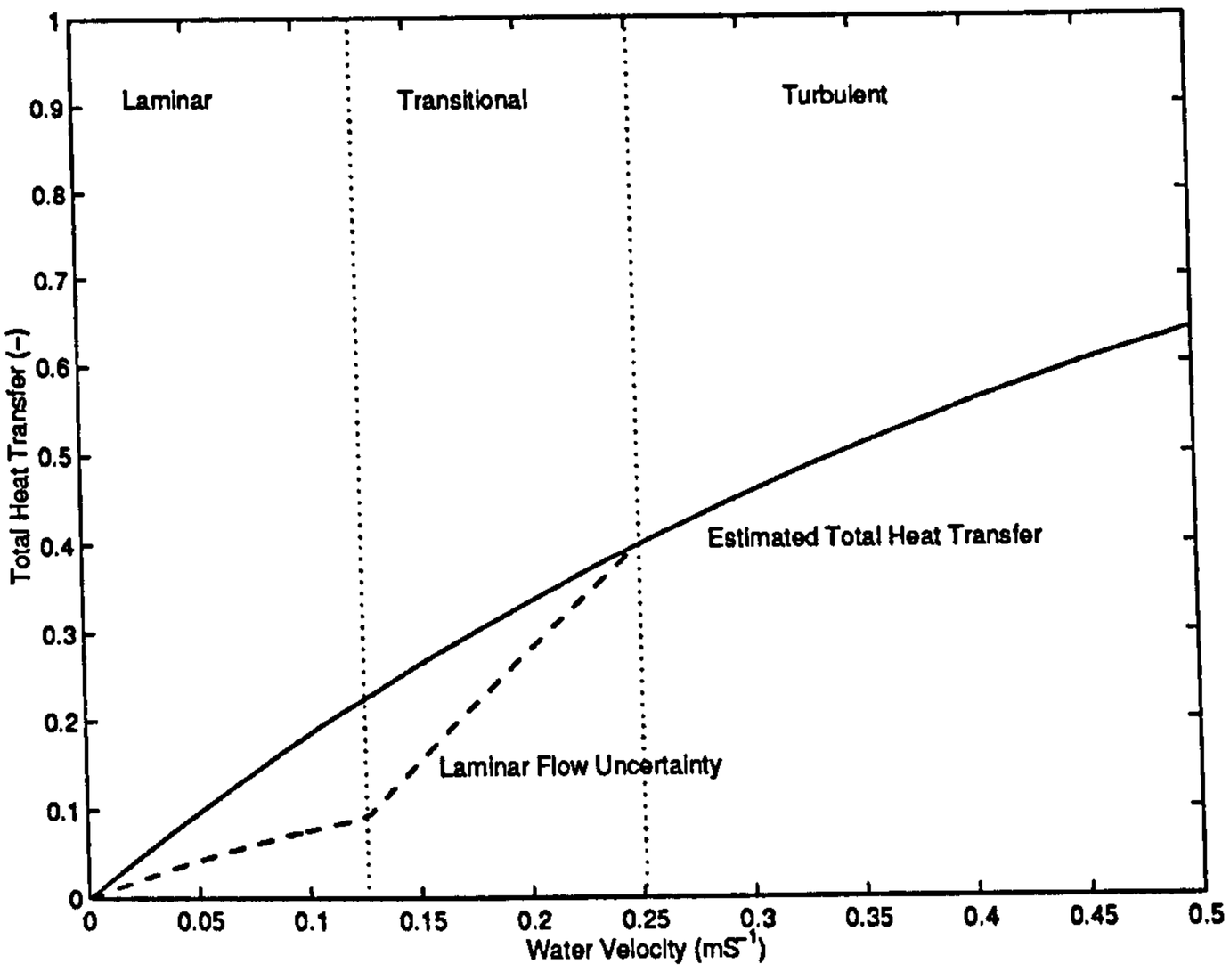

Figure 5.10: Demonstration of the Additional Uncertainty in the Total Heat Transfer That can be Associated With the Laminar Flow Region.

the laminar/transitional region. Figure 5.10 demonstrates the asymmetrical uncertainty envelope given by the approach. For a cooling coil operating with a maximum water mass flow rate of 2kgs^{-1}, the uncertainty region covers more than 25% of the operating region.

5.4 Uncertainty in Heat and Mass Transfer

The additional calculations associated with the computation of heat and mass transfer result in further uncertainty in the model. Initially, the presence of dehumidification affects the uncertainty in the UA and effectiveness calculations, discussed here in the first section. Additional uncertainties affecting the model output are then discussed in terms of the following:

- fully wet operation;
- partially wet operation;

- and iteration convergence.

5.4.1 Effect of Mass Transfer on Effectiveness

The uncertainty associated with the crossflow/counter flow assumptions is independent of the temperature difference between the water and air. However, as the air moisture content increases the effectiveness uncertainty is affected. Figure 5.11 shows plots of the mean effectiveness and effectiveness uncertainty for varying on coil air moisture contents with T_{wi} =6℃ and T_{ai} =35℃. Under wet conditions, the SHR effectively reduces the influence of the air-side capacity rate resulting in the minimum capacity rate being on the water-side for more of the operating range. This becomes more significant as the latent load on the coil increases. The effect on the mean effectiveness is to skew the capacity ratio line. This effect is also evident in the uncertainty plots, but more significant is how the uncertainty shifts as the duty increases. As the latent duty increases, the effectiveness exhibits an increase in uncertainty and then decreases at high duty. This would indicate that the crossflow/counter flow assumption is more precise at the extremes of operation. This is due to the dependence in the heat-exchanger characteristics on the C_r/N_{tu} relationship, depicted in the first plot of Figure 5.5. At lower values of C_r a larger difference exists between $\dot{C}_{min}$ and $\dot{C}_{max}$, which results in a smaller difference between the counter flow and cross flow heat-exchanger characteristics and hence less uncertainty. At the very high duties depicted in the g_{ai} =0.030kgkg$^{-1}_{air}$ plot of Figure 5.11, C_r is at a minimum, $\left(i.e.\ C_r = \frac{\dot{m}_a \cdot Cp_a \cdot SHR}{\dot{m}_w \cdot Cp_w} = \frac{5.0 \cdot 1.03 \cdot 0.3}{5.0 \cdot 4.12} \approx 0.12\right)$. It is the SHR that affects the uncertainty, by affecting the air-side more than the water-side, except where $g_{ai} \rightarrow$ 0.030kgkg$^{-1}_{air}$ when almost the entire operating space is affected to the same extent.

5.4.2 Fully Wet Operation

The air-side heat transfer often uses an estimation of fin efficiency to take account of various characteristics of the coil configuration. From Bayazitoglu and Ozisik (1988),

$$\eta = \frac{\tanh al_{fin}}{al_{fin}}, \tag{5.33}$$

$$al_{fin} = l_{fin}\sqrt{\frac{2\kappa}{kl_t}}, \tag{5.34}$$

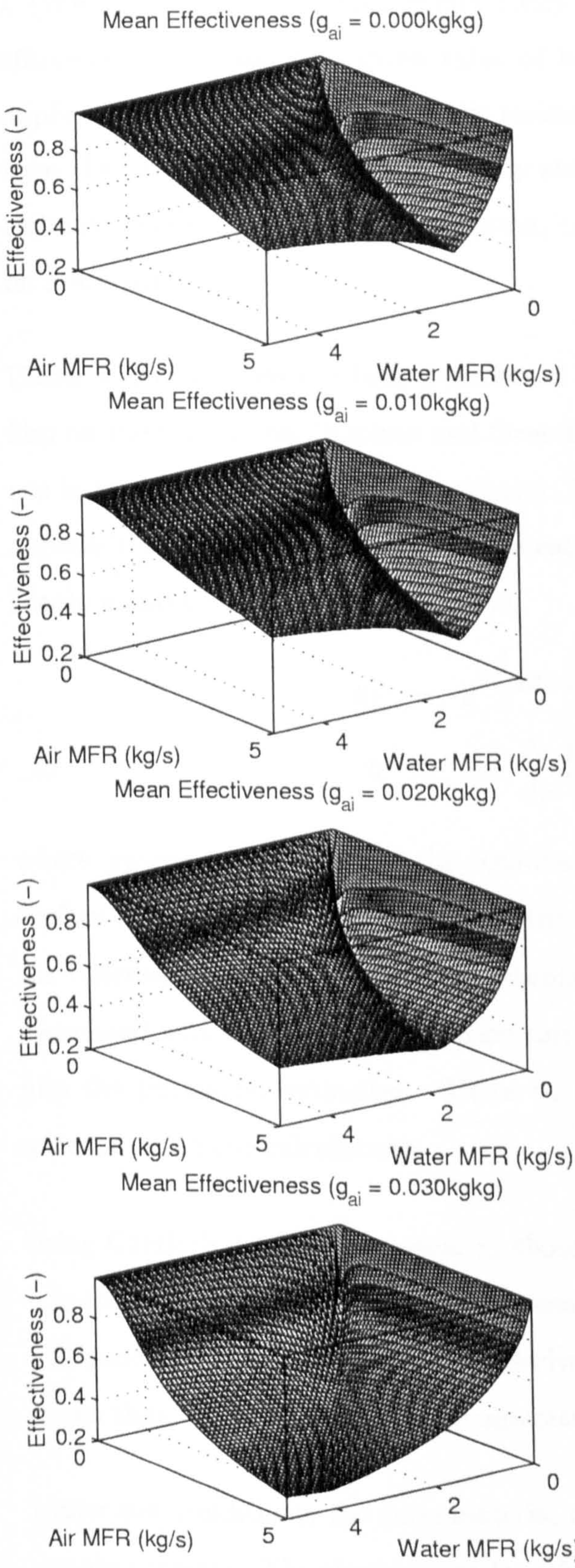

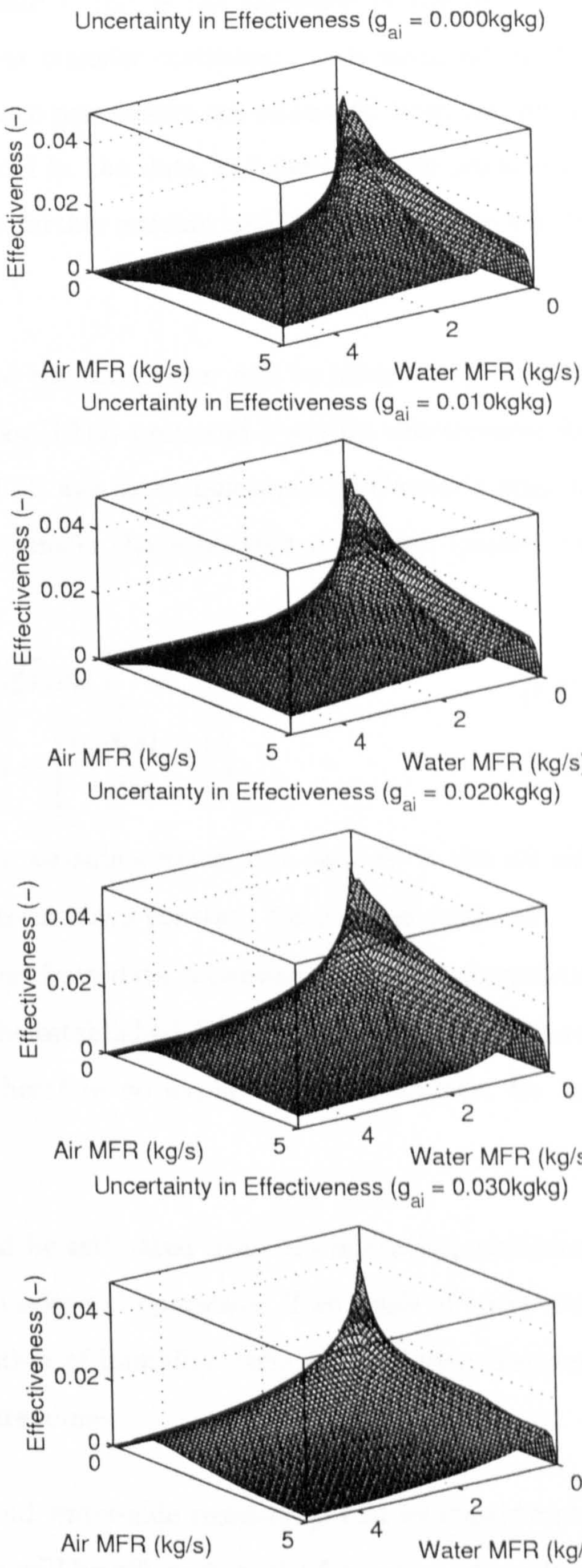

Figure 5.11: The Mean Effectiveness and Effectiveness Uncertainty for Varying on Coil Air Moisture Contents with T_{wi} =6℃ and T_{ai} =35℃.

where κ ($\mathrm{WK^{-1}m^{-2}}$) is the heat transfer coefficient, l_{fin} (m) is the length of the fin, k ($\mathrm{WK^{-1}m^{-1}}$) is the thermal conductivity and l_t (m) is the thickness of the fin. The efficiency is constant for a given value of heat transfer coefficient. It is assumed in the application of these models that if the resistance parameters are estimated from real data, then the fin efficiency will be implicitly stored in the data and hence in the parameter estimate. Since the correction is constant, no further account need be taken of the effects on a dry coil.

Under wet conditions the heat transferred to the air stream will be affected by a water film on the fin surface. Stephan and Gruschka (1994) proposed a wet fin effectiveness for use in the calculation of the bypass factor. This was an enhancement of Carrier's original approach which assumed no change in heat transfer characteristics under wet conditions. Stephan and Gruschka's proposal gave,

$$b_f = e^{-\left(\frac{n_r A_f \eta}{SHR\, r_a v_a^{\nu} \dot{m}_a C_{pa}}\right)}, \tag{5.35}$$

$$\eta = 1 - \frac{A_s}{A_o}\left(1 - \left[\frac{\tanh a l_{fin}}{a l_{fin}}\right]\right), \tag{5.36}$$

where $\frac{1}{SHR r_a v_a^{\nu}} = h_{wet}$, A_s is the secondary air-side surface area and A_o is the air-side surface area. As for the dry coil case the term stays constant for a given resistance. If the resistance parameters are to be estimated from data, however, then the uncertainties associated with dry and wet operation can be established from the data and incorporated into the parameter estimates. There is, therefore no explicit need to account for this uncertainty in the calculations.

Using Carrier's original approach, r_a should be estimated from dry operating conditions. It is then the uncertainty that will increase under wet operation. Two levels of uncertainty will almost certainly exist since the derivation of humidity ratio requires more measurements than the consideration of temperature alone.

Under wet conditions, the tube material and water-side resistances can be considered to remain constant. The air-side heat transfer will be affected by the formation of condensation. A change in the value of r_a under wet conditions is not appropriate with the use of Carriers bypass factor, however, the uncertainty about r_a can be adjusted to account for the uncertainty in the predictions under wet conditions. This can be achieved by using

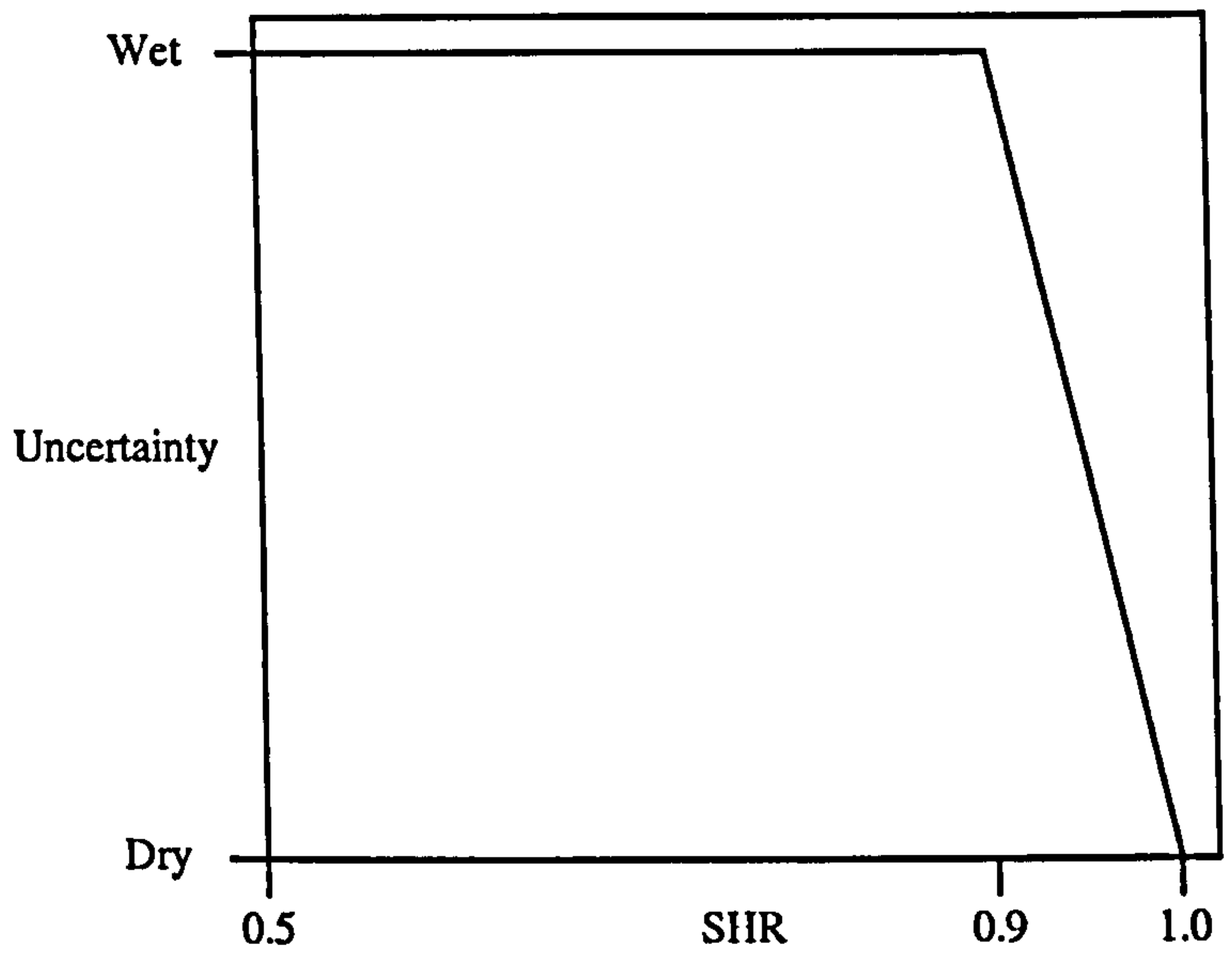

Figure 5.12: Demonstration of the Uncertainty Associated with r_a in Wet and Dry Operation.

the wet and dry data set to re-estimate the uncertainty, but not the value of, r_a. The process can therefore be described by three stages:

1. by using a range of dry coil operating conditions to establish r_a, R_m and r_w,

2. generating the parametric uncertainty intervals from the differences between the model predictions and the data,

3. using a range of fully wet operating conditions and generate differences between the model predictions and re-estimate the uncertainty about r_a with the wet *and* dry data sets.

If it is possible to carry out sufficient tests it would be possible to generate an uncertainty profile over partially wet conditions. Since this is not usually practicable, an approximation can be applied under the assumption that the uncertainty varies linearly across the partially wet condition, as Figure 5.12 demonstrates. Where it is not practicable to carry out the extensive data collection required by the above approach, the data can be collected under wet or partially wet conditions only. The uncertainty in r_a of the same coil under dry conditions will be less.

5.4.3 Partially Wet Operation

Braun et al. (1989) used Differential Complexity to derive an estimate of the uncertainty in the heat transfer under partially wet conditions. In the study, a detailed finite element model of a cooling coil was compared to the simpler effectiveness relationship to evaluate the error in the estimated total heat transfer generated by assuming the coil was either all wet or all dry. The detailed model determined the location along the air path where condensation begins. The longitudinal temperature gradient will approximate to counter-flow where there are many passes of the water stream along the air stream. The surface temperature will also vary in the transverse direction and so conceivably wet and dry sections could occur in this plane as well in the air flow plane. Braun found that predictions assuming that a partially wet coil was either all wet or all dry could generally be made within 5% of the total heat transfer.

The coil was assumed to be completely wet if the surface temperature determined by the dry analysis was less than the outlet air dew point temperature. If the surface temperature at the air inlet determined with the wet analysis, is greater than the air entering dew point temperature, the coil is partially wet. The selection of the largest total heat transfer is selected. This knowledge can be applied to the SHR approach. An SHR of 1.0 describes a dry coil. Carrier suggests that coils may be considered all wet if SHR < 0.9. The 5% uncertainty can therefore be applied to this 10% band. Figure 5.13 demonstrates the application.

5.4.4 Iteration Convergence

Equations 5.12 through to 5.29 require iteration to yield a solution when the coil is operating under wet conditions. This iteration solution is based on the convergence of successive estimations of total heat transferred to within a preset criterion[4]. There are two issues that effect uncertainty in the model:

- the convergence criterion implicitly generates uncertainty in the output prediction;

[4]See Appendix A for discussion on the solution of heat-exchanger calculations.

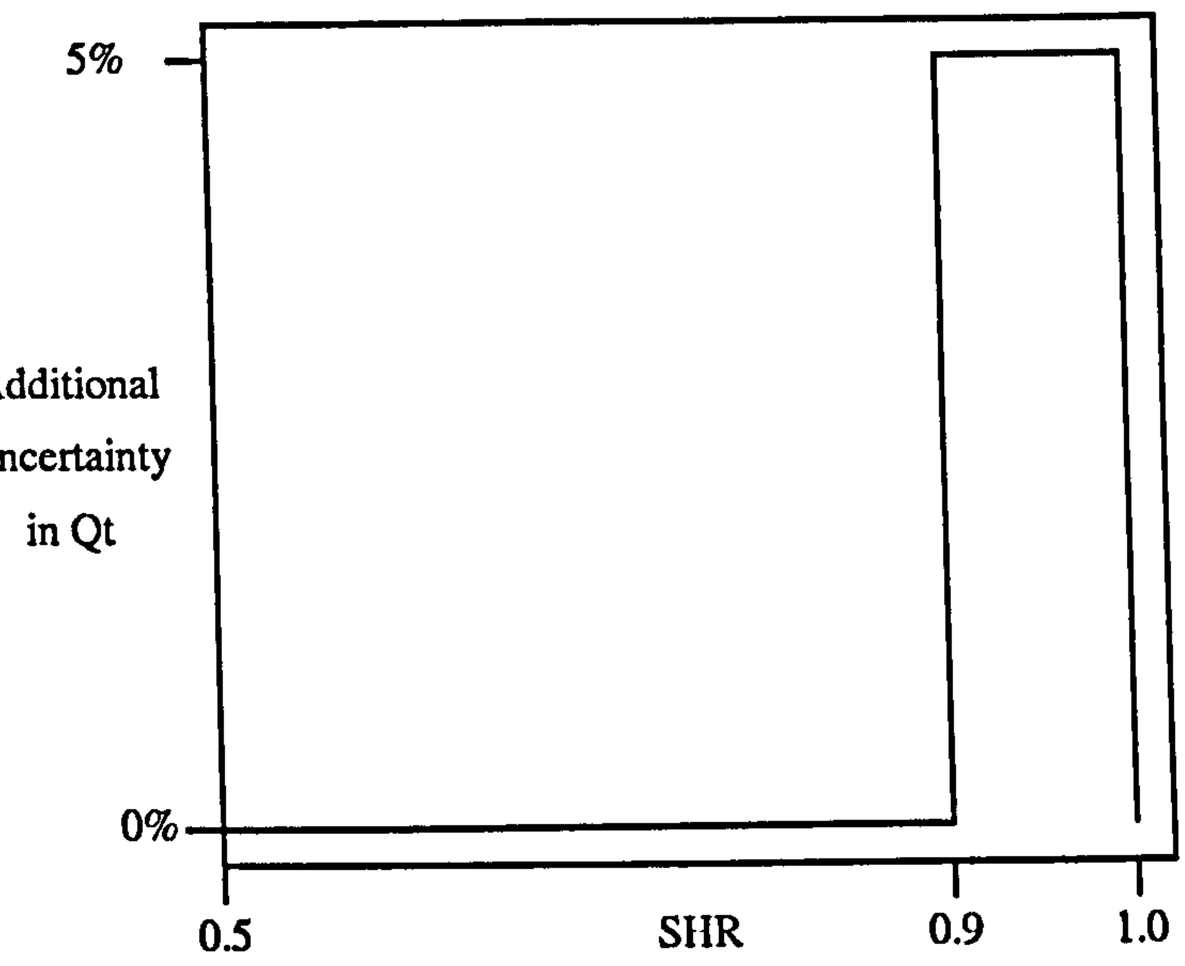

Figure 5.13: Demonstration of the Uncertainty Associated with the Prediction of Q_t Under Partially Wet Operation.

- the numerical calculation of the uncertainty sensitivity coefficients is complicated by the iterative procedure.

The convergence criterion affects the number of iterations required to achieve the solution. On this basis, uncertainty analysis can be used to formally set the criterion, rather than basing it purely on judgement. The uncertainty in the subject of the successive substitution is equivalent to the band set by the criterion. The contributions to the uncertainty in the subject can be evaluated over the whole range of operating conditions setting the convergence criterion to a level where it just becomes insignificant. This then will give the minimum number of iterations with no significant increase in uncertainty in the output.

Some degree of uncertainty needs to be established against which the insignificance of the convergence criterion can be measured. The structural uncertainty associated with the counter flow/crossflow relationship is directly calculable and always present in the model output. Since the uncertainty is not dependent on external factors and that any subsequent uncertainty, from measurements etc., will only serve to increase the overall uncertainty, this fulfills the criteria for comparison. The total uncertainty is given by,

$$U_t = \sqrt{U_{EMS}^2 + \left(\frac{\partial \varepsilon}{\partial Q_t} \cdot U_{CC}\right)^2}$$

Where U_{EMS} is the uncertainty in the effectiveness model structure and U_{CC} is the uncertainty in the convergence criterion.

Using Uncertainty Percentage Contributions, UPCs, for the CC and EMS, the source effects can be compared in the total uncertainty in the mean effectiveness. The EMS does not require differencing for calculation; $UPC_{EMS} = \frac{U_{EMS}^2}{U_t^2}$. However, the CC uncertainty affects Q_t which does require a sensitivity coefficient in the calculation; $UPC_{CC} = \frac{\partial \varepsilon}{\partial Q_t} \cdot \frac{U_{CC}^2}{U_t^2}$. Generating an approximation to the first derivative numerically, needs the selection of a differencing interval and requires a non-iterative solution for ε with Q_t as the governing input. It can be shown that once convergence on a value for Q_t has been established, the following iteration is closer to the solution. Using the converged value of Q_t, the iteration is carried out once more gaining Q_t^1 and again using $Q_t + \delta$ (where δ is the differencing interval) as the input yielding Q_t^2. The local sensitivity coefficient is then calculated by $\frac{Q_t^2 - Q_t^1}{\delta}$. It should be noted that the differencing interval and the convergence criterion are not interdependent under this regime.

Selection of the Convergence Criterion

Using the inputs T_{wi} =6℃, 0.5kgs^{-1}< $\dot{m}_a$ < 5.0kgs^{-1}, 0.5kgs^{-1}< $\dot{m}_w$ < 5.0kgs^{-1}(both in 0.5kgs^{-1}steps), 0.006kgkg$_{air}^{-1}$< g_{ai} < 0.030kgkg$_{air}^{-1}$and 7℃< T_{ai} < 35℃, a set of inlet conditions that represented the operating region most sensitive to uncertainty in Q_t was selected (T_{ai} =7℃ and g_{ai} = 0.006kgkg$_{air}^{-1}$). The convergence criterion was exercised in nine steps from 30% to 0.05%, and the normalised total number of iterations and mean squared error was used to establish the approximate optimum value of convergence criterion. Figure 5.14 shows this optimum value, with < 4.6% at a total of 190 iterations, compared against an arbitrary level selected for use in previous work (Buswell and Wright, 1998; Norford et al., 2000), < 0.005% at 1774 iterations and the preferred level of < 0.1% at 660 iterations. The preferred level sacrifices some computational effort to achieve insignificance in the effect of the uncertainty in Q_t in the uncertainty in ε. There are, however,

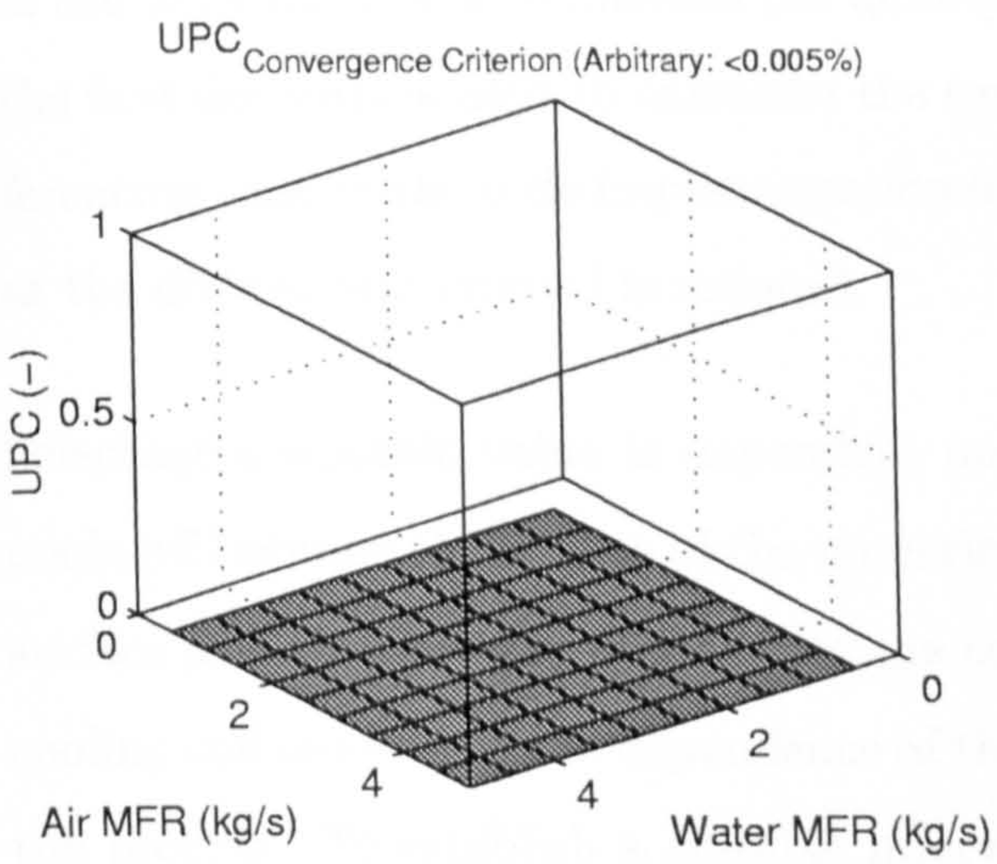

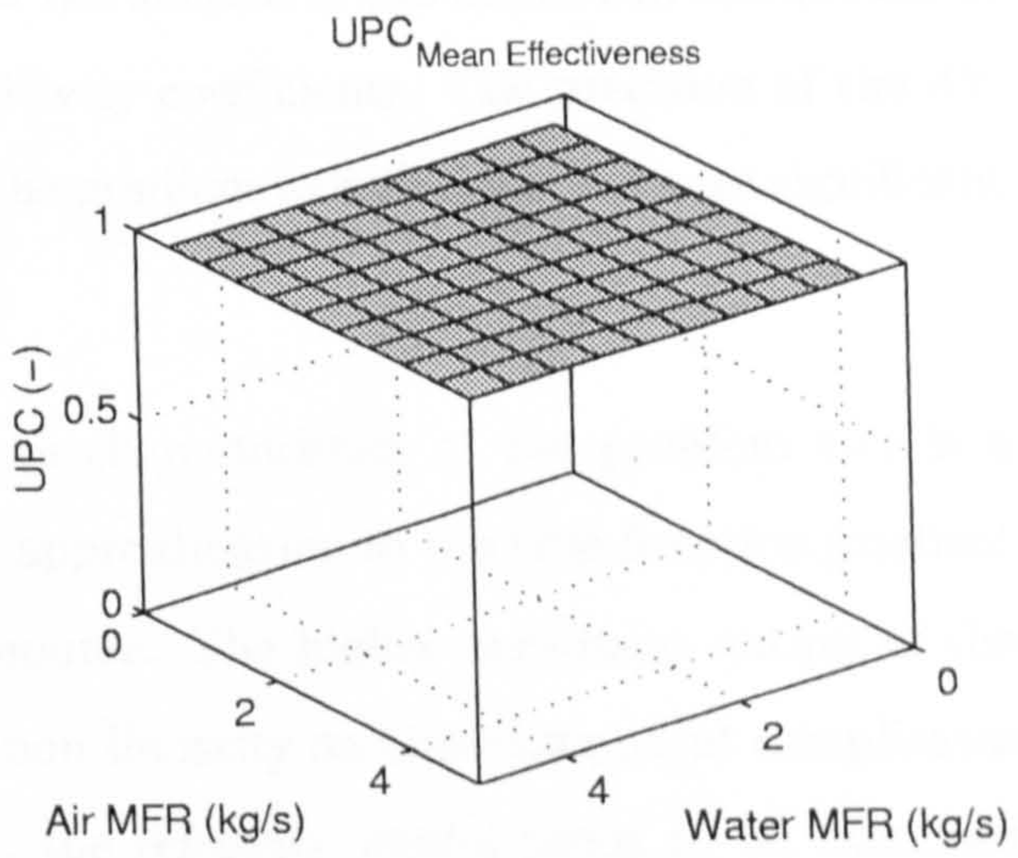

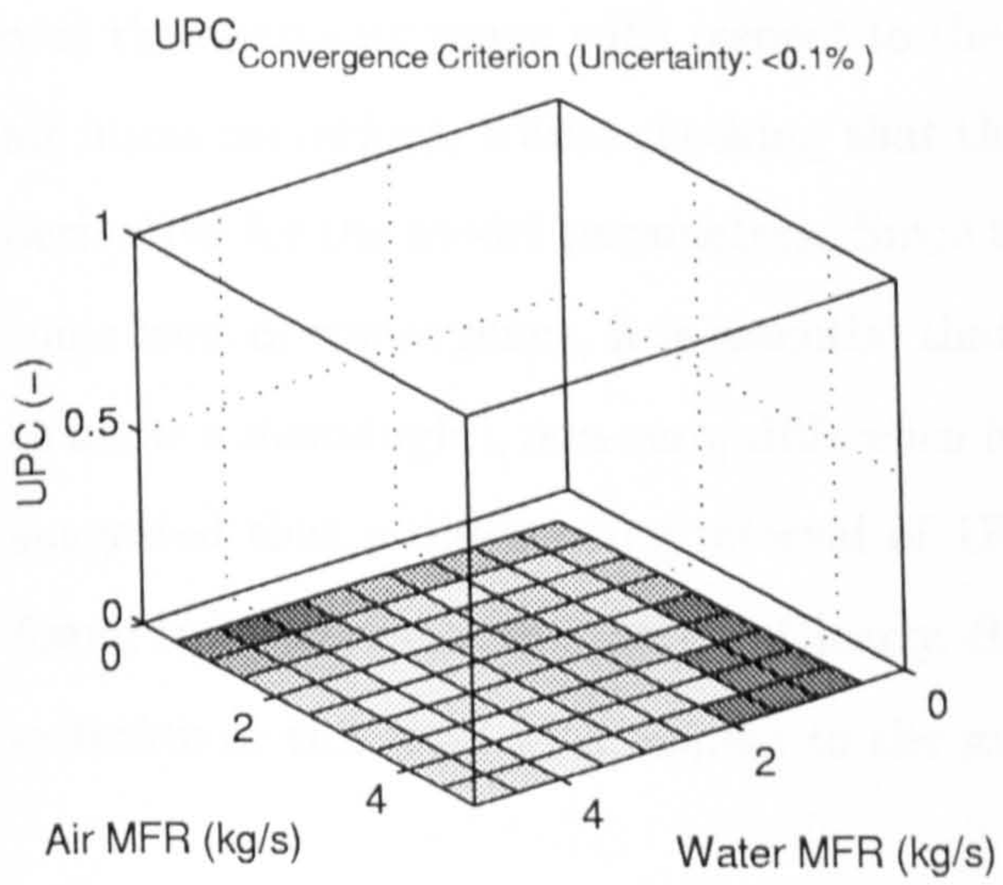

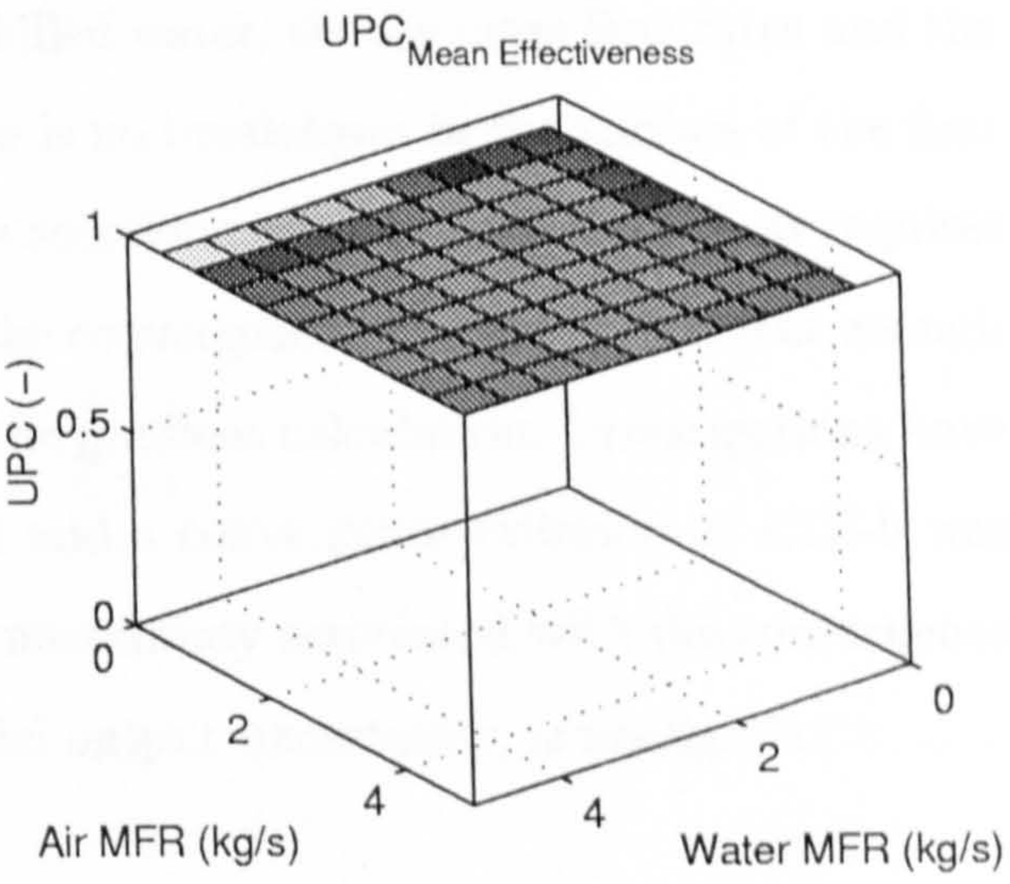

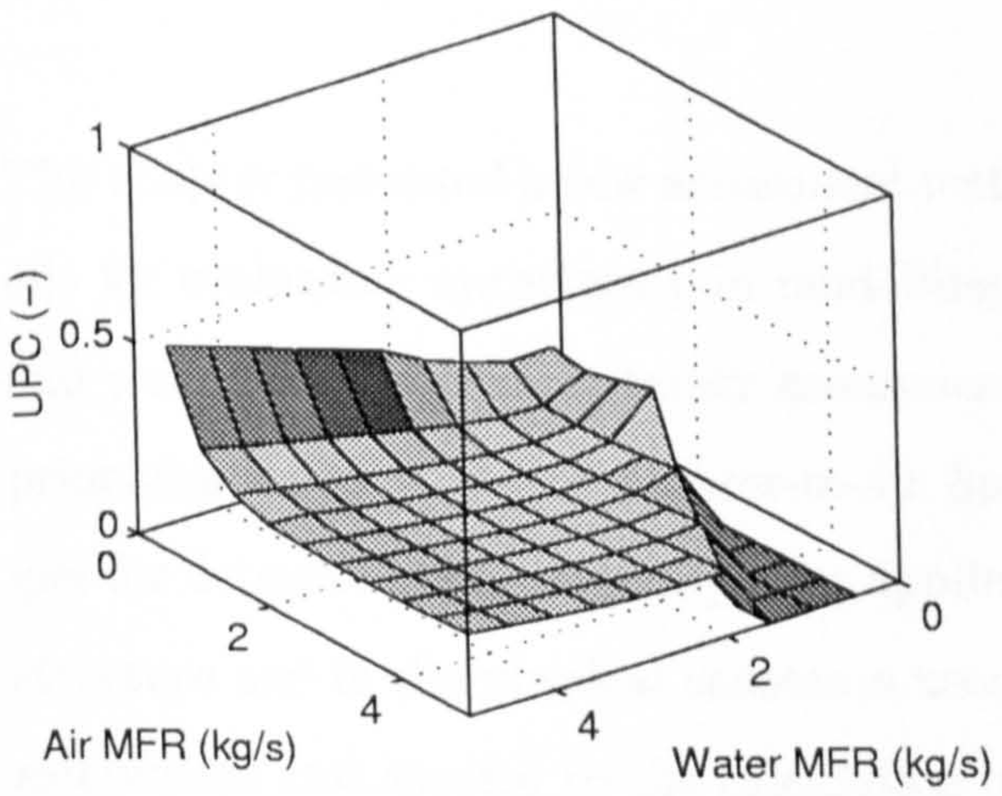

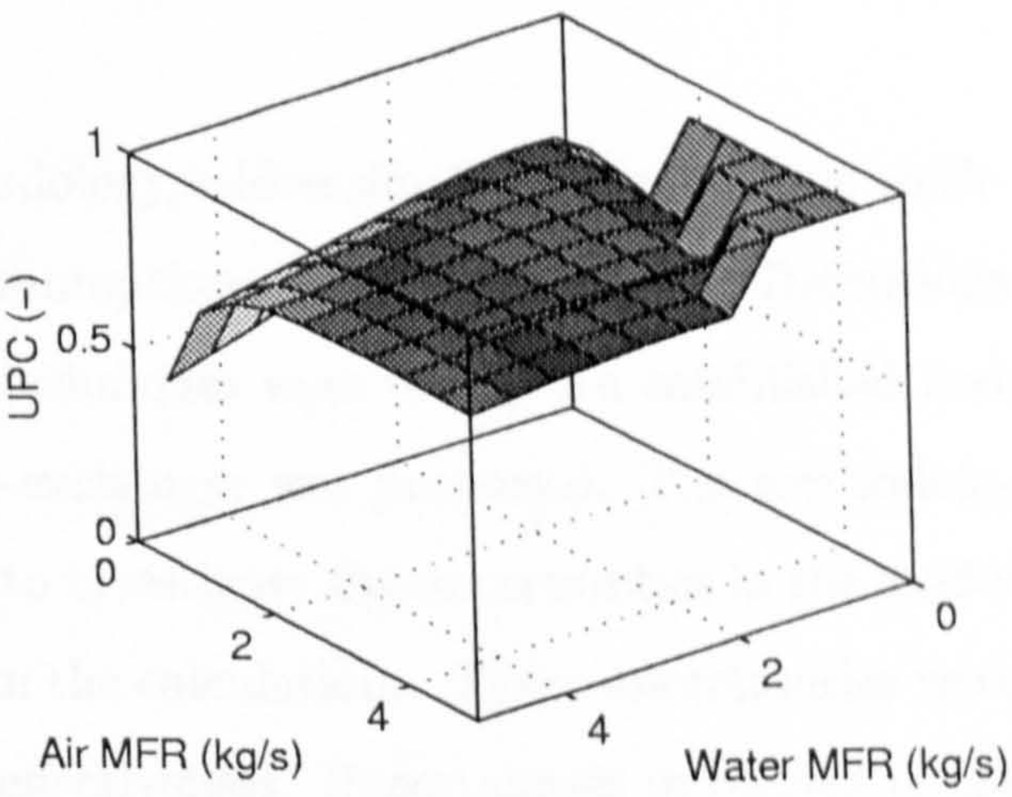

Figure 5.14: The Effect of the Uncertainty in the Convergence Criterion About Q_t on Effectiveness Uncertainty.

additional considerations for the convergence criterion. The accuracy of the convergence of the iterative process influences the quality of the surface of the numerical calculation of the first derivatives used to calculate the sensitivity coefficients. The precision of the differencing used in the code implementation of the gradient calculations becomes significant as the differencing interval is reduced.

Selecting a suitable value is dependent on the characteristics of the problem and is a trade-off between the quality of the numerical approximation to the true function gradient surface and the machine precision of the computer. The highly non-linear nature of the cooling coil model and the dependence of the non-linearity on operating point complicates the process. To establish a suitable interval, the reference model needs to be exercised over the operating range with respect to the chilled water, the air mass flow rates and the air input conditions, whilst checking that there is no breakdown in the surface of the first derivative for the model parameters. Since the solution under wet coil conditions requires some level of convergence, it is essential that the convergence criterion is stringent enough to allow a meaningful, non-zero, difference in the gradient calculation. Investigations have suggested that a differencing interval of 1E-4 and a convergence criterion of <1E-9 was found to be workable in practice. Clearly, the uncertainty associated with the convergence criterion at this level with respect to the model output uncertainty, is negligible.

5.5 Conclusions

This chapter presented a new assessment methodology, addressing the current lack of methods for evaluating uncertainty in modelling assumptions and simplifications. Definitions and classifications of uncertainty assessment techniques were listed. An established first principles based model of a water-to-air heat-exchanger was presented. The methodologies for determining uncertainty were applied to investigate the uncertainties in the model structure and in the physical constants used in the calculations. These uncertainties were established and applied to the calculation of effectiveness. Uncertainties in respect of the model parameters and the implications of their derivation from data were introduced and these are extended in Section 7.2. Specific Comments are:

- four methods of uncertainty evaluation were defined as, Empirical Quantification, Differential Complexity, Absolute Range and Differential Composition;

- it was established that to apply structural uncertainty to a model requires the uncertainty effects to be numerically realisable and that the uncertainty can be described by variance;

- it was established that uncertainty exists in the calculation of effectiveness because this class of heat-exchanger falls between the cross flow and counter flow definitions that are used to construct the model;

- there is uncertainty in the UA calculation induced through the overall approximations for temperature/enthalpy difference and heat transfer coefficients;

- the investigation showed that there will always be some influence from the uncertainty in the physical constants (demonstrated in Section 7.3);

- it was established that uncertainty due to the flow regime on the air side of the coil will be negligible since HVAC coils operate predominantly in the laminar flow region;

- the water side flow regime is more involved and it was argued that if data used to identify the resistance parameters for a specific coil were taken from the whole range of likely mass flow rates, then the uncertainty would be implicit in the uncertainty in the parameter estimates (introduced through the data) and no further uncertainty measures need be taken;

- a similar statement is also true for the uncertainty in the air side resistance coefficients due to the effect of water on the coil surface under partially or fully wet operating conditions;

- uncertainty in the heat transfer due to partially wet conditions was accounted for by applying an established level of uncertainty to this region;

- it was demonstrated how uncertainty can be used as a formal criterion for the selection of internal iteration convergence in models. It was however, demonstrated that where differencing is employed, numerical stability becomes the critical issue, often leading to insignificant uncertainty in the convergence criterion.

The significance of the level of uncertainty present in the model structure is inevitably dependent on the application of the model. Uncertainties in the variables and in estimated model parameters contribute also to the uncertainty in the model prediction. Section 7.3 demonstrates the significance of model structural uncertainty in terms of a condition monitoring scheme applied to a HVAC cooling coil.

Chapter 6

Test System Validation

This chapter describes the configuration and characteristics of the system used to demonstrate the uncertainty in condition monitoring presented in Chapter 7. The description focuses on the cooling coil (and adjacent sections). The system performance was studied over a twelve month period, monitoring three periods exemplifying summer, winter and spring operation.

The measurements used in the analysis in Chapter 7 require validation. The calibration/validation of sensors in their natural[1] environment is desirable. It allows the observation of operational characteristics that may influence the measurements. Although there has been some work developing *in situ* performance testing techniques in HVAC equipment (Phelan et al., 1997a), there are no *in situ* sensor validation methods reported in the literature to date. Accordingly, a new methodology is proposed. The methodology is applied to data collected from the test system. The principal aims are to remove persistent bias in the measurements, thus reducing the uncertainty in subsequent calculations. Sensor offsets applicable to the critical measurements for the condition monitoring scheme described in Section 7.1 are established for the test system.

[1]The term 'natural' is used here to describe the locations of the sensors used in the normal control of the system.

6.1 Test System Description

The experimental programme was conducted at the Energy Resource Station (ERS), a full size test facility located in Ankeny, Iowa, USA. A brief outline of the building and HVAC equipment follow. Further information can be found in Norford et al. (2000) and Price and Smith (1998).

6.1.1 Building

One of two identical AHUs was used. This served four test rooms made up of an interior room and one facing east, one south and one west. The test rooms were unoccupied and so false sensible heat loads were applied to generate the 'occupancy' profile for the rooms.

The general construction of the ERS building includes a structural steel frame with pre-cast concrete panels, a blanket of insulation on the warm side of the wall panels and concrete flooring. The building has a flat roof and a floor area of $\sim 860 m^2$. The east, south and west test rooms have window areas of $\sim 6 m^2$ and are double glazed.

6.1.2 HVAC Equipment

The heating plant was not considered in the investigation and was isolated for the duration of the test periods. However, some pre-heating of the outside air was required in the winter period to force the plant into 'economiser mode'. The heating plant supplied a pre-heat coil installed in the outside air duct. The winter test conditions were selected to generate conditions that required no load on the cooling coil. The heater was then used to adjust these conditions to allow the coil operation to be observed under low duty.

Due to system constraints the cooling coil was served by two chilled water sources during the tests periods. In winter a local 35 kW two-stage, reciprocating, air-cooled chiller, was used. In the spring and summer test periods, chilled water was supplied by a central plant serving the Energy Center and other buildings in the vicinity. The chilled water circuits local to the cooling coil were served by a fixed speed pump and the coil was controlled

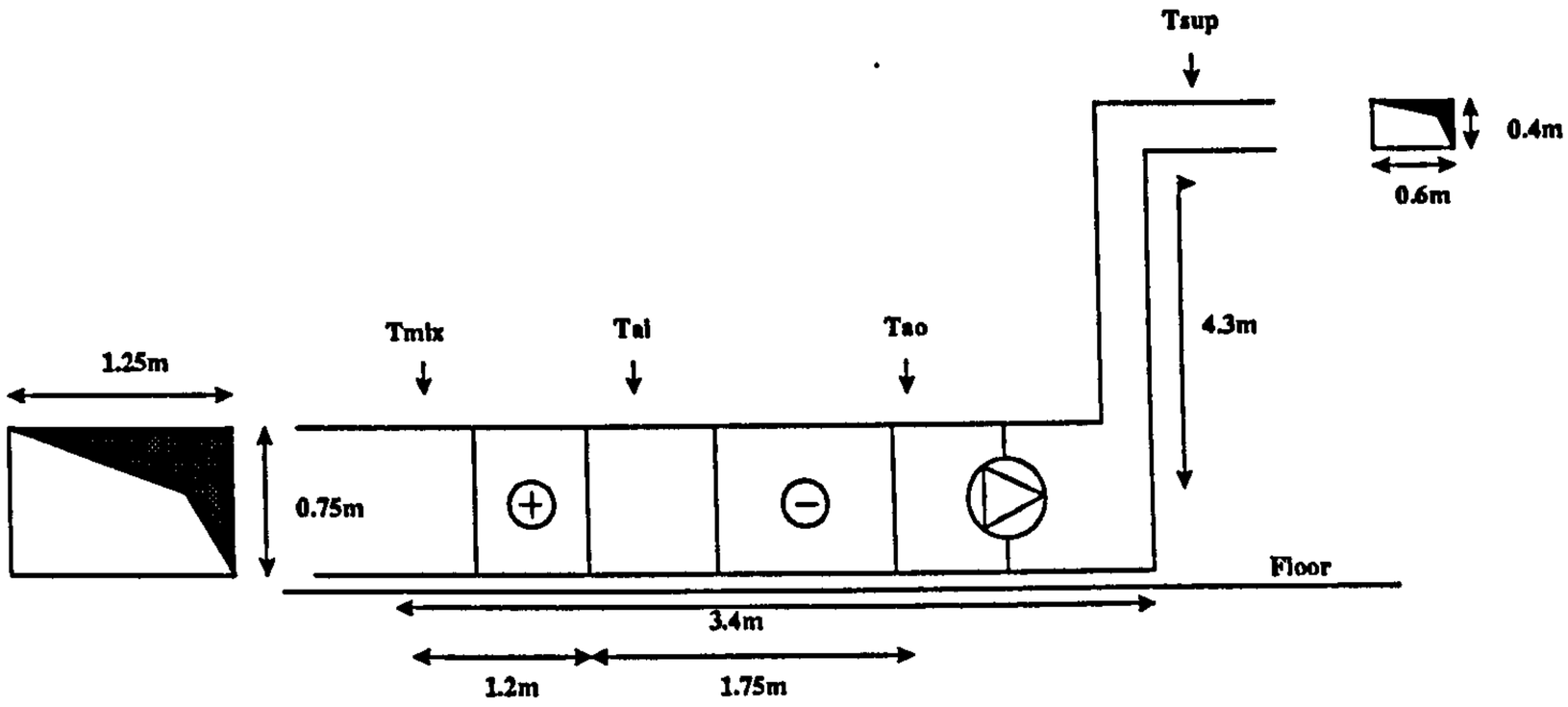

Figure 6.1: Test Plant Configuration.

by varying the water mass flow rate via a three port mixing valve installed in a diverting application.

6.1.3 Air Handling Unit

The major components of the AHU are the supply air and return air fans; cooling and heating coils; heating and cooling control valves; recirculated air, exhaust air, and outdoor air dampers; and the ducts to transfer the air to and from the conditioned spaces. The speed of the supply and return fans are controlled with variable frequency drives. The outside air temperature and humidity were measured at a weather station located on the roof of the ERS building. Air from the AHU's is supplied to Variable Air Volume (VAV) box units, each having electric or hydronic reheat. Figure 6.1 gives the approximate dimensional characteristics of the AHU. T_{mix}, T_{ai}, T_{ao} and T_{sup} indicate the location of the air temperature sensors at the mixed air condition, at the inlet and outlet of the cooling coil and at the supply air condition respectively.

6.1.4 The Cooling Coil Sub-System

The focus of the investigation is based around the cooling coil sub-system depicted in Figure 6.2, and nominally rated at 35kW. Air temperature measurement is available either side of the coil (T_{ai} and T_{ao}). Air volumetric flow rate measurements are available on the

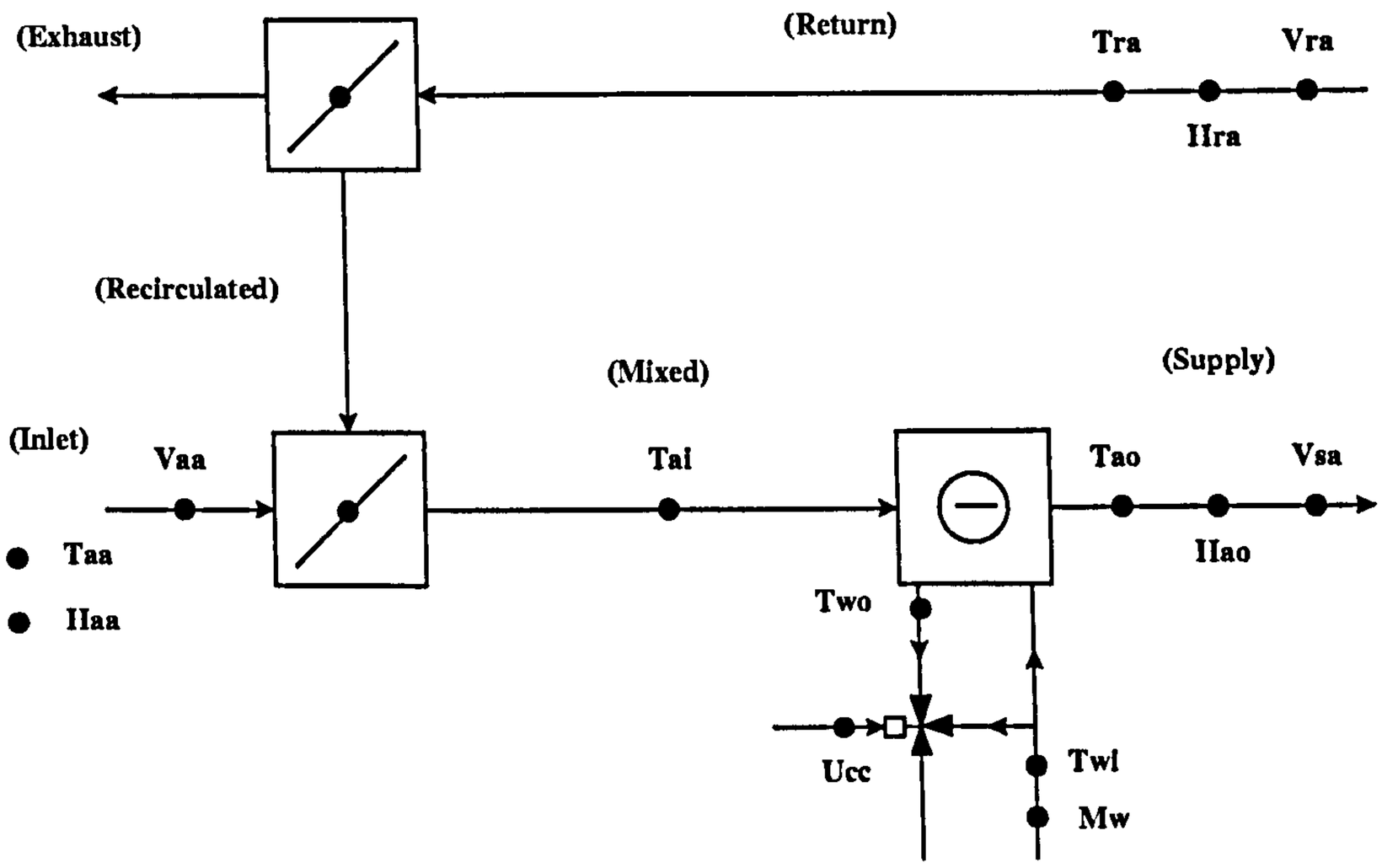

Figure 6.2: The Test subsystem.

return air (V_{ra}), ambient (V_{aa}) and supply air (V_{sa}) paths. The relative humidity and temperature (local to the humidity sensors) measurements are available for the recirculated (H_{ra} and T_{ra}), ambient (H_{aa} and T_{aa}) and supply air (H_{sa} and T_{sa}). The mixed air humidity, therefore has to be estimated from the ambient and return measurements. This is typical of the configuration of HVAC systems. Water temperatures are available entering (T_{wi}) and leaving (T_{wo}) the coil, although when the valve is closed the outlet sensor sits in a stagnated flow. Finally, the primary circuit water mass flow rate ($\dot{m}_w$) is measured. The mass flow through the coil is not normally measured in HVAC systems. In this instance, the part load mass flow rate needs to be estimated using a model that has the cooling coil control signal (u_{cc}) as an input. A suitable model can be found in Appendix B, the calibration of which is discussed in Section 7.2. This chapter is concerned with sensor validation and considers only full or zero coil duty.

The HVAC System Operational Characteristics

The control system maintains a pre-determined space temperature in the test rooms by varying the volume of air entering the space, via a control loop local to the VAV terminal boxes serving each room. During the course of the day the loads on each space varies

through the load scheduling and as a function of ambient influences. The HVAC equipment responds to the subsequent varying volume flow requirement by adjusting the supply air volumetric flow rate by maintaining a prescribed static pressure at some point in the supply air duct. The return fan tracks the supply fan by maintaining 90% of the measured supply air flow. The cooling coil seeks to maintain an off coil temperature by varying the amount of chilled water flowing through the coil. At certain times of the year, the cooling load drops to the point where the mixing of the correct proportions of the outside and return air can maintain the desired conditions in the space. This means there is no water mass flow rate through the coil and the outside and return air dampers modulate to provide temperature control. There are some operational characteristics associated specifically with the experimental programme:

- the water mass flow rate in the primary circuit fluctuates which is due to a flow imbalance in the cooling coil circuit (due to a poorly sized balancing valve) and due to the change in configuration of the primary water circuit (to accommodate campus chilled water and the local chiller in different seasons);
- some reconfiguration of system took place between each test period to accommodate other uses at the facility, although every effort was made to ensure that everything was the same at each test period;
- occasional reverse air flow in the exhaust duct was observed which was due to a short exhaust duct (hence low resistance) making an easier path for air flow than the ambient duct (which had the pre-heat coil installed for the testing) when the supply fan demanded more air flow than the return fan could supply;
- and a loss of the return fan tracking of the supply fan was observed when the fans went to their respective minimum speed settings resulting in negligible leakage through the ambient mixing box damper at 100% recirculation (cleaners set back at the end of the occupancy period).

6.2 *In Situ* Sensor Validation Methodology

It is desirable to calibrate sensors as close to their natural environment as possible, but this is practically impossible for most HVAC measurements. In model based condition monitoring, the relationships between measurements are more important than accuracy in the absolute sense. HVAC sensors can be validated by comparison to each other, using the normal operational modes of the equipment. This has the advantage of characterising the operational characteristics that affect the measurements, which can be significant. The *in situ* validation methodology can be broken down into the following procedure:

1. set system to an understood mode of operation;
2. gather data;
3. correct offsets to data;
4. validate with other data;
5. validate all offset corrections with air/water-side energy balance.

The critical measurements typically used for condition monitoring based on thermal data are those needed to characterise the energy exchange between the fluid streams. These measurements are split here into three categories: humidity, temperature and flow rate. Differencing (between measurements) is used where possible to achieve synergy in the readings, while it is assumed that the factory calibration and installation settings are faithful in the absolute sense.

A hierarchical approach to the validation of the sensors is required where there are dependencies of bias in some measurements as a function of the system characteristics that are measured by other sensors. The following investigation sequence should therefore be applied: air flow rate; air temperature; air moisture content; water flow rate; and water temperature.

The operational modes (driven by the control signals) of the equipment should be excited to identify any influences on the measurements. Stratification at different mixing box damper

positions, is an example (Section 6.3.2). There are two approaches to the treatment of observed offsets that are considered to be persistent or reoccurring as a function of some operating condition:

- they can be 'corrected' which will in general lead to increased precision and little if any additional uncertainty;
- or they can be accommodated by estimating the additional uncertainty associated with subsequent calculations using that data, resulting in poorer precision and greater uncertainty.

6.3 Sensor Validation

6.3.1 Air Flow Rate

The air volumetric flow rates are measured in the outside air duct, supply air duct and in the return path prior to the diverging section that divides the recirculated air from that which is exhausted. When comparing the flow rates between the outside air and supply air flow rate and the return air and supply air flow rate, when the mixing box is at either extreme, certain characteristics become apparent.

Figure 6.3 shows test data from the three test periods under full recirculation (u_{mb}=0%) and full outside air (u_{mb}=100%). The correlation coefficient for the data in each plot is shown in the bottom righthand corner labelled, 'cc'. The 'Test (Summer)' plot depicts data gathered from an open loop test in which the mixing box dampers were moved in stages that gave a steadily increasing proportion of recirculated air in the mixed air condition. The other plots are generated using data from operational days in each test period under normal closed loop control. When the plant is operating at 100% outside air (u_{mb}=100%), it can be seen across the test period that there is a persistent offset that increases with flow rate. This is typical evidence of leakage through the close recirculation damper and has been demonstrated in other similar systems (Buswell et al., 1997; Salsbury and Diamond, 2000). As the supply fan increases in duty, the return fan tracks it at $\sim$ 90% of full flow ($0.142 m^3 s^{-1}$). The pressure behind the recirculation damper is increased accordingly and

hence leakage is inevitable. This effect is exacerbated in this plant due to the addition of a pre-heat coil in the outside air path which has the effect of lowering the relative resistance across the closed damper. This effect is not reciprocated at full recirculated air. Under closed loop control, there is a negligible difference between the measured flow rates which suggests that there is no significant leakage through the closed outside air damper. This is apparent because there will be a relatively high pressure in the mixing box due to some velocity pressure being converted to static pressure where the air turns through 90°. Evidence from a recent CFD simulation of the mixing boxes in the test system supports this (Kelso et al., 2000). The effect may be sufficient at certain conditions to encourage flow out through the closed outside damper, which would explain the slightly higher return air to supply air flow rate observed above $\sim 0.6 m^3 s^{-1}$. This point also delimits the transition into a region of poor control, where the return fan (at the lower flow rates) is no longer able to maintain tracking of the supply fan because it is slightly oversized. This affects the operational data at the 'cleaners setback' period at the end of the day when the plant goes into full recirculation. Here the supply fan reduces the air flow which will increase the pressure and hence any leakage across the exhaust and the outside air damper. The open loop testing conditions have a tendency to exacerbate these effects, as can be seen in the upper righthand plot.

These effects culminate in the characteristics displayed in Figure 6.4. The actual measured ratio of outside air in the supply air stream, (V_{aa}/V_{sa}), is given as a function of the control signal to the mixing box (u_{mb}). There is clearly a lack of leakage at full recirculation compared to ~10% present at the full outside air condition. This plot demonstrates that the outside air fraction is more precisely represented by using the volumetric flow rate measurements than by inferring in from the control signal to the mixing box.

6.3.2 Air Temperature

Recent work by Norford et al. (2000) used the measurements of air temperature taken at the outlet of the mixing box and at some distance past the outlet of the supply fan for a fault detection and diagnosis scheme applied to the test system described in Secion 6.1. The work demonstrated that the two measurements did not correlate well when there was

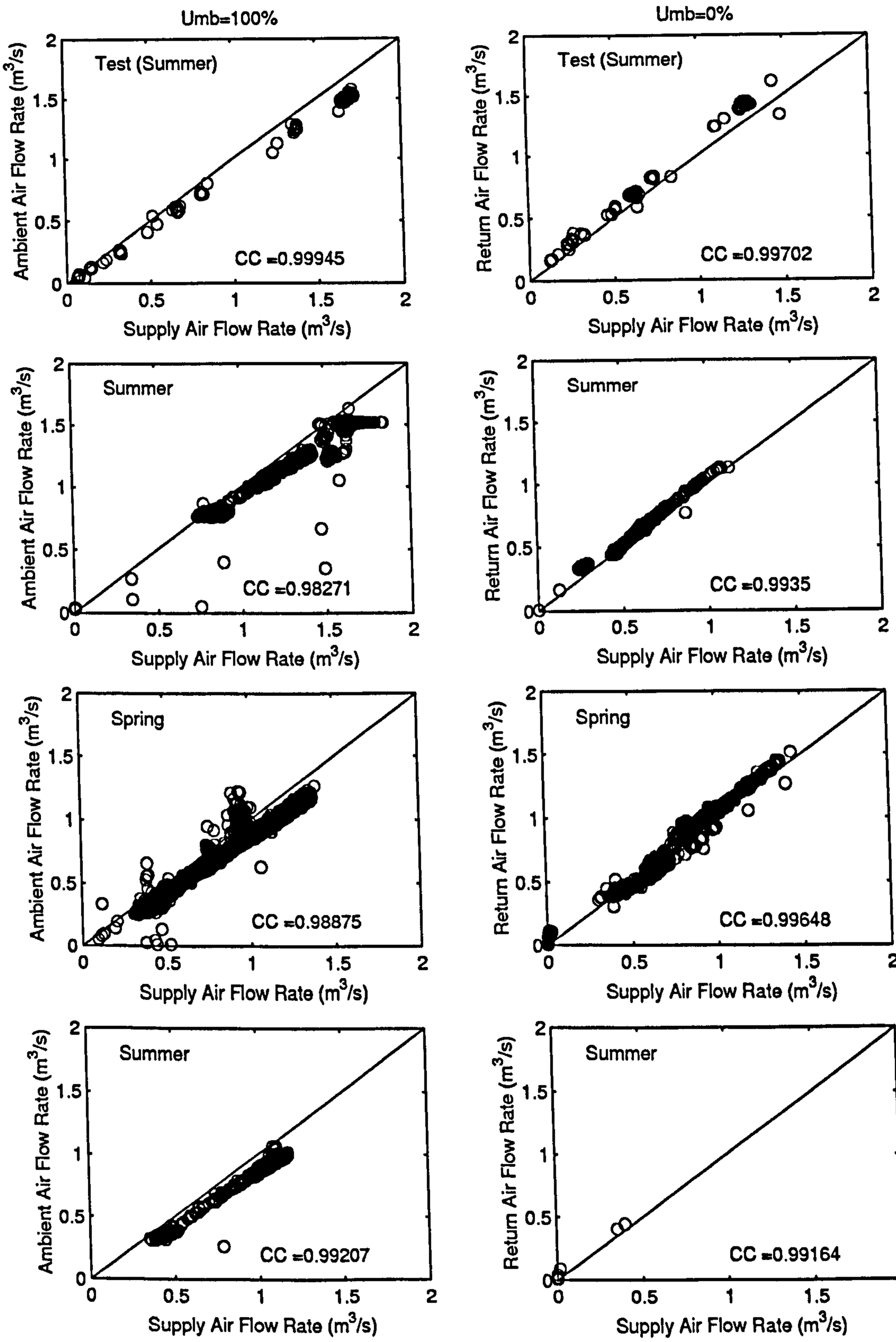

Figure 6.3: The Outside and Return Air Volumetric Flow Rates Compared Respectively to the Supply Air Volumetric Flow Rate for Each Test Period.

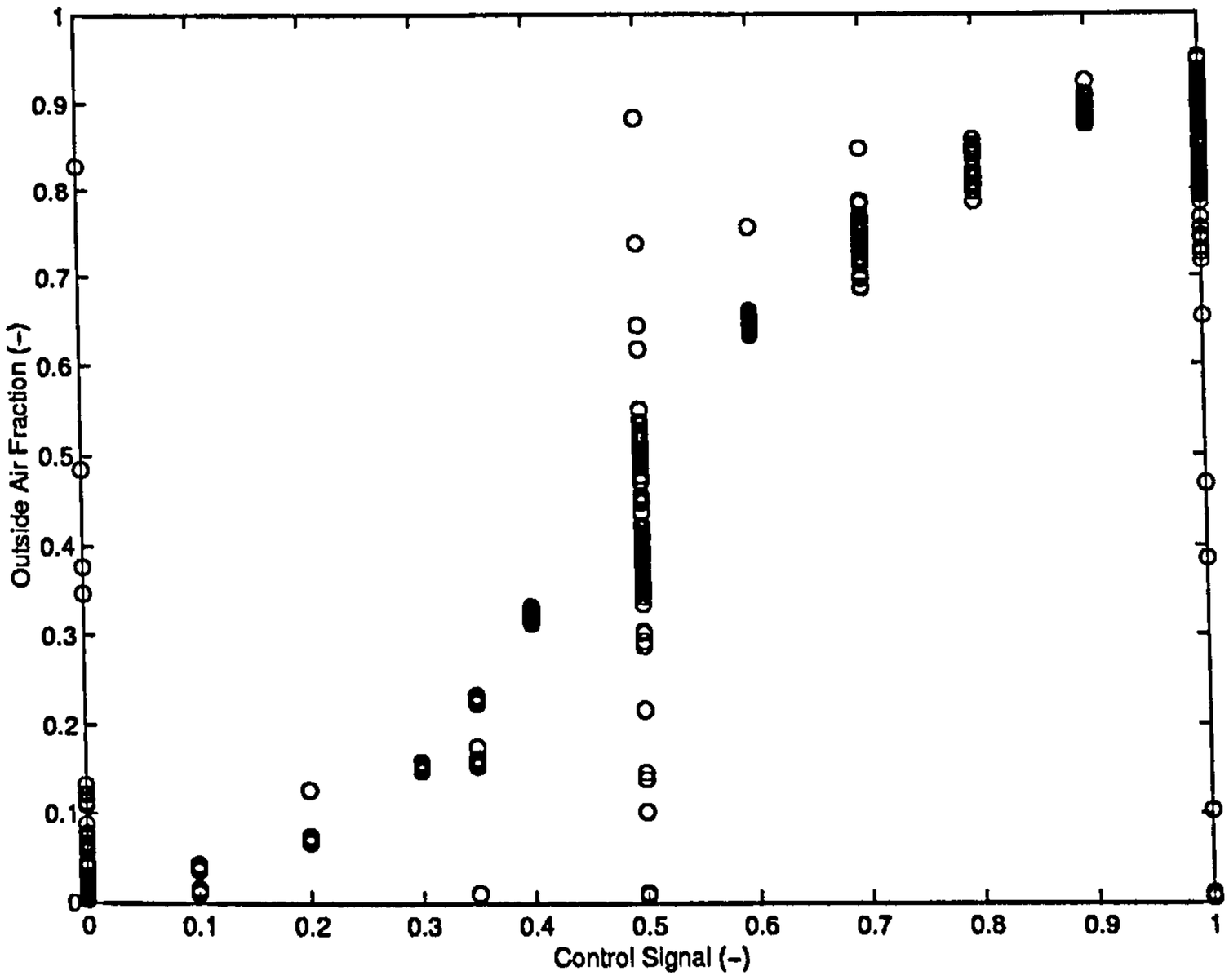

Figure 6.4: The Mixing Box Characteristics in Terms of the Measured Ratio of Outside Air in the Supply Air as a Function of the Mixing Box Control Signal.

no load across the coil sections. It was not obvious how the energy introduced into the air stream by the fan, or duct gains/losses affected the temperature measured at the supply condition. The mixed air sensor and the supply air sensor are also of different types and so there will be a lack of correlation in the uncertainties. When studying the residual from the difference between the measurements, this will result in significantly larger uncertainty in the calculated value.

For this work the air temperatures measured entering and leaving the coil have been selected over the others available (at the exit to the mixing box and the supply air temperature off the AHU) on the following basis:

- radiative effects appear to be minimal;
- heat lost to the external environment is negligible;

- sensors are 'identical', which maximises the correlations between them (which is advantageous where differencing between sensors is employed; the negative first derivative reduces uncertainty in correlated measurements).

To establish any persistent offset between the sensors and any other characteristic effects, certain conditions are necessary:

- cooling coil needs to be inoperative, preferably with the chilled water circulation pump off, in case there is any unknown leakage in the control valve;
- there needs to be a method of varying the temperature onto the coil to check non-linearity in sensor offset, which can be achieved by stepping the mixing box between extremes given the correct ambient conditions;
- the primary condition variables, such as mixing box position and air flow rate, should be exercised (data gathered at more than one operation condition) to account for any characteristic influences on the measurements.

The 'step test' as described in Salsbury (1996) and Buswell et al. (1997) is a systematic way of achieving the required system excitation. For this system, the mixing box was stepped from full fresh air to full recirculated air at the mixed air point. The supply fan speed was also adjusted in open loop whilst the return fan was left under 'normal' system control (tracking supply air flow rate at 90% of flow). The test was undertaken in summer and in order to get a large temperature difference (~10K or more) across the ambient and return air paths, all the space heat sources were turned on so that the return air was hotter than the ambient. Some issues and considerations for the application of such tests in real buildings are:

- excessive heating of the space (~48°C) may cause damage to finishes, particularly laminated plastics. In addition, this can be outside the specified operating range of computing equipment, although no ill effects were observed during the experimental period;

- the serviced space needs a means of loading if the mixed air condition is the driving force behind the test. Since the space air condition during the test is likely to result in discomfort for the space users, this load is unlikely to be generated by the occupants. Additional heat load is therefore required, which increased the cost of the testing;
  - load can be applied by the opposing coil (i.e. by the heating coil while testing the cooling coil) or by a combination of the opposing coil and the mixing box providing the system/sensor configuration allows the test component to be isolated;
  - stepping the mixing box does offer some 'combined' information about how the mixing box position affects the air temperature measurements. Recent work is showing these effects to be significant (Carling and Isaksson, 1999; Robinson, 1999; Robinson, 1998; Kelso et al., 2000; Lee, 2000).

The temperature difference between the air off the coil and the air on the coil ($\delta T_a = T_{ao} - T_{ai}$) from the step test as a function of the outside air fraction,

$$j = V_{aa}/V_{sa}, \tag{6.1}$$

is shown in Figure 6.5. The solid line shows the best fit to the data in a least-squares sense, and is given by,

$$\delta T' = -0.32388 \cdot \left(\frac{V_{aa}}{V_{sa}}\right) - 0.13366,$$

where $\delta T'$ is the predicted temperature difference. The plot includes the data that would be considered to contain some transients, however, due to the nature of the test, the majority can be regarded as being in steady-state[2]. The leakage through the outside air damper as described in Figure 6.4 can be seen to the right hand end of the plot up to $j \approx 0.9$, but the most obvious feature is the inconsistent offset with respect to the outside air fraction. This is due to poor mixing of the return and outside air streams at entry to the coil section and the type and location of the temperature sensors used. Figure 6.6 depicts the approximate dimensions and geometry of the sensors as they are installed in the test system.

[2]True steady state is not achievable in real systems and so a quasi-steady-state is referred to here. The dominant transients are due to the steps in the mixing box position and the subsequent mixing of the air and subsequent heating or cooling of the cooling coil mass due to the new air condition.

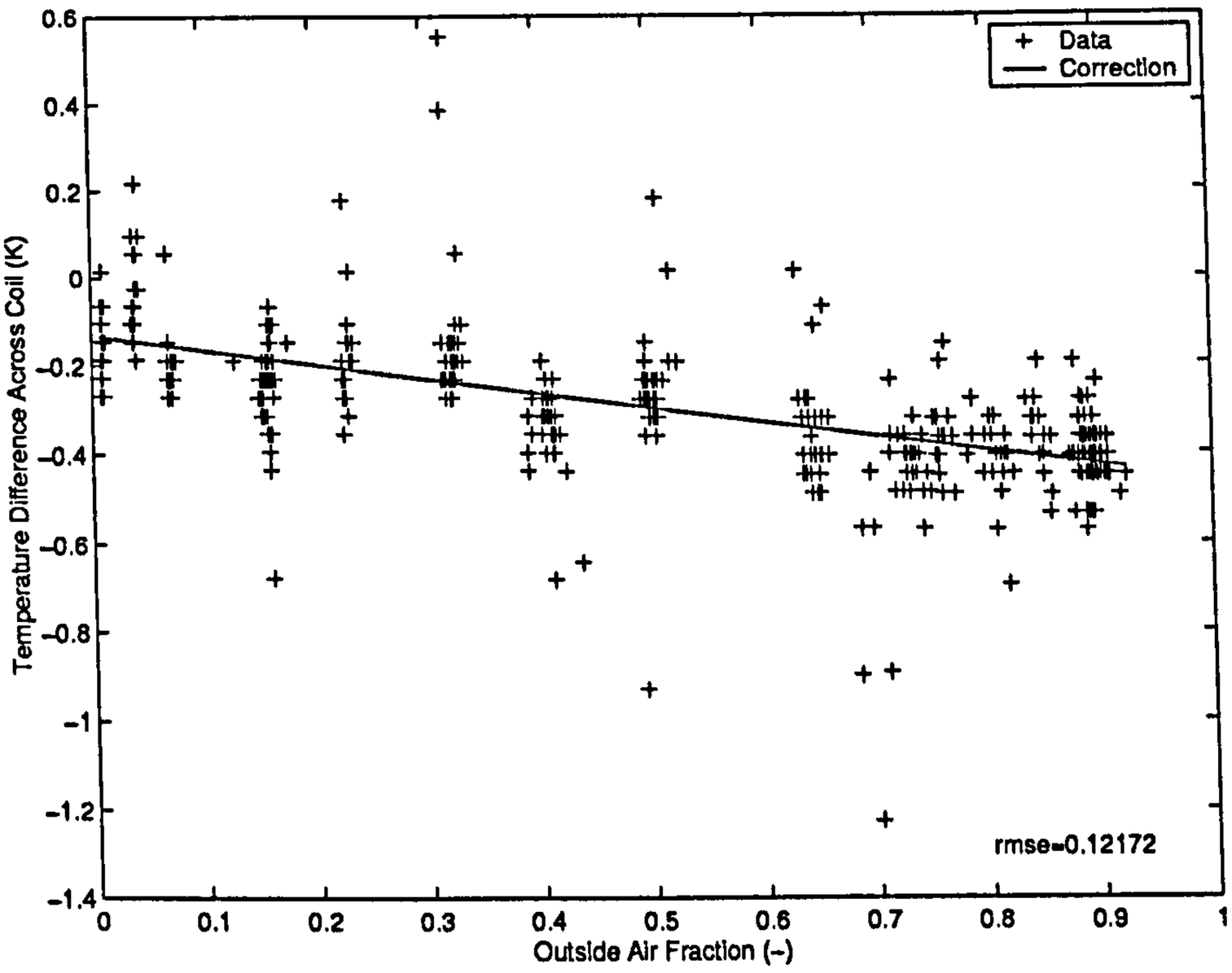

Figure 6.5: The Temperature Difference Between the Air Off the Coil and the Air on the Coil From the Step Test as a Function of the Outside Air Fraction, Where 'rmse' Refers to the Root Mean Square Error.

A model of the sensors and the stratified air flow was developed that assumed that the sensors were perfectly round and were a maximum of 1000mm long (Section 3.2.1). The level of stratification in the duct was varied from 0% Outside Air Fraction to 100%. A 'band' of set width equally distributed about the stratification level was assigned the average temperature of the two streams to simulate some mixing. Increasing the width of the band relates to better mixing of the air. Given the location of the inlet and outlet sensor, the amount of the sensor that is exposed to each of the three temperature 'bands' can be calculated. This was converted to three respective resistances from the inlet sensor calibration certificate. With the assumption that series resistance applies, these were subsequently added to give a total sensor resistance, which could then be related to the calibration certificate data to give the temperature 'as measured'. In order to demonstrate the effects of quite small changes (in installation terms) in the relative sensor geometry, in the presence of differences in the level of mixing, three parameters were adjusted with respect to the inlet and outlet sensors:

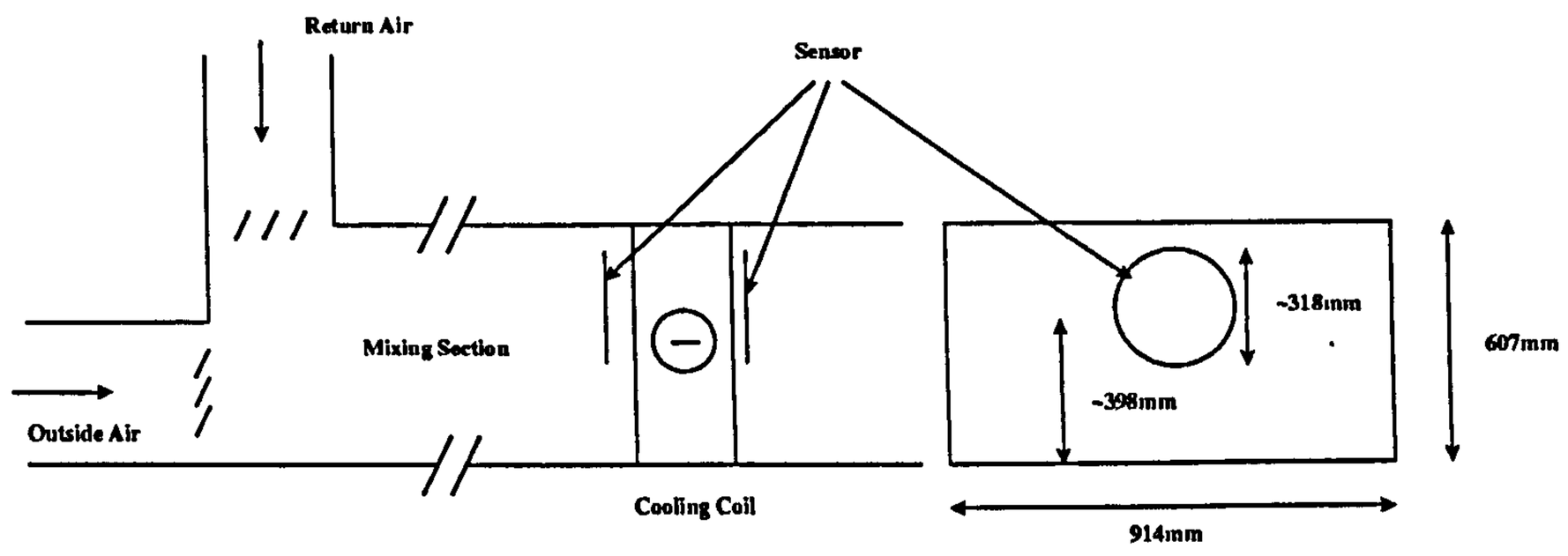

Figure 6.6: Installed Sensor Geometry and Configuration.

- the diameter of the sensor;
- the height of the sensor;
- and the width of the mixing.

Figure 6.7 depicts the results from the analysis. The notation 'D' describes the difference in the diameters between the two sensors. 'H' defines the difference between the height to the centre of each sensor. 'W' describes the width of the 'well mixed' band of air between the two air streams.

Although the model is crude, the results demonstrate that persistent offsets are inevitable. There is a dependence of the bias (the difference in the temperatures, 'DT' in Figure 6.7) on the Outside Air Fraction and the order of magnitude of the bias is similar to that observed in the data. There is, therefore, a strong argument for the observed bias (shown in Figure 6.5) to be attributed to geometrical differences in the sensors (shown in Figure 6.7).

The warmer air stream was the return in the tests on the real system. If the outside air was warmer, the sign of the bias would change. Of the available data, however, the only suitable points for checking were those where the return was the warmer stream, so this could not be formally validated. If the geometry of the sensors is constant and the characteristics of the effect established, the bias can be removed from the temperature difference. The validation plots in Figure 6.8 show some test data where the offset correction has been applied to the air inlet temperature. The scattered points are evidence of latent dynamics

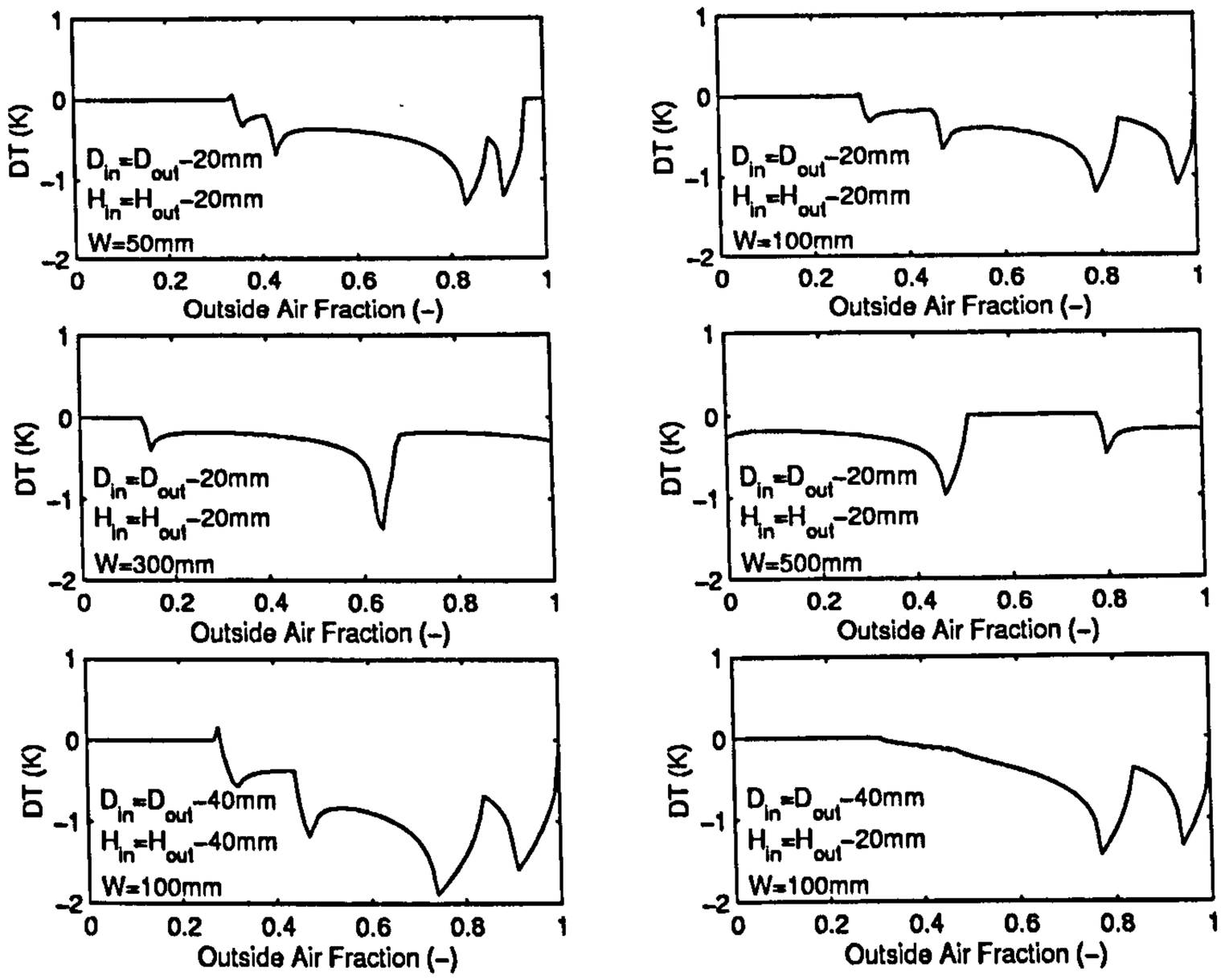

Figure 6.7: Results from Analysis of the Temperature Difference, 'DT', Sensitivity to the Sensor Configuration in Light of Varying Magnitude of Outside Air Fraction.

as the system approaches steady-state.

It should be noted that the bias discussed above is in addition to the bias in the approximation of the true bulk average temperature of the air on and off the coil. In a sense this removes the uncertainty associated with the geometrical issue when the measurements are used for differencing but it does affect the uncertainty in the estimation of the bulk mean average. For cases shown in Figure 6.7 where the geometry is the same for both sensors, Figure 6.9 shows the deviation of each to the true mean air temperature at different levels of mixing. 'W' describes the width of the 'well mixed' band of air bwteen the two air flows in the model. The magnitude of errors that might be expected is demonstrated. These values seem to be reasonable when compared to Robinsons work (1999) where a similar temperature differential (~10K used in the simulation discussed here) was generating in the order of 7K across the height of the duct. Using the detailed uncertainty analysis techniques however, these uncertainties would be considered to be correlated. Consequently, the uncertainty (in terms of the absolute effect on the the accuracy of the calculated result) will most certainly be less than Figure 6.9 suggests when considering differencing

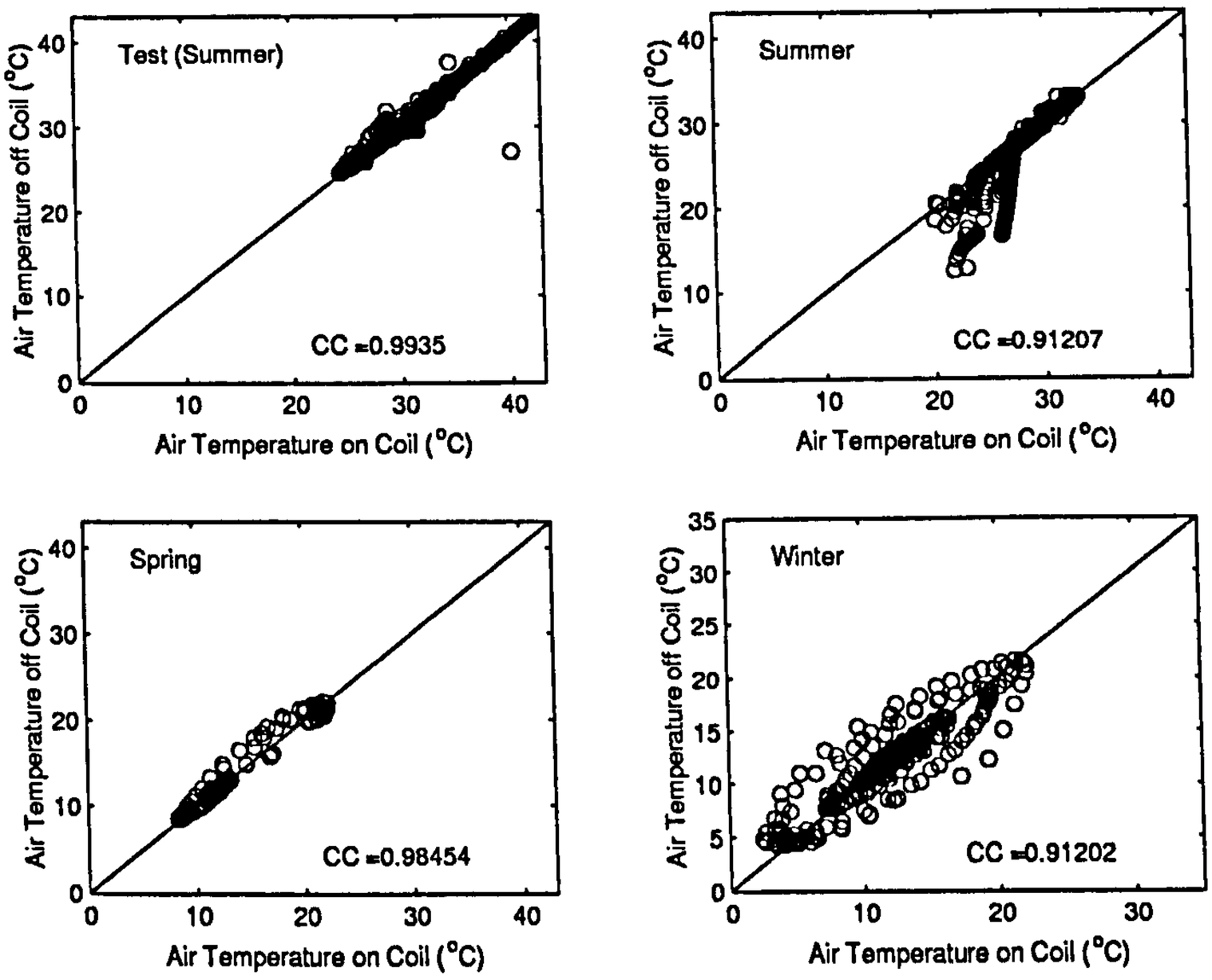

Figure 6.8: Plots Validating the Applied Sensor Offset Correction for the Air Temperature Difference across the Cooling Coil for Data from each Test Season.

type equations.

6.3.3 Air Moisture Content

In general, in HVAC equipment it is the relative humidity and dry bulb temperature of the air that is measured. Most analysis requires humidity ratio, which can be calculated from these two measurements. The enthalpy difference across the cooling coil is of interest here, but humidity measurements are rarely made on the inlet to the coil. The humidity of the air entering the coil has to be estimated using the humidity measurements of the return and ambient air.

One of the problems with the measurement of relative humidity in HVAC grade sensors is that these will most certainly be the poorest, in terms of accuracy, in the system. The bulk average uncertainties are one of the largest contributions to the uncertainty in a given measurement (Section 3.2.1). One grace with the humidity measurements is that the air can be considered to be well mixed in terms of moisture content. The ambient air should

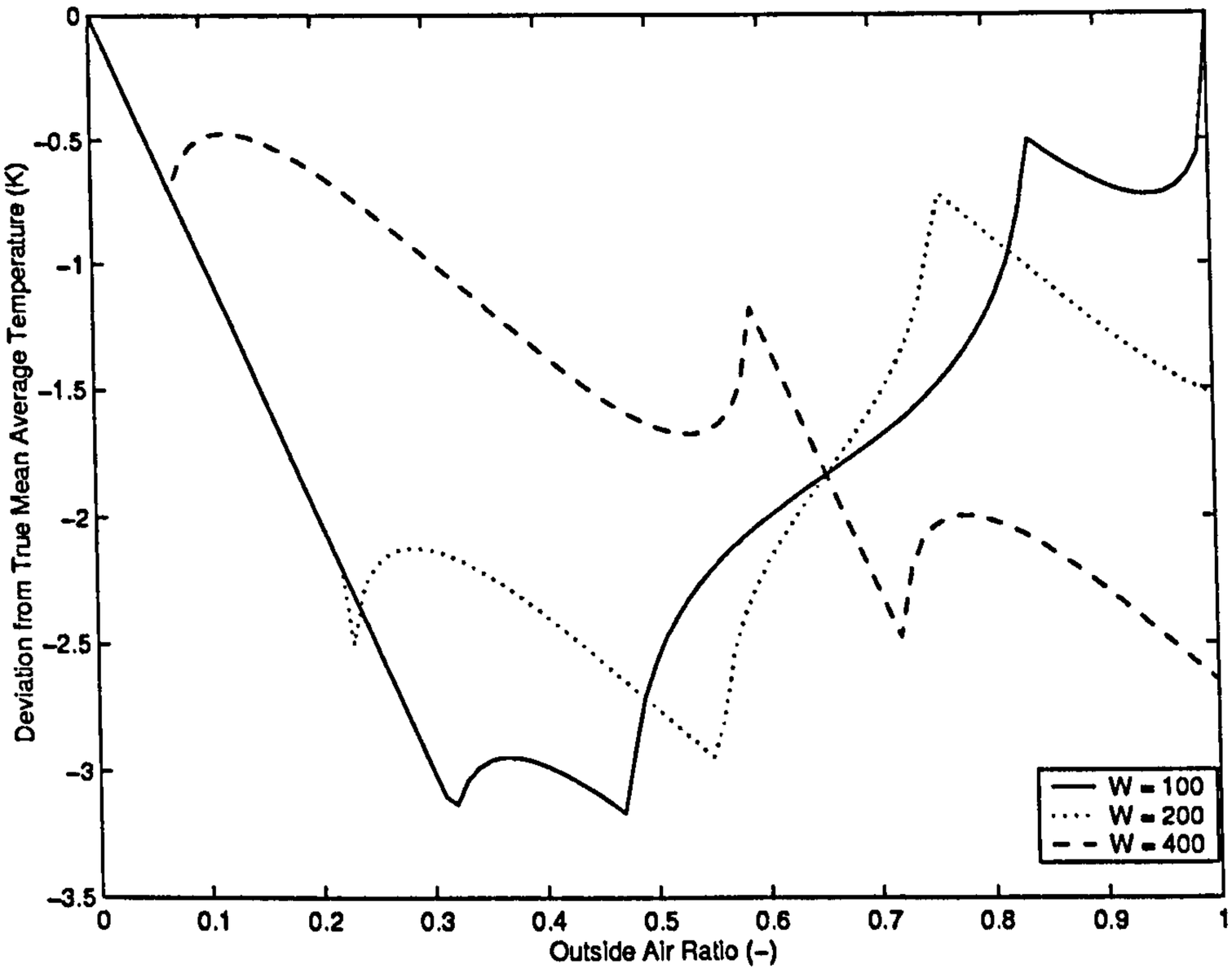

Figure 6.9: Deviation from the True Mean Temperature at Different Levels of Mixing Using the Sensor Model.

be well mixed in terms of the location of the sensor in relation to the inlet duct; the return air should be well mixed in the conditioned space because there are no latent gains in the duct and, the air from the space should be well mixed. The supply humidity measurement should be representative of the bulk average because it is in a location after the fan where it is likely that the mixing is reasonable. Any spatially induced uncertainty is most likely to come from stratification effects that affect the temperature measurement used in the calculation of humidity ratio.

The only observed change in air humidity in the HVAC equipment, will occur over the cooling coil when it is active and when the prevailing conditions dictate. A comparison of the dew point temperatures of the outside air and that based on the chilled water entering the cooling coil showed that dehumidification was only possible during the summer period. We can therefore restrict the inclusion of air moisture content to summer season calculations. The removal of these measurements where possible is desirable because they introduce increased levels of uncertainty and reduce the precision in the calculations (Comparison of Figures 7.7 and 7.8 in Section 7.3 demonstrate this).

In order to assess the precision of the measurements there must be no dehumidification across the cooing coil. The simplest method of defining this is when the cooling coil control signal is zero having first demonstrated that there is no valve leakage present. The air temperature sensors are some distance apart resulting in duct and equipment (fans) losses/gains that are difficult to estimate and hence calibration between the sensors is difficult. These sensors are, however, local to the respective humidity measurements and so it is proposed here that any persistent bias in the estimation of the air moisture contents will implicitly describe the biases local to each sensor pair. By comparing the calculated moisture contents, corrections to any offset found can be applied directly.

The moisture content of the air onto the cooling coil needs to be estimated by assuming that the proportion of water vapour in the mixed air stream is in the same ratio as the volumetric flow rates of the two serving air streams (ambient and return). Figure 6.10 shows the validation plot for the mixed air moisture content without any corrections. There is some offset apparent in the summer, but none in the spring and winter testing periods. This could either be due to, or a combination of, some improved on site calibration of the sensors that took place after the summer and/or some non-linearity in the offset. For the purposes of this work, it is sufficient to say that the applied offset should be applicable to the summer period only. Calculating the mean offset in $g_{sa} - g_{ra}$, using data from the step test used to characterise the air temperature sensors when u_{mb}=0.0, the bias was calculated as -7.015e-004kgkg$^{-1}_{air}$. Likewise for $g_{sa} - g_{aa}$, using data when u_{mb}=1.0, the bias was calculated as -8.745e-004kgkg$^{-1}_{air}$. These were applied to the summer data and Figure 6.11 shows the results. The scattered data in the right hand plot shows some humidification of the air generated by water evaporation of the coil surface after the chilled water supply to the coil has ceased. The coil was previously dehumidifying.

6.3.4 Water Flow Rate

The chilled water supply to the coil is fed from a primary circuit similar to that depicted in Figure 1.1. A three port mixing valve in a diverting application controls the proportion of water flowing through the coil. At design, the maximum mass flow rate through the coil will be specified and assumed to be constant. There are a number of reasons why this

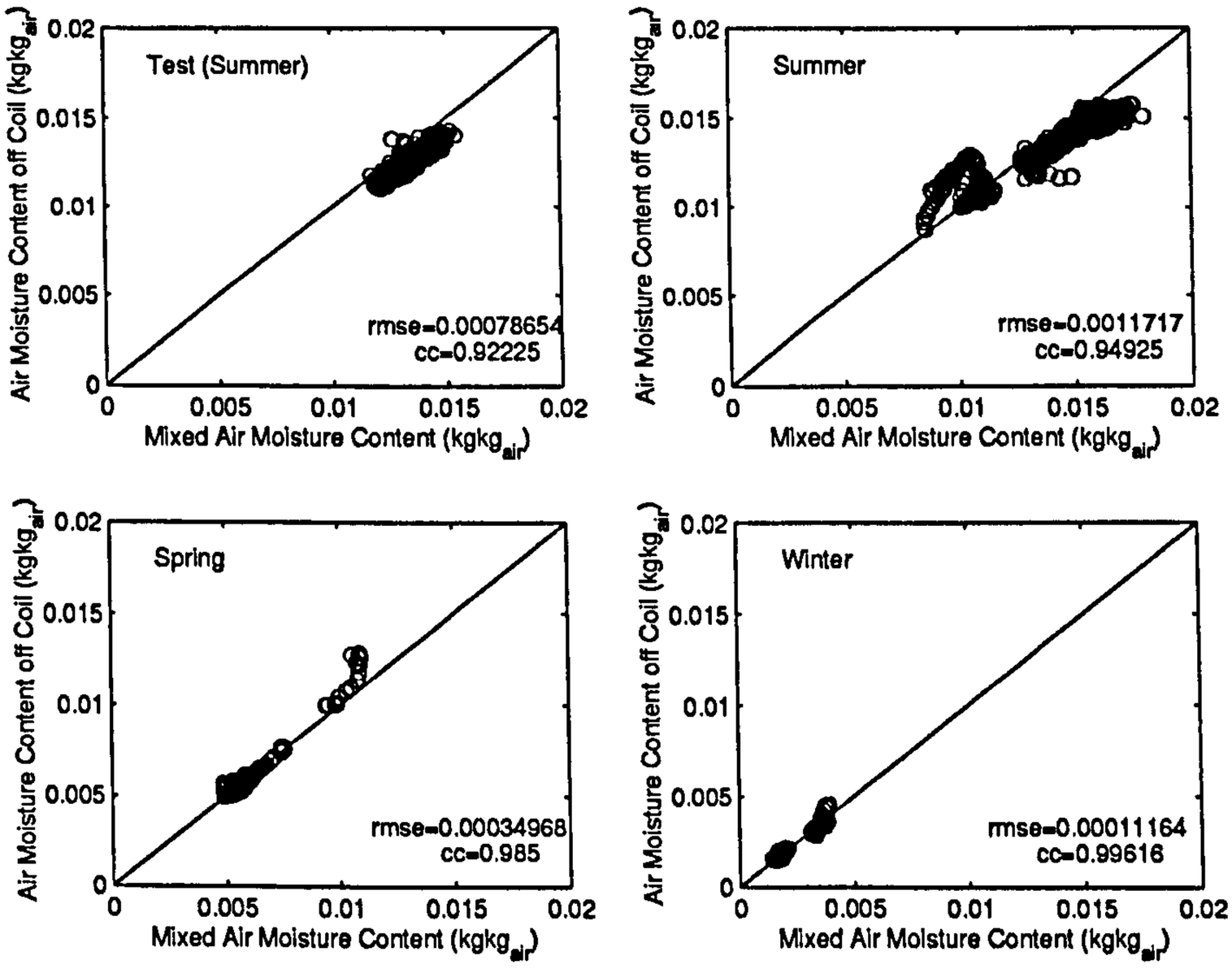

Figure 6.10: Validation Plot for the Mixed Air Moisture Content Without Any Corrections.

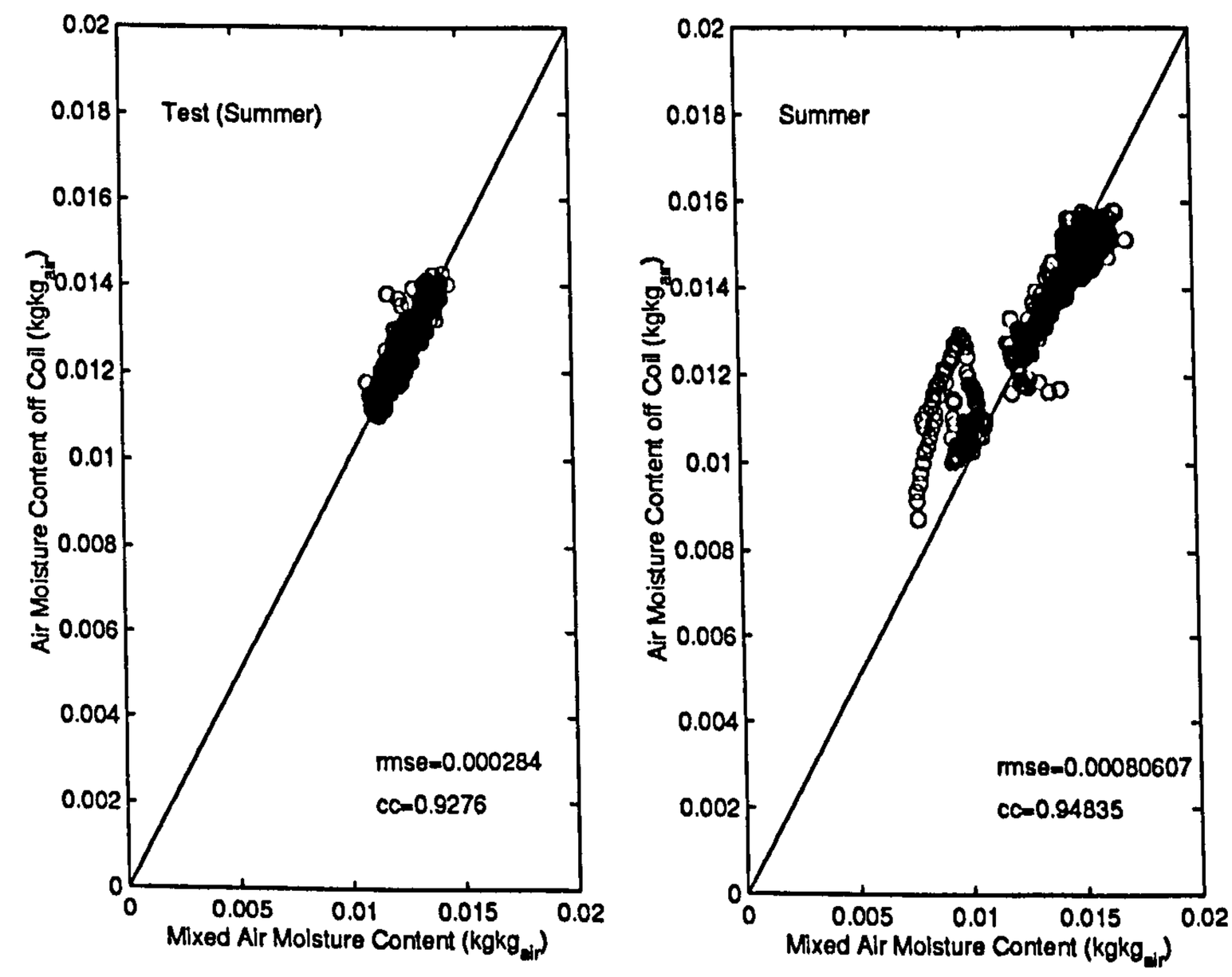

Figure 6.11: Validation Plot for the Mixed Air Moisture Content For the Summer Test Period With Bias Corrections.

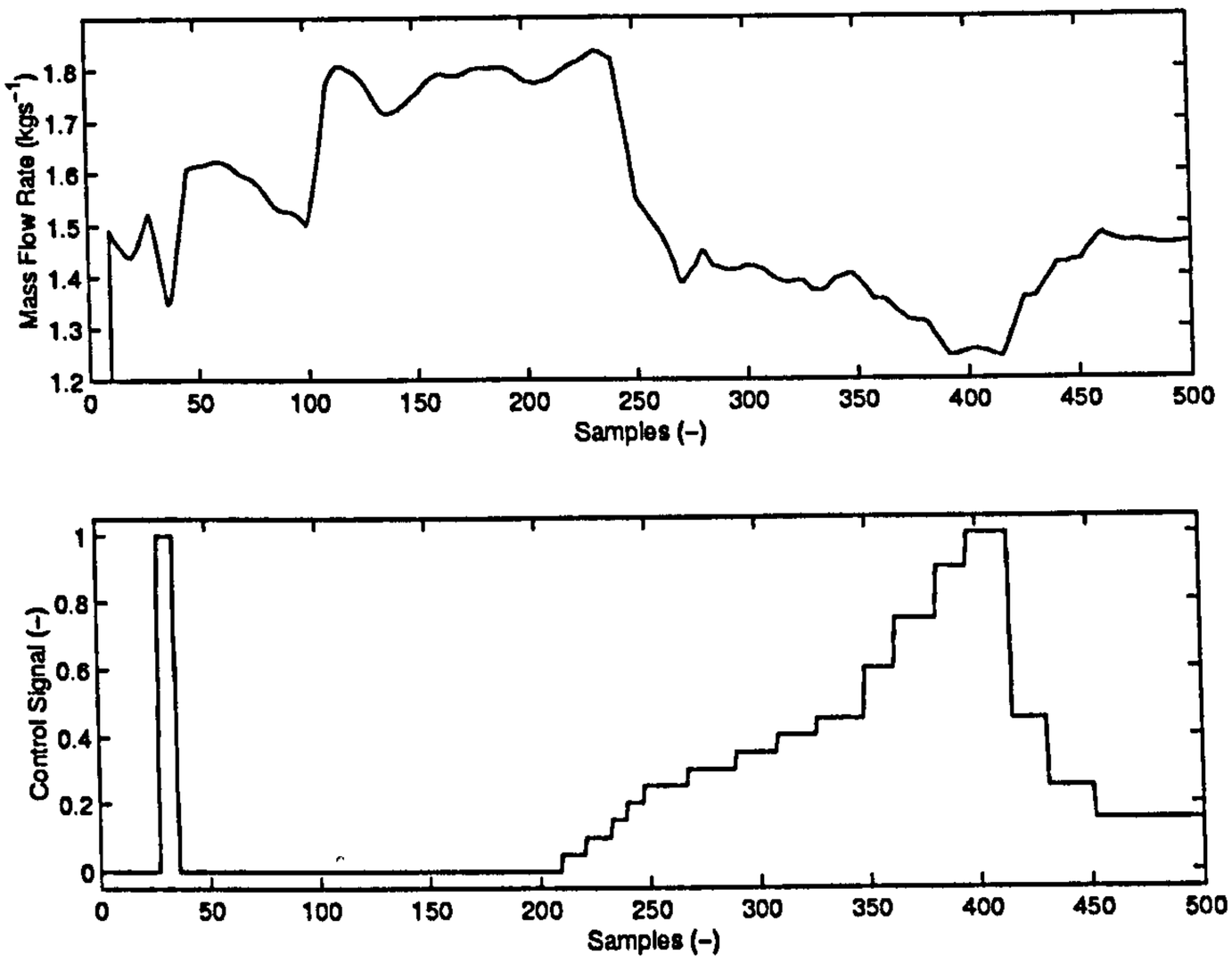

Figure 6.12: The Chilled Water Mass Flow Rate Measurement for a Range of Control Positions.

may not be realised in the installation:

- under/over flow due to primary circuit load;
- change in system configuration;
- variable pump speed (when it should be constant).

The mass flow rate measurement of the chilled water cannot be validated against another sensor. The resistances to flow in the circuit and diverting leg are unbalanced which causes fluctuations in the primary circuit mass flow rate (there will always be some flow fluctuations even with perfect balancing due to conflicting valve inlet and bypass ports). These effects can be seen in Figure 6.12. As the coil valve is stepped open, the mass flow rate is seen to vary when it should stay constant. There are also other disturbances that could be attributed to pressure fluctuations in the campus chilled water system that feeds the primary circuit. Each sequence of steps was carried out on separate days and the difference in the measurement at similar valve positions is considerable. The circuit imbalance will mean that the maximum flow rate will change as a function of valve position. These effects should remain constant and will contribute to the curvature of the combined

valve/coil characteristics. Figure 6.13 demonstrates this by plotting the test data measured mass flow rates against cooling coil control signal. The left hand plot show data when the valve is opening and the right hand when the valve is closing to eliminate hysteresis effects. The maximum chilled water mass flow rate is attributed to the flow rate when the valve is 100% open. There were also some changes to the configuration of the system to run on the local chilled water supply from a two stage chiller which has affected the circuit characteristics. The winter period is relatively unaffected since the coil valve is normally closed. Figure 6.14 shows the mean chilled water mass flow rates as measured when u_{cc} =100% for the summer and spring test periods. There is nearly 30% difference between the minimum and maximum observed value (based on the maximum flow rate) which, at a temperature difference of 10K across the coil, is ~25kW. In light of these fluctuations and since the flow meter is a calibrated instrument, the obtained mean mass flow rates have been used to set the maximum mass flows for each test day. Where the mass flow rate at 100% is not available, the measurement from the nearest available day is used. The 95% confidence estimates about the estimated means is used as additional uncertainty associated with the sensor.

Clearly, flow/pressure disturbances in the primary circuit will have a pronounced effect on the accuracy of calculations. There are two possible solutions:

- measure the mass flow into the coil;
- or set sufficiently large confidence limits about a mean to account for any expected fluctuations.

The measurement of flow directly into coil will clearly improve the accuracy, but would require more instrumentation. Adjusting the confidence limits is a more robust approach, but will be less accurate and much less precise.

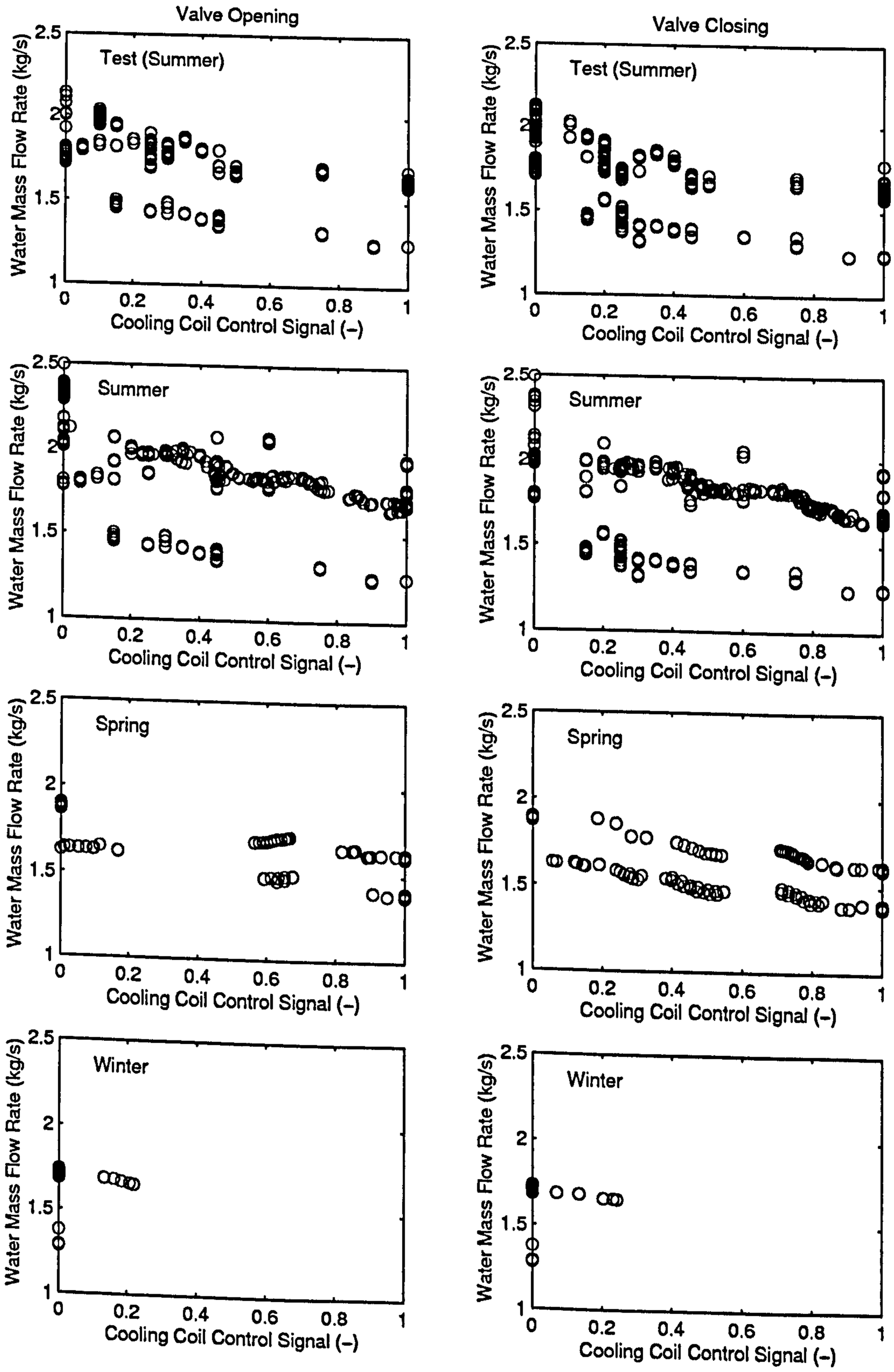

Figure 6.13: The Chilled Water Mass Flow Rate against Control Signal for the Test Data.

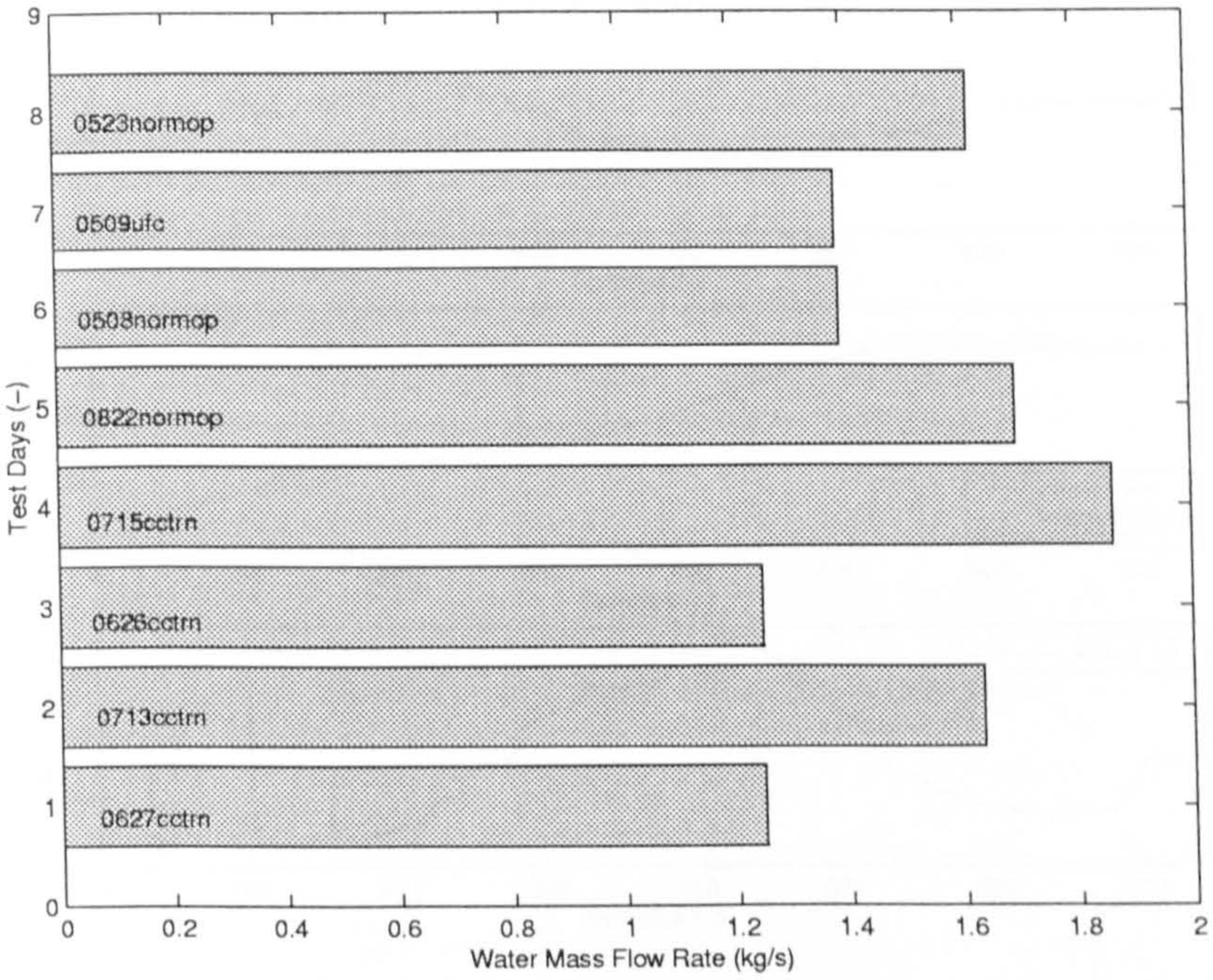

Figure 6.14: The Mean Chilled Water Mass Flow Rates at u_{cc} =100% for the Test Data used from the Summer and Spring Test Periods.

6.3.5 Water Temperature

The three test periods (summer, winter and spring) should have seen the plant operating under identical conditions. From the data it is apparent that the chilled water inlet temperature was measured on the coil side of the loop in June and July. This is characterised by the drift towards the ambient temperature when $u_{cc} = 0$. When the valve is opened, chilled water flows past the sensor and a sharp drop in temperature is observed. The August measurement, however, was made on the pump side and hence the same jump was not evident in the coil water temperature.

These observations also confirmed that the water temperature measurements are only of use when there is flow between them. In fact, the temperatures measured close to the coil can be influenced by the air temperature in the duct. Figure 6.15 shows these measurements (middle plot), with the difference between the means and the associated uncertainty on the top plot and the mixed air temperature on the bottom plot. The steps in the mixed air temperature are the result of the mixing of two air streams at dissimilar temperatures by stepping the mixing box open. The cooling coil was inactive during these

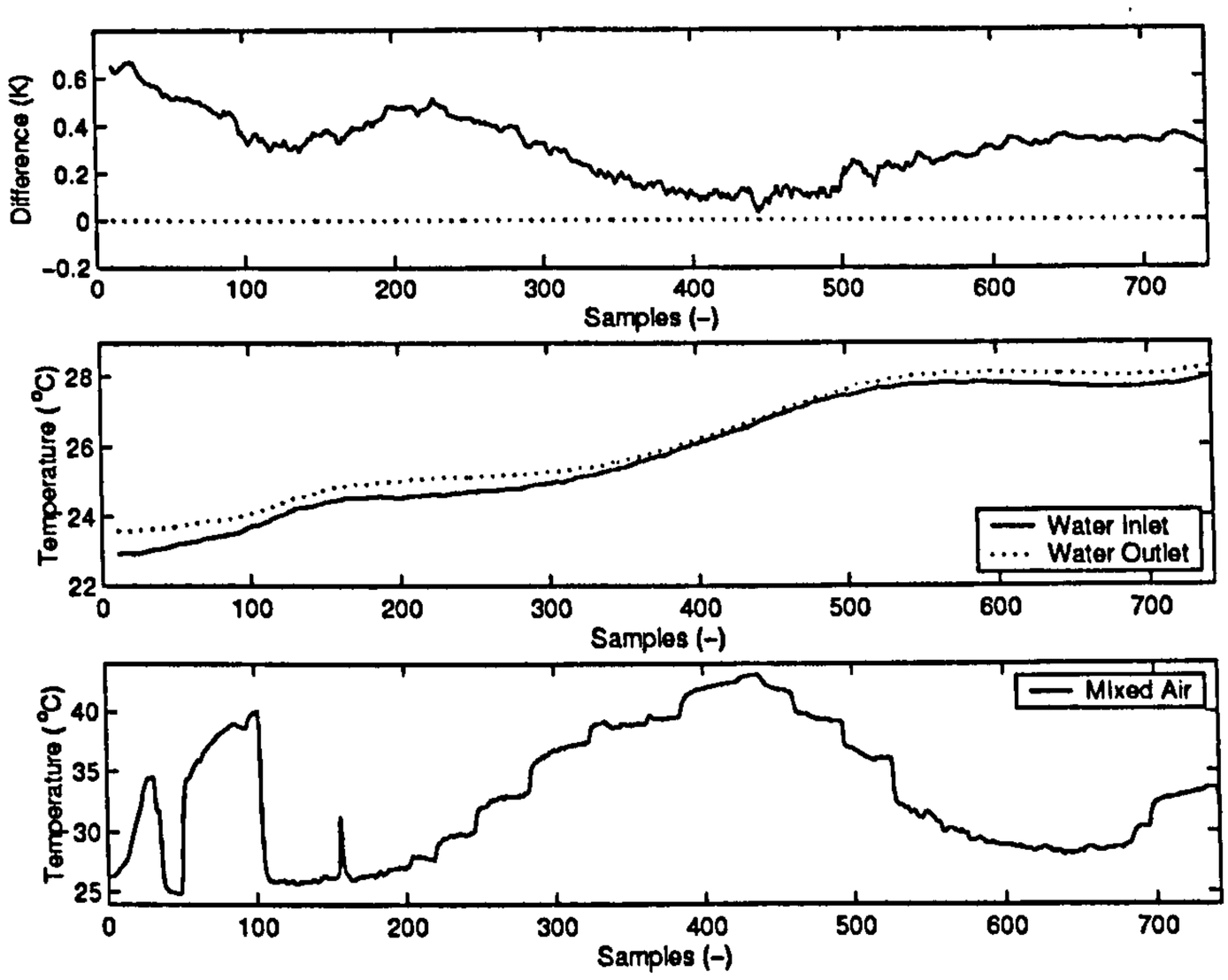

Figure 6.15: The Significance of the Observed Differences between the Chilled Water Temperature Sensor Measurements, Entering and Leaving the Cooling Coil.

tests. The chilled water is stationary in the coil and the circulation pump is off, hence the water temperature is closer to the ambient room temperature (≈ 20°C) than the normal operating chilled water temperature. The ambient temperature during the course of the test drifted up because the space temperature increased as the heat input to the space during the mixing box step test was persistently maintained. The principal feature of the plot are the similarity in the characteristic trends between in mixed air temperature (bottom plot) and the magnitude of the difference between the measurements (top plot). The step test (starting at sample $\approx$150) moved the system operating point from 100% ambient air to 100% recirculated air (at sample $\approx$425), and back. Stratification of the air flows could account for the difference. If the inlet is at the bottom and the outlet at the top of the AHU, the air flow path could mean that a stratified layer causes the lower sensor to be cooler that the higher one. The stratification argument is further supported by work by Kelso et al. (2000). For generating an estimate of the offset in the temperature measurements the water mass flow rate is assumed to be correct, as for the air-side case. Corrections are then made to minimise the bias in the air temperature measurements using data collected under 'special' conditions. Similarly, the air moisture content difference across the coil is 'corrected'. At 100% chilled water through the coil it

Table 6.1: Offsets Applied to Chilled Water Outlet Temperature Measurements.

Data	Offset (K)
June	0.776
July	0.110
August	1.226
May	-0.855
January/February	0.000

is then possible to check the offset present in the water temperature sensors. Figures 6.16, 6.17, 6.18 and 6.19 show the difference between the measured temperature difference and that calculated by energy balance for the summer data, detailing the instances where no offsets (corrections to bias in the measurements) are applied; offsets except the water-side temperature measurement applied; all offsets applied; and the spring data with all the offsets applied. The left hand plots show the data used to calculate the offset estimates and the right hand plot shows the validation data where possible and Table 6.1 details the sign and magnitude of the offsets as applied to T_{wo}. The legend in the top left hand corner of each plot refers to the respective date ('ddmm') and data filename. The winter period value has to be assumed since there is no data available for validation. This offset is unimportant with respect to the test data in this work because only operation where the control signal is 0% is considered. Each row of plots shows data collected from distinctly different test periods. Between these times the plant was used for other work and while the best endeavours were undertaken to ensure that the system was returned to the same condition at each new period, the plots show that this did not occur. The validation test seems to show that during each period the offsets were consistent, while between tests they differ. This means that the offsets need to be checked and applied separately for each test period. This is unlikely to be a problem in a real system, where constant changes to plant and control systems are atypical, but it does highlight how sensitive such calculations are on the disturbance of sensors and plant. In terms of condition monitoring, some of these offsets would show up as a fault.

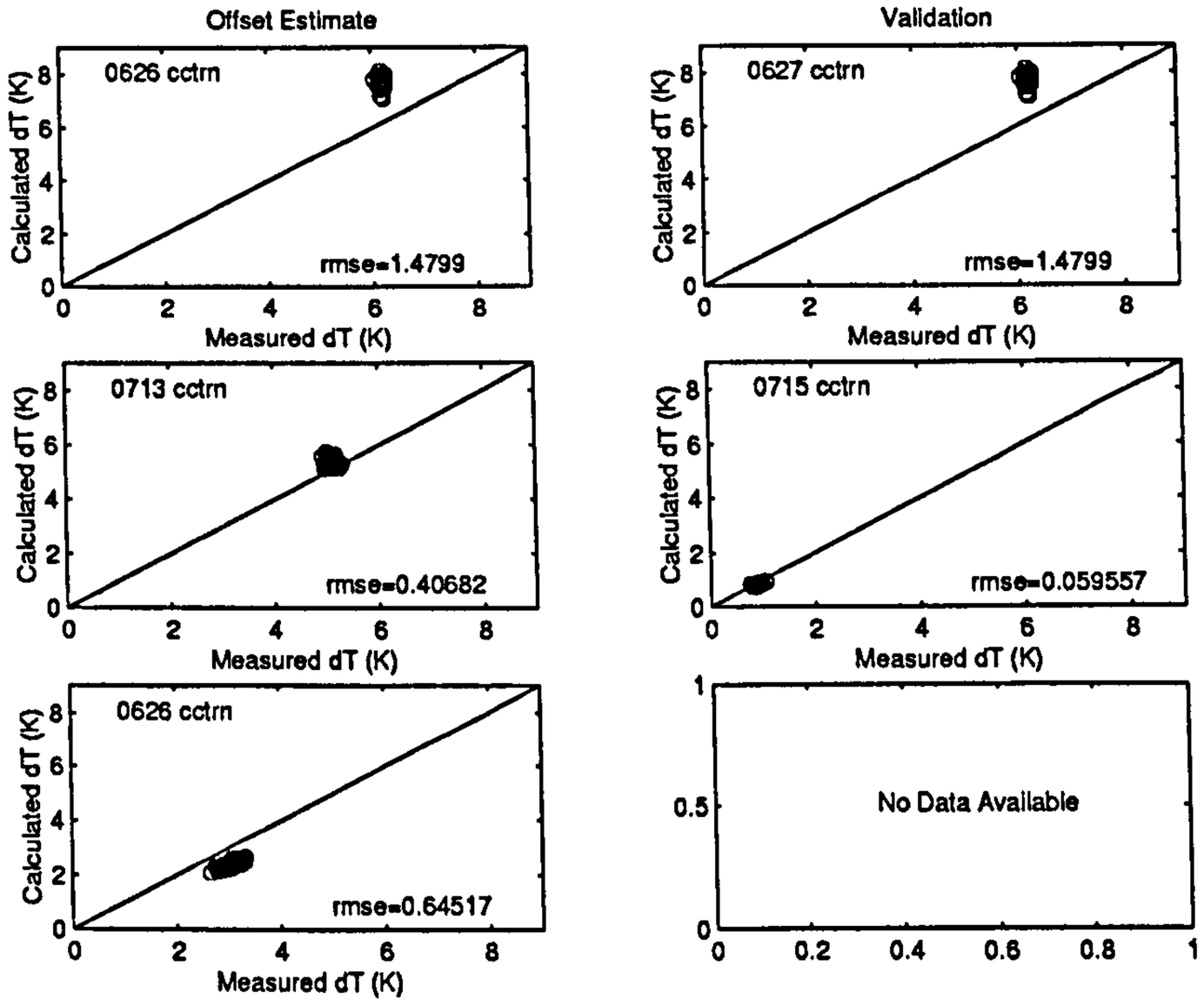

Figure 6.16: The Difference between the Measured Temperature Difference and that Calculated by Energy Balance for the Summer Data with no Offsets Applied, Where 'rmse' Refers to the Root Mean Square Error.

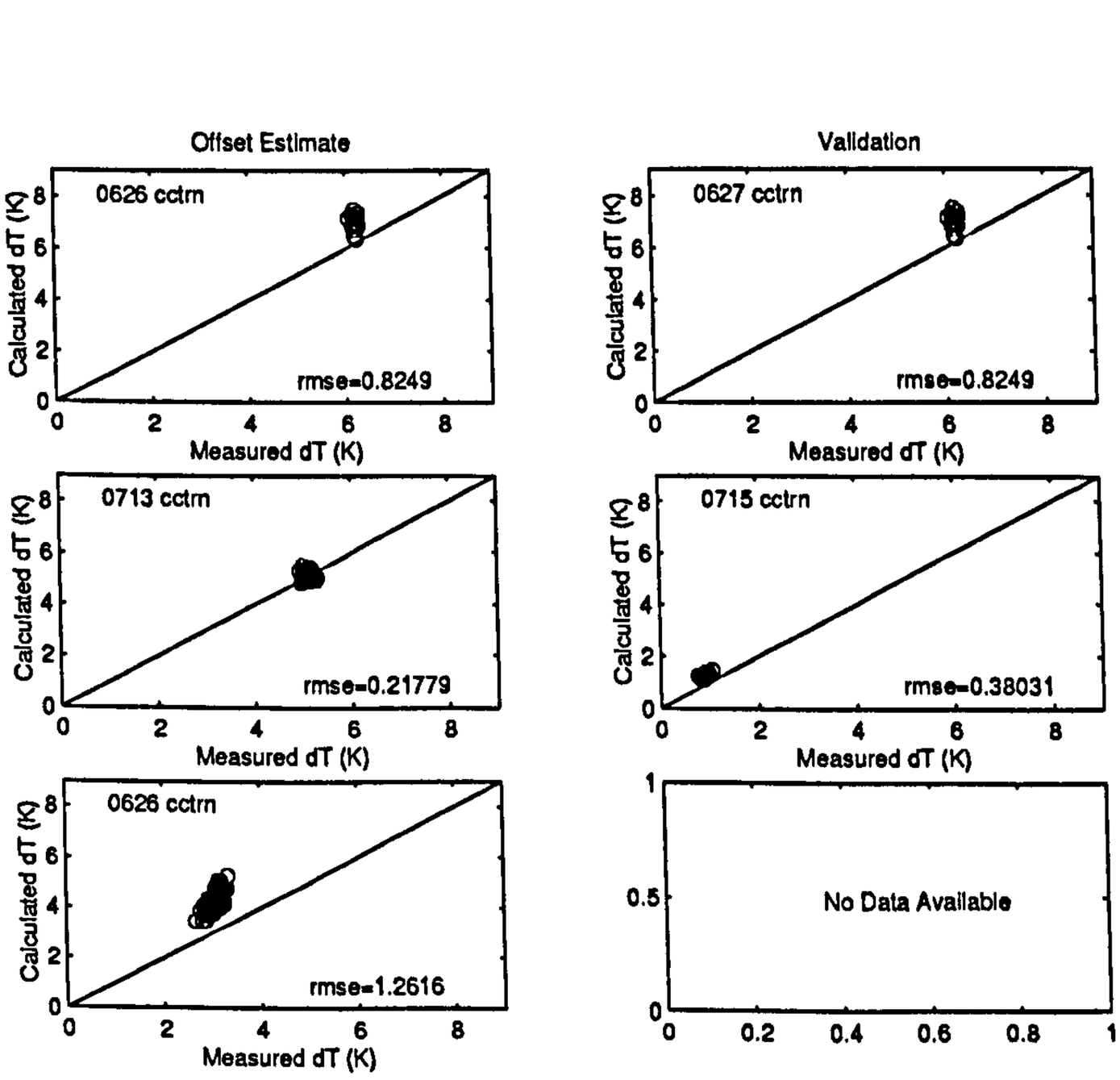

Figure 6.17: The Difference between the Measured Temperature Difference and that Calculated by Energy Balance for the Summer Data with All Offsets Applied, Except that Associated with the Chilled Water Temperature Measurements, Where 'rmse' Refers to the Root Mean Square Error.

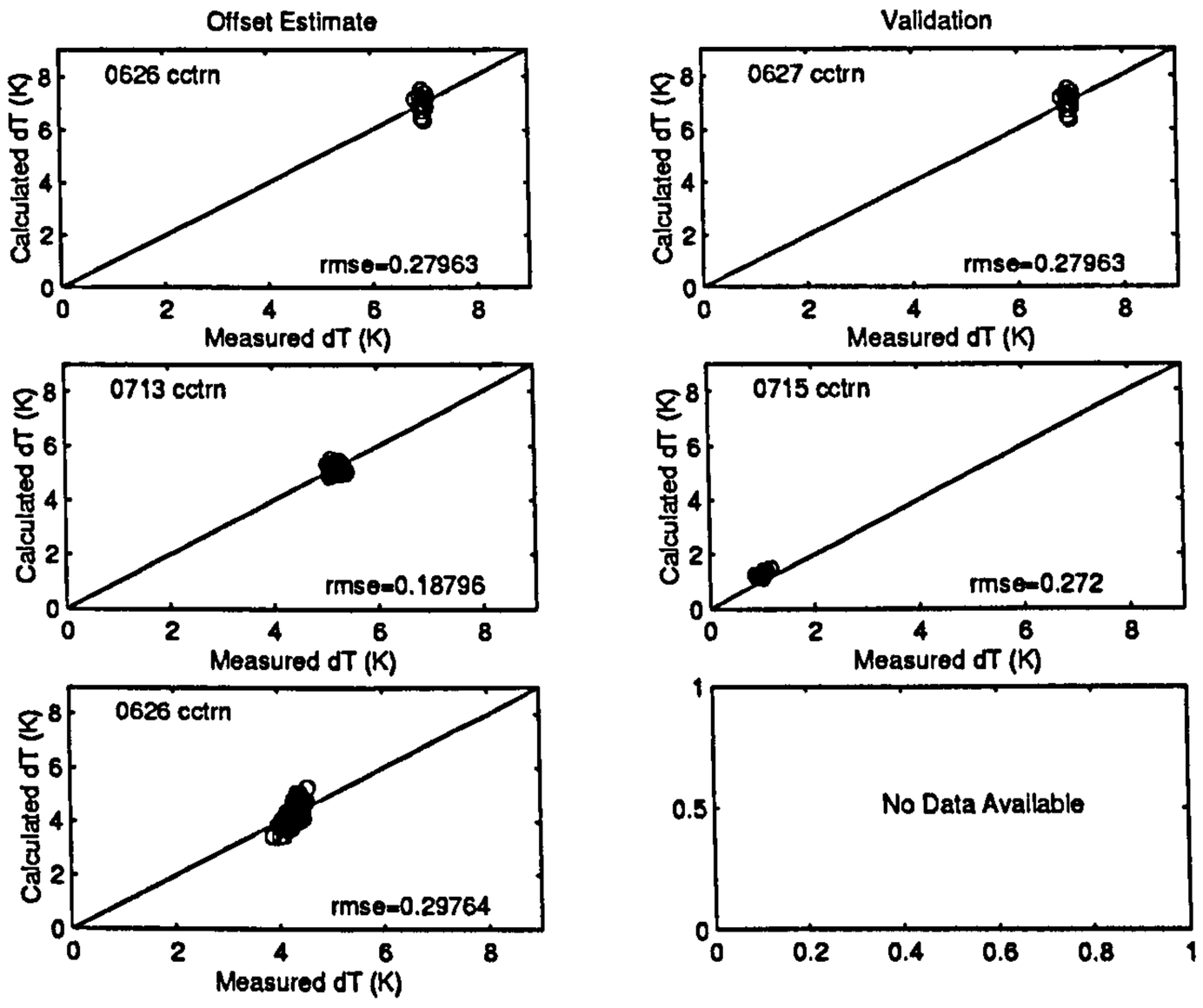

Figure 6.18: The Difference between the Measured Temperature Difference and that Calculated by Energy Balance for the Summer Data with All Offsets Applied, Where 'rmse' Refers to the Root Mean Square Error.

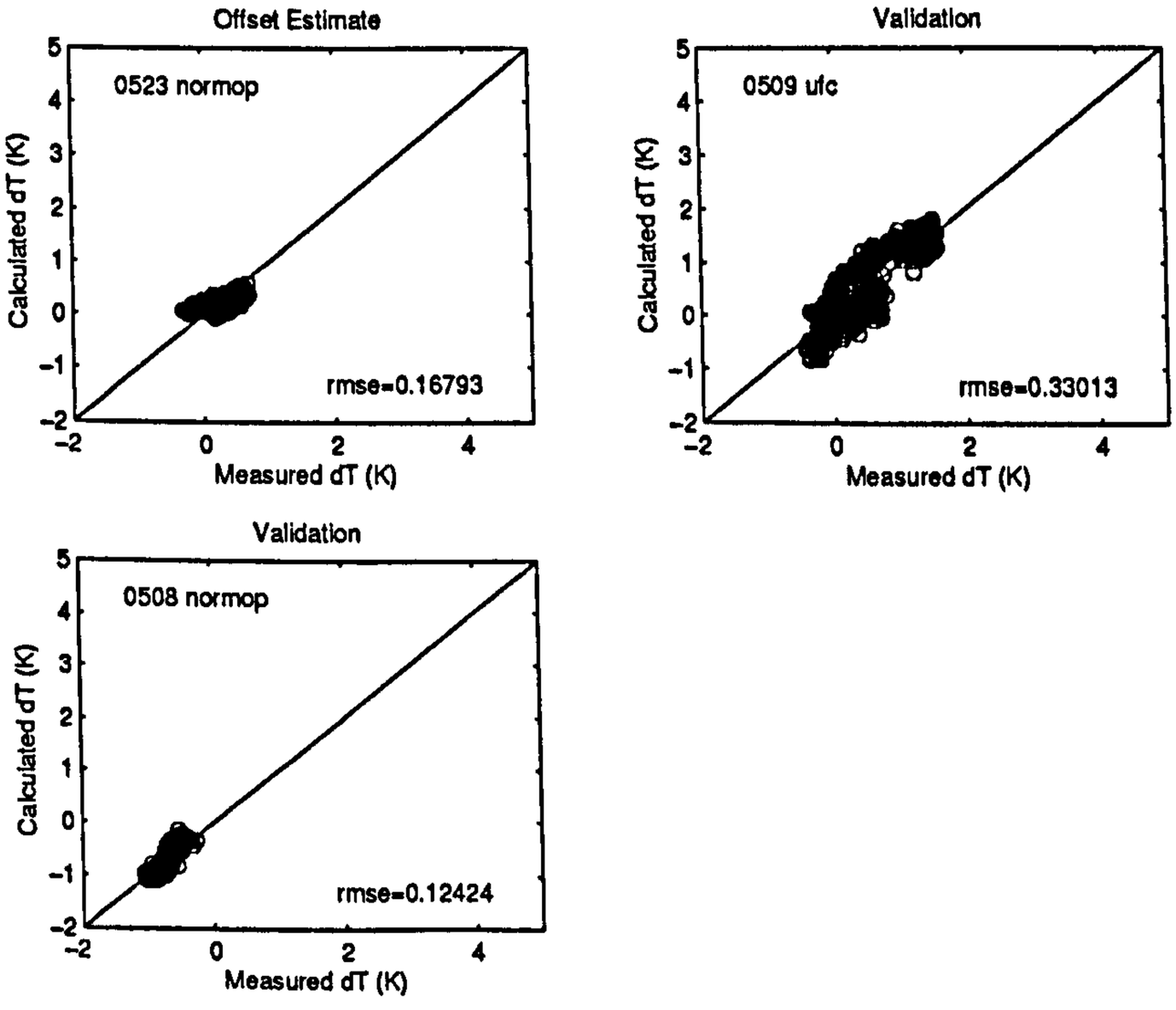

Figure 6.19: The Difference between the Measured Temperature Difference and that Calculated by Energy Balance for the Spring Data with All Offsets Applied, Where 'rmse' Refers to the Root Mean Square Error.

6.4 Uncertainty Validation

Validation of the offsets applied to the sensor measurements to account for persistent bias can be achieved by calculating the sample-wise uncertainty for the air/water-side energy balance equation given by,

$$\xi = \dot{m}_w C_{P_w} (T_{wi} - T_{wo}) - \dot{m}_a (h_{ai} - h_{ao}) . \tag{6.2}$$

Confirmation that the estimates of uncertainty in the measurements and the bias corrections are valid are indicated when $\xi - U_\xi < 0.0\text{kW} < \xi + U_\xi$, where U_ξ is the uncertainty in the residual error, ξ. This comparison can be made for the coil at 100% and 0% duty since the water mass flow rate through the coil is known for both conditions.

Tables 6.2 and 6.3 detail the uncertainties and the correlations between measurements respectively used for the uncertainty plots. In Table 6.3 the 'C' and 'A' indicate the correlations in the Calibration and Acquisition (analogue to digital conversion) uncertainties that exist between some of the sensors (these are also referenced in Table 6.2). Values of uncertainty marked '*' refer to percentage of range uncertainties which are calculated at each data sample. The other uncertainties are in absolute terms.

Correlations arise through calibration using the same instrument/method and acquiring the data through a common conversion component; principally the analogue to digital converter in the control system out-station. The correlation results in two or more measurements being biased either positively or negatively with similar magnitude. For this system, the uncertainties due to bulk averaging and radiation effects are not considered to be correlated in this respect (Chapter 3). The random uncertainty and the uncertainty in the use of dynamic data for steady-state analysis is calculated in accordance with the methodology set forth in Chapter 4. The Figures 6.20, 6.21 and 6.22 show the energy balance residual with the 95% confidence limits for the summer, spring and winter operating seasons. The plots only show the residual when the cooling coil is either at full or zero duty and the plant operating conditions are considered to be 'normal'. One difference between the plots is that the level of uncertainty reduces from summer → spring → winter. This is due to the decreasing levels of the participating uncertainties and the reduction in the uncertainty magnification factors (with respect to total duty, see Section 2.1.1 for a

Table 6.2: Details of the Bias Uncertainty Estimates Used to Generate the 95% Confidence Intervals About the Energy Balance Calculations.

Sensor	**Calibration 'C'**	**Acquisition 'A'**	**Bulk Average 'B'**	**Radiation 'R'**	**Units**
T_{ra}	0.15	0.02	0.25	0.0	K
T_{aa}	0.15	0.02	0.25	0.0	K
T_{sa}	0.15	0.02	0.25	0.0	K
T_{ai}	1.67	0.05	0.25	0.003	K
T_{ao}	1.67	0.05	0.25	0.02	K
T_{wi}	0.139	0.05	0.0	0.0	K
T_{wo}	0.139	0.05	0.0	0.0	K
H_{ra}	2.0*	0.024	2.0	0.0	%
H_{aa}	2.0*	0.024	2.0	0.0	%
H_{sa}	2.0*	0.024	2.0	0.0	%
V_{aa}	0.02*	0.00023	0.06*	0.062	m^3s^{-1}
V_{ra}	0.02*	0.00023	0.06*	0.131	m^3s^{-1}
V_{sa}	0.02*	0.00023	0.06*	0.0	m^3s^{-1}
$\dot{m}_w$	0.006 ($0 < \dot{m}_w < 1.1$)	0.0028	0.0	0.0	kgs^{-1}
	0.5 ($1.1 < \dot{m}_w < 10.0$)				%

Table 6.3: Details of the Sensor Uncertainty Correlations Used to Generate the 95% Confidence Intervals About the Energy Balance Calculations.

	T_{ra}	T_{aa}	T_{sa}	T_{ai}	T_{ao}	T_{wi}	T_{wo}	H_{ra}	H_{aa}	H_{sa}	V_{aa}	V_{ra}	V_{sa}	$\dot{m}_w$
T_{ra}														
T_{aa}														
T_{sa}	CA													
T_{ai}	A	A	A			A	A							
T_{ao}	A	A	A	CA		A	A							
T_{wi}	A	A	A											
T_{wo}	A	A	A			CA								
H_{ra}														
H_{aa}														
H_{sa}								C						
V_{aa}												CA		
V_{ra}														
V_{sa}											CA	CA		
$\dot{m}_w$														

definition of the uncertainty magnification factors) as the loads on the coil reduce. Plot specific comments are:

Summer is the most uncertain of the three plots which can be attributed to the inclusion of the air moisture content in the calculations due to the latent exchange occurring on the coil. This has the effect of increasing uncertainty and reducing precision. One conclusion that can be drawn is that it is desirable to discard the moisture content from calculations whenever possible. Other components will not be as affected under the same circumstances (mixing box/heating coil/fan-duct, etc.). The large error at the beginning of the day is due to dynamics, but it can be seen that the uncertainty assessment attributed to the uncertainty in the dynamics results in sufficiently wide confidence bounds to give no significance to the difference.

Spring is a little improved compared to the summer season in terms of precision and uncertainty for the reasons stated above. Here both the air and water-side capacities contribute to the calculation.

Winter exhibits better precision and uncertainty than the previous seasons. This is due to the water-side capacity rate assumed to be zero when $u_{cc} = 0\%$, hence only the sensible air-side measurements contribute to the calculation of the difference and its associated uncertainty.

6.5 Conclusions

In this chapter, the experimental equipment used for the analysis of uncertainty in condition monitoring a cooling coil sub-system was described. A new *in situ* sensor testing methodology was introduced and used to validate the critical sub-system measurements. The sensor uncertainties and uncertainty correlations were listed. Where possible, the measurements were corrected for persistent bias and then validated by an energy balance between the primary and secondary fluid. Conclusions from this work with regard to: uncertainty in HVAC measurements; the *in situ* methodology; and the implications of these findings, are discussed below.

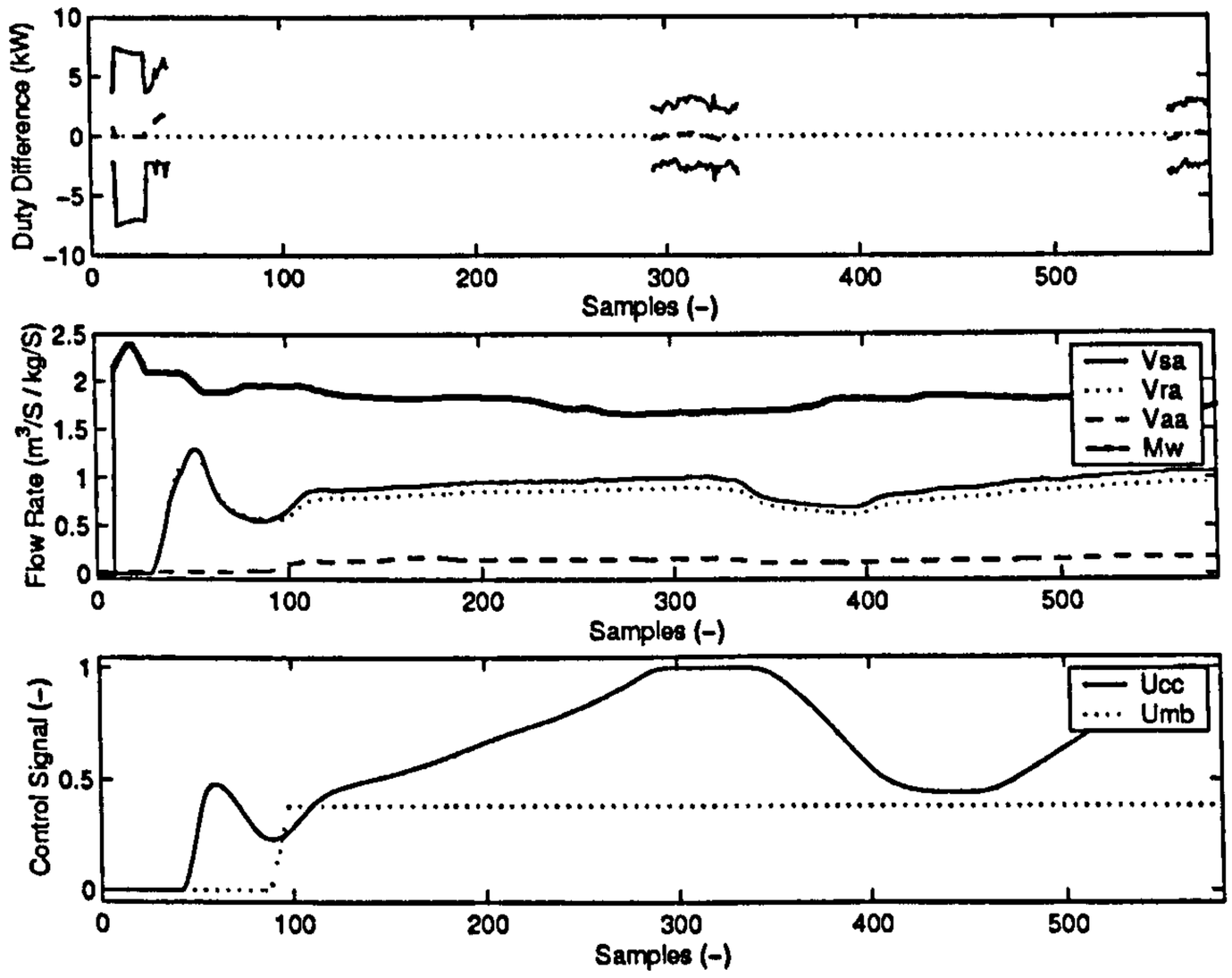

Figure 6.20: Energy Balance With Uncertainty Intervals for 'Normal' System Operation in the Summer.

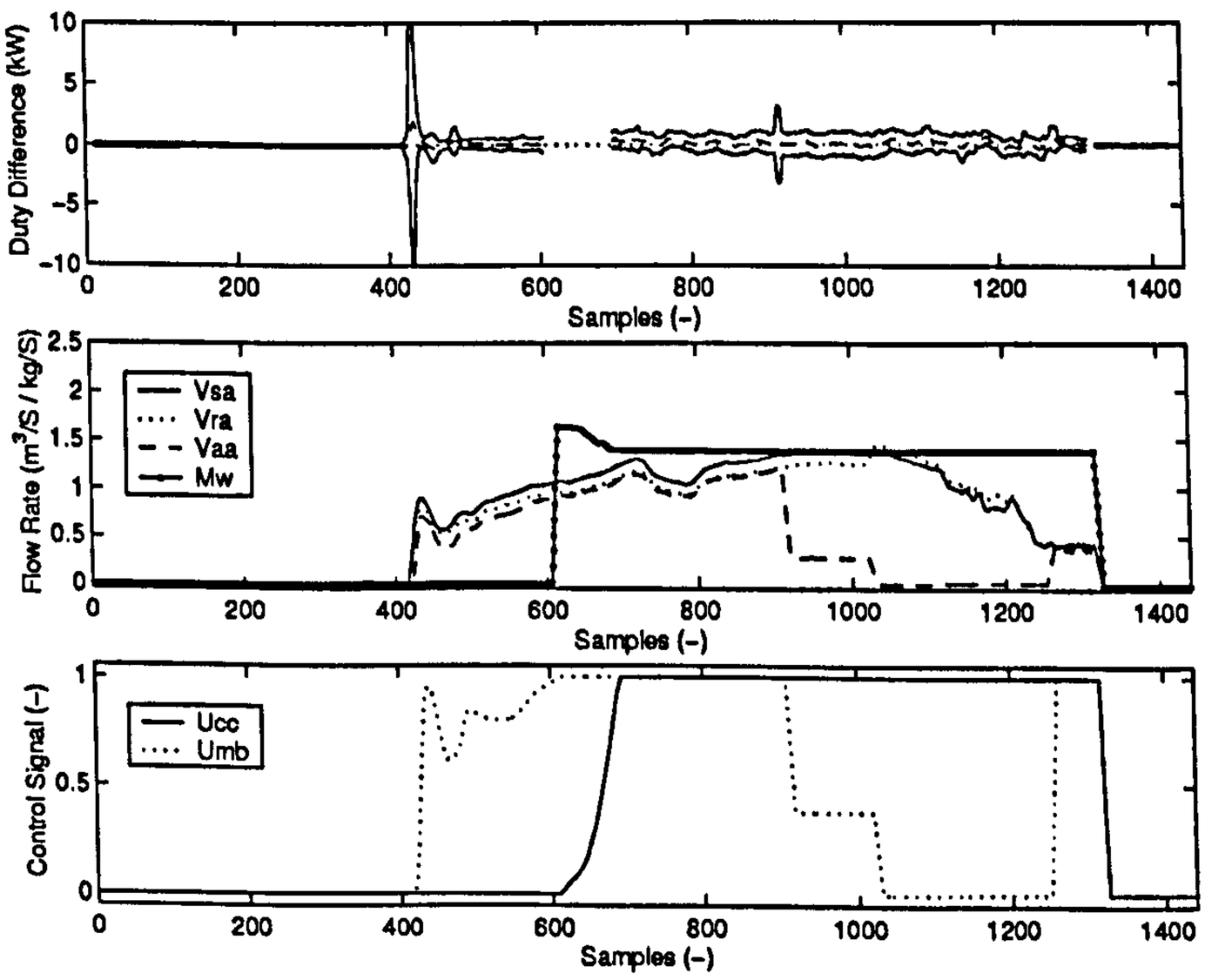

Figure 6.21: Energy Balance With Uncertainty Intervals for 'Normal' System Operation in the Spring.

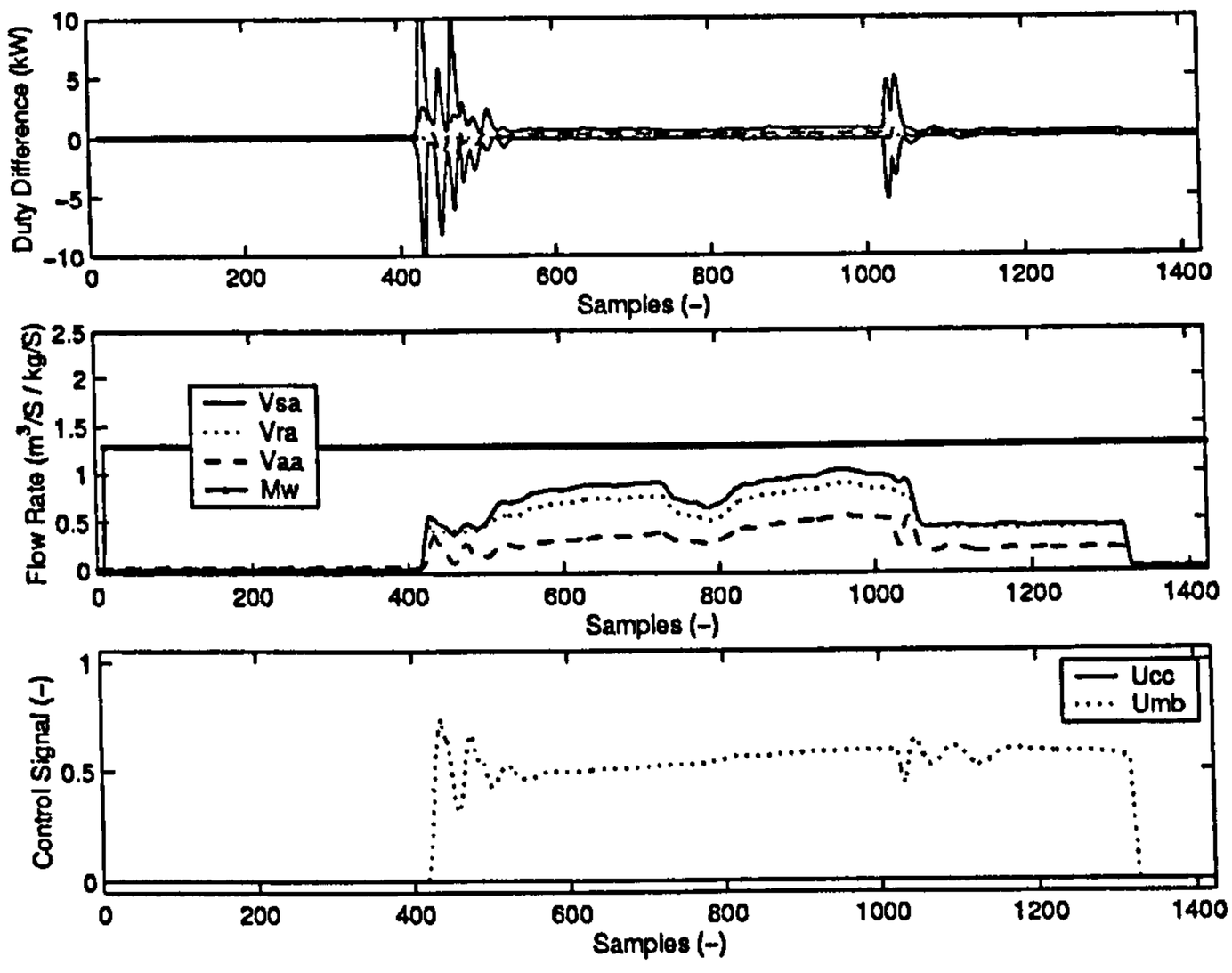

Figure 6.22: Energy Balance With Uncertainty Intervals for 'Normal' System Operation in the Winter.

6.5.1 Uncertainty in HVAC Measurements

Generally where the bias cannot be explained (which allows correction) between *in situ* sensors, the uncertainty should be increased to accommodate these values. The approach here has been to gain the highest precision that could be reasonably expected from typical HVAC measurements. The extraction of the necessary bias information from an *in situ* testing (which would lead to the automation of the process) has been investigated. The procedure has yielded some quite precise and accurate calculations of an energy balance across a cooling coil installed in a real VAV HVAC system. The resultant sensor offsets and corrections have been validated on 'normal' operation data. Some specific comments:

- calibration, acquisition, radiation and, in particular, estimates of bulk averages (single value representation of a spatially distributed quantity or property) are the most significant sources of uncertainty and further work is needed to gain a better understanding of uncertainty due to the two latter sources;

- correlations are generally restricted to those that share common A to D converters and/or are calibrated to the same instrument/standard;

- where conversion of temperature/relative humidity to air moisture content is required, the temperature in the humidity sensor should be used where possible: use of separate sensors will increase uncertainty.

6.5.2 Implementation of the *in situ* Validation Methodology

Summarising the methodology procedure based on the application to the sub-system described in Section 6.1 follows.

1. Check and explain differences between air flow measurements at 0% and 100% outside air.

2. With the coil sections off, check for stratification effects on air measurements, explain effects and remove any persistent offset. Validate with alternate data.

3. Check air moisture content estimates at 0% and 100% outside air. Ideally this should be done over a range of humidities since there can be non-linearities in the sensors/between the relative humidity and temperatures sensors/between each sensing pair. Special care should be taken over the effects of the mixing box on the measurements. The test data and validation should be done over the whole mixing box range.

4. Some measurements of the water mass flow rates in the primary circuit are needed to assess the variation that can be expected. Ideally the mass flow rate of water through the coil would be measured also. Typically though, a reference model will be required to estimate the part load mass flow rates (See Appendix B and Section 7.2).

5. One way to obtain a good estimate of the sensor offset between the chilled water inlet and outlet sensors is to turn the fans off and open up the valve fully. In addition, if insulation is placed either side of the coil, the measurements would be improved. Where this is not available, energy balance at 100% chilled water flow through the coil can be used.

Further, more specific comments are:

- water temperature offset should be measured at several flow rates through the coil;
- the location of the air temperature sensors with respect to the stratification of the mixing box is a major uncertainty issue and further research is needed to identify better solutions to the problem;
- the addition of a mixed air humidity sensor is most likely to realise poorer representation of the bulk average at that point due to air stratification effects. Multiple sensors would be expensive and would not guarantee greater precision;
- trying to account for the temperature rise across a fan is difficult to achieve and should be avoided. Estimations of the energy introduced to the air stream from the fan (affecting the air temperature 'seen' at the sensor) cannot be estimated reliably;
- precise and accurate calibration of the flow sensors are paramount, since the *in situ* testing relies on theses measurements as the reference for some of the 'corrections' of certain measurements. This is particularly important since these cannot be validated against each other without some major physical interaction with the plant.

6.5.3 Discussion of Implications

- Sensor reliability, accuracy and precision is at the centre of data usefulness.
- The testing over different periods demonstrated how sensitive measurements are to manual intervention and especially how measurement characteristics (with respect to equipment configuration) can be altered. This confirms the advantages of an *in situ* testing regime *in addition to* the usual calibration methods.
- The alteration of the plant configuration is not typical of real buildings, but the consequences are the same. Clearly in a real system, tight control over plant disturbance is needed and it is likely that after maintenance/repairs, etc. there will need to be some calibration checks to see if the plant is operating as it was before the disturbance occurred. Again this is an advocate for an automated *in situ* testing procedure.
- It is not the quality of the sensors that are responsible for the lack of precision

and/or presence of significant uncertainty. The positioning in relation to complex and partially unpredictable effects is far more influential; principally stratification.

- Poorly balanced secondary water circuits and their susceptibility to under and over flow is an issue when the coil circuit chilled water flow rate is not measured. Errors on the water-side temperature and flow measurements have a four-fold effect on the corresponding sensible air-side measurements. This is particularly significant where there are multiple coils fed from a common circuit. One solution is to measure the flow in each circuit, although this would increase the cost of the monitoring plant.

Chapter 7

Uncertainty in Condition Monitoring

Automated Condition Monitoring in HVAC is a concept designed to assist operators in the detection of undesirable equipment behaviour. The application of model based techniques makes it possible to detect abnormal operation that would otherwise go undetected (Hyvärinen, 1997b; Hyvärinen, 1997c).

For a scheme to be useful to the operator, it must be sufficiently sensitive so that small changes in the condition of operation can be detected. Abrupt changes in the system usually result in relatively large changes in the expected values of the measured variables and so the current practice of 'limit checking' to raise an alarm would be sufficient. Secondly, field trials have shown (Vaezi-Nejad et al., 1997) that if condition monitoring is to be applied successfully and accepted by equipment operators, it must not generate false alarms (indicate abnormal operation when the equipment is operating normally). The belief in an alarm becomes the principal issue when applying condition monitoring techniques to equipment installed in real buildings (Visier, 1998). To date, this robustness issue has not been successfully addressed in the literature.

Recent research has demonstrated the viability of first principles based, steady-state models for generating accurate predictions of the performance of HVAC equipment installed in real buildings (Buswell et al., 1997; Buswell and Wright, 1998; Norford et al., 2000). This chapter presents a condition monitoring scheme applied to an HVAC cooling coil

subsystem based on such models. The scheme is applied to the system described Chapter 6. The robustness of the scheme output, in terms of false alarm rate, is assured by the appropriate incorporation of all the significant contributing uncertainties. The sources of these uncertainties have been discussed and demonstrated in Chapters 3 through to 6. The introduction of uncertainty via the parameter identification process is addressed in this chapter. The relative magnitudes of the contributions to the uncertainty in the scheme output are analysed.

The robustness and sensitivity of the condition monitoring scheme is evaluated using data from three operating conditions: summer, winter and spring. The plant was operated under two conditions: 'fault free' and 'fault present'. The two faults used in the analysis were valve leakage and coil under capacity.

7.1 Scheme Design

Model based condition monitoring compares the measured performance of the target system with a model that describes the system operating correctly. The difference between the model output and the actual system output is the 'prediction error' (see Figure 1.2 in Section 1.2.1). The significance of the prediction error indicates whether the system can be regarded as operating correctly or not. The uncertainties in the model structure, model parameters, measurements and in the system's proximity to steady-state are used to ascertain the uncertainty in the prediction error. If the confidence limits, given by the uncertainty $\pm U_\xi$, about the prediction error, ξ, are such that $\xi - U_\xi < 0.0\text{kW} < \xi + U_\xi$, the system is operating correctly. If $\xi - U_\xi > 0.0\text{kW}$ or $\xi + U_\xi < 0.0\text{kW}$ then the system performance is significantly different from that predicted by the model. The system operation is therefore abnormal, and, for the purposes of this research, is considered to indicate the presence of a fault in the system[1].

Figure 7.1 depicts the information flow diagram for the proposed condition monitoring scheme. The parenthesis indicates arrays of data, detailed in Table 7.1. u_{cc}, s, m_w, Q_t and Q_t' refer to the control signal to the cooling coil, valve stem position, water mass flow

[1]Generally the existence of a fault is conditional on there being some cost/benfit associated with correcting the abnormal behaviour (Rossi and Braun, 1994).

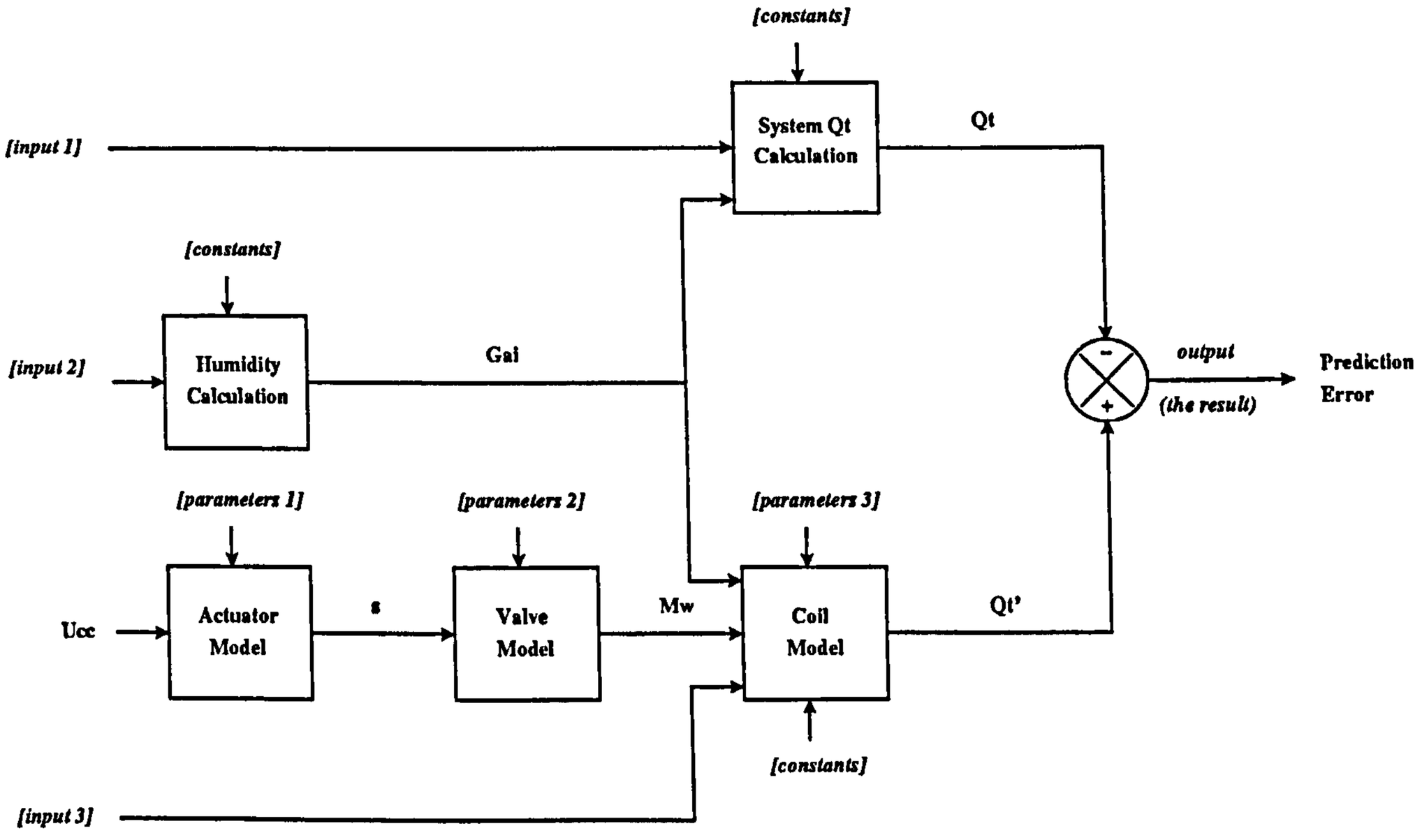

Figure 7.1: Information Flow Diagram for the Condition Monitoring Scheme.

rate (kgs^{-1}), actual total heat transfer (kW) and predicted total heat transfer, respectively. The 'humidity calculation' block generates the humidity ratio of the air into the coil using the ratio of the outside air to return air in the supply air stream (see Equation 6.1 in Section 6.3.2 and Section 6.3.3). The 'system Q_t calculation' block represents the air side total heat transfer calculation, $Q_t = \dot{m}_a (h_{ai} - h_{ao})$, where h_{ai} and h_{ao} are the air inlet and outlet enthalpies respectively ($kJkg^{-1}$). The reference model predicts the total heat transferred in the heat exchange process. The model consists of three components: a valve model, an actuator model (Appendix B) and a heat-exchanger model (Section 5.2).

The reference model is calibrated to more precisely represent the test subsystem. This is achieved by the adjustment of a number of parameters. The parameters are estimated by inspection of the equipment, design information and training data. The training data is generated by open loop tests that step the system throughout the range of operation. ω, a_l, a_h and β represent the actuator and valve parameters relating to hysteresis, low activation point, high activation point and valve curvature characteristic (A fuller account of the model and parameters can be found in Appendix B). The UA scaling factor, S_{UA}, is dimensionless and describes the increase/decrease in the UA (WK^{-1})of the target coil

Table 7.1: Arrays of Input Data in the Condition Monitoring Scheme.

Input 1	Input 2	Input 3	Param. 1	Param. 2	Param. 3	Constants
$\dot{V}_{sa}$	$\dot{V}_{sa}$	$\dot{V}_{sa}$	ω	β	S_{UA}	Cp_a
T_{sa}	$\dot{V}_{aa}$	T_{ai}	a_l	γ	l_w	Cp_w
T_{ai}	T_{aa}	T_{wi}	a_h	$\dot{m}_{w_{max}}$	l_h	ρ_a
T_{ao}	T_{ra}	-	-	-	d_t	ρ_w
H_{sa}	H_{aa}	-	-	-	n_r	-
-	H_{ra}	-	-	-	n_c	-
-	-	-	-	-	R_a	-
-	-	-	-	-	R_m	-
-	-	-	-	-	R_w	-
-	-	-	-	-	ν_a	-
-	-	-	-	-	ν_w	-

with respect to a reference coil at 100% duty. These five parameter are estimated from the training data after the other parameters listed in Table 7.1 have been established. The parametric uncertainty is evaluated from the data source used to generate the respective estimates. In terms of model calibration, the uncertainty in the parameter estimates is derived from the calibration data measurements.

The scheme is formulated for *on line* application. At each new sample the new mean value for each input and output variable is calculated, based on Equation 4.2. The magnitude of the prediction error is then calculated using the mean values. The assessment of the random uncertainty and the uncertainty due to the proximity of the system to steady-state is calculated simultaneously, based on Equation 4.3. Any 'percent of range' measurement uncertainties and the model structural uncertainties are also updated at every new sample. Fixed bias errors in the measurements and parameters remain constant. All the uncertainties are quoted at the 95% level, hence the 95% confidence in the scheme output can be calculated. Appendix C details the derivation of the uncertainty calculation procedure.

The condition monitoring scheme generates an alarm when the prediction error becomes significantly non-zero. There must be a flow of air over the coil and water flow through the primary circuit if the measurements are to be applicable to the calculations. The scheme, therefore, only allows alerts to a significant change in system operation when these mass flow rates are non-zero.

7.2 Subsystem Model Calibration

7.2.1 Calibration Methodology and Parametric Uncertainty

The subsystem model has 17 parameters and their values and uncertainties need to be evaluated. The width and height of the coil air-side face area, the numbers of circuits and rows and the internal diameter of the tubing used for the water circuits can be determined directly from inspection of manufacturers' data. The maximum chilled water mass flow rate through the coil needs to be measured. Uncertainty will be introduced and should be estimated based on the available data. There will not usually be any uncertainty associated with the numbers of circuits and rows.

The estimation of the resistance parameters can be made from manufacturers' data as suggested by Holmes (1982). Regression can be used to generate confidence limits in the parameters. Holmes also gives some typical resistance coefficients for HVAC coils if this detailed information is not available. The coefficients published in the work can be used to generate mean values and 95% confidence estimates. These resistances then remain constant in the model and an additional parameter is added. This parameter is termed the UA scaling factor, (S_{UA}) (Buswell et al., 1997); it simply scales the water/air/material resistances and is adjusted until the reference model output matches the test data at 100% duty. No additional uncertainty is introduced into the model. The uncertainty in the measurement is assigned to the valve parameter describing the maximum flow in the primary circuit, $\dot{m}_{w_{max}}$ and $\dot{m}_{w_{max}}$ is estimated prior to S_{UA}. The exponents of the air-side and water-side resistance coefficients are reported in the literature (Holmes, 1982; Rabelil et al., 1999) to lie between 0.7 and 0.8. The average is taken and the 95% confidence is estimated from these values.

This leaves the actuator parameters (a_l, a_h and ω) and the valve curvature parameter (β) to be estimated. The valve authority is fixed such that $\gamma = 0.5$. This is because the information in typical HVAC measurements, is not sufficiently rich to support the estimation of more than one parameter that contributes to the process curvature characteristics. These are estimated from the steady-state step-test data collected from the system. This data is generated by stepping the valve control signal from $u_{cc} = 0\% \rightarrow u_{cc} = 100\% \rightarrow u_{cc} = 0\%$

in 5% or 10% steps. After each step, the system is left to reach steady-state. As the valve closes, the steps are usually coarser than when the valve is opening and are required to determine the magnitude of the hysteresis. The water temperature measurements were available on the inlet and outlet of the coil in this installation and so the water mass flow rates were calculated from,

$$\hat{m}_w = \frac{\dot{m}_a \left(h_{ai} - h_{ao}\right)}{Cp_a \left(T_{ai} - T_{ao}\right)}, \tag{7.1}$$

where $\dot{m}_a$ is the air mass flow rate, T_{ai} and T_{ao} are the air inlet and outlet temperatures and Cp_a is the specific heat capacity of air. This data was used to calibrate the remaining model parameters and the uncertainties in the measurements were used to generate the uncertainty in $\hat{m}_w$.

The selection of the low activation point is based on two consecutive points generated while increasing the control signal to the valve. The first point is required to yield no significant flow through the coil and the second point should exhibit significant flow. It can be stated that there exists 99.9% confidence that the valve will always open between these points (see Section 5.1 for details of the 'Absolute Range' uncertainty assessment technique). The activation point is therefore defined by the mean of these and the 99.9% limits scaled down to 95% (a factor of 0.595). A similar task is repeated for the high activation point.

Only the data in between the activation points as the valve is opening are used to establish the valve curvature, β. The estimation is made in the least squares sense. The uncertainties are calculated for each data point by,

$$U_{\bar{x}} = \sqrt{\left(\frac{\sum_{i=1}^{i=n} U_{x_i}}{n}\right)^2 + \left(\frac{tS_{x_p}}{\sqrt{n-1}}\right)^2}, \tag{7.2}$$

where $U_{\bar{x}}$ is the uncertainty in the averaged point, n is the number of points in each sample (10) of each of the p steps. $\frac{tS_{xp}}{\sqrt{n-1}}$ is the 95% confidence limit where S is the standard deviation of the mean on the points at each step and t is the Student-t statistic. The uncertainty in the parameter, β, can then be calculated from,

$$U_\beta = \sqrt{\left(\left[\frac{\delta\bar{x}}{\delta\beta}\right]^{-1} U_{\bar{x}}\right)^2}. \tag{7.3}$$

The uncertainties vary across the range of operation and so the parametric uncertainty in β is given as a function of control signal. The function uses linear interpolation to estimate

between points. The uncertainty that exists from the last data point before the activation points is linearly reduced to a point nominally half way between the activation point and fully open/closed position. This ensures that the uncertainty at the point of transition from the stationary/moving valve is accounted for. This is particularly important at the low end of operation. In addition, the gradient in the inactive region at the low end of operation will generate sensitivity coefficients equivalent to zero. Additional measures are required to ensure that a gradient can be calculated to show the correct level of uncertainty.

Using the valve closing data ω, is adjusted to minimise the error in a least squares sense. The value of a_l needs to be adjusted simultaneously to take account of the structure of the actuator model, although the relationship between a_l and the real activation point remains constant. The uncertainty in the hysteresis parameter can be accounted for by including the uncertainty in the closing data points in the evaluation of the uncertainty in β.

7.2.2 Calibration Test Data

Figure 7.2 demonstrates the step tests in terms of the calculated water mass flow rate. The tests were carried out on two separate days approximately two weeks apart during summer (high load) conditions. At $u_{cc} = 1.0$, the maximum mass flow rate is different for each day as the result of changes in the system configuration (Chapter 6). After $u_{cc} > 0.2$, there is a slight increase in the uncertainty as $u_{cc} \rightarrow 1.0$ due to the corresponding increase in UMFs[2]. There appears to be some heat transfer when $u_{cc} < 0.2$ in both plots, which is due to the presence of a difference in the water inlet and outlet temperatures. This occurs because the temperature sensors are sited in the stagnant legs (when $u_{cc} = 0$) immediately outside the coil. Both tend to the ambient temperature when there is no flow through the coil at similar rates. If the coil has been operational, the different initial temperatures will mean the difference between the inlet and outlet will not significantly decrease with time (of the order of tens of minutes). The magnitude of the uncertainty when the valve is closed, however, confirms the lack of significance of this characteristic. At approximately sample number 375 on the righthand plot, the confidence is very high and indicates no

[2]Uncertainty Magnification Factors, see Section 2.1.1 for a definition.

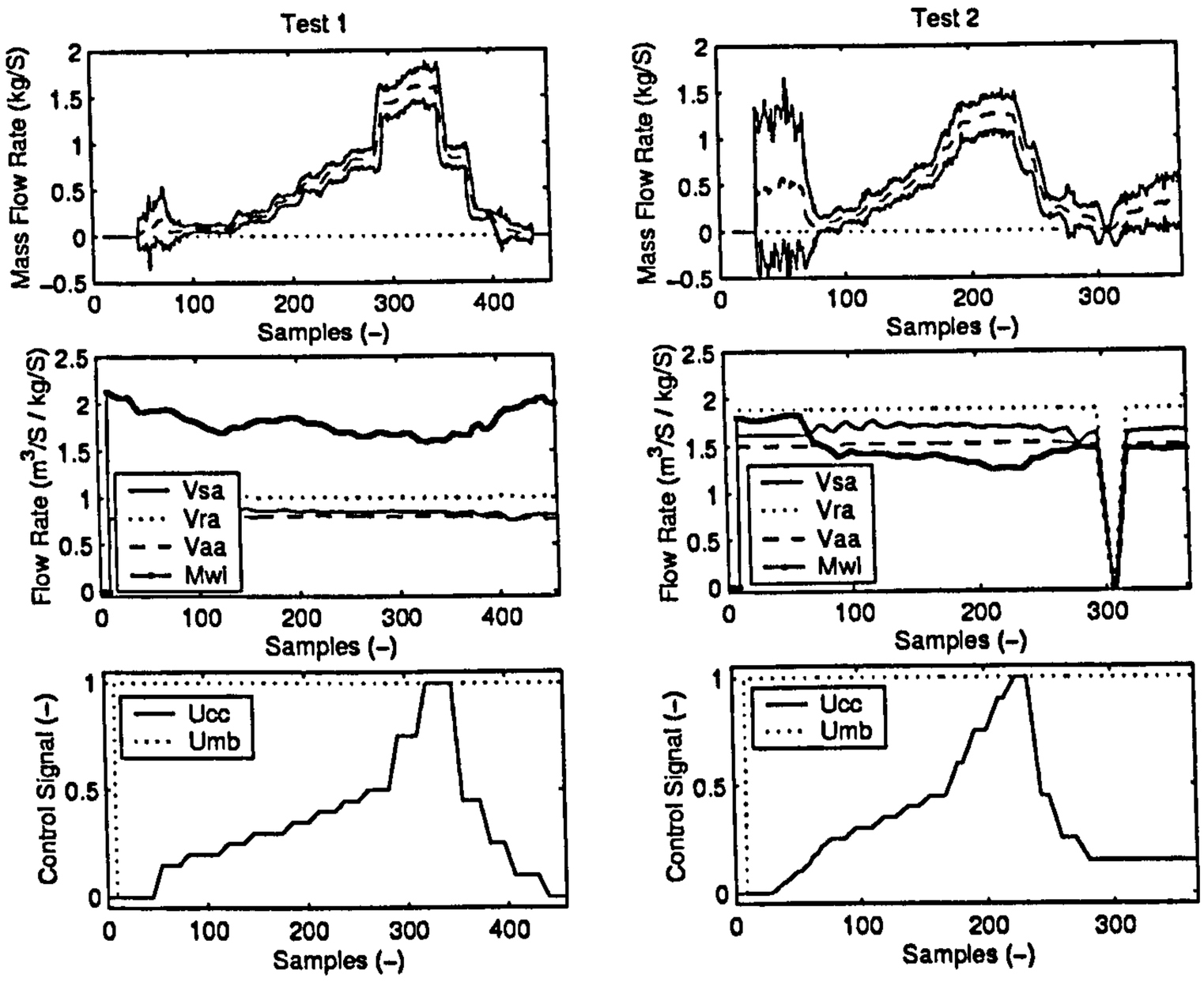

Figure 7.2: Using the Energy Balance Between the Air and Water Sides of the Cooling Coil to Calculate the Actual Water Mass Flow Rate and Uncertainty at Part Load.

water mass flow rate. At this point the plant shut down for a short period. This resulted in no water mass flow rate in the primary circuit and no air flow. There is no heat transfer and therefore no mass flow rate. This also results in negligible uncertainty[3].

The plots in Figure 7.3 shows the water mass flow rate characteristics and uncertainty derived from the tests shown in Figure 7.2. Test 1 in Figure 7.2 was carried out at 100% supply fan speed which relates to the middle plot in Figure 7.3. Test 2 Figure 7.2 was carried out at 50% supply fan speed and relates to the uppermost plot in Figure 7.3. The bottom plot in Figure 7.3 shows the significance of the difference between the two tests. The right hand plots show the mean mass flow rate corresponding to the control signal. The solid line refers to the valve opening data and the broken line refers to valve closing data. The left hand plots illustrate the significance of hysteresis.

Both tests confirm that there is 10%→12% (of full flow) hysteresis in the mass flow rate (6kW in terms of water-side ΔT=10K) and that it is just significant in terms of the

[3]It should be noted that this feature was not planned in the original test.

uncertainty in the calculation of $\hat{m}_w$. The valve is observed to become inactive when $0.75 > u_{cc} > 0.9$. Both plots show significant flow at $u_{cc} = 0.25$, based on the filtered data; a 'lag' in the measurements is introduced by the filtering process. Consideration of the raw water inlet/outlet temperature data shows that the Test 1 day opens $0.2 > u_{cc} > 0.25$ and Test 2, $0.15 > u_{cc} > 0.2$. One possible explanation is that the higher flow rate in Test 2 could indicate higher pressures across the valve control port, hence significant flow would be achieved at a smaller mechanical opening (lower valve position).

7.2.3 Calibration Results

The subsystem model parameter estimates and the uncertainties associated with each are summarised in Table 7.2. Figure 7.5 shows the level of uncertainty in the parameter β. Estimated from the data it represents the uncertainty in β, γ and ω as calculated using Equations 7.2 and 7.3. Figure 7.4 demonstrates the application of the calibrated valve and actuator model. The Test 1 data has been used to train the model and the Test 2 data to validate the results. There are some points outside the confidence limits. The model is static as are the uncertainties associated with its predictions. The data plotted over the model prediction are time continuous and are generated by stepping the control signal, see Figure 7.2. The data between each of the steps will introduce uncertainty due to the transients present. This uncertainty is not accounted for in the plots shown in Figure 7.4 and hence some of the intermediate samples between the larger steps appear to violate the model uncertainty.

At the lower end of operation the uncertainty issues surrounding the drifting temperatures apply as discussed in Section 7.2.2. The evaluation of the uncertainties in the scheme in combination with the model will result in robust predictions in terms of the prediction error.

7.3 Analysis of Uncertainties

The parametric, measurement, transient and model structural uncertainties are applied to the test subsystem condition monitoring scheme. Samples of the test data from each

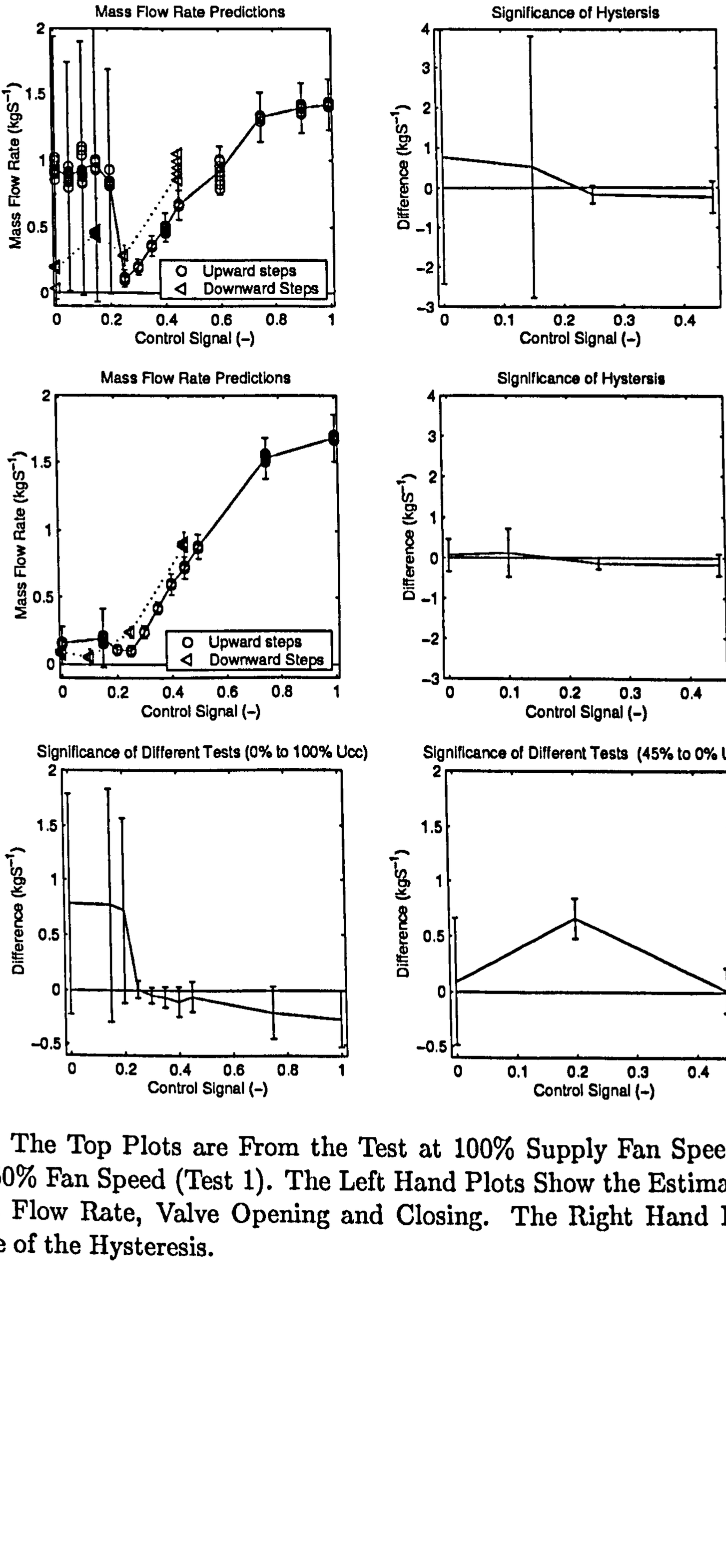

Figure 7.3: The Top Plots are From the Test at 100% Supply Fan Speed (Test 2), the Middle at 50% Fan Speed (Test 1). The Left Hand Plots Show the Estimation of Steady-State Mass Flow Rate, Valve Opening and Closing. The Right Hand Plots Show the Significance of the Hysteresis.

Table 7.2: Subsystem Model Parameters and the Associated Uncertainties.

Parameter	Estimate	Uncertainty (±)	Units
ω	0.080	(included in β)	(-)
a_l	0.230	0.05	(-)
a_h	0.825	0.08	(-)
β	0.720	$f(u_{cc})$	(-)
γ	0.500	(included in β)	(-)
$\dot{m}_{w_{max}}$	(See Chapter 6)	0.198	kgs^{-1}
S_{UA}	0.916	(accounted for in $\dot{m}_{w_{max}}$)	(-)
l_w	0.914	0.010	m
l_h	0.607	0.010	m
d_t	0.013	0.001	m
n_r	6	N/A	(-)
n_c	18	N/A	(-)
r_a	1.03	0.32	$_{(rows)}Km^2s^{\nu}W^{-1}m^{-\nu}$
R_m	0.417	0.055	WK^{-1}
r_w	0.280	0.12	$_{(rows)}Km^2s^{\nu}W^{-1}m^{-\nu}$
ν_a	-0.750	0.05	(-)
ν_w	-0.750	0.05	(-)

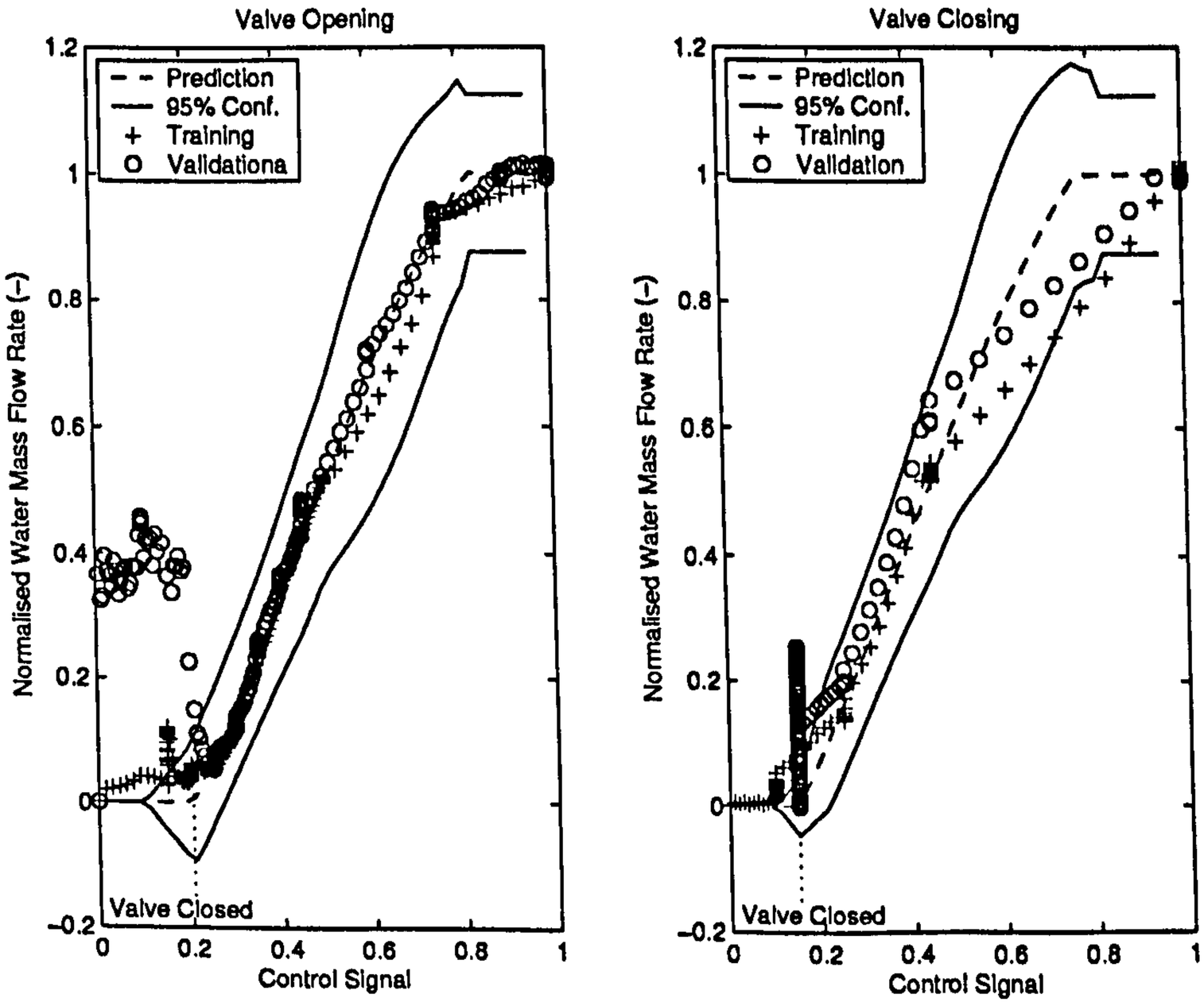

Figure 7.4: The Valve Actuator Model Calibrated from Data and Engineering Knowledge.

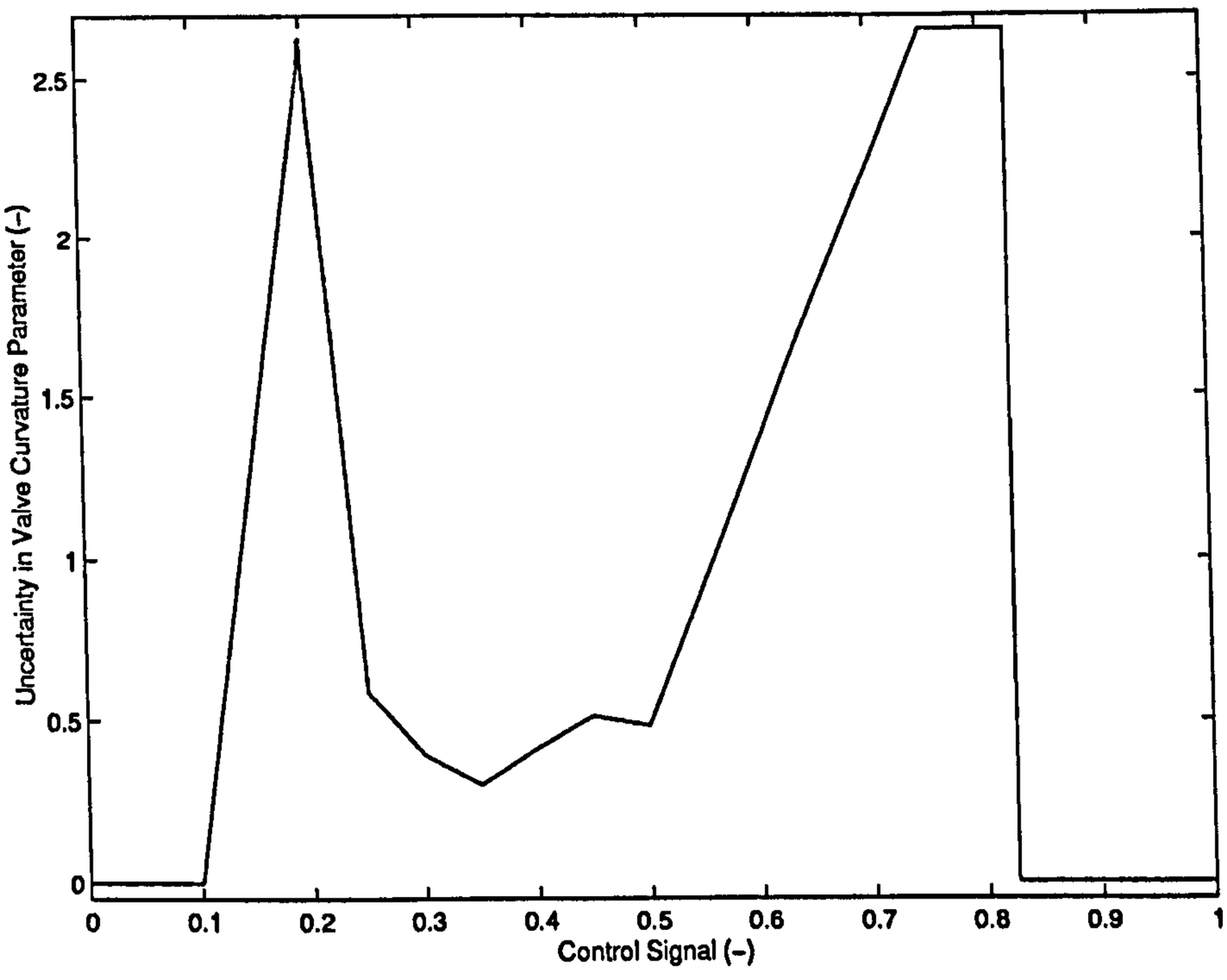

Figure 7.5: The Uncertainty in the Parameter β.

test period (summer, winter and spring) have been selected to illustrate the varying levels of uncertainty contributions from classified sources. Figures 7.6 through to 7.9 show the UPCs to the uncertainty in the prediction error.

The upper most plot in each figure gives the magnitude of the total uncertainty in kW. The combined static uncertainties and the uncertainty due to transients is also plotted. Note that the static and transient uncertainties are combined in quadrature, not summed, to generate the total uncertainty. The second plot from the top gives the UPCs[4] in four classes: air flow rate measurement, air temperature measurement, water temperature measurement and air moisture content measurement (where the uncertainty sources are a combination of the air temperatures and relative humidity measurements used to calculate humidity ratio). These are labelled as 'M_a', 'T_a', 'T_w' and 'G_a' respectively on Figures 7.6 to 7.9. The uncertainties from *all* the measurements in each class are included. This allows the primary correlations between measurements to be accounted for in the UPC[5]. The third plot gives the UPCs for the model parametric and the model structural uncertainties and

[4]Uncertainty Percentage Contributions, see Section 2.1.1 for definition.

[5]The UPCs can only be directly calculated from a general uncertainty analysis, i.e. ignoring the correlations. Here the affects of any correlations between like sensors is accounted for in the UPC calculation.

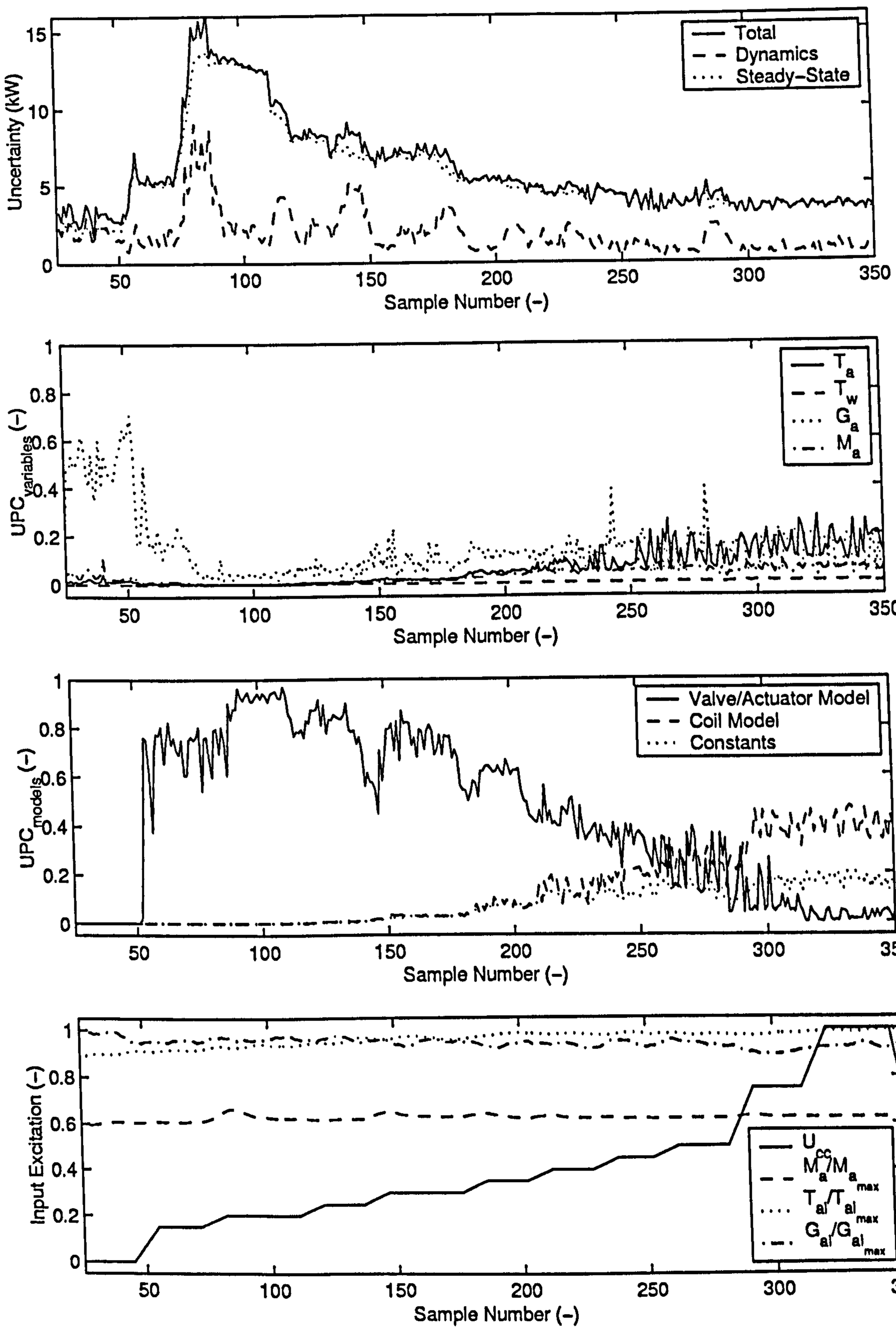

Figure 7.6: Summer Conditions (Wet Coil) Showing High Sensible and High Latent Heat Exchange Contributions to the Total Heat Transfer. When $u_{cc} = 0.0$, $Q_t = 0.0$kW and When $u_{cc} = 1.0$, $Q_t \approx 35.0$kW.

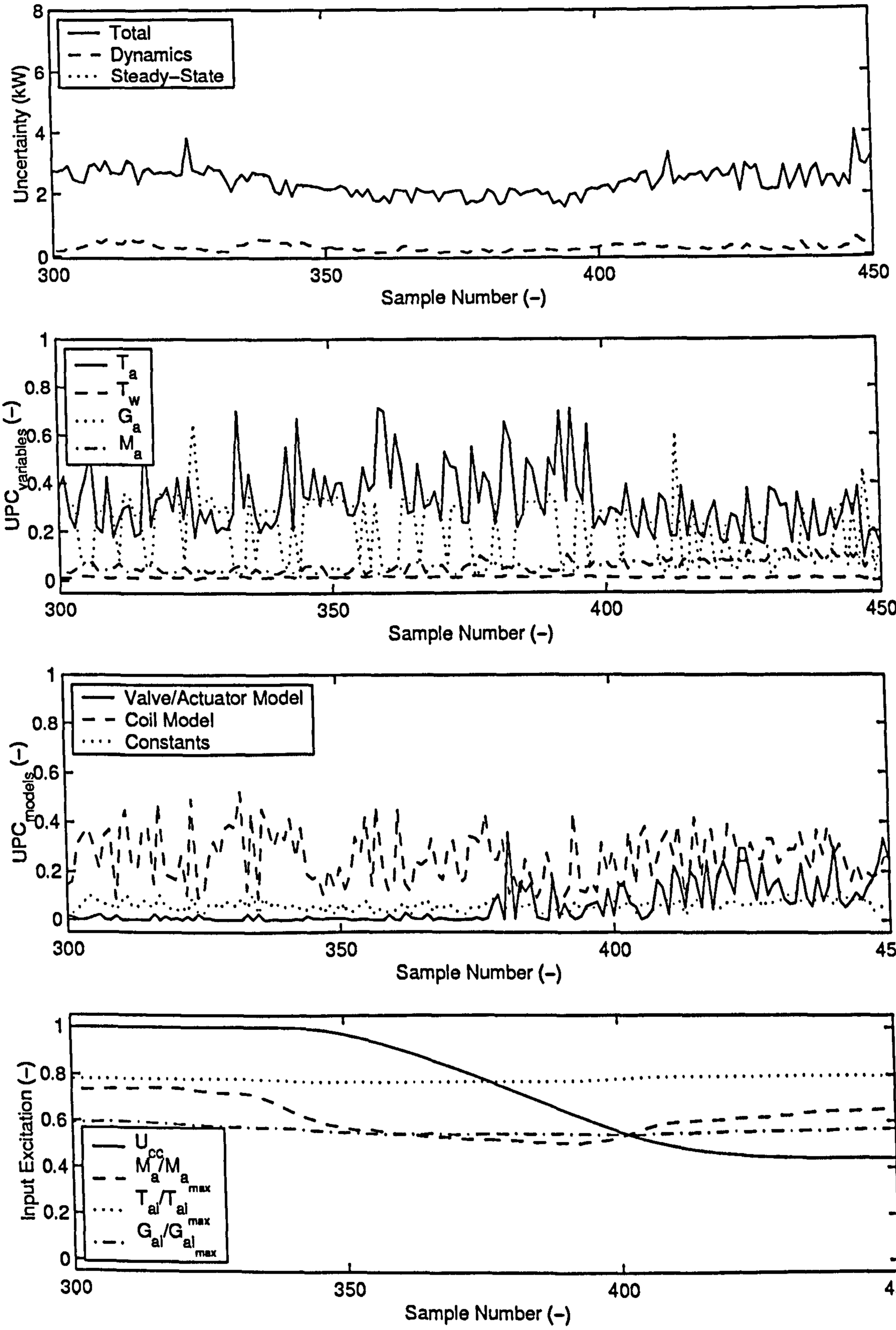

Figure 7.7: Summer Conditions (Dry Coil) Showing High Sensible Heat Exchange Only, but Including the Latent Component in the Calculation. When $u_{cc} = 1.0$, $Q_t \approx 21.0$kW.

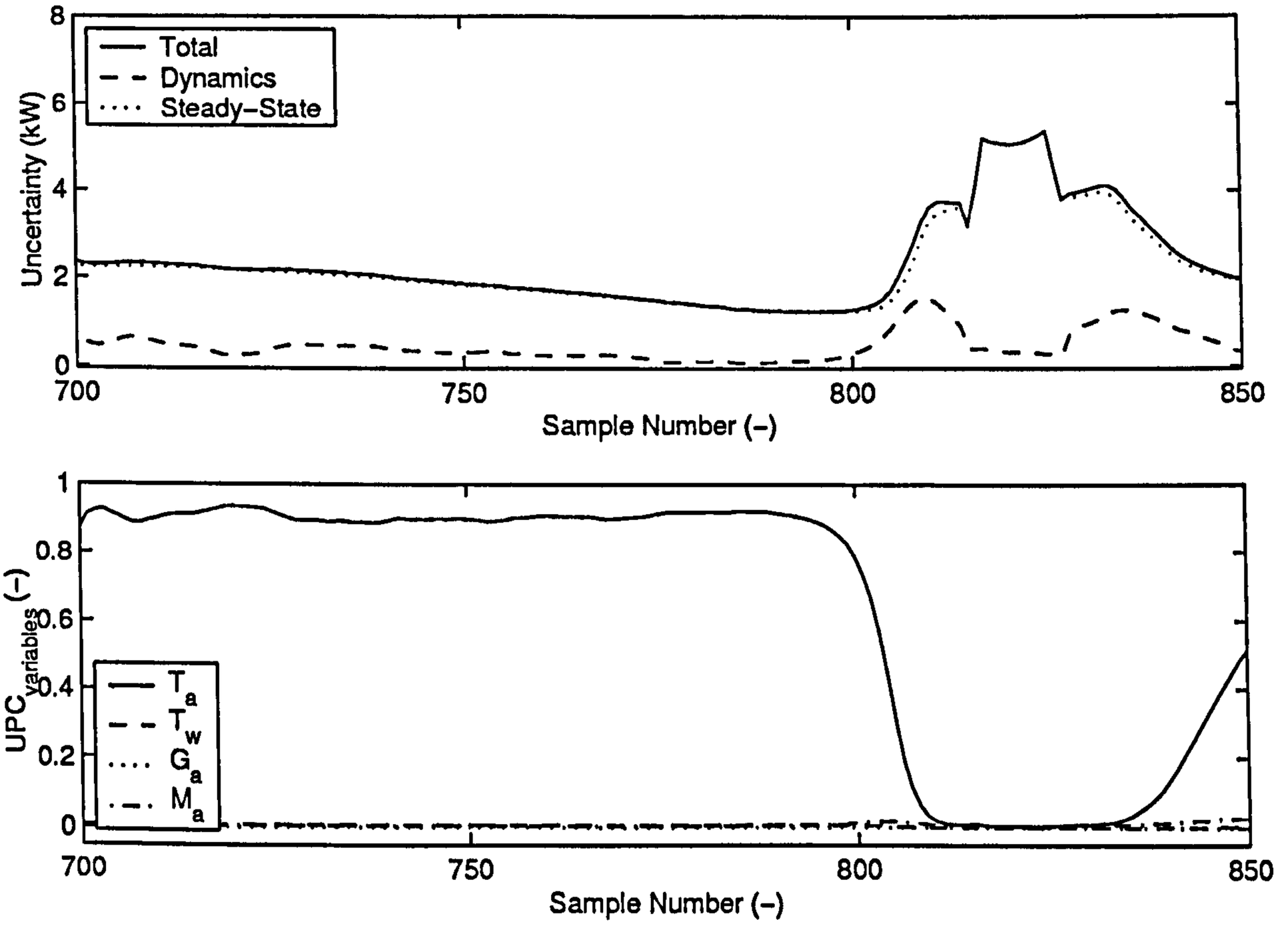

Figure 7.8: Spring Conditions (Dry Coil) Showing Moderate Sensible Heat Exchange. When $u_{cc} = 1.0$, $Q_t \approx 14.0$kW.

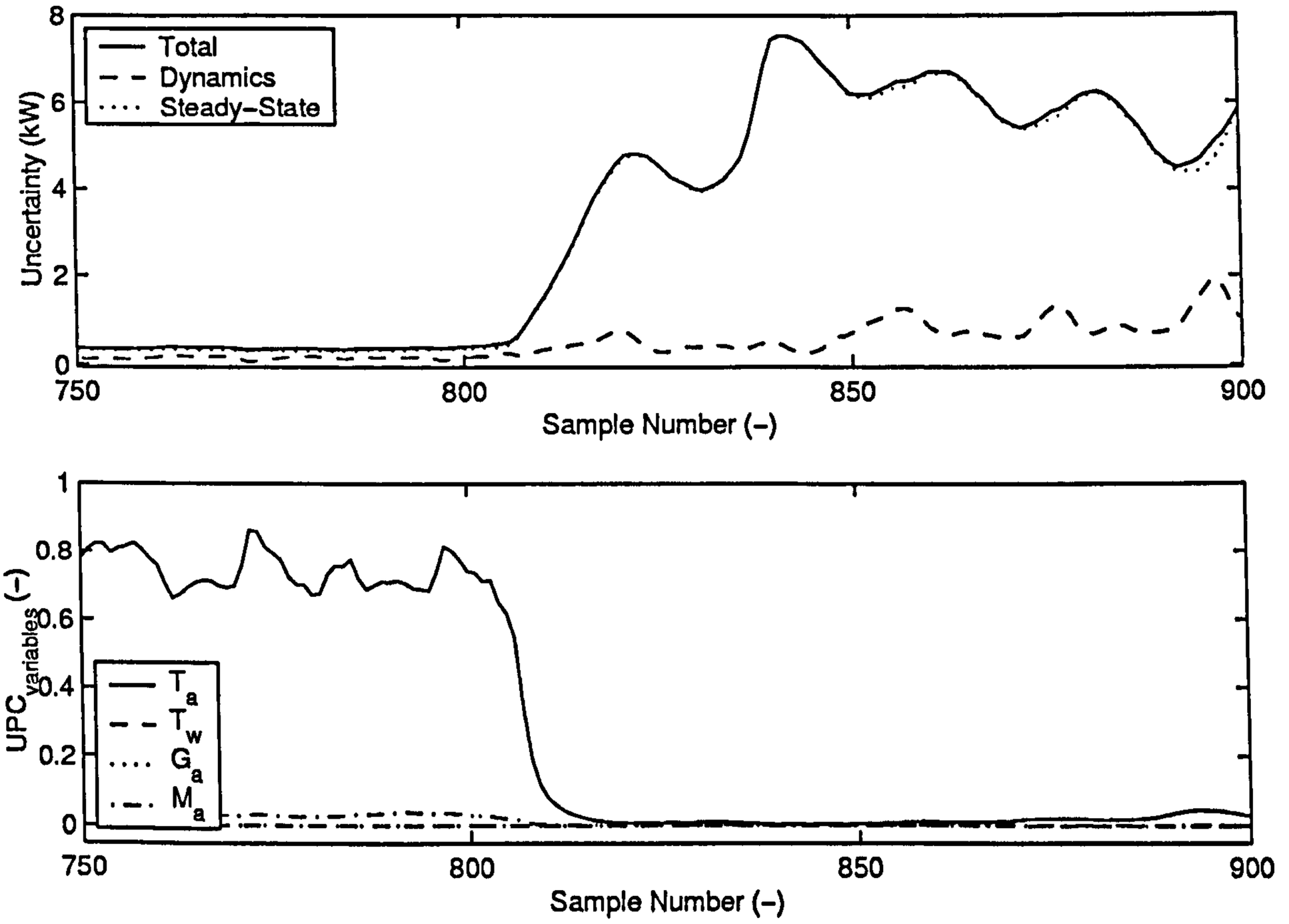

Figure 7.9: Winter Conditions (Dry Coil) Showing Low Sensible Heat Exchange. Q_t is Nominally Zero During this Period.

includes the uncertainties due to the physical constants. The bottom plot shows the input excitation expressed as the ratio of the measurements over maximum values encountered in the test period. The input excitations are the control signal, supply air mass flow rate, inlet air temperature and inlet humidity ratio, labelled as, 'U_{cc}', 'M_a', 'T_{ai}' and 'G_{ai}' respectively.

Figure 7.6 shows the first half of one of the step-tests recorded in July. The coil surface was wet and the coil was operating at the highest duty observed in the test periods. Figure 7.7 depicts a typical August day. The summer conditions result in high duty, but on this day the inlet air humidity was sufficiently low to yield dry coil operation. However, since it was established that the summer conditions could generate wet coil operating conditions, the latent component was left in the calculation of prediction error. This plot demonstrates the effect of the humidity on the uncertainty in the prediction error under sensible load conditions. When compared to Figure 7.6, it shows the difference in uncertainty between wet and dry coil operation. Figure 7.8 details the results from a day in May, representing the spring seasonal conditions. The conditions have been tested and are known to preclude wet coil operation. The 'system Q_t Calculation' block depicted in Figure 7.1 is simplified to sensible heat transfer only as a consequence and the uncertainty contribution from the humidity class is correspondingly zero. The inlet air temperature is approximately 50% of the full duty case but the air mass flow rate is the highest of the test periods. Figure 7.9 shows similar dry coil operation to Figure 7.8, but for the winter period, where the cooling coil is off for the majority of the time. The data was taken from a day in March.

7.3.1 Results of Uncertainty Analysis

Consideration of Figures 7.6 through to 7.9 lead to a number of observations:

- the 'noise' in the summer data is due to the humidity measurements;
- the contribution of uncertainty due to transients is minimal, particularly when the system is close to steady-state. Although not obvious from these plots, the evaluation is required to prevent spurious uncertainties being generated during significant (and rapid) changes in operating condition. This can be seen as the valve opens in

Figure 7.6 at sample 80-85 the dynamic uncertainty contribution is ~2kW (~15%);

- the uncertainty contributions of the water inlet temperature can be neglected;
- the uncertainty in the physical constants and the air mass flow rate measurements do make a significant contribution to uncertainty at very high duties;
- the structural uncertainty associated with the coil model is highly significant during the summer periods;
- the uncertainty when the valve is just open dominates the uncertainty in the prediction error. This is due to the high gain of the subsystem at this operating region;
- the uncertainty at $u_{cc} = 100\%$ during the summer ranges from ~3kW to ~4kW. In spring this value is ~2kW. During the winter the uncertainty when $u_{cc} = 0\%$ is ~0.5kW;
- when $\dot{m}_w \neq 0 \text{kgs}^{-1}$the air temperature uncertainty dominates the uncertainty in the prediction error. During the summer conditions the uncertainty due to the air humidity and temperature is more evenly distributed;
- the steps in the total uncertainty in Figure 7.9 between sample 800-850 is due to the evaluation of uncertainty at the point at which the actuator reverses.

7.4 Analysis of the Implications for Condition Monitoring

In order to evaluate the implications of uncertainty on condition monitoring, two operational modes are required: 'fault free' and 'fault present'. Section 6.1.4 describes the normal operating characteristics under the 'fault free' condition. Under 'fault present' operation the control system parameters are the same as for normal operation. The system has a single fault condition imposed on it. The system seeks to maintain the desired space conditions despite the fault and will achieve this unless the fault is so severe as to cause the system to saturate. Two fault conditions have been selected on the basis that the conditions affect opposite ends of the operating range and they can both be implemented in the system in a repeatable manner. The fault conditions are:

- control valve leakage;
- and coil under capacity.

The leakage fault is implemented by incorporating an additional valved leg that, if open, allows water to by-pass the control port of the valve. Thus, there can be water flow through the coil when the control valve is closed. This fault is most apparent when the valve is closed and hence should be most visible in winter, less so during spring and will be unlikely to be observed during the summer period.

There were three levels of leakage implemented. The magnitude of the leakage at each level was established by closing the control port of the mixing valve and opening the by-pass leg valve. The flow rate through the leg was measured and set to an established value. In this way the leakage effect could be reproduced in different seasons. One issue with implementing the fault in this way is that there is a parallel flow path at all times and this will affect the balancing of the circuit. The effect, however, is negligible compared to the normal flow imbalance (Section 6.3.4). In addition, as the valve opens the relatively high resistance to flow in the by-pass leg results in the normal flow path through the control port being favoured, and the leakage effect disappears in terms of significance.

The coil capacity fault introduces a reduction in the maximum duty of the coil in a controllable and reproducible manner. The fault condition was also introduced in three levels of magnitude. This was implemented by increasing the effective mixing valve control port resistance by the installation of an additional valve. The increased resistance reduced the flow of chilled water through the coil. The level of the reduction was measured at 100% flow through the coil ($u_{cc} = 1.0$). Table 7.3 gives the approximate magnitude of each fault level relative to the maximum water mass flow rate (taken as 1.6kgs^{-1}), for both faults.

The leakage fault was implemented in spring and winter and the under capacity fault in spring and summer and all three seasons had fault free days. No fault detection is possible if either $V_{sa} = 0.0 \text{m}^3\text{s}^{-1}$ or $\dot{m}_w = 0.0 \text{kgs}^{-1}$ and the fault indicators used are set to zero in these cases. This is most noticeable in Figure 7.12 from sample 0 to 350. The data used to calibrate the reference model was collected during summer and is shown in Figure 7.10. The fault free and fault present data for each season is shown in Figures 7.11 to 7.16. The

Table 7.3: Approximate Magnitudes of the Fault Levels Implemented as a Percentage of Maximum Water Mass Flow (1.6kgs^{-1}), in Ascending Order of Severity.

Fault Level	Leakage (%)	Under Capacity (%)
No Fault	0.0	100
1	2.5	70
2	4.5	40
3	7.0	25

following observations can be made:

- all faults are detected and there were no false alarms (Figures 7.10 to 7.17);
- the summer and winter seasons (Figures 7.12 and 7.14) show up the respective faults more convincingly than the faults introduced in the spring season (Figures 7.16 and 7.17);
- the valve opening error in the model is present in all plots, but to a lesser extent on those plots with lower coil duties (Figures 7.13 and 7.17);
- the summer fault free operation and under capacity days (Figures 7.11 and 7.12) happen to have less latent duty than the test day (Figures 7.10), which is reflected in the reduction in uncertainty;
- the 'fuzzyness' present in the confidence limits for the summer under capacity day is due to the uncertainty in the humidity sensors (Figure 7.12)).

7.4.1 Magnitude of Detectable Faults

The precise magnitude of the fault in a particular component of the system is difficult to ascertain since the effect on the fault detection criterion is dependent on the operating conditions. The magnitude of the faults therefore refers to the effect of the causal fault on the detection criterion. The following conclusions can be drawn.

The maximum duty in a cooling coil will often mean high latent exchange in addition to sensible heat transfer. Uncertainty in the system under such conditions, would require

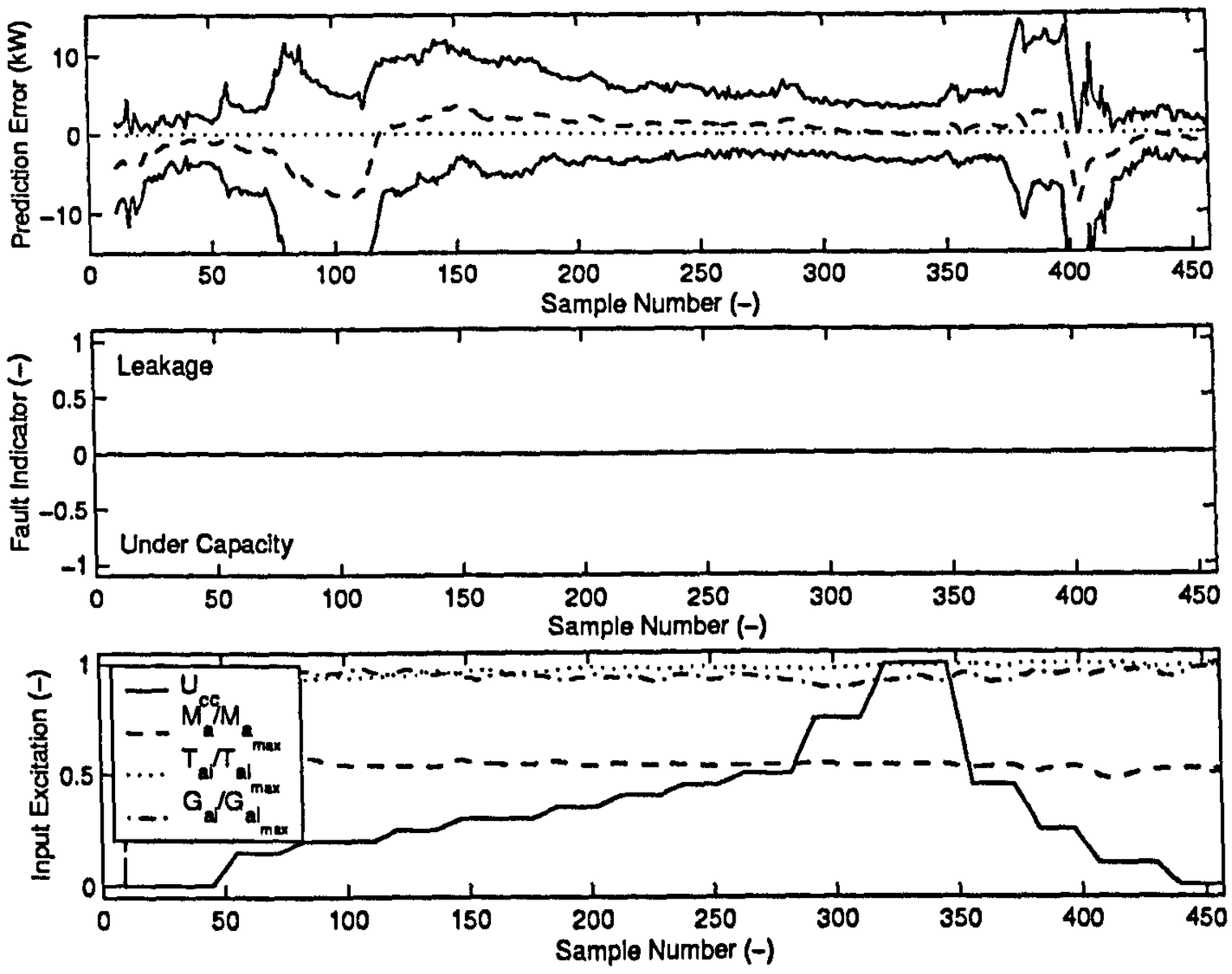

Figure 7.10: Sub-system Model Calibration Data (No Fault).

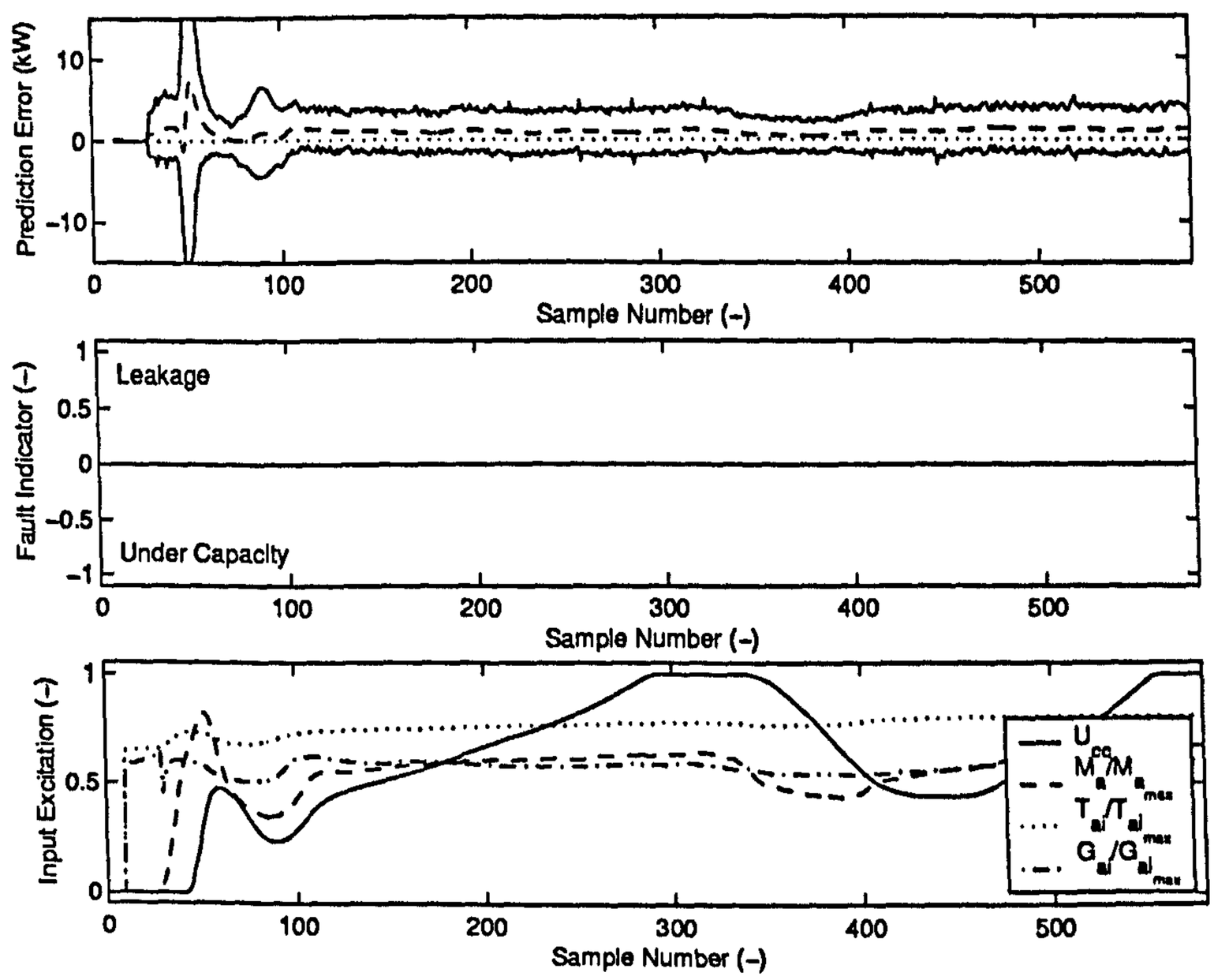

Figure 7.11: Summer Normal Operation (No Fault).

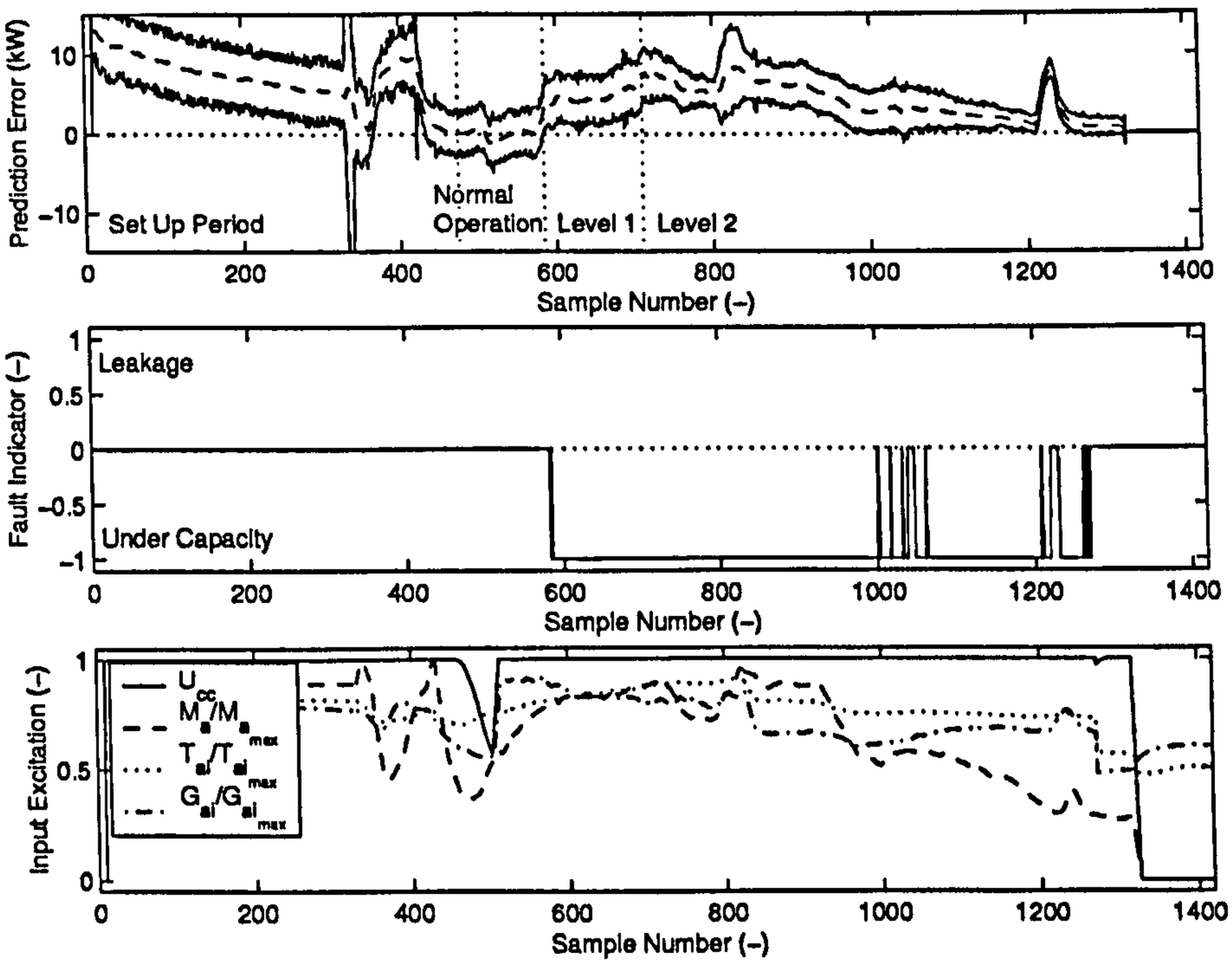

Figure 7.12: Summer Under Capacity (Fault Levels 1 and 2).

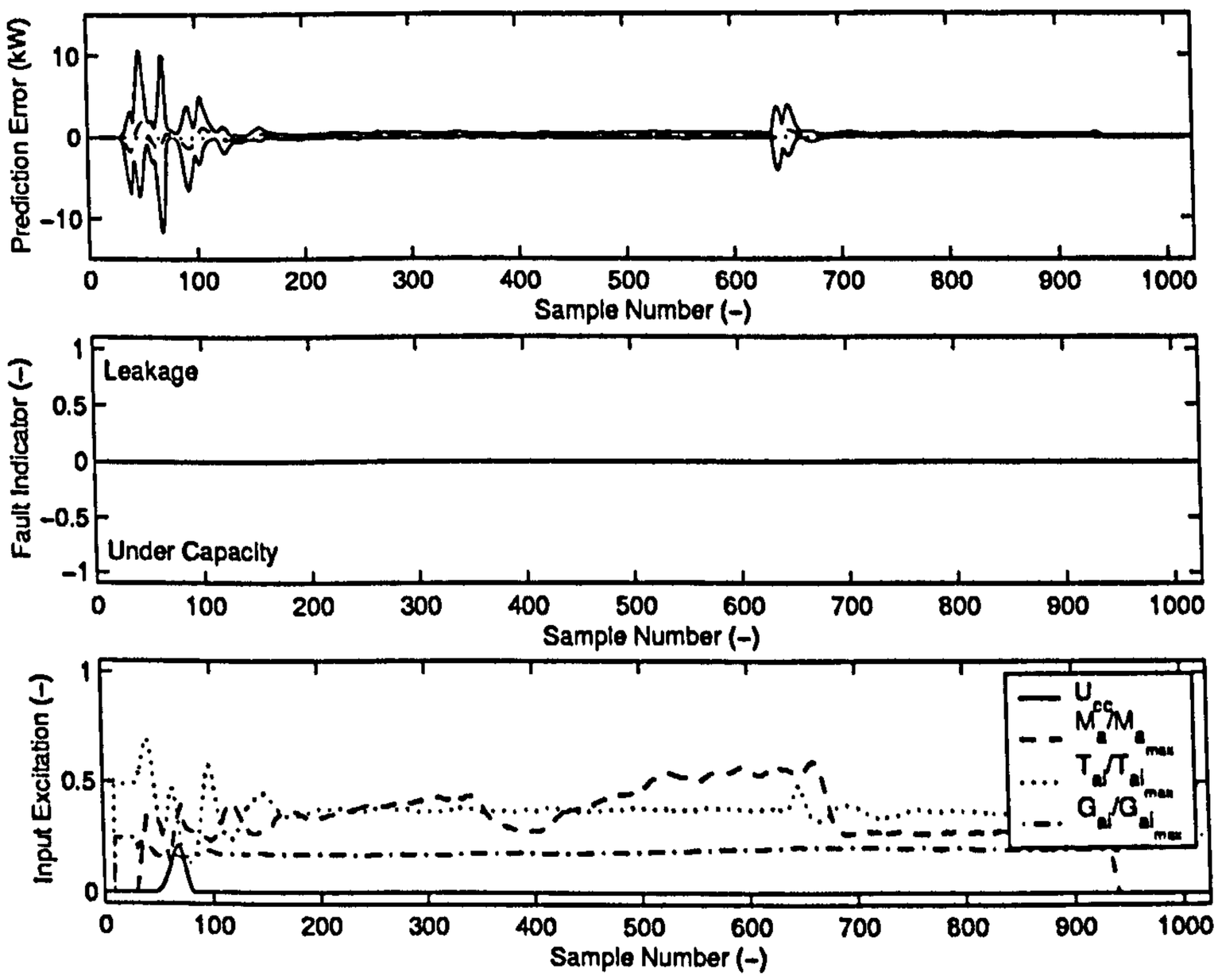

Figure 7.13: Winter Normal Operation (No Fault).

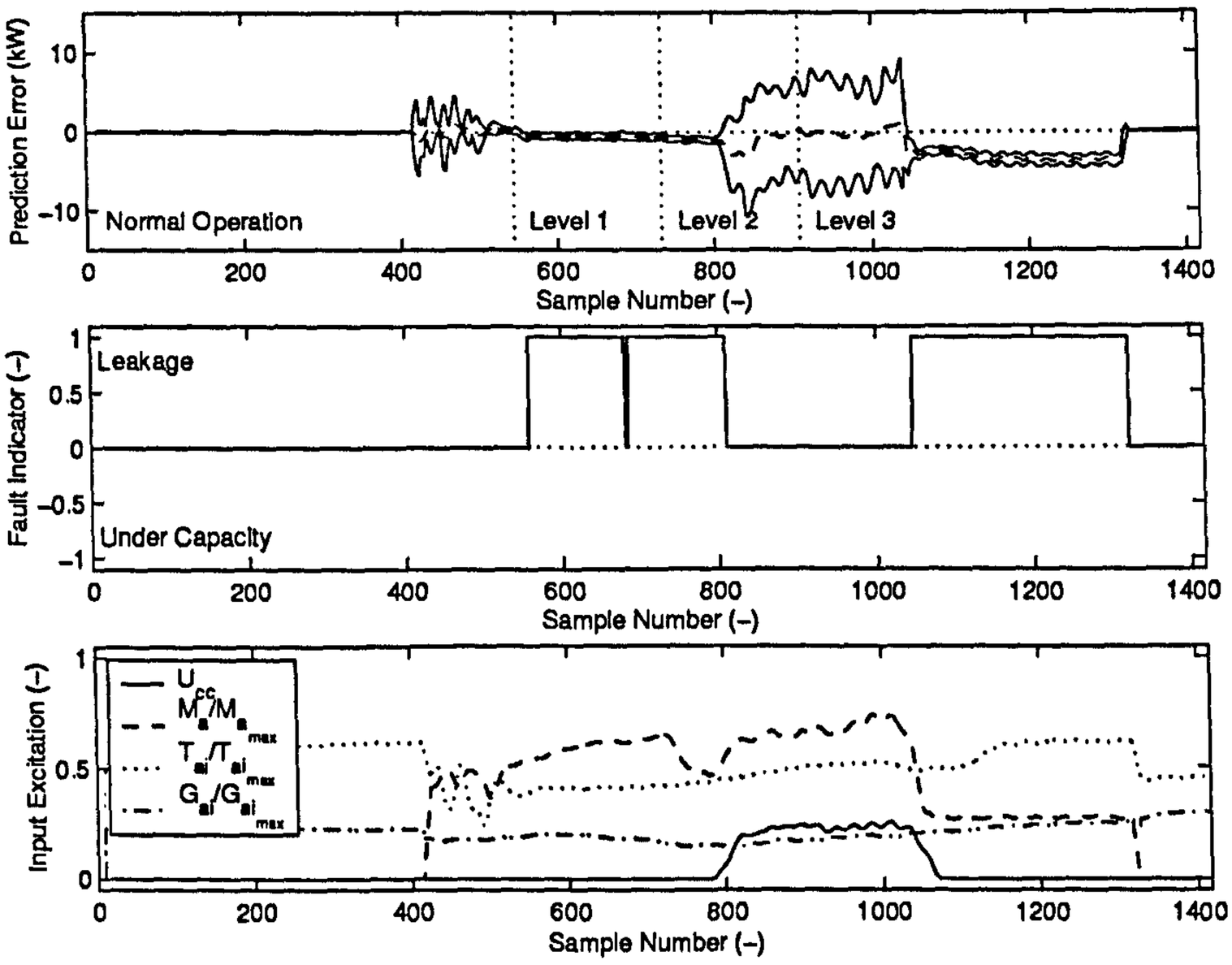

Figure 7.14: Winter Leakage (Fault Levels 1, 2 and 3).

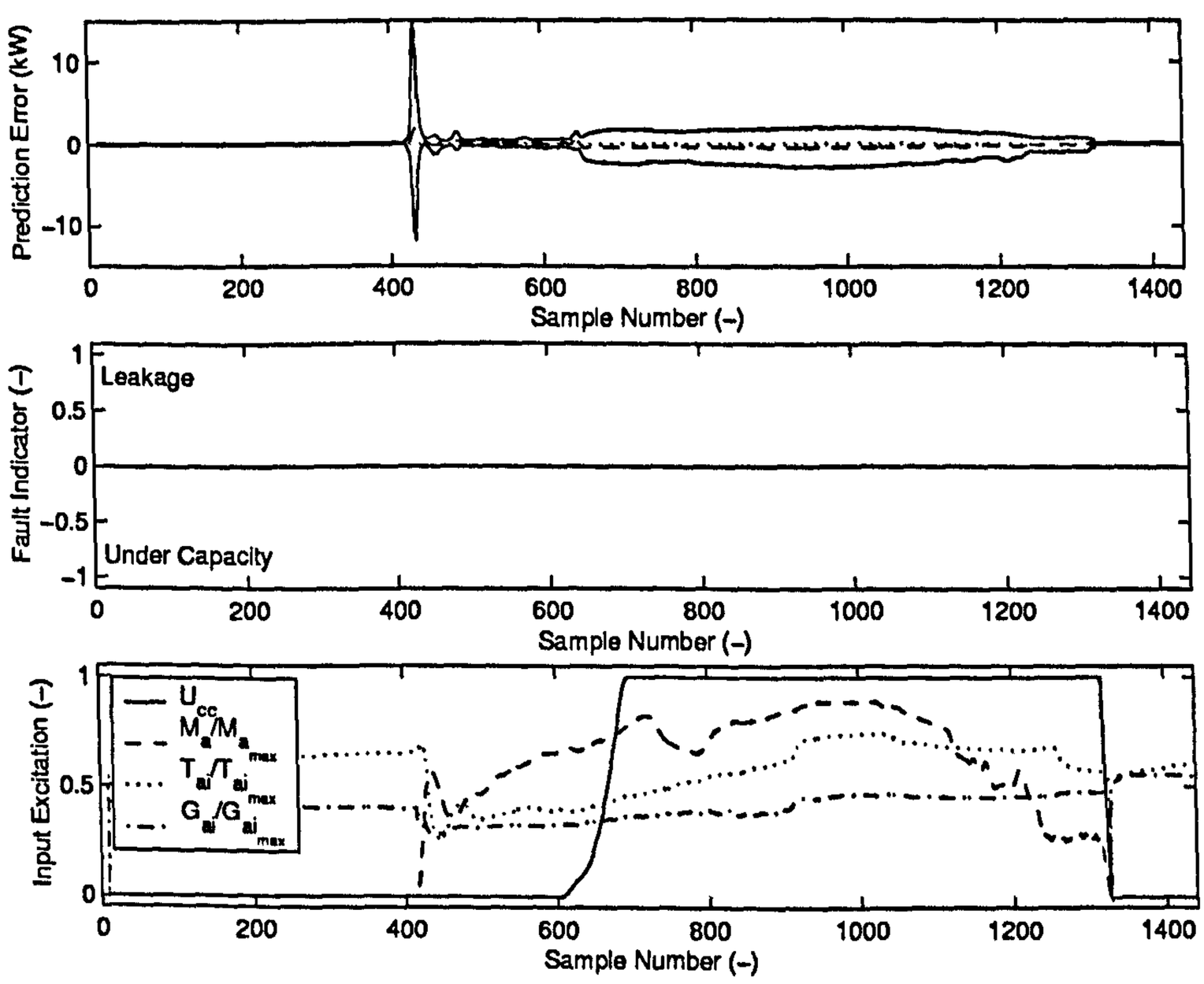

Figure 7.15: Spring Normal Operation (No Fault).

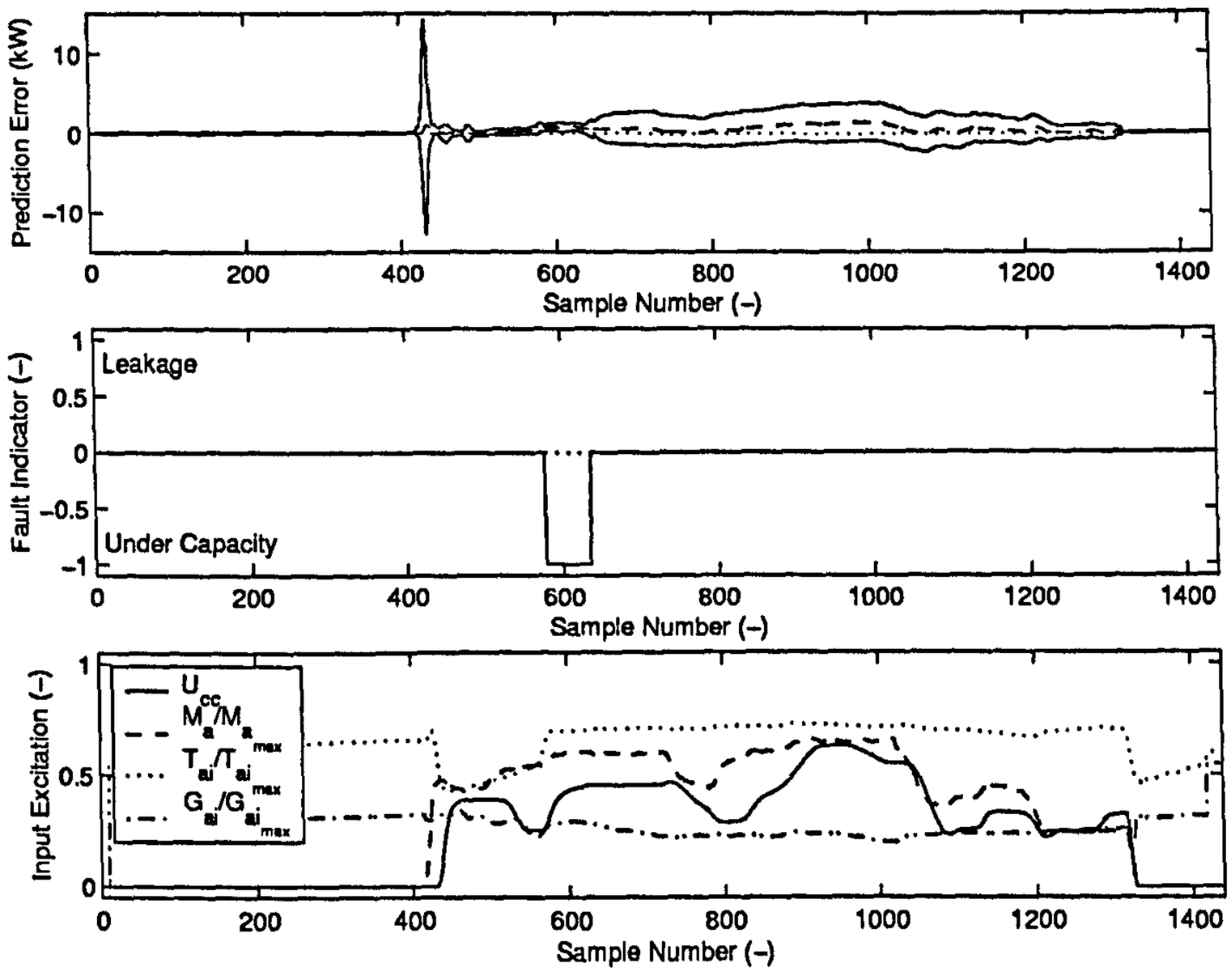

Figure 7.16: Spring Under Capacity (Fault Level 3).

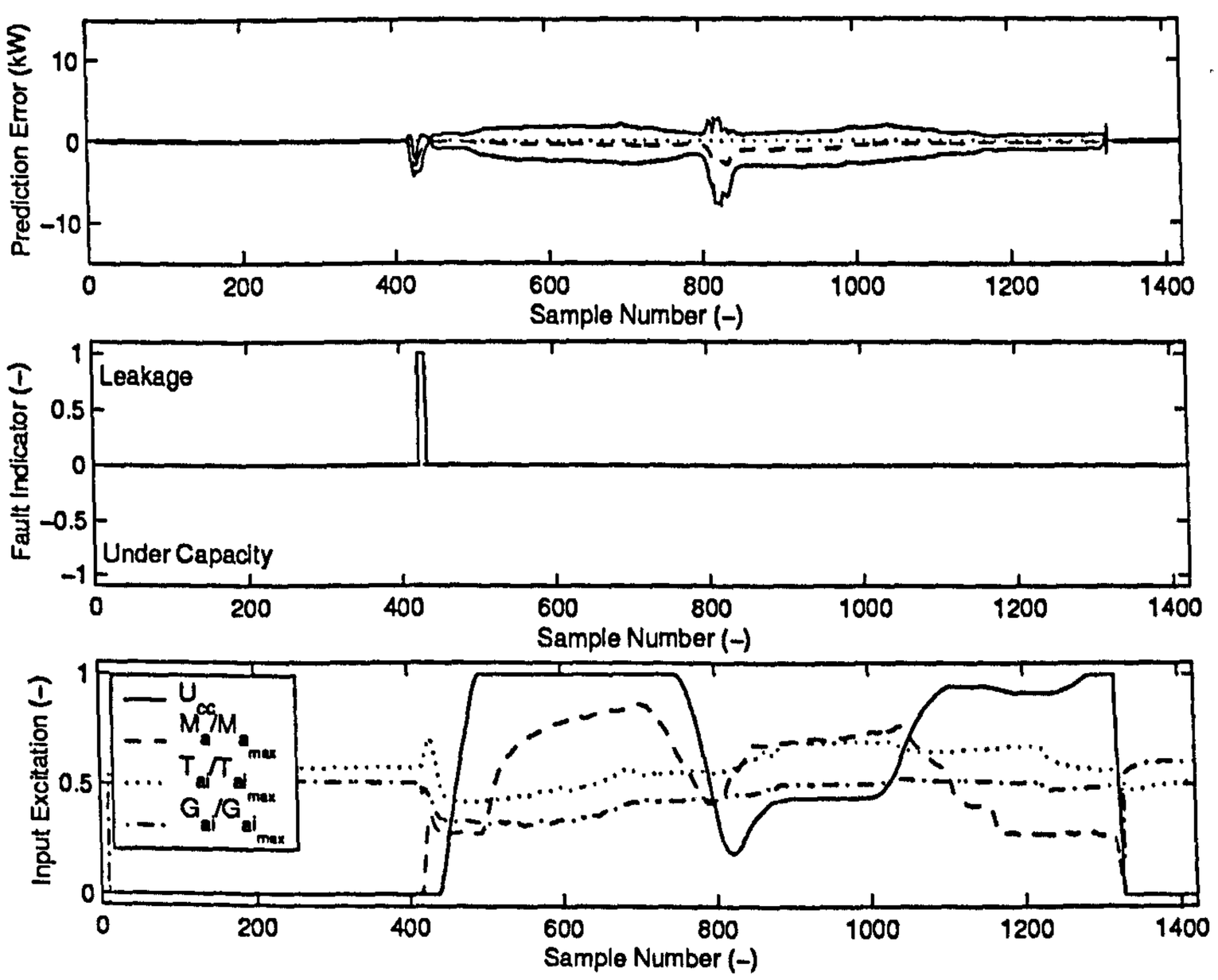

Figure 7.17: Spring Leakage (Fault Level 3).

faults of the following magnitude to be reliably detected; under capacity > 5.0kW and leakage >3.0kW (14% and 9% of the rated duty of the coil respectively). In addition, the valve would need to be fully closed for any control port leakage to be detected. Uncertainty at part load increases the uncertainty in the difference.

The latent load on the coil on the normal operation day in the summer was much less than on the day when calibration data was collected. This was mainly due to the system operating close to 100% recirculated air (minimal latent load). This reduced the uncertainty to ≈4kW over the range of operation. In fault free operation on typical summer days, detection of a leakage in the valve is not likely, unless the control valve is held closed for a sufficient period just after start-up.

The under capacity fault in the summer could be detected at the smallest level implemented. A 30% reduction in maximum flow rate (≈0.5kgs^{-1}), generated a 5kW prediction error. The uncertainty under those condition was calculated at approximately ±4kW and so an alarm was generated.

The uncertainty during the spring season is greatly reduced due to the reduction in coil load. As an additional consequence, the effect of the faults in terms of heat transfer is also reduced resulting in little or no detection occurring. Faults need to have a larger magnitude in spring than in the summer or winter if they are to be detected.

During the winter period the system loads reduce again. The data here is slightly artificial in the sense that for leakage to be detected, pumps need to be circulating chilled water in the primary circuit at a temperature that allows some heat transfer. Typically in winter the cooling system would be shut down, rendering fault detection impossible. Given the test system conditions, however, the smallest level of leakage, 0.04kgs^{-1}, resulted in a 0.75kW prediction error. The uncertainty was calculated at approximately ±0.5kW and hence the fault was detected.

7.5 Conclusions

A condition monitoring scheme for a cooling coil subsystem has been described. The scheme generates robust indicators of abnormal equipment operation because it accounts for all the uncertainties associated with HVAC system measurements and models. The models were calibrated to more precisely represent the target system. This model calibration and parametric uncertainty assessment procedure were described.

The uncertainty contributions were classified into several groups: air temperature, water temperature, humidity ratio, air mass flow rate, valve/actuator model, coil model and physical constants. These groups were used to investigate the respective UPCs at different load conditions. The implications of the uncertainties on the condition monitoring scheme were investigated. The analysis used data collected from three seasons, describing fault free operation and operation with valve leakage and under capacity present.

7.5.1 Scheme Design and Model Calibration

In concept the scheme design is simple. Obtaining the uncertainty estimates may be time consuming, but the process is direct. One advantage of the model calibration is that it is non-iterative. It allows the determination of parameter estimates individually. The solution of the cooling coil subsystem model is a highly dimensioned problem that was previously solved by Salsbury (1996) using the non-linear optimization technique set proposed by Box (1965). In addition, the approach presented here is appropriate for automation.

The most significant modelling problem in terms of uncertainty and precision is when the valve is opening. The rangeability in typical HVAC valves means that the water flow is uncontrollable at significant mass flow rates when the valve is nearly closed. Small errors in the low activation point result in very large prediction errors. This is exacerbated because of the highly non-linear coil characteristic due, in this case, to the poorly designed coil circuit. In the test system the mass flow fluctuation in the primary circuit also contributed to this reduction in model precision. The coil output non-linearity also generates the high

Table 7.4: Significant Uncertainty Contributions for Dry and Wet Coil Operation.

Dry Operation	Wet Operation
Valve/Actuator Model	Valve/Actuator Model
Air Temperatures	Air Temperatures
Coil Model	Coil Model
-	Humidities
-	Physical Constants
-	Air Flow Rates

degrees of uncertainty in this operating region, which preserves the robustness of the scheme output.

7.5.2 Uncertainty Contributions

The model parametric and structural uncertainties are significant during high duty. The uncertainty in the air temperature measurements is the most significant uncertainty from the input variables used in the condition monitoring scheme. The transient uncertainty is required to prevent the calculation of spurious uncertainty values. The uncertainty in the water temperature measurements can be neglected. Where sensible heat exchange is assured, the uncertainties in the physical constants and humidities can be neglected. If latent heat exchange is possible, the uncertainties in the humidities must be included. Table 7.4 summarises the static uncertainty contributions that should be considered for sensible, and sensible and latent, heat transfer.

7.5.3 Implications for Condition Monitoring

The condition monitoring scheme yielded no false alarms. Every fault implemented over the three trial periods were detected. Winter provided the most decisive detection of the presence of valve leakage. The summer operating conditions clearly identified the presence of under capacity. The spring conditions demonstrated that detection was possible, but the evidence is likely to be more sparse, unless the fault magnitude is increased. Some specific comments are:

Table 7.5: The Magnitudes of Faults that can be Detected in Each Season, in Terms of Total Heat Transfer and as a Percentage of Full load (35.0kW).

Season	Leakage (kW)	(%)	Under Capacity (kW)	(%)
Summer	>3.0	9	>5.0	14
Spring	>1.0	3	>2.5	7
Winter	>0.5	1	-	-

- in absolute terms, leakage is easier to detect than under capacity, due to the nature of the non-linear, high gain, heat-exchanger characteristics at the low end of operation;
- the valve needs to be closed if leakage is to be detected, but the detection of under capacity is not as sensitive in this respect.

Table 7.5 summarises the magnitudes (in terms of their effect on Q_t) of uncertainties that could be expected to be detected under the stated conditions.

Chapter 8

Conclusions

This thesis has investigated the uncertainty associated with the first principle model based condition monitoring of HVAC systems. The research focused on a cooling coil subsystem installed in a real system. The influence of the uncertainty sources were investigated in terms of relative magnitude of contribution. The implications for the sensitivity and robustness in fault detection was evaluated. The proposed scheme was demonstrated to be sensitive to the detection faults and generated no false alarms. The accuracy of the model predictions comes through:

- minimising the effects of persistent bias in the measurements;
- calibration of the reference model to the target system.

The robustness of the scheme is generated by the consideration of all the significant uncertainty contributions:

- fixed bias in the measurements;
- random influences on the measurements;
- proximity of the system to steady-state;
- model structure;
- model parameter calibration.

The conclusions of the work with respect to the aims and objectives set out in Section 1.4 are listed below.

- Uncertainty analysis techniques have not been extensively used in HVAC engineering to date. The correct treatment of uncertainty is critical to the usefulness of data. This is especially so for minimising the false alarm rate of condition monitoring technologies applied to HVAC systems.

- The HVAC sensors identified in the investigation are sufficiently accurate for the purposes of condition monitoring. The precision of the sensors suffers principally due to the bulk averaging of spatially distributed properties or quantities. Stratification is the primary causal factor of this source of uncertainty. Methodologies for the evaluation of this uncertainty were introduced.

- For the discrete data sampling applications investigated, a fixed window filtering method implicitly generated less uncertainty than an exponentially weighted filter method. An approach to evaluating the uncertainty in the use of steady-state analysis with data containing transients was derived based on the fixed window filter.

- There is uncertainty associated with the approximation of HVAC heat-exchangers to the cross flow/counter flow arrangements on which the ϵ-N_{tu} method is based. There is uncertainty associated with the physical constants used in such calculations. Uncertainty exists in the estimation of the resistance parameters for a given coil. The fluid flow regimes encountered may influence the uncertainty in subsequent predictions using the model. The significance of the model structural uncertainty in terms of the use of the model is dependent on application.

- Validation of persistent bias or measurement characteristics induced by the system operating conditions need to be evaluated to maximise the precision and accuracy of subsequent analysis. An *in-situ* sensor validation methodology suitable for HVAC systems was presented.

- The correct incorporation of uncertainties in a condition monitoring regime generates robust indicators of changes in system operating condition. It is possible to detect under capacity in the investigated HVAC system during high and moderate coil

duties. It is possible to detect leakage through a cooling coil three-port control valve in any season, provided the valve is closed.

8.0.4 An Overview of the Approach

The research has led to the establishment of a procedure for appropriating a robust condition monitoring scheme for HVAC equipment, realised through the correct incorporation of the uncertainties. This procedure has generic application to systems with 'permanent' instrumentation. Once the target system has been selected:

review suitable models: consider the published and/or derive suitable models for the required prediction purposes.

evaluate the measurements: identify the available measurements. Evaluate these in conjunction with the available models in terms of input/output requirements. Implement additional or amendments to the existing instrumentation as required.

evaluate bias uncertainty in the measurements: evaluate the uncertainties due to calibration, the data acquisition process, and system operational characteristics. Use manufacturers information, instrument calibration results and system observations. Identify operational characteristics that generate persistent bias. Remove bias from the measurements where possible. Amend the uncertainty estimates where is is not possible to remove the bias. Establish correlations in the uncertainties.

evaluate random uncertainty in the measurements: evaluate the characteristic system time constants with respect to the desired information. Select the filter used to generate the mean and variance for each measured variable (See Section 4.3). Establish a suitable sampling interval and number of samples the filter will base the measurement estimates (mean and variance) on. If steady-state models are used and transients are likely to be present in the data, apply the technique described in Section 4.4. This requires the estimation of the magnitude of the maximum likely input and the expected minimum/maximum variance magnitudes.

evaluate uncertainty in the model structure: establish the assumptions and simplifications used to formulate the model. Apply the evaluation techniques described in

Section 5.1. Establish the influence of convergence criteria used to terminate iterations used internally in the model. If numerical differencing is required, check the integrity of the gradients generated over the expected range of operation.

calibrate model: if model calibration is required, collect suitable data form the system. Identify the model parameters. Section 7.2 describes one approach suitable for steady-state models.

evaluate uncertainty in the model parameters: use the uncertainty in the measurements and/or available information to evaluate uncertainty in the estimated parameters. If measured data from the system is used: check to avoid incorporating uncertainty more than once. Ensure that the data is rich enough to allow the estimation of the selected parameters. If calibration testing is used to collect data, determine the effect of the prevailing conditions in terms of: the identification of the characteristics (are the system features 'visible' in the data?) and the level of uncertainty in the data (how significant is it with respect to the desired model output uncertainty?).

identify significant uncertainty sources: identify the uncertainties that contribute to the desired output significantly. The uncertainty percentage contribution method is a powerful tool for this purpose (Section 7.3). Observe the magnitude of uncertainty across the expected range of operation. Check that the level of uncertainty in the output renders it useful. If not, re-evaluate the measurement quality/model type/calibration data, making amendments where required.

***on line* implementation:** the uncertainty code derived in Appendix C can be used. The fixed bias uncertainties in the measurements and parameters (including those representing the model structural uncertainty) are entered in the bias uncertainty matrix. The correlation matrix is configured. Uncertainties that are dependent on operating region are updated at every new a sample. The random uncertainty and the uncertainty due to the system's proximity to steady-state is evaluated at every sample and updates the random uncertainty matrix accordingly. The sensitivity coefficients for each uncertainty source with respect to the scheme output is calculated at each new sample. The uncertainty of the scheme output is consequently calculated for the current sample.

8.0.5 Uncertainty and Measurements

Chapters 3, 4 and 6 discuss uncertainty in the measurements critical to the condition monitoring of an HVAC cooling coil subsystem. The following conclusions can be drawn:

uncertainty contribution to prediction error: in the condition monitoring scheme investigated, the air temperatures were the dominant uncertainty contribution from the measurements. In practice, establishing suitable estimates of bulk average uncertainty in the air temperature measurements is a significant problem. As a result, the reliability of the estimate lies with the evaluation of the system characteristics made by the investigator. The contribution from the water temperature measurement was negligible. This was because the scheme used the air side measurements as the inputs to calculate the actual total heat transfer (Section 7.1). The air mass flow rate measurements only influence the uncertainty during high duty conditions. The precision of the air measurements are important where they influence other system measurements/estimations (such as the air humidity ratio entering the coil, Section 6.3.1). The air humidity should be excluded from calculations where possible. The precision of the model predictions decreases significantly when it is included.

air temperature measurements and stratification: achieving an accurate estimate of the bulk average air temperature is difficult with typical HVAC instrumentation. The problem occurs because simplified models generate prediction based on 'lumped' process characteristics. The air temperature, as an input, is a single value and can not be represented in spatial terms. With regard to the analysis, this simplification is a conceptual error. Its effect is one of the dominating influences on the uncertainties in the scheme, although in some cases it is possible to minimise the effect (Section 6.3.2). There are a number of possible solutions: ensure the air is mixed to near perfect conditions; better representation of the bulk mean average of the stratified air (improve the measurements (Section 3.2.1) or mapping the characteristics using another model); generate a spatially distributed model (computational fluid dynamics). In terms of *on line* condition monitoring, the second solution is the most promising.

water mass flow rate estimation: a common configuration of cooling coil subsystems varies the chilled water mass flow rate for controlling the coil output. Not only is it expensive to measure the flow rate for individual coils, but it is difficult to obtain a sensor that will measure the range of flows that can be experienced (Section 6.3.4). In addition to this, the water mass flow rate is not required for control and so it is not typical to find this measurement in HVAC systems. Given the valve/actuator characteristics as a function of control signal, the water mass flow rate through the coil can be estimated. These characteristics can be obtained from data collected from the system. At low duty (valve nearly closed) there is a lack of precision and high degree of uncertainty. Reasonable levels of uncertainty at valve closed and fully open can be achieved. At high duties, this renders the condition monitoring scheme insensitive in the mid ranges of coil duty. This problem is unlikely to be solved by applying a direct measurement for the reasons stated above. One solution is a better model and model calibration procedure discussed in Section 8.0.7.

uncertainty due to the proximity to steady-state: when the process is at or close to steady-state, the significance of the uncertainty due to transients in the data is negligible. In fact, the magnitude of the bias uncertainty in the measurements is sufficient to ensure that all but the largest disturbances make a negligible contribution to the uncertainty in the prediction error. Generally, the large disturbances are restricted to the system start up period (Figure 7.15). The evaluation of the uncertainty is required if false alarms are to be avoided.

correlations in uncertainties: correlations in the random uncertainties are not considered to exist, which is generally the case in engineering systems. Two principal sources of correlations in the bias uncertainties are typical in HVAC systems: in calibration to the same standard and in analogue to digital conversion. The latter is especially apparent when using the same sensors from the same manufacturer. The former occurs because of the sharing of components in the data acquisition equipment used in the control system. The effects of the correlations can be very significant, demonstrated by the air temperature measurements in the scheme applied here.

disturbance of equipment and sensor validation: the validation of sensor measurement in relation to the other measurements used in an analysis is more important

than accuracy. The validation process can be time consuming in HVAC systems and may require physical intervention with the equipment if good results are desired. This process helps identify operational characteristics that generate persistent bias in measurements. However, the instrumentation is sensitive to movement. Replacement of sensors and re-calibration must always be implemented in related sensor groups. Disturbances to the equipment (maintenance on the mixing box dampers, for example) can alter the operational characteristics of the system. This may necessitate the re-validation of the instrumentation.

estimating air temperature gain not attributed to the coils: the measurement of air temperature either side of cooling coils do not occur in every HVAC installation. Commonly, the supply air measurement (usually some distance from the coil section) is the only 'off coil' air temperature available. Often, the supply fan is installed between the coils and the sensor (usually a point sensor). In VAV systems it is difficult to predict the temperature rise that is 'seen' at the sensor, due to the fan. Duct losses and leakage exacerbate the problem. Practically, imprecise and highly uncertain differences between the air measurement into the coil and the supply air measurement exists. Air temperature measurements are required either side of the coil if reasonable precision and accuracy is to be realised.

8.0.6 Uncertainty and Heat Exchanger Modelling

Chapter 5 describes a simple first principles based model of a heat-exchanger in Section 5.2. A four class description of the methods of assessing model structural uncertainty is introduced and applied to the model. Section 7.2 describes the calibration of the model to the test system. The influence of the model structural uncertainty on the uncertainty in the prediction error is demonstrated in Section 7.3. The following conclusions can be drawn:

uncertainty contribution to the prediction error: the uncertainty in the coil model contributes to the uncertainty in the prediction error; significantly at high duties. The model generates no contribution when the valve is closed. The uncertainty in the modelling assumptions should not be neglected in analysis.

performance of the model: without a precise measurement of the chilled water flow rate, the model representation of the installed coil is impossible to assess. The coil adequately describes the process considering the uncertainties and precision associated with the valve/actuator model (Section 8.0.7). Sensible heat transfer is simpler to predict than latent and sensible transfer. A possibility would be to predict the former case using the sensible heat transfer model. The uncertainty in doing so could be evaluated using both models.

iteration convergence criteria and uncertainty: internal iterations introduces uncertainty into the model. The model structural uncertainty can be used to select a suitable level of convergence. The criteria affects numerical differencing. Generally, the convergence of the model must be smaller than the differencing interval applied (Section 5.4.4). The size of the differencing interval affects the gradient function surface and this must be adequate for the proposed task. One particular issue with the cooling coil models is divergence in the solution. This is undesirable and the measures described in Appendix A were implemented to prevent this.

evaluating structural uncertainty: the uncertainty in the model structure must be realisable in terms of: an estimate of variance; representation by a parameter, measured variable or internally calculated variable. Identifying the uncertainties in the process model is difficult. Care is required to ensure that the same uncertainty source is not incorporated into the model twice, which is a particular issue with regard to models of complex processes.

8.0.7 Model Calibration and Parametric Uncertainty

The subsystem model used in the condition monitoring scheme was constructed from three component models. The heat-exchanger was described in Chapter 5 and the valve and the actuator models are both described in Appendix B. Section 7.2 described the estimation of the parameter estimates and associated uncertainties. The following conclusions can be drawn:

reduction of the heat-exchanger model parameters: the fixing of the ratio of the

resistances (water side/tube wall material/air side) is a reasonable simplification (negating the requirement for manufacturers information detailing the coil performance). The loss of characterisation of the coil is negligible compared to the uncertainty in the installed valve/actuator model, derived from data from the system.

estimating the parameter values: the activation points and hysteresis are relatively easy to estimate directly by observation of the equipment or from calibration data. The heat exchanger parameter can be estimated directly as can the maximum water mass flow rate (which needs to be measured). The curvature parameters associated with the model can be estimated from the data, either by calculating the water mass flow rate or inferring it by incorporating the coil model into the estimation process. Using HVAC grade data it is not possible to estimate more than one parameter that is associated with the curvature of the process.

estimating the parametric uncertainties: the estimation of the low activation point is critical to low duty model precision. This estimate can be correct in a mechanical sense, but fluctuations in the circuit pressure causes the relationship between the coil output and the control signal to change. This inevitably increases the uncertainty round the activation point with respect to the prediction error. Consequently, the uncertainty as the valve opens is very high as discussed in Section 8.0.5. It is also impossible to separate the uncertainties associated with parameters estimated from the same data. The uncertainty in the data needs to be modelled explicitly, or attributed to one of the estimated parameters (setting the uncertainties associated with the other parameters to zero).

performance of the valve/actuator model: most parameters retain their 'physical' meaning in terms of the process because they are estimated separately where possible. Methods that estimate all parameters together increase the dependency between parameter estimates. The uncertainty in the system characteristics derived from data can be modelled explicitly. The analytical structure of the model with respect to process curvature is not therefore required. Better model precision could be realised by the application of *blackbox* techniques, such as neural networks, or fuzzy modelling approaches.

collecting the calibration data: there are two principal considerations regarding the

prevailing conditions when collecting the calibration data: the characteristics that are required to be described by the data must be 'visible'; and the higher the coil duty, the greater the uncertainty in the calibration data (particularly if latent heat exchange is present). In addition, there must be flow past sensors if the measurements are to be useful.

8.0.8 Uncertainty and Condition Monitoring

Chapter 7 describes a HVAC condition monitoring scheme that incorporates all the uncertainties in the calculation of prediction error. Section 7.4 demonstrates the implications of uncertainty in the condition monitoring of an HVAC cooling coil subsystem. The code derived in Appendix C is used to evaluate the uncertainty in the prediction error based on the uncertainties discussed and identified in Chapters 3 through to 7. The following conclusions can be drawn:

performance of the scheme: the scheme generated no false alarms and detected all the faults implemented in each season. Valve leakage can only be detected when the valve is closed. The uncertainty in the valve model at just-open precludes detection otherwise. Under capacity can be detected when the control signal is approximately 40% or more. This is due to the highly non-linear system characteristics. The appropriate consideration of the uncertainties present in the scheme generates robust estimations of the prediction error.

detectable fault magnitude: at very low duties a level of leakage that generates a prediction error >0.5kW (1.4% of full duty, ~35kW) can be detected. The scheme is less sensitive in this respect to the detection of under capacity. The high load generated by the prevailing conditions, however, result in high uncertainty. At full duty, the effect of under capacity needs to be in excess of >5.0kW (14.2%) to be detected. At intermediate loads, an effect of >1.0kW (2.9%) and >2.5kW (7.1%) is required for leakage and under capacity respectively.

8.1 Further Work

Possible further research could be implemented in the following areas:

measurement uncertainty: needs further research especially in the assessment of the bulk average uncertainty, which is critical to the accuracy of calculations. More work is needed to gain a better understanding of these effects. Further work is required for the assessment of the effects of radiation on sensors.

model structural uncertainty: could be enhanced by studying the differences between a detailed finite element model and the simplified models used here, an extension of Braun's work. The assessment methodology could be applied to different models and investigate how generic the approach is. In addition, this would lead to a better understanding of the uncertainties that exist in models and calculations that are traditionally assumed to be negligible.

model parametric uncertainty: could be developed by collecting stepped training data from several operating conditions and investigating the local/global parameter identification issues in terms of precision, robustness and uncertainty. Further work is required to improve the knowledge regarding valve opening characteristics.

***in situ* sensor validation:** should be applied to other systems. This would improve the method. Step tests could be refined and the whole approach could be automated.

condition monitoring: could be extended to other HVAC subsystems such as the mixing box and fan/duct systems. The configuration of the input/output relationships with respect to the generation of prediction error could be investigated. This would identify any particular arrangement that would yield the minimum uncertainty and the most sensitive response to changes in system operation.

Appendix A

The Solution of Heat-Exchanger Calculations

There are two issues that affect the successful solution of water-to-air heat-exchanger models operating under fully or partially wet conditions:

- psychrometric feasibility,
- iteration convergence.

Here both issues are discussed and solutions are proposed to ensure that the model solutions are correct and feasible.

A.1 Psychrometric Feasibility

The use of numerical differencing in water-to-air heat-exchanger models to find an approximation to the first derivative requires careful application. If the fluid streams conditions result in a value very close to or on the 100% saturation line associated with psychrometric process, the differencing may result in a solution attempt at an infeasible condition. This will result in excessive iterations and a possibly spurious solution value. Prevention of these possible occurrences can be augmented by first; implementing a check to ensure the inputs do not generate operating points that are sub-cooled and then by checking the

differencing value does not violate the same rule. In both cases, if the rule is violated, steps can be taken to address the problem.

A.1.1 Feasibility of the Input Data

For a given air moisture content, g (kgkg_{air}^{-1}), and dry bulb air temperature, T (°C), $(h_{g_{sat}} - h_{T_{sat}}) \leq 0$ should *not* be violated, where h denotes the enthalpy (kJkg^{-1}). If the rule is not satisfied there would be a difference between the saturation enthalpies, $h_{x_{sat}}$, at both conditions and the resulting inlet conditions would be sub-cooled. Assuming a linear relationship between enthalpy, dry bulb temperature and air moisture content in the sub-cooled region, the conditions at the 100% saturation conditions can be taken as the 'corrected' inlet conditions. Given T_{ai} and g_{ai} and using psychrometric functions, this 'correction' can be implemented using the following sequence of operations,

$$\begin{aligned} h_{ai} &= f(T_{ai}, g_{ai}), \\ T_{h_{ai_{sat}}} &= f(h_{ai}), \\ \forall(T_{h_{ai_{sat}}} > T_{ai})\Big\{T_{ai_{new}} &= T_{h_{ai_{sat}}} \\ g_{ai_{new}} &= f(T_{ai_{new}}, h_{ai})\Big\}, \end{aligned} \tag{A.1}$$

where $T_{h_{ai_{sat}}}$ is the saturation temperature at h_{ai} and $T_{ai_{new}}$ and $g_{ai_{new}}$ are the 'corrected' inlet conditions.

A.2 Iteration Convergence

Stoecker (1989) highlights problematic issues when using the Gauss-Seidel method for successive substitution. These issues can result in slow convergence or divergence in the solution of a set of simultaneous linear equations. Steady state models of fully or partially wet operation of water to air heat-exchangers, such as those described by Salsbury (1996) and Buswell et al. (1997), use successive substitution and can fail to converge. Under certain conditions, the iteration convergence exhibits oscillatory behaviour about the solution in consecutive iterations. A method to ensure convergence on a solution to within a preset tolerance is required to ensure correct model output predictions.

A.2.1 Solution Proposal

If computational efficiency is of lesser importance than the convenience and simplicity of the convergence method, partial substitution in successive substitution can be employed. Stoecker gives,

$$x_{j,i+1} = \varsigma x_{j,i+1*} + (1 - \varsigma) x_{x_{j,i}}, \tag{A.2}$$

where ς is the partial substitution factor, x_j is the variable being computed, i and $i+1$ are the subscripts indicating the previous and new values and $i+1*$ indicates the new value computed directly from the equation.

In this implementation the method should insure convergence under a reasonable number of iterations. Trials were based around a nominally counter flow, steady-state, water-to-air, ε-N_{tu}[1] heat-exchanger with latent and sensible load, where the substitutions used the calculated total heat transfer. The investigation revealed that no one value for ς would satisfy the convergence criterion for all points in the operating space. It was found that if the partial substitution was implemented at one value of beta, the result was non-convergence or the oscillatory behaviour returned but within a smaller band around the solution.

To prevent this, an algorithm was developed that reduced the oscillatory band to an acceptable degree. With this approach, the solution is deemed to converge if the oscillations were below a certain threshold, the *convergence criterion.* The convergence criterion, ξ, is given as a percentage of the total heat load, Q. The algorithm decreases ς in stages until convergence was achieved and is described by,

$$\begin{aligned} initialise \quad i &= 0 \\ and, \quad n &= 0 \end{aligned}$$

$$\forall \left(\left| \frac{1 - Q_{i+1}}{Q_i} \right| > \xi \right) \{$$

$$Q_i = Q_{i+1} \rightarrow \cdots \rightarrow Q_{i+1*} = f(\cdot)$$

$$\forall (i > X + [Y + iY]) \{$$

[1] effectiveness-Number of (heat) Transfer Units, see (Kays and London 1984).

Table A.1: The Extent of the Algorithm Testing Range.

Variable	Range	Units
Water Mass Flow Rate	$0.0 \rightarrow 5.0$	kgs^{-1}
Air Mass Flow Rate	$0.0 \rightarrow 5.0$	kgs^{-1}
Air Moisture Content (on coil)	$0.00 \rightarrow 0.03$	kgkg_{air}^{-1}

$$
\begin{aligned}
\varsigma &= \left(\frac{0.9}{10^n}\right) - \left(\frac{i-9n}{10^{(n+1)}}\right) \\
IF \quad i &= 8+(9n) \quad THEN \quad n = n+1 \\
Q_{i+1} &= \varsigma Q_{i+1*} + (1.0-\varsigma) * Q_i \\
and, \quad i &= i+1 \ \} \Big\}, \qquad \text{(A.3)}
\end{aligned}
$$

where i and n are incremental counters, X is the operator that controls the 'waiting' for natural convergence and Y controls the 'lingering' of iterations at a ς level.

A.2.2 Results

This algorithm was implemented and the model exercised over a wide operating range. Table A.2.2 details the extent of the investigation. Figure A.1 shows the results from one trial with the air moisture content at $0.03\mathrm{kgkg}_{air}^{-1}$, over part of the test area. Note that SHR is the sensible heat ratio defined as $\frac{Q_s}{Q_t}$. Some influence of the degree of latent heat exchange can be observed in the number of iterations required for a solution, however, the tests investigation demonstrated that convergence within 20 iterations was assured for the input space considered. Values of $X = 5$ and $Y = 1$ were found to be suitable values for this application, and an extreme convergence criterion of $1E-10$ was tested and found to be achievable in less than 100 iterations.

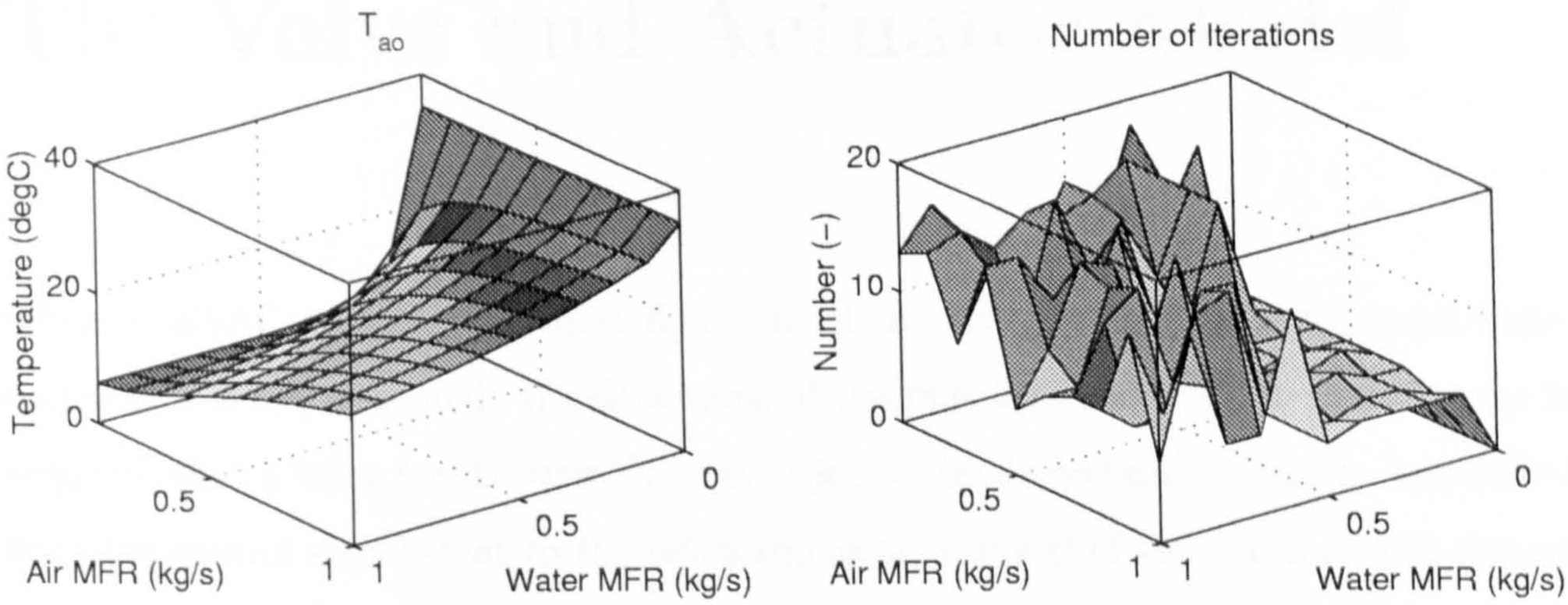

Figure A.1: Some Results from Testing the Convergence Algorithm.

Appendix B

The Valve and Actuator Model

Often in HVAC systems, the mass flow rate of the primary fluid in water-to-air heat-exchangers is not measured. If calculations of the part load duty of a heat-exchanger is required, then a value for the mass flow rate needs to be determined. This can be inferred from the control signal (sent to the actuator) using a model of the actuator and control valve.

A combination of valve and actuator models, based on those proposed by Clarke (1985), were implemented by Salsbury (1996). The valve model has been successfully demonstrated in work by Buswell et al. (1997) and Buswell and Wright (1998). A simplified version of this model is described here. The hysteresis component of the actuator model, however, was found to be deficient for on-line applications in subsequent work by Norford et al. (2000). A robust actuator model was developed as part of this work and is also described. In addition, the uncertainty associated with both models is identified.

B.1 The Valve Model

Typical HVAC heat-exchanger systems have inherently non-linear (exponential) characteristics. In an attempt to produce a linear relationship between demand (control signal) and heat output, the valve is designed to have approximately opposing characteristics. These characteristics are also influenced by the circuit resistances, affecting the authority of the valve. It can be shown that the installed valve characteristics can be represented

by,

$$\dot{m}_w = \frac{\dot{m}_{w_{max}}}{\sqrt{1+\gamma\left(\left[\left(\left[1-e^{\beta s}\right]\left[1-e^{\beta}\right]^{-1}\right)^{-2}\right]-1\right)}}, \tag{B.1}$$

where s is the valve stem position, $\dot{m}_w$ (kgs^{-1}) is the mass flow rate of water through the coil, $\dot{m}_{w_{max}}$ is the maximum mass flow rate, typically the mass flow in the primary circuit. The parameters β and γ are the valve curvature coefficient and valve authority respectively. The valve curvature can be estimated from manufacturers data. Valve authority needs to be determined empirically. It can be convenient to estimate both parameters from using empirical data gathered from the existing HVAC measurements. Derivation using this data, however, usually requires that one parameter is fixed (often $\gamma = 0.5$) and the other (β) is estimated. This is because the data that is readily obtainable from HVAC plant is not sufficiently rich enough to be used to identify both parameters (both effectively adjust the curvature of the model). It should be noted that some tuning of these parameters is usually necessary if reasonable model precision is desired. This can be attributed to the non-linearities that are introduced to the system through poor selection of the circuit water flow regulation (control/balancing valves) and poor commissioning. Often, therefore, the practically implemented model is 'greyer' than the derivation of Equation B.1 might first suggest[1].

B.1.1 Model Uncertainty

The principle valve model simplifications are:

- valve rangeability and 'real' closure characteristics are not modelled;
- valve characteristic may not be truly exponential;
- the derivation of the authority correction is based on fully developed turbulent flow in the subsystem;
- the system is correctly balanced.

[1]The full derivation of the model, on which Equation B.1 is based, can be found in Salsbury (1996).

These all contribute to the inherent structural uncertainty that will affect the accuracy of the estimation of $\dot{m}_w$. If the parameters (β and γ) are estimated from data collected using typical HVAC measurements, the high uncertainty in the data will be transferred to the parameters. The uncertainty in the parameters will usually be greater than the uncertainty due to the modelling assumptions. It is assumed for the work presented in this thesis that the uncertainty in the valve model parameters will dominate and so the uncertainty in the valve model structure can be neglected.

B.2 The Actuator Model

A typical feature of HVAC systems are regions of inactivity in the subsystem output at the extremes of control signal. The 'dead-band' when $u_{cc} \to 0\%$ duty is a characteristic of the actuator, is often not compensated for in the control software. When $u_{cc} \to 100\%$ duty the observable effects may in-part be attributed to the actuator. The apparent magnitude of the dead-band, however, is exacerbated by the non-linearities in the system output that will almost certainly exist. In addition to the dead-bands, hysteresis is often present. The hysteresis in a system can be attributed to 'slack' in the mechanical linkage between the actuator and the valve stem.

The actuator model accounts for both features, describing the relationship between the control signal and the position of the valve stem. Typically in HVAC systems the magnitude of either can be significant (Buswell et al., 1997; Norford et al., 2000). The reduction in operating range can be up to 40% and hysteresis in motor driven actuators is often between 5% to 10% (Buswell et al., 1997; Buswell and Wright, 1998; Norford et al., 2000).

The dead-bands are modelled by reducing the control signal, ($u \in \{0, 1\}$), to that dictated by the high and low activation points (a_h and a_l respectively),

$$u^{sq} = \frac{u - a_l}{a_h - a_l}, \tag{B.2}$$

where u^{sq} is the normalised active range. The hysteresis model is applied within this active range. The hysteresis model effectively describes an 'envelope' bounding the feasible valve stem positions, demonstrated in Figure B.1.

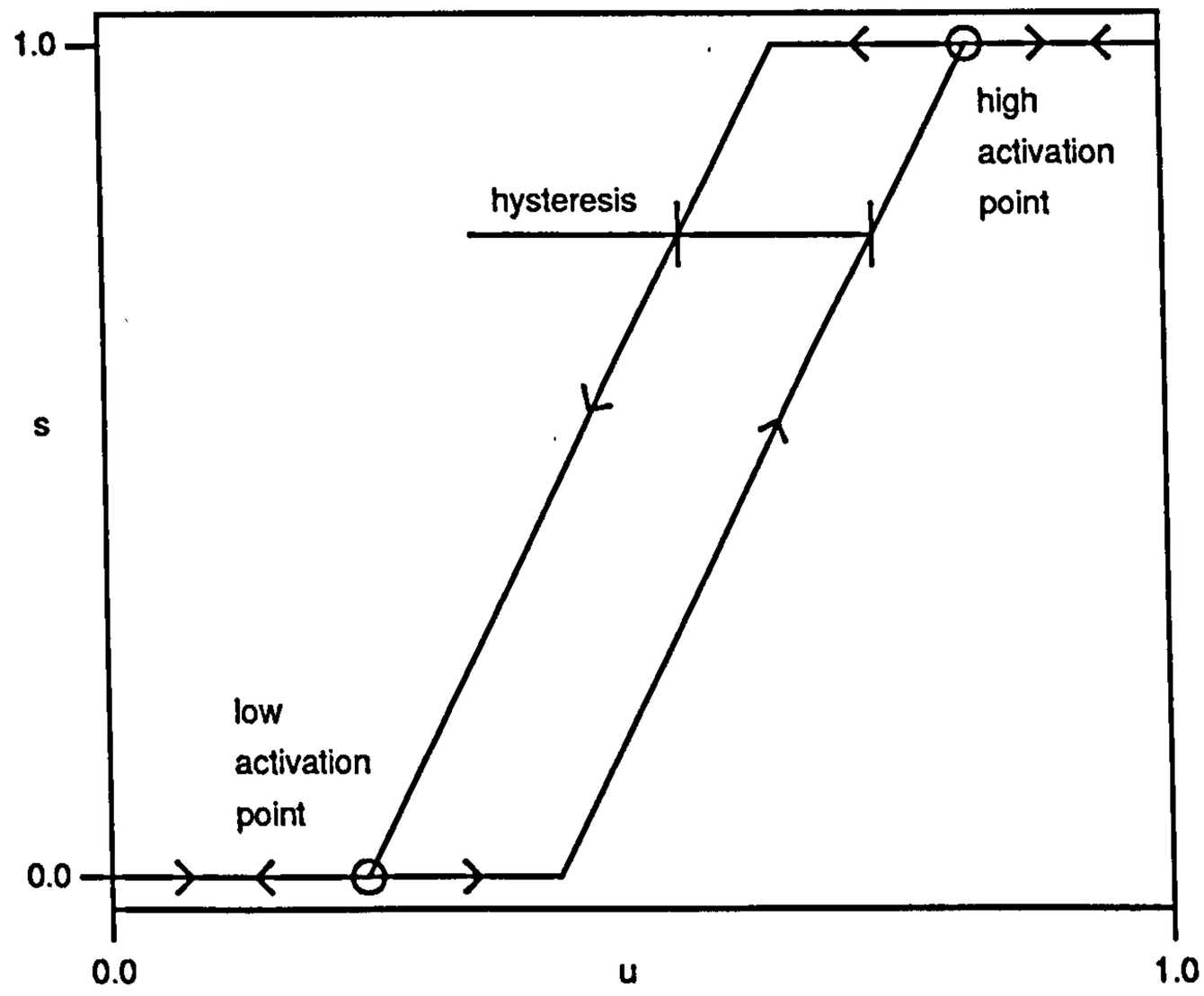

Figure B.1: Control Element Position as a Function of Control Signal.

The hysteresis model described by Clarke (1985) only requires the retention of one historical information data (the last position of the valve stem) and a single parameter (the hysteresis) to predict the current stem position. The model has been shown to give incorrect stem positions when it was applied to an on-line model of a heat-exchanger subsystem used to track the performance of real systems. This was been attributed to the model's ability to track actuator reversal.

The proposed model tracks the valve stem position at every sample, ϱ. One parameter describes the level of hysteresis present in the subsystem, ω. The retention of three historical data are required: the valve stem position, $s(\varrho-1)$; the control signal at the last time step, $u^{sq}(\varrho-1)$; and the direction of movement at the last time step where there was movement, $dir(\varrho-x)$. The current movement direction is calculated by $dir(\varrho) = u^{sq}(\varrho) - u^{sq}(\varrho-1)$ and the valve stem position found by the application of the following rules,

$$\forall\Big(dir(\varrho)>0\Big)\Big\{$$

$$\forall\Big(dir(\varrho-x)=\uparrow_o \;\; AND \;\; u^{sq}(\varrho)>\omega\Big) \;\; s(\varrho) \;\; = \;\; u^{sq}(\varrho)-\omega,$$

$$\forall\Big(dir(\varrho-x)=\downarrow^c \;\; AND \;\; dir(\varrho)>\omega\Big) \;\; s(\varrho) \;\; = \;\; u^{sq}(\varrho)-\omega,$$

$$ELSE \;\; s(\varrho) \;=\; s(\varrho-1) \;\Big\}$$

$$\forall\Big(dir(\varrho)<0\Big)\Big\{$$

$$\forall\Big(dir(\varrho-x)=\downarrow^{c} \;\; AND \;\; u^{sq}(\varrho)<1-\omega\Big) \;\; s(\varrho) \;=\; u^{sq}(\varrho),$$

$$\forall\Big(dir(\varrho-x)=\downarrow^{c} \;\; AND \;\; |dir(\varrho)|>\omega\Big) \;\; s(\varrho) \;=\; u^{sq}(\varrho),$$

$$ELSE \;\; s(\varrho) \;=\; s(\varrho-1) \;\Big\}$$

$$ELSE \qquad\qquad s(\varrho) \;=\; s(\varrho-1), \tag{B.3}$$

where $s(\varrho)$ is the true position of $s^{sq}(\varrho)$ given by,

$$s^{sq}(\varrho) = s(\varrho)\frac{\delta s}{\delta u}, \tag{B.4}$$

where $\frac{\delta s}{\delta u}$ is the gradient of the hysteresis characteristic and is given by,

$$\frac{\delta s}{\delta u} = \frac{1}{1-\omega}. \tag{B.5}$$

$s^{sq}(t)$ is then used as the input to the valve model. The model has been validated on real systems (Norford et al., 2000).

B.2.1 Model Uncertainty

The three parameters need to be estimated for the target system. Some uncertainty will exist in the estimates and will therefore affect the accuracy of the prediction of the valve stem position.

If it is assumed that there is no hysteresis and no uncertainty in a_h, then the influence of the uncertainty in the location of a_l in the estimated position of the valve stem, $\hat{s}$, will diminish as the operating point approaches a_h as Figure B.2 demonstrates. The uncertainty associated with a_h has similar characteristics, but it is a_l that is assumed to have no uncertainty.

Figure B.3 shows the effect of uncertainty in the hysteresis parameter. Uncertainty in the hysteresis parameter affects the one side of the envelope only, dependent on the formulation of the model. It should be noted that the gain of the model is dependent on the size of the hysteresis parameter, as well as the distance between activation points. The

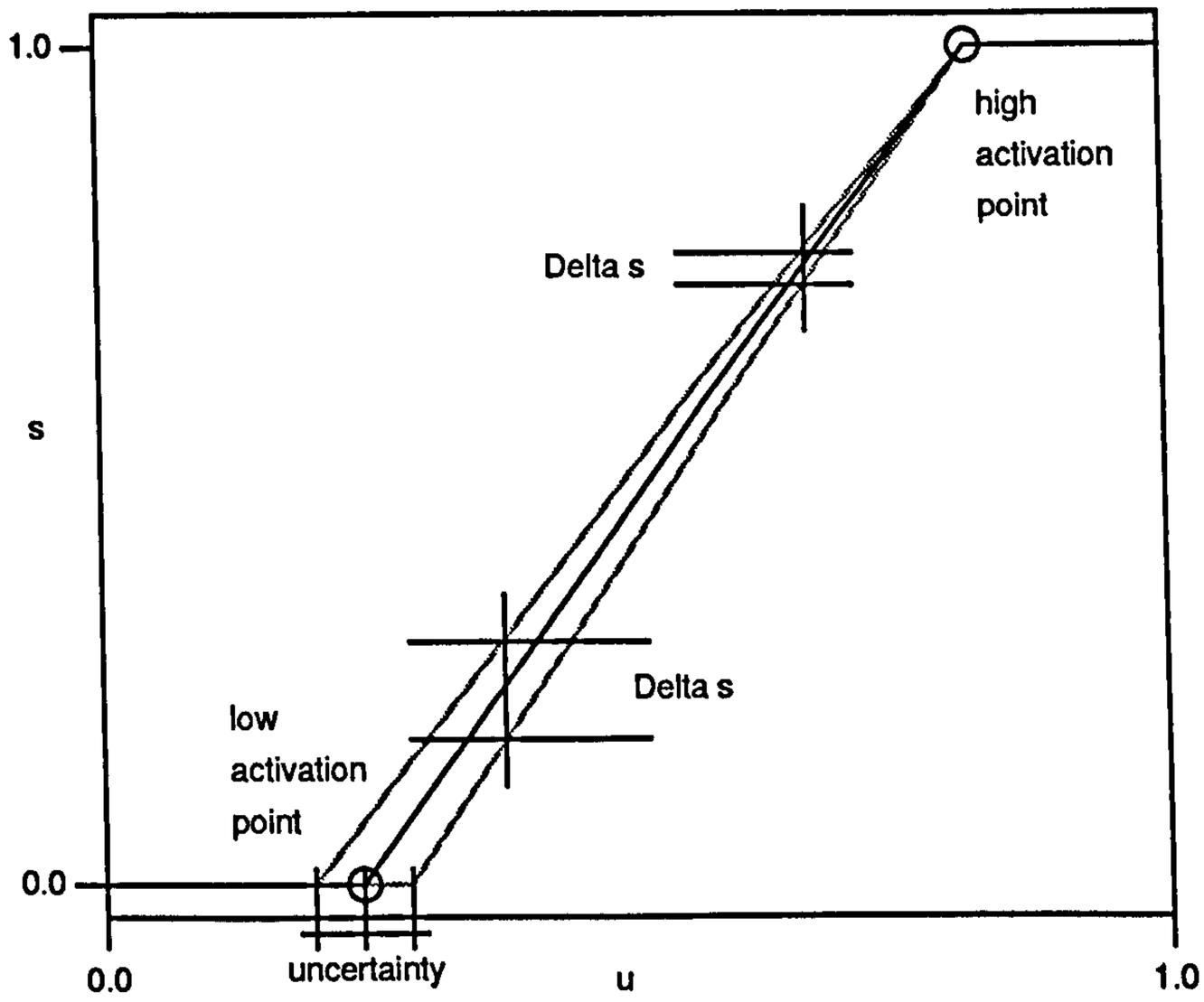

Figure B.2: The Effect of the Uncertainty Associated with the Low Activation on Estimated Damper Position

consequence of this is that the three parameters cannot be estimated in isolation. While one activation point can be estimated directly, the other and the hysteresis have to be evaluated simultaneously. The estimation of these parameters can be by inspection or from empirical data. Appropriate estimates of uncertainty can then be applied to each parameter. The actuator model is not based on first principles but on an explicit representation of the observed behaviour and as such has no implicit modelling assumptions. The only uncertainty in the model is present in the parameter estimates.

It should be noted that a further complication occurs when numerical differencing is used to generate an estimate the sensitivity coefficient associated with the valve stem position and the hysteresis parameter. If the differencing is applied when the valve stem is 'floating' in the region between the boundaries of the hysteresis envelope, the gradient will be zero. This results in the uncertainty contribution from the hysteresis parameter being evaluated as zero. To prevent this, the sensitivity coefficient needs estimating when $\omega = 0$ and a_l adjusted such that the gain of the model is equivalent to the model where $\omega \neq 0$.

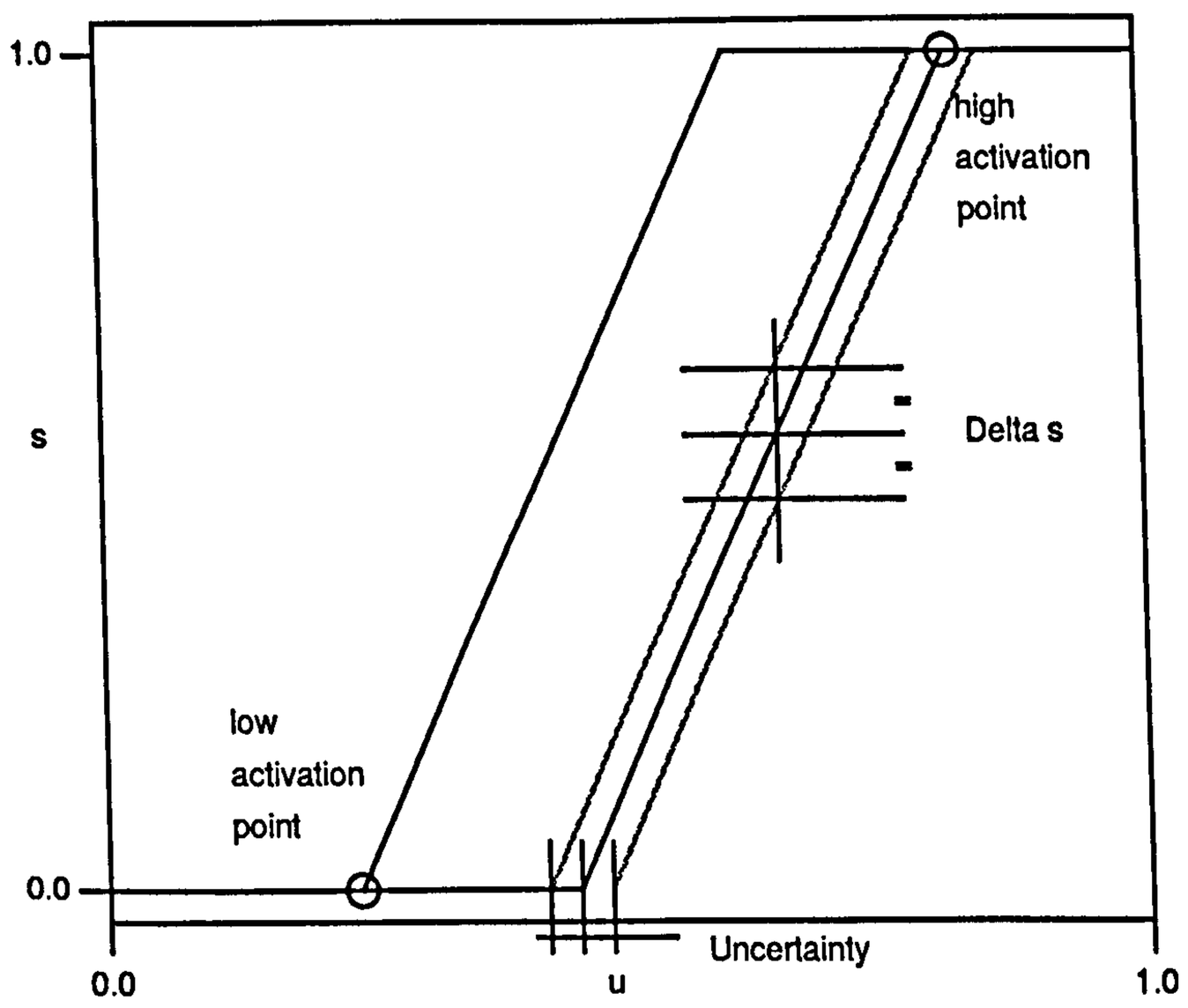

Figure B.3: Shows the Effect of Uncertainty in the Hysteresis Parameter on the Estimation of Damper Position

Appendix C

Derivation of Uncertainty Code

The representation of the uncertainty propagation equation for 95% confidence limits that allow treatment of the correlations in the uncertainties was proposed by Coleman and Steel in the form,

$$U_y^2 = B_y^2 + P_y^2, \tag{C.1}$$

where, U_y is the uncertainty in the result, y, and B_y and P_y represent the 95% estimates of the bias and random uncertainties, denoted by M in the general equation,

$$M_y^2 = \sum_{i=1}^{J} \theta_i^2 M_i^2 + 2 \sum_{i=1}^{J-1} \sum_{k=i+1}^{J} \theta_i \theta_k \rho_{M_{ik}} M_i M_k, \tag{C.2}$$

where J is the number of variable and $\theta_i = \frac{\partial_y}{\partial x_i}$. Given the standard deviation S_i and assuming the large sample assumption is applicable, $P_i = 2S_i$. $\rho_{M_{ik}}$ is the correlation coefficient that relates the correlations between uncertainty sources, assumed to be 1 or estimated by,

$$\rho_{M_{ik}} = \sum_{j=1}^{L} (M_i)_j (M_k)_j \tag{C.3}$$

where L is the number of elemental uncertainties that are common for the variables x_i and x_k.

There are a number of shortcomings with the representation shown in Equations C.1 to C.3, which are:

- only variable uncertainty is treated;

- does not allow the application of the method to automated operations on the data.

Here, the representation is developed to demonstrate the coding operations and to facilitate the application of a generalised approach to treat variable, parametric and model structural uncertainties. The model structural uncertainties are introduced at intermediate calculation points (temporary variables) and are termed *intermediate variables.*

Taking the standard (not correlated) uncertainties associated with each non-operator element of the model $[Z_1, Z_2, \ldots, Z_n]$, the vector of the first derivatives of y with respect to all non-operator elements of the model (i.e. the parameters, variables and intermediate variables) is given by,

$$\Theta = \begin{bmatrix} \frac{\partial y}{\partial Z_1} \\ \frac{\partial y}{\partial Z_2} \\ \vdots \\ \frac{\partial y}{\partial Z_n} \end{bmatrix}. \tag{C.4}$$

Θ is the vector of sensitivity coefficients. The elemental uncertainties associated with each model element Z can be represented by the elemental uncertainty matrix, m, where the rows correspond to $[Z_1, Z_2, \ldots, Z_n]$ and the columns to each type of elemental uncertainty, of which there are a maximum of L possible. m is initially a null matrix representing complete certainty in the elements of Z. Non-zero elements indicate the appropriate uncertainty levels associated with Z_i. The sum squared uncertainty matrix, $\widetilde{M}$ is given by,

$$\widetilde{M} = m^T m, \tag{C.5}$$

Discarding the elements with unwanted information, the sum squared uncertainty vector, M is given by,

$$M_i = \widetilde{M}_{ii} \Big|_{i=1}^{n}. \tag{C.6}$$

The calculation of the correlated uncertainties require further notation. The matrix of correlated derivatives Φ is given by,

$$\Phi = \Theta_i \Theta_k \Big|_{i=1}^{n} \Big|_{k=1}^{n}, \tag{C.7}$$

and Ψ_{jik} is a three dimensional matrix $(L \mathrm{x} n, \mathrm{x} n)$ where the $n \mathrm{x} n$ matrix is upper triangular in the j dimension. The elements of Ψ_{jik} represent the correlation coefficients of the

elemental uncertainties with each non-operator element in the model where $\rho \in [0, 1]$,

$$\Psi_{jik} = \left[\begin{bmatrix} \rho_{ik} & \cdots & \rho_{n1} \\ \vdots & \ddots & \vdots \\ \rho_{1n} & \cdots & \rho_{nn} \end{bmatrix}_{j=1,} \begin{bmatrix} \rho_{ik} & \cdots & \rho_{n1} \\ \vdots & \ddots & \vdots \\ \rho_{1n} & \cdots & \rho_{nn} \end{bmatrix}_{j=2,\ \ldots,} \begin{bmatrix} \rho_{ik} & \cdots & \rho_{n1} \\ \vdots & \ddots & \vdots \\ \rho_{1n} & \cdots & \rho_{nn} \end{bmatrix}_{j=L} \right]. \quad \text{(C.8)}$$

The correlated uncertainties are represented by the $(L \mathrm{x} n, \mathrm{x}\, n)$ matrix $\boldsymbol{N}$,

$$\boldsymbol{N} = \Psi_{jik} m_{ij}^{\frac{1}{2}} m_{kj}^{\frac{1}{2}} \Big|_{i=1}^{n} \Big|_{k=1}^{n} \Big|_{j=1}^{L}. \quad \text{(C.9)}$$

U_M^2 is the scalar output of the 95% confidence estimate for one uncertainty type (random or bias) and is given by,

$$U_M^2 = \sum_{i=1}^{n} \Phi_{ii} M_i + 2 \sum_{j=1}^{L} \sum_{i=1}^{n} \sum_{k=1}^{n} \Phi_{ik} \boldsymbol{N}_{jik}, \quad \text{(C.10)}$$

where the equation is evaluated for bias and random uncertainty. If j represents the *maximum* elemental uncertainties assigned to either the bias or random uncertainty components and both m matrices are of the order $(n \mathrm{\ x\ } max(L))$ where the unwanted elements in the matrix with less information are equal to zero, the uncertainty about the model output, U_y, is given by,

$$U_y = \left[\sum_{i=1}^{n} \Phi_{ii} \left(M_i^B + M_i^P \right) + 2 \sum_{j=1}^{L} \sum_{i=1}^{n} \sum_{k=1}^{n} \Phi_{ik} \left(\boldsymbol{N}_{jik}^B + \boldsymbol{N}_{jik}^P \right) \right]^{\frac{1}{2}}. \quad \text{(C.11)}$$

Solution Structure

The sensitivity coefficients in Θ are in a specific order: those relating to the variables first, parameters next and intermediate variables last. These coefficients are derived in one of three ways:

1. where the algebraic derivative is known *a priori*, the value is calculated directly;

2. where the algebraic derivative is difficult to ascertain, differencing is employed;

3. where the uncertainty is calculated directly (generally in the representation of model structural uncertainty), Θ_i is set to unity.

Uncertainty estimates that are expressed as values describing the total uncertainty associated with a parameter or variable (rather than as elemental sources) are treated as a bias uncertainty in the matrix formulation and the corresponding elements in the random uncertainty matrix are set to zero.

Bibliography

Abernathy, R. B. (1973). *Handbook, Uncertainty in Gas Turbine Measurements.* National Technical Information Service, US Department of Commerce.

Abernethy, R. B., R. P. Benedict, and R. B. Dowdell (1985, June). Asme measurement uncertainty. *Journal of Fluids Engineering 107.*

ANSI/ASME-MFC-2M (1983). *Measurement Uncertainty for Fluid Flow in Closed Ducts.* The American Society of Mechanical Engineers, New York.

ANSI/ASME-PTC-19.1 (1986). *Measurement Uncertainty, (ANSI/ASME PTC 19.1-1985).* The American Society of Mechanical Engineers, New York.

ASHRAE (1991). *Method of testing air-to-air heat exchangers.* American Society of Heating Refrigerating and Air-Conditioning Engineers, Atlanta.

ASHRAE (1996). *Engineering Analysis of Experimental Data.* American Society of Heating Refrigerating and Air-Conditioning Engineers, Atlanta.

Bayazitoglu, Y. and M. N. Ozisik (1988). *Elements of Heat Transfer.* McGraw-Hill.

Benouarets, M., A. L. Dexter, R. S. Fargus, P. Haves, T. I. Salsbury, and J. A. Wright (1994, December). Model-based approaches to fault detection and diagnosis in HVAC systems. In *Proceedings of System Simulation in Buildings '94*, Liège, Belgium.

Bilal, M. A. (Ed.) (1998). *Uncertainty Modeling and Analysis in Civil Engineering.* CRC Press.

Binder, K. and D. W. Heermann (1992). *Monte Carlo Simulation in Statistical Physics.* Springer-Verlag Berlin Heidelberg, New York.

Box, M. J. (1965). A new method of constrained optimisation and a comparison with other methods. *The Computer Journal.*

Brandemuehl, M. J., S. Gabel, and I. Andresen (1993). *A Toolkit for Secondary HVAC Systems Energy Calculations.* ASHRAE.

Bratko, I., I. Mozetic, and N. Lavarac. Automatic synthesis and compression of cardiological knowledge.

Braun, J. E., S. A. Klein, and J. W. Mitchell (1989). Effectiveness models for cooling towers and cooling coils. *ASHRAE Transactions 95, Pt. 2.*

Breuker, M. S. and J. E. Braun (1997, August). Demonstration of a statistical, rule-based fault detection and diagnostic method on a rooftop air conditioing unit. In *Proceedings of Clima 2000*, Prague, The Czech Republic.

Breuker, M. S. and J. E. Braun (1998). Evaluating the performance of a fault detection and diagnostic system for vapour compression equipment. *HVAC & R Research 4 No. 4.*

Breuker, M. S. and J. E. Braun (1999). Common faults and their impacts for rooftop air conditioners. *HVAC & R Research 4 No. 3.*

Bronson, D. J., S. B. Hinchey, J. S. Haberl, and D. L. O'Neal (1992). A procedure for calibrating the DOE-2 simulation program to non-weather-dependent measured loads. *Transactions of the American Society of Heating, Refrigerating and Air-Conditioning Engineers 98, Pt. 1.*

Brown, K. K., H. W. Coleman, and W. G. Steele (1998). A methodology for determining the experimental uncertainty in regressions. *Journal of Fluids Engineering 120, No. 3.*

Brown, K. K., H. W. Coleman, W. G. Steele, and R. P. Taylor (1996, May). Evaluation of correlated bias approximations in experimental uncertainty analysis. *American Institute of Aeronoutics and Astronautics 34, No. 5.*

BSRIA (1993a). *Commissioning of VAV Systems in Buildings.* BSRIA, Berkshire, England.

BSRIA (1993b). *The commissioning of air conditioning systems in buildings.* BSRIA, Berkshire, England.

Buswell, R. A. (1998, April). Documenting and transfer of data sets. Working paper presented at Annex 34 meeting, Loughborough, UK.

Buswell, R. A., P. Haves, A. L. Dexter, N. D, and R. Fargus (1997). Introducing faults into hvac plant installed in real buildings. Working paper presented at Annex 34 meeting, October, 1997, Boulder, Colorado, USA.

Buswell, R. A., P. Haves, and T. I. Salsbury (1997, August). A model-based approach to the commissioning of hvac systems. In *Proceedings of Clima 2000*, Prague, The Czech Republic.

Buswell, R. A. and J. A. Wright (1998). Practical application of fault detection and diagnosis: Final report on condition monitoring.

Buswell, R. A. and J. A. Wright (1999, April). Model based condition monitoring of a hvac cooling coil sub-system installed in a resl building. Working paper presented at Annex 34 meeting, Fontainebleau, France.

Carling, P. (1998a, September). Comparisons of air temperature sensors in ahu. Working paper presented at Annex 34 meeting, Oulu, Finland.

Carling, P. (1998b). Comparisons of air temperature sensors in ahu. Working paper presented at Annex 34 meeting, Oulu, Finland.

Carling, P. (1999). Swedish results from measurements in an office building. Working paper presented at Annex 34 meeting, Fontainebleau, France.

Carling, p. and P. Isaksson (1999). Temperature measurement accuracy in an air-handling unit mixing box. In *The Third International Symposium on Heating, Ventilation and Air-Conditioning.*

Carrier, W. H., R. E. Cherne, and W. A. Grant (1940). *Modern Air Conditioning, Heating and Ventilating.* Pitman.

Ciepliski, D. L., R. W. Besant, and C. J. Simonson (1998). Some recommendations for improvements to ashrae standard 84-191. *ASHRAE Transactions 104 Pt. 1.*

Clarke, R. C. (1985). *HVACSIM+ Building Systems and Equipment Simulation Program Reference Manual.* U.S. Department of Commerce, National Bureau of Standards, National Engineering Laboratory, Center for Building Technology, Building Equipment division, Gaithersburg, MD 20899.

Coleman, H. W. and W. G. Steele (1995, October). Engineering application of experimental uncertainty analysis. *American Institute of Aeronoutics and Astronautics 33, No. 10.*

Coleman, H. W. and W. G. Steele (1999). *Experimentation and Uncertainty Analysis for Engineers* (4th ed.). John Wiley and Sons.

Coleman, H. W., W. G. Steele, and R. P. Taylor (1995, December). Implications of correlated bias uncertainties in single and comparative tests. *ASME Transactions 117*.

Dexter, A. L. and M. Benouarets (1995). Generic modelling of hvac plant for fault diagnosis. In *Proceedings of the 4th IBPSA International Conference: Building Simulation*, Madison, Wisconsin, USA.

Dexter, A. L. and M. Benouarets (1996). A generic approach to identifying faults in HVAC plant. *Transactions of the American Society of Heating, Refrigerating and Air-Conditioning Engineers 102, Pt. 1.*

Dietrich, C. F. (1973). *Uncertainty, Calibration and Prbability*. Adam Higler, London.

Dobson, A. J. (1983). *An Introduction to Statistical Modelling*. Chapman and Hall.

Elmahdy, A. H. and R. C. Biggs (1979). Finned tube heat exchanger correlation of dry surface heat transfer data. *Transactions of the American Society of Heating, Refrigerating and Air-Conditioning Engineers 85, Pt. 2.*

Eurachem (1995). *Eurachem: Quantifying Uncertainty in Analytical measurement* (1st ed.). Department of Transport and Industry.

Fargus, R. and A. L. Dexter (1994, December). Non-linear black-box modelling of HVAC systems. In *Proceedings of System Simulation in Buildings '94*, Liège, Belgium.

Geshwiler, M. (1996). *Technical Data Bulletin: Fault Detection and Diagnosis for HVAC Systems*. ASHRAE.

Glass, A. S., P. Gruber, M. Roos, and J. Tödtli (1995, August). Qualitative model-based fault detection in air-handling units. *IEEE Control Systems*.

Gruber, P. (1996). Determination of the tuning parameters of the steady state detector for a central air handling unit (cahu). *IEA Annex 25 Final Report, Volume II - Real Time Simulation of HVAC Systems for Building Optimization, Fault Detection and Diagnosis, Technical Papers of IEA Annex 25*.

Han, C. Y., Y. Xiao, and C. J. Ruther (1999). Fault detection and diagnosis of hvac systems. *ASHRAE Transactions 105, Pt. 1.*

Hasselman, T. K., M. C. Anderson, and W. Gan (1998, February). Principal components analysis for nonlinear model correlation, updating and uncertainty evaluation. In *Proceedings of the 16th International Modal Analysis Conference*, Volume 1 and 2, Vol. 3243, Ch. 262, Santa Barbara, USA.

Haves, P., T. I. Salsbury, and J. A. Wright (1995). Condition monitoring in hvac subsystems using first principles models. *Transactions of the American Society of Heating, Refrigerating and Air-Conditioning Engineers 102, Pt. 1.*

Hofer, E. (1999). Sensitivity analysis in the context of uncertainty analysis for computationally intensive models. *Computer Physics Communications 117, Pt. 1-2.*

Holman, J. P. (1984). *Experimental Methods for Engineers* (4th ed.). McGraw and Hill.

Holmes, M. J. (1982, December). The simulation of heating and cooling coils for performance analysis. In *Proceedings of System Simulation in Buildings '82*, Liège, Belgium.

House, J. M. and J. Whitcomb (1999). A case study of the application of a rule-based fdd method for air-handling units to field data. Working paper presented at Annex 34 meeting, Fontainebleau, France.

Hyvärinen, J. (1997a). *IEA Annex 25 Final Report.* VTT, Espoo, Finland.

Hyvärinen, J. (1997b). *IEA Annex 25 Final Report, Volume I - Building Optimization and Fault Diagnosis Source Book.* VTT, Espoo, Finland.

Hyvärinen, J. (1997c). *IEA Annex 25 Final Report, Volume II - Real Time Simulation of HVAC Systems for Building Optimization, Fault Detection and Diagnosis, Technical Papers of IEA Annex 25.* VTT, Espoo, Finland.

ISO (1976). *Measurement of Fluid Flow - Estimation of a Flow Rate Measuremnent, (ISO 5168).* International Organization for Standardization, Geneva, Switzerland.

ISO (1993). *Guide to the Expression of Uncertainty in Measuremnent.* International Organization for Standardization, Geneva, Switzerland.

Johnson, A. B., C. J. Simonson, and R. W. Besant (1998). Uncertainty analysis in the testing of air-to-air heat/energy exchangers installed in buildings. *ASHRAE Transactions 104 Pt. 1B.*

Kammerud, R., K. L. Gillespie, and M. M. Hygeman (1999). Economic uncertainties in chilled water design. *ASHRAE Transactions 105 Pt. 2.*

Kaptipamula, S., R. G. Pratt, D. P. Chassin, T. Z. Taylor, K. Gowi, and M. R. Brambley (1999). Automated fault detection and diagnostics for outdoor-air ventilation systems and economizers: Methodology and results from field testing. *ASHRAE Transactions 105, Pt. 1.*

Kays, W. M. and A. L. London (1984). *Compact Heat Exchangers* (Third ed.). Krieger Publishing Company.

Kärki, S. H. and S. J. Karjalainen (1999). Performance factors as a basis of practical fault detection and diagnostic methods for air-handling units. *ASHRAE Transactions 105, Pt. 1.*

Kelso, R. M., P. H. Marshall, and A. J. Baker (2000, September). A cfd study of airflow in a mixing box. In *Proceedings of CIBSE/ASHRAE Conference.*

Kline, S. J. and F. A. McClintock (1953, Jan.). Describing uncertainties in single-sample experiments. *Mechanical Engineering 75 No. 3.*

Kreider, J. F. and J. S. Haberl (1994). Predicting hourly building energy use: The great energy predictor shootout - overview and discussion of results. *Transactions of the American Society of Heating, Refrigerating and Air-Conditioning Engineers 100, Pt. 2.*

Lee, A. (2000). Air mixing through a cooling coil; results from a cfd analysis. Presentation at the University of Oxford.

Li, X., J.-C. Visier, and H. Vaezi-Nejad (1996). A neural network prototype for fault detection and diagnosis of heating systems. *IEA Annex 25 Final Report, Volume II - Real Time Simulation of HVAC Systems for Building Optimization, Fault Detection and Diagnosis, Technical Papers of IEA Annex 25.*

Li, X., J.-C. Visier, and H. Vaezi-Nejad (1997). A neural network prototype for fault detection and diagnosis of heating systems. *ASHRAE Transations 103, Pt. 1.*

Moffat, R. J. (1982, June). Contributions to the theory of single-sample uncertainty analysis. *Transactions of ASME 104.*

Moffat, R. J. (1985, June). Using uncertainty analysis in the planning of an experiment. *Journal of Fluids Engineering 107.*

Moffat, R. J. (1988, January). Describing the unceratinties in experimental results. *Experimental and Fluid Science 1.*

Ngo, D. and A. L. Dexter (1998). Fault diagnosis in air-conditioning systems using generic models of hvac plant. In *Proceedings of the International Conference on System Simulation in Buildings*, Liege, Belgum.

Ngo, D. and A. L. Dexter (1999a, April). Automated commissioning using a multi-step approach to fault diagnosis. Working paper presented at Annex 34 meeting, Fontainebleau, France.

Ngo, D. and A. L. Dexter (1999b). A robust model-based approach to diagnosing faults in air-handling units. *ASHRAE Transactions 105 Pt. 1.*

Norford, L. K. and S. B. Leeb (1996). Non-intrusive electrical load monitoring in commercial buildings based on steady-state and transient load-detection algorithms. *Energy and Buildings 24.*

Norford, L. K., J. A. Wright, R. A. Buswell, and D. Luo (2000). *Final Report of ASHRAE Research Project 1020-RP: Demonstration of Fault Detection and Diagnosis in Real Building.* Massachusetts Institute of Technology and Loughborough University.

Oughton, R. J. (1985). *Applications Manual: Automatic Controls.* CIBSE, London, England.

Pearson, K. (1902). On the theory of errors of judgement with special reference to the personal equation. *Philosophical Transactions of the Royal Society of London 198, Series A.*

Phelan, J., M. J. Brandemuehl, and M. Karti (1997a). In-situ performance testing of chillers for energy analysis. *ASHRAE Transactions 103 Pt. 1.*

Phelan, J., M. J. Brandemuehl, and M. Karti (1997b). In-situ performance testing of fans and pumps for energy analysis. *ASHRAE Transactions 103 Pt. 1.*

Price, B. A. and T. F. Smith (1998). Description of the iowa energy center energy resource station:facility update 1.

Rabehl, R. J., J. W. Mitchell, and W. A. Beckman (1999). Parameter estimation and the use of catalog data in modelling heat exchangers and coils. In *ASHRAE Transactions.* Volume , Part.

Reddy, T. A., J. S. Haberl, and J. S. Elleson (1999). Engineering uncertainty analysis in the evaluation of energy and cost savings of cooling system alternatives based on field-monitored data. *ASHRAE Transactions 105 Pt. 2.*

Reddy, T. A., J. S. Harbel, and J. S. Elleson (1999). Engineering uncertainty analysis in the evaluation of energy and cost savings of cooling system alternatives based on

field-monitored data. *ASHRAE Transactions 105 Part 2.*

Robinson, K. D. (1998). Damper control characteristics and mixing effectiveness of an air-handling unit combination mixing/filter box. In *ASHRAE Transactions.* Volume 104, Part 1A.

Robinson, K. D. (1999). Mixing effectiveness of ahu combination mixingt/filter box with and without filters. In *ASHRAE Transactions.* Volume 105, Part 1.

Rogers, G. F. C. and Y. R. Mayhew (1988). *Thermodynamic and Transport Properties of Fluids* (Fourth ed.). Basil Blackwell Ltd.

Rossi, T. M. and J. E. Braun (1994). Reducing operating costs with optimal maintenance scheduling. Working paper, distributed at the 8th meeting of IEA Annex 25, Stuttgart, Germany.

Rossi, T. M. and J. E. Braun (1997). A statistical rule-based fault detection and diagnostic method for vapor compression air compressors. *HVAC & R Research 3 Pt. 1B.*

Salsbury, T. and R. Diamond (2000). Performance validation and energy analysis of hvac systems using simulation. *Energy and Buildings.*

Salsbury, T. I. (1996). *Fault Detection and Diagnosis in HVAC Systems using Analytical Models.* Loughborough University, UK. PhD Thesis.

Schwarzenbach, J. and K. F. Gill (Eds.) (1992). *System Modelling and Control* (Third ed.). Edward Arnold, London.

Seem, J. E., J. M. House, and R. H. Monroe (1999, July). On-line monitoring and fault detection. *ASHRAE Journal 41, No. 7.*

Sontay (1998). *Sontay Product Catalogue, 1999.* Sontay, England.

Steele, W. G., R. P. Taylor, R. E. Burrell, and H. W. Coleman (1993, October). Use of previous experience to estimate prescision uncertainty of small sample experiments. *American Institute of Aeronoutics and Astronautics 31, No. 10.*

Stephan, W. and Gruschka (1994). Comparison of different models for cooling coils under wet conditions. In *Proceedings of the 4th International Conference on System Simulation in Buildings, Liege.*

Stoecker, W. F. (1989). *Design of Thermal Systems* (Third ed.). McGraw-Hill.

Taylor, B. N. and C. E. Kuyatt (1994). *Guidelines for Evaluating and Expressing the Uncertainty of NIST Measturement Results.* U.S. Government Printing Office. Washington.

Taylor, J. R. (1982). *An Introduction to Error Analysis.* University Secience Books, California.

Taylor, J. R. (1986). *Computer-Based Data Aquisition Systems.* Instrument Society of America.

Threlkeld, J. L. (1970). *Thermal Environmental Engineering.* Prentice-Hall: Englewood Cliffs, NJ.

Underwood, C. P. (1999). *HVAC Control Systems: Modelling, Analysis and Design.* E and FN Spon, London.

Underwood, C. P. (2000). Robust control of hvac plant 1: Modelling. In *Building Services Engineering and Research Technology*, pp. 53–61. Volume 21, Part 1.

Vaezi-Nejad, H., P. Simon, P. Correleas, M. Kerdoncuff, and M. DelTreil (1997). Assessment and improvement of emma software. Working paper, presented at IEA Annex 34 meeting in Boulder, Colorado, USA.

Visier, J. C. (1998). Customer benefits, user needs and user interface. Working paper, distributed at IEA Annex 34 meeting in Fontainbleau, France.

Visier, J. C., H. Vaezi-Nejad, and P. Corrales (1999). A fault detection tool for school buildings. *ASHRAE Transactions 105, Pt. 1.*

Walpole, R. E. and R. H. Myres (1989). *Probability and Statistics for Engineers and Scientists.* Macmillan.

Yoshida, H. and S. Kumar (1999). Rarx algorithm based model development and application to real time data for on-line fault detection in vav units. Working paper presented at Annex 34 meeting, Fontainebleau, France.